SOUND TRANSMISSION THROUGH LIGHTWEIGHT PARALLEL PLATES

BY

R. Sean Smith

This thesis is submitted in accordance with
the requirements of Heriot-Watt University for
the degree of Doctor of Philosophy.

Department of Building Engineering and Surveying
Heriot-Watt University

December 1997

CONTENTS

LIST OF FIGURES

List of Tables

List of Symbols

B	Bending stiffness for a beam (Nm)
	Bending stiffness per unit width for a plate (Nm)
$D_{1\text{-}2}$	Level difference (dB)
D_y	Bending stiffness for a beam about the x-axis
E	Youngs modulus (N/m^2)
E_i	Energy of subsystem i
E_0	Reference energy (10^{-12}J)
E_a	Youngs modulus in the axial plane
E_r	Youngs modulus in the radial plane
E_t	Youngs modulus in the tangential plane.
F	Shear force (N/m)
G	Torsional stiffness
I	Moment of inertia
K	Bulk modulus of air (1.4×10^5 N/m)
L	Subsystem dimension (m)
$L_{1\text{-}2}$	Junction length (m)
L_a	Acceleration level (dB re 10^{-12} J)
L_e	Energy level (dB re 10^{-12} J)
Lp	Sound pressure level (dB re 2×10^{-5} N/m)
L_v	Velocity level (dB re 10^{-12} J)
Lw	Sound power level (dB re 10 W)
M	Moment
N	Number of nails
S	Surface area (m^2)
	Cross sectional area
T	Reverberation time (sec.)
T_{60}	Reverberation time (sec.)
U	Perimeter length (m)
V	Volume (m^3)
W	Power (W)
W_i	Power input to subsystem i (W)
W_{ij}	Power flow from subsystem i to j
W_{id}	Power lost internally from subsystem i
Y_p	Mobility of a plate (m/Ns)
Y_b	Mobility of a beam (m/Ns)
Z	Impedance (Ns/m)
a	Acceleration (m/s^2)
b	Width of beam
c	Wavespeed (m/s)
c_0	Wavespeed in air
c_B	Bending wavespeed (m/s)
c_g	Group velocity (m/s)
c_L	Longitudinal wavespeed (m/s)
c_T	Transverse wavespeed (m/s)

f	Frequency (Hz)
f_c	Critical frequency (Hz)
f_0	Mass-spring-mass resonance (Hz)
f_p	Transition frequency for line to point connection
f_x	Frequency for first cross resonance in cavity
h	Thickness (m)
i	$\sqrt{-1}$
k	Wavenumber (rad/m)
k_B	Bending wavenumber (rad/m)
k_L	Longitudinal wavenumber
k_T	Transverse wavenumber
k_n	Nearfield wavenumber (rad/m)
k_x	Wavenumber in the x direction (rad/m)
k_y	Wavenumber in the y direction (rad/m)
l	Depth of cavity (m)
m	Mass (kg)
n_b	Modal density of a beam (modes/Hz)
n_c	Modal density of a cavity
n_p	Modal density of a plate
n_r	Modal density of a room
p	Pressure (N/m^2)
s	Spacing of point connections
t	Time (sec.)
v	Velocity (m/s)
α	Absorption coefficient
γ	Flexural displacement in the z-direction (m)
ζ	Inplane displacement in the y-direction
η	Loss factor
η_i	Total loss factor of subsystem i
η_{id}	Internal loss factor of subsystem i
η_{ij}	Coupling loss factor from subsystem i to j
θ	Angle of incidence (rad)
λ	Wavelength (m)
μ	Poisson's ratio
ξ	Inplane displacement in the x-direction
π	3.14159....
ρ	Density (kg/m^3)
ρ	Surface density (kg/m^2)
σ	Radiation efficiency
τ	Transmission coefficient
ϕ	Angle of rotation (rad)
CLF	Coupling loss factor
ILF	Internal loss factor
MSM	Mass-spring-mass
SEA	Statistical energy analysis
SRI	Sound reduction index (dB)
TLF	Total loss factor

Acknowledgements

The author would like to extend his sincere thanks to his supervisor, Prof. Robert Craik, for the guidance and encouragement during the course of this research. In addition, the author would like to acknowledge the assistance provided in the way of SEA computer software written by Prof. Craik, which allows the potential that statistical energy analysis offers as a predictive design tool to be realised.

Most of this work was carried under on behalf of the Engineering and Physical Sciences Research Council (EPSRC) and the Defence Evaluation Research Agency (DERA). The author would like to thank Dr. Ken Heron from DERA for his constant support and interest in the project during his many visits. Prior to this period the author was supported on an EPSRC studentship to which the author gratefully acknowledges their support. During the period of the studentship the author was able to visit the Acoustics Research Department of the National Research Council of Canada. The author would like to thank the EPSRC who funded the visit and Dr. Alf Warnock and Dr. Trevor Nightingale for allowing temporary access to their exhaustive collection of measured data.

The author would like to thank the staff of the Dept. of Building Engineering and Surveying and of Heriot-Watt University for their support and encouragement. Many thanks are also extended to the RA's and PhD students within the Department who created a stimulating and enjoyable environment within which to study.

Finally the author would like to thank his girlfriend Anna Biavati and her family for their tireless support and endless encouragement throughout the course of this study.

Dedication

This work is dedicated to my mother Marean who passed away prior to this study being completed.

Nessun maggior dolore,
Che ricordarsi del tempo felice,
nella miseria. (Dante)

Abstract

This thesis examines the transmission of sound through lightweight parallel plates, (plasterboard double wall partitions and timber floors). Statistical energy analysis was used to assess the importance of individual transmission paths and to determine the overall performance.

Several different theoretical models were developed, the choice depending on the frequency range of interest and method of attachment of the plates, whether point or line, to the structural frame. It was found that for a line connected double wall there was very good agreement between the measured and predicted results, where the dominant transmission path was through the frame and the cavity path was weak. The transition frequency where the coupling changes from a line to a point connection is when the first half wavelength is able to fit between the spacings of the nails.

For point connected double walls, where the transmission through the frame was weaker than for line connection, the cavity path was dominant unless there was absorption present. When the cavity was sufficiently deep, such that it behaved more like a room, the agreement between the measured and predicted results was good. As the cavity depth decreases the plates of the double wall are closer together and the agreement between the measured and predicted results were not as good.

Detailed experiments were carried out to determine the transmission into the double wall cavities and isolated cavities. It was found that the transmission into an isolated cavity could be predicted well. However, for transmission into double wall cavities the existing theories could not predict transmission accurately when the cavity depth was small.

Extensive parametric surveys were undertaken to analyse changes to the sound transmission through these structures when the material or design parameters are altered. The SEA models are able to identify the dominant mechanisms of transmission and will be a useful design tool in the design of lightweight partitions and timber floors.

Chapter 1
Introduction

1.1 General Introduction

This thesis examines sound transmission through lightweight parallel plates. Structures to which this work is applicable include lightweight double leaf partitions and timber floors. Using Statistical Energy Analysis (SEA) theoretical models are presented to predict the sound transmission through such structures and the behaviour of the individual components. Other structures to which this work is applicable include wing sections of aeroplanes and the fuselage of helicopters.

For the purpose of this work the structures under study are specifically lightweight plasterboard double walls and timber floors. In domestic construction it is often important that the walls and floors possess a high sound insulation to prevent sound being transmitted between dwellings and between rooms within dwellings as this can represent a nuisance to the occupants. When party walls or floors are constructed they must meet the stipulations of the Building Regulations [1,2] and the relevant British or International Standards [3,4,5,6].

Lightweight parallel plate structures consist of two thin lightweight plates which are coupled by a connecting structural frame resulting in cavities being formed between the plates and frame. The principle material used for the structural frame in such constructions is timber. This is a cheap, fast to construct and workable material providing easy handling for the labourers on site.

In recent years the designs of timber floors and partition walls have become more complex incorporating elaborate fixing connections and improved types of absorption,

made from a variety of different materials, for the purpose of achieving higher sound insulation. As designers, architects and specifiers push for improved sound insulation between and within dwellings, it is becoming increasingly important to determine the principle transmission paths through such designs and what components of the structure could be improved.

There are numerous sound transmission paths which may take place in a double wall. There is the interaction between the plates of a double wall or timber floor and the cavity. The structural isolation which is lost due to the frame coupling the plates of a double wall at points (such as screws and nails) or along a line (if glued) also will affect the overall performance of the structure. Whilst some walls may be designed to have very high sound insulation properties, as tested in a laboratory, when built in the field (on site) the connection with other components of the building may cause flanking paths. These are sound transmission paths which allow sound to pass from one room to another, bypassing the wall, resulting in poor sound insulation but not at the fault of the separating wall.

One method of determining the performance of such structures is to carry out extensive experimental work and from the collection of empirical data decisions could be made on how best to improve the design. However, this is a long, drawn out and not particularly accurate process and may not identify the best areas for improvement, particularly on how each component behaves in the overall performance of sound insulation.

A second method is to try to predict the overall transmission by determining mathematical equations based on empirical data. This approach has been widely used on double wall structures, but does not identify the transmission mechanisms involved.

The best method is to predict the performance of the structures entirely based on knowing the material properties of the components and using mathematical models determine the contributions from the individual transmission paths and how they collectively affect the overall performance. This method is adopted for this study and uses the modelling technique of Statistical Energy Analysis (SEA).

Statistical energy analysis (SEA) is a flexible approach to modelling the behaviour of complex systems and it is able to overcome most of the failings of the classical theories. When using SEA the system or structure is subdivided into its various components called subsystems making it easier to model and more manageable.

The behaviour of double walls or timber floors is a complicated process to model. Using SEA allows specific transmission mechanisms to be studied in addition to determining the overall sound transmission through such structures.

To quote the words of A. Powell "*the essentially random nature of the process can be seized upon with great advantage, instead of it being a burden*" [7].

1.2 Aims of this thesis

This thesis aims to develop the work of Craik and Wilson [8,9,10] and others by studying sound transmission through lightweight parallel plates. Firstly to develop theoretical models to predict the acoustic performance of double leaf lightweight partitions. Secondly to verify these theories with measurements made on real partition systems and on particular components of the construction. Thirdly to identify the dominant mechanisms of transmission through such structures.

The interaction of the various components of the double walls are analysed and in particular the structural coupling which takes place at the frame. By expanding on the work of Wilson all types of waves such as flexural, longitudinal and transverse are included in a study of structure borne sound transmission for a line connection between the plates of a double wall. The interaction of the lightweight plates and the frame when the plates are connected by few point are also studied using mobility models. Attention is also given to the effect of the cavities on the walls behaviour and their interaction with the plates and rooms.

The approach of this study was to identify and examine each transmission mechanism to produce and then verify, theoretical models to predict transmission. Where possible existing theories were used. New theories were developed when existing theories were

found to be inappropriate or non-existent. Numerous test lightweight walls were built and experiments carried out to obtain measured data to compare with the predicted results. By combining the transmission of each of the mechanisms in a statistical energy analysis (SEA) framework, predicted data was obtained that included the effects of individual transmission paths and their effect on the overall predicted sound transmission.

Most of the following chapters deal with a specific subject area which is relevant to a particular transmission path. Measured and predicted results are shown together with the theoretical models where the test structures that the experiments were carried out on were only analysing that specific transmission path.

1.3 Outline of the thesis

Chapter 2 gives a review of the previous work on double walls and the application of statistical energy analysis. The work of previous authors using the classical theories and SEA is discussed. The basic theory is also contained in this chapter and is referred to in later chapters. Only the principle equations for basic SEA are given which are specific to their use for double walls. For further discussion on the use of and theory of SEA works by Lyon [11,12] and Craik [13] provide indepth analysis.

Chapter 3 describes the measurement procedures, experimental facilities and test structures that were used and built during the course of this work. Discussion on the accuracy of the measurements is given along with data showing the 95% confidence intervals of various tests.

Chapter 4 describes the transmission between parallel plates with point connection. A review of the existing theory is given and the types of connection possible are described. Theory is presented for the case where the plasterboard is attached to the frame at discrete points. A parametric survey is carried out to study the effect on the structural transmission path through the frame when the material parameters of the frame are altered. Finally measured results are given from tests on specific structures built to study only this transmission path so that comparison may be made with predicted data.

Chapter 5 gives a detailed theoretical model that allows transmission between the plates, where the coupling to the frame occurs along a line. A review is also carried out of previous authors work in this area. Two principle models are presented where the frame may be modelled as a beam or as a finite plate. Comparisons are shown of the predicted results for these and other models for transmission for a line connection. A parametric survey is carried out for the plate model where the material parameters of the frame are altered.

Chapter 6 gives extensive comparison between measured and predicted data for line connected parallel plates where certain plates were omitted and the frame depth was altered. These tests were carried out on freely suspended plate structures to analyse the line coupling transmission path only.

Chapter 7 examines the transmission into an isolated cavity and also for a double wall cavity. No new theory is presented but existing theories are examined in detail. Contributions from the various SEA transmission paths are compared to identify the dominant mechanism. The effect of the cavity to the overall sound transmission through point connected double walls is studied.

Chapter 8 brings together all the theories presented, from Chapter 2 to Chapter 7, into an SEA framework so that comparisons can be made between predicted and measured results for full scale double walls. Results are presented for single plate walls, ribbed walls, point and line connected walls and finally results from a full scale timber floor. The timber floor was constructed so that flanking transmission could also be examined and the contribution from these paths is discussed and results presented.

Chapter 9 contains a summary of the conclusions and gives suggestions for further work.

Chapter 2

Review of Previous Work on Double Walls and the Application of Statistical Energy Analysis

2.1 Introduction

This chapter describes the construction of double walls and the various sound transmission paths that occur. A review of work done by previous authors on research into sound transmission through double walls is presented. The use of statistical energy analysis (SEA) by past authors as a method of predicting sound transmission through these structures is also discussed. Following these reviews the framework for SEA theory and how it may be applied to double wall structures is described.

2.2 Double wall construction

Fig 2.1 shows a typical section through a double wall partition and the various SEA sound transmission paths. Sound transmission can take place through the structural frame, the cavity and the interaction of the structure with the source and receiving rooms. The structure and sound transmission paths of a double wall partition are similar to that of a basic timber floor.

Generally the material used for the partition plates is 12.5mm thick plasterboard which has a density of approximately 800 kg/m^3 and a longitudinal wavespeed of 1700m/s. These are connected by nails or screws to a structural timber frame. In the case of partitions used in offices the structural frame is a steel or aluminium alloy channel. For the purpose of this study, most of the test structures studied have involved timber structural frames so that the theories presented could also be applied to domestic timbers floors.

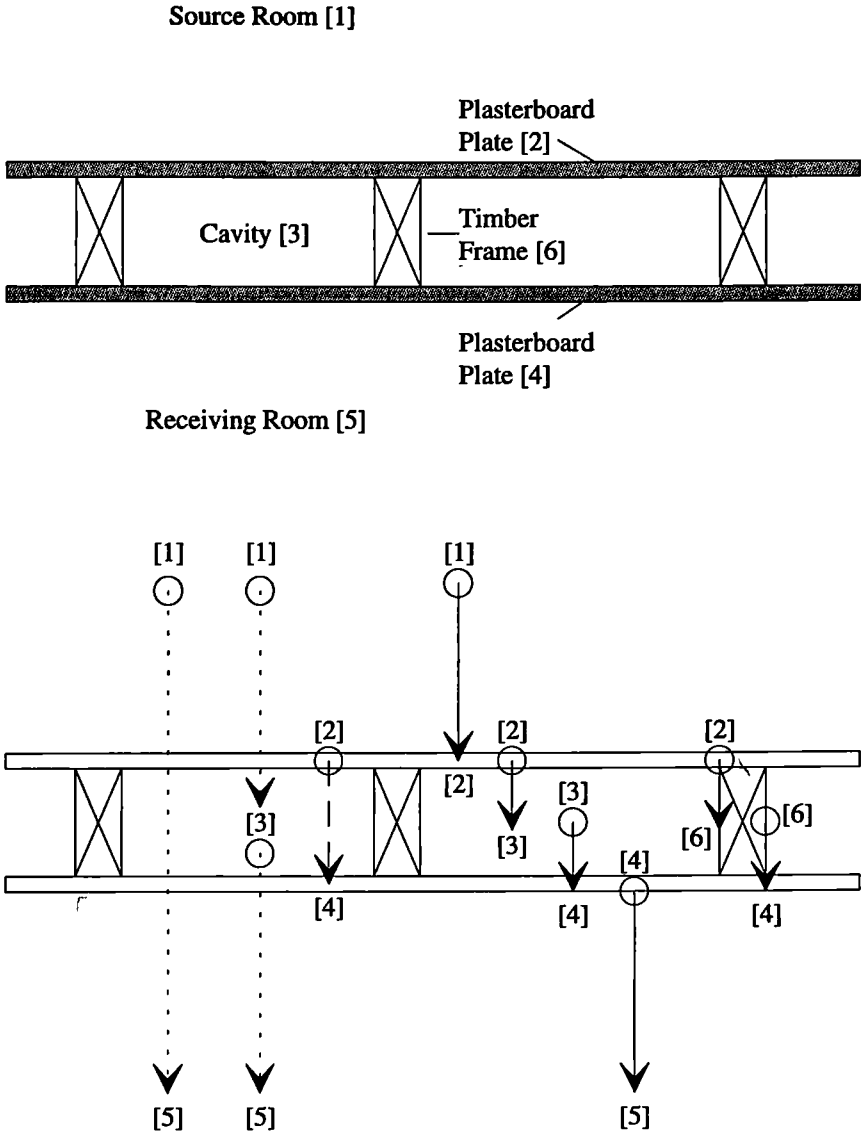

Sound transmission paths for a double wall structure

Non resonant paths [1]-[5] Room to room
[1]-[3] Room to cavity
[3]-[5] Cavity to room
Airtie [2]-[4] Plate to plate

Resonant paths [1]-[2] Room to plate
[2]-[3] Plate to cavity
[3]-[4] Cavity to plate
[4]-[5] Plate to room
[2]-[6] Plate to frame
[6]-[4] Frame to plate

Figure 2.1 Double wall structure of a lightweight partition showing sound transmission paths

The timber structural frame in a partition or a floor has a width of normally 40-55mm. However, the depth of the frame may vary from 25mm, for a non load bearing partition, up to 250mm for a floor joist [2]. The spacing of these frame elements varies from 400mm to 600mm depending on the load requirements and design specification. The standard type of timber used in internal domestic partitions or joists in timber floors is softwood timber [14]. Examples of softwood include, Norway spruce, Douglas fir, Scots pine and Yellow pine. Timber as a material can be defined as a low density, cellular and polymeric composite which does not conveniently fall into any one class of material [15]. Due to its high strength and low cost it is an attractive material for the construction industry.

The direction of grain and growth rings in timber results in an orthotropic material with different material properties depending upon the plane under study. Fig 2.2 shows a cross section through a wedge shaped segment of softwood tree. There are three planes of study when using timber. These are the axial plane, which is the vertical growth direction of the tree, the radial plane, the direction of the growth rings (radiating outwards from the centre of the tree), and the tangential plane, which as the term describes, is the tangential to the direction of the growth rings. Due to 90-95% of the tree cells being aligned in the axial direction, or vertical axis, the remaining cells are aligned in the radial and tangential axis and this also causes anisotropy in the timber [15]. This was not initially thought to be important but subsequent calculations showed that this orthotropicity can have a significant effect.

Fig 2.3 shows a typical cut section as would be used for joists and partition frames. The term used for the structural frame in a partition is 'stud'. Fig 2.4 shows the direction of loading and direction of sound propagation through the structural element. The longitudinal wavespeed in the tangential direction, $C_{L(t)}$ is as much as two to four times less than in the axial direction, $C_{L(a)}$. As a result of this the bending stiffness in the various directions are different and should be accounted for when predicting the structure borne sound transmission through the frame. Further discussion of this is presented in Chapter 5.

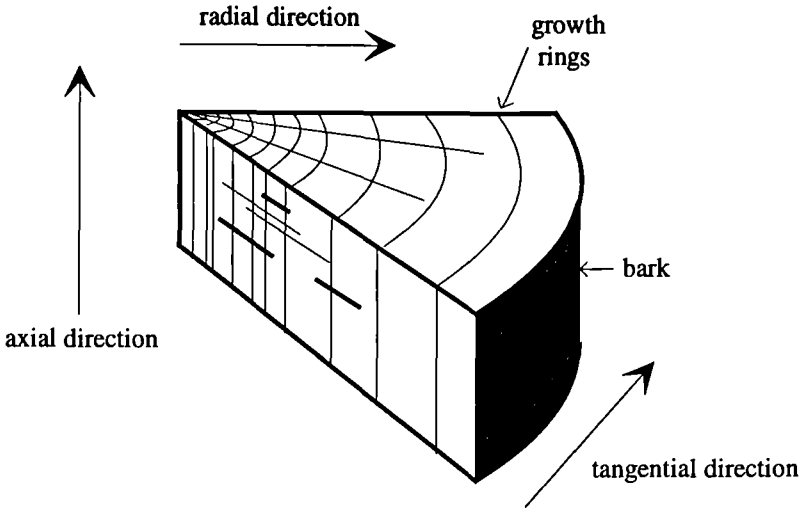

Figure 2.2 Cross section through a wedge shaped segment of softwood tree

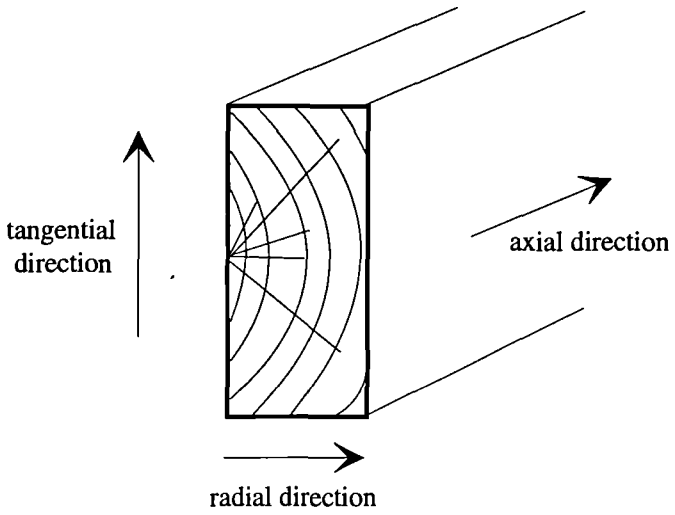

Figure 2.3 Typical cut section of timber for joists and studs

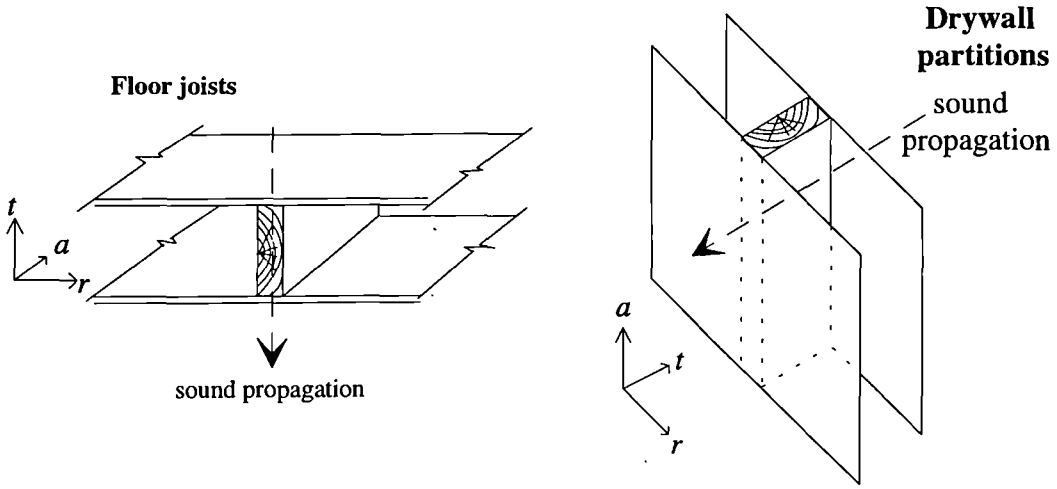

Figure 2.4 Direction of loading and sound propagation for floor joists and drywall partitions.

The spacing of nail or screw point connections also varies due to the difference in mechanical coupling that occurs. Nails have a weaker mechanical coupling than screws and therefore require to be positioned at closer spacings due to design load requirements. Typical spacings for nails in a plasterboard partition are 150mm and for screws 300mm [16,17]. Further discussion on the implications of this spacing and the choice of nail or screw connections is discussed in Chapter 4.

2.3 Review of previous work on double walls

This section outlines some of the principal theoretical work by previous authors for sound transmission through double walls.

Beranek and Work [18] produced a theoretical model for the transmission of waves at normal incidence to a double wall. The stimulus, in part , for Beranek and Work producing this theory was experimental work by Nichols *et al* [19] who studied a series of attenuating structures as part of a World War II program for "quieting noise in aircraft". The double wall studied consisted of two impervious layers, an air space and two acoustical blankets. They were able to obtain a ratio of pressures on any two surfaces by solving the wave equation for the different sections of the wall using the continuity of acoustic impedance at each interface. From this an expression could be derived for the difference between the incident and transmitted sound pressure levels on the wall. Equations for more simple structures could be derived from the general case by setting some of the parameters equal to zero. Beranek and Work's theory had the advantage of being theoretically exact and could be applied to various forms of construction. The disadvantage being that they only provided a solution for normal incidence.

London [20] found that the normal incidence theory was "totally inadequate" in explaining the behaviour of a double wall as normal incidence overestimates the performance of double walls. Real walls are subjected to diffuse sound fields and as a result lower transmission loss is obtained. London obtained a solution for sound transmission for random incidence. London considered the problem as a continuity problem with forward and reverse travelling waves between the two plates and a

forward wave beyond the second plate. This theory predicted that the improvement of a double wall over a single wall could be small and sometimes even negative. This behaviour of the double wall was explained by the effect known as Lower London frequency or mass-spring-mass frequency.

At low frequencies the double wall behaves like a single wall with the same total mass. The air in the cavity appeares to have no sound reduction effect. Instead it behaves as if it had an infinite stiffness causing the two plates of the double wall to move as one. The mass-spring-mass (MSM) frequency, f_0, occurs where the cavity behaving like a spring with a stiffness equal to that of the air, joining the two plates (masses) of the wall, would have its first resonance. The transmission loss rises rapidly above this frequency as the effect of the cavity influences the sound reduction. Further dips in the transmission loss occur at higher frequencies where standing waves may be supported in the cavity.

Using this random incidence theory London compared his predicted data with measured data for double wall structures with varying widths of the cavity. For some of the structures there was good agreement but for structures with narrow cavities and for high frequency results the theory underestimated the walls performance. This may have been due to the fact that he analysed all angles of incidence with equal weight. In addition London introduced a resistance term R which assisted in aligning the theoretical values of the transmission loss with the measured values. This was criticised by Mulholland *et al* [21] and White and Powell [22], because no physical mechanism could be related to R.

Mulholland, Parbrook and Cummings [21] calculated the transmission loss of an infinite double wall using ray theory. The solution assumed that an obliquely incident wave upon entering the cavity would under go repeated reflections between the two plates of the double wall with sound being transmitted on each occasion. The wave was attenuated with each reflection by introducing absorption in the cavity on the surface of the two plates. Whilst their model did not predict any better the transmission loss than Beranek and Work or London they claimed that at least it allowed examination of the effects of absorbing surfaces. When predicted and measured data was compared for

their model with absorption in the cavity they did find good agreement. However they did not measure the absorption factor of the material in the cavity and chose at random the value to give the best fit. The theory was modified later by Cummings and Mulholland [23] by the introduction of absorption at the edges of the cavity to attenuate the cavity waves which created a finite wall behaviour. They integrated the expression over a limited angle of incidence and found good agreement with measured data without the need to randomly select absorption values. But this theory was criticised by Sewell [24], who did not agree on the use of ray theory in the cavity where the frequencies under study had a much larger wavelength than the cavity depth. Mulholland continued his research in this area with studies on experimental work with Utley [25] for trying to identify an optimum spacing for the cavity between the two plates and with Hudson [26] on real masonry cavity walls.

Sewell [24] produced a two dimensional solution for sound transmission through a finite double wall based on wave theory. The wall was modelled as two simply supported plates each set in their own infinite rigid baffle. For mathematical reasons the cavity was assumed to be infinite and left open. The purpose being that once sound passed between the baffles it was assumed it never returned. Sewell did not treat the coincidence region between the plates and air. Solutions were provided for above and below critical frequency, for both resonant and non-resonant transmission. By varying the internal loss coefficient of the plates the transmission loss could vary significantly. When comparing other authors measured results with his theory which shows an impressive agreement Sewell noticeably omitted the value of the internal loss coefficient he had used for his comparison. Good agreement between measured and predicted results was obtained when the internal damping was chosen.

Sharp [27] produced three approximate expressions based on the sound field being incident over a limited angle of incidence for predicting double wall performance. The three expressions were dictated by the frequency boundaries of MSM and first cross cavity resonance. The first expression was for frequencies below the MSM where the double wall behaved as a single wall and the transmission loss increased at 6dB per octave. The second expression was for frequencies between MSM and the first cross cavity resonance where the transmission loss increases at 18dB per octave and was

similar to Schiller's [28] expression. The third expression was used for frequencies above the first cross cavity resonance where transmission through the double wall is more dependant upon the individual double wall plates. The data provided by these approximate theories compared well with experimental data until absorption was placed in the cavity. The third expression had poor agreement at the higher frequencies.

The theories presented so far have dealt with infinite double walls, had unwarranted or unmeasured factors inserted to assist in their agreement or have been solved for normal incidence. They have at some time been building blocks in assisting the understanding of sound transmission through double walls. One factor which perhaps is absent in most of the above mentioned theories is the effect of structural coupling. Real double walls are coupled by structural supports (as in lightweight partitions) or are tied together by returning one of the plates (as in cavity walls).

Sharp [27] produced expressions based on impedance models for the effect that a structural tie or line may have on the airborne performance of a cavity wall. However these do not permit the structural coupling to be examined in detail and are for flexural wave motion normally incident on the joint. Real walls will have inplane waves and these may or may not form a contributory factor. Also as has been mentioned before solving a solution for normal incidence does not reflect the behaviour of real walls. Bhattacharya, Mulholland and Crocker [29] have examined structural coupling through a double wall using a wave model and modelling the frame as a plate. This presupposes that the frame is deep enough to support modal behaviour. Their research lacked an indepth analysis of the parameters of the double wall and how any changes to these properties might affect the overall sound transmission. Vinokur [30] also investigated structural coupling via the foundation strip at the base of a double wall. Approximate expressions were found for its contribution on airborne performance.

These authors and others are discussed in more detail in Chapter 5, *Parallel Plates with a Line Connection*, for their contributions to the prediction of structural sound transmission through double walls. Other authors such as Donato [31], Lin and Garrelick [32], Gu and Wang [33] and Davy [34] have studied double walls and have produced solutions which are specific to a particular transmission path or problem or

are a modification to a previous suggested theory. Further discussion and a more in depth analysis of some of the various theories mentioned above can be found in Fahy [35].

The overall effect of varying any parameter or analysing all paths simultaneously is not possible in the solutions presented so far. The finite nature of the cavity and its interaction with the plates, for resonant transmission, or with the room, non resonant transmission, cannot be grasped from the previous theories. Any changes to the structure under study result in laborious calculations for the smallest of changes. The quick approximate theories such as Sharp's are only useful when no structural coupling is present. In the present and future real world of double walls the designers and architects require a fast and reliable method of predicting the performance of double walls without the need for laborious and for some difficult calculations.

In order to overcome some of the limitations of the classical theories statistical approaches based mainly on SEA were adopted. The next section introduces SEA and shows how it was used to study double walls.

2.4 Statistical energy analysis and double walls

This section provides a brief description of Statistical energy analysis (SEA), the major contributors to SEA for building structures and past work by previous authors on double walls using SEA.

Brief outline of SEA

The general theory and background necessary to use SEA is described by Lyon [12] and for applications of SEA to buildings by Craik [13]. Statistical energy analysis allows the behaviour of complex systems to be modelled [12]. SEA is a technique that was developed during the 1960's to allow complex structures to be modelled with relative ease. Whilst the original ideas were spawned in the 1940's by Smith [36] the momentum to use SEA due to its fast feedback and quick calculations came about during the development of space vehicles and aircraft during the 60's. The general principles of SEA can be applied to any type of structure and provides a means of

representing and describing a structure in a simple manner.

In SEA a structure (system) is broken down into smaller more manageable sections called subsystems. Each has its own identifiable energy which is assumed to be stored in resonant modes. The subsystems are coupled to each other, whether structurally such as a two plates connected along a line, or by a transmission path, such as two rooms divided by a wall for a non resonant transmission path. The net power (energy) flows through the system from subsystems of high modal energy to subsystems of low modal energy. Some of the principle attractions of SEA are its ability to examine specific transmission paths, change subsystem parameters without laborious calculations and see their overall effect on the sound transmission through the entire system. Using this technique can make it possible at an early stage in the design process of any structure to identify the principle or dominant transmission paths. This allows attention to be concentrated on these paths and can create further understanding of the mechanisms involved. Also the effects of less important paths can be analysed individually, such as flanking paths, which though minor may when summed with the other indirect paths still play a contributory role.

Some of the first papers that described power flow through structures employing statistical-mechanics and heat transfer may be found in Heckl [37], Lyon and Maidanik [38] and Lyon and Eichler [39].

It is important to mention that though there are great benefits of using SEA this technique draws heavily on other disciplines from the classical theories for describing the properties of the subsystems and the coupling that occurs between them. Also that SEA is an analysis framework which is statistical, in that it is not an exact understanding of a specific system [13]. It's aim is to understand the behaviour of a wide variety of structures and to provide a mean response not a deterministic solution as might be found using Finite Element Analysis.

SEA and building structures

Towards the end of the 1960's SEA started to be applied to building structures. As mentioned previously SEA uses many of the classical theories to assist in predicting the

performance of building structures. For structures such as walls and floors the energy is assumed to be stored in the resonant bending modes. For rooms the energy is assumed to be stored in the rooms resonant modes and the theory of room acoustics is used to describe the properties of the subsystems.

To describe the radiation from structures, bending wave theory is used. Sewell [24], Maidanik [40], and Leppington *et al* [41-43] have all studied radiation and these theories can be incorporated into SEA to predict the coupling between walls and rooms. Mass law theory can be used to describe the transmission between rooms for non resonant transmission.

Structural coupling between elements in a structure may also need to be predicted. The structural coupling is obtained from the transmission coefficients which can be derived from wave models of structural joints. Theory provided by Cremer *et al*[44], Kihlman [45], Gibbs [46], Craik [9] and Langley [47] allow many of the joints found in building structures to be examined.

Application of SEA to double walls

This section describes the application of SEA to double wall structures studied by previous authors and Fig 2.5 shows some of the SEA models and transmission paths investigated.

White and Powell [22] produced the first work on double walls using SEA. White and Powell were critical of London [20] and other classical theorists for their assumptions. Their paper was in turn criticised by Sewell [24] and Donato [31] for only concentrating on resonant transmission and for an error in an assumption in their paper.

Crocker and Price [48] developed an SEA model for two rooms separated by a wall which investigated resonant and non resonant transmission, shown in Fig 2.5a. This was then extended in a second paper, Price and Crocker [49], for double walls, shown in Fig 2.5b. The cavities were lined at their edges with absorption to reduce the effect of the cavity resonant modes and this is not how real walls are constructed. Although the theories presented in this paper have been criticised by Donato [31] and Brekke [50] for

not taking into account any change to the cavity depth it was important in understanding the basics and the usefulness of SEA in predicting resonant and non resonant transmission through double walls. It also showed that a wide variety of elements of a structure could be modelled as subsystems such as plates, rooms and cavities.

Bhattacharya [51] also investigated double walls in his thesis producing wave models for the structural sound transmission, discussed in this study in chapter 5, and developing theory for transmission into cavities. Bhattacharya also wrote a paper with Price and Crocker [96] on double walls using SEA where they modelled the structural ties as subsystems, shown in Fig 2.5c. It appears from their paper that the ties under discussion are narrow tie beams and it may not be possible to model these ties as subsystems due to the lack of resonant modes, as found by Wilson [8].

They also studied double walls connected by channel section panels (plates) but do not make clear in SEA terms if these were modelled as subsystems. In the final figure, figure 13, of their paper the authors show good agreement between the predicted transmission loss between the double wall parallel plates coupled by channel sections (plates) and the difference in the measured transmission loss for a wall with and without channel sections. They account for the difference in the two walls as entirely due to the channel coupling. The difference in behaviour of a double wall with and without connecting plates can be due to a number of factors, not just the connecting channel sections. When channel sections are present, coupling the parallel plates, the cavity is split into a number of individual cavity subsystems and its modal properties are changed. The coupling between the cavity and the adjacent plates is also affected due to the smaller panel area bounded by the channels. From work presented later in this study the panels would also be split into SEA subsystems, their size being dictated by the connection spacing of the channels. This was not mentioned in their paper. It may have been more prudent to have shown the overall predicted and measured transmission loss for the line connected double wall, rather than subtracting one walls results from another. In addition they used two values for the plate damping of 0.005 for frequencies less than 800Hz and 0.02 for frequencies above 800Hz. This when calculated into dB is a 6dB change which greatly assists the agreement but is never justified for its use.

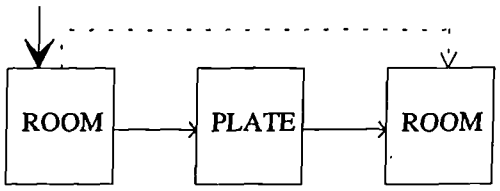

(a) 3 subsystem model of two rooms separated by a wall. (Crocker and Price)

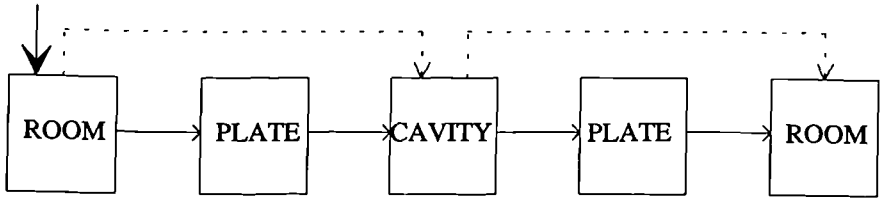

(b) 5 subsystem model of two rooms separated by a double wall with no structural frame (Price and Crocker)

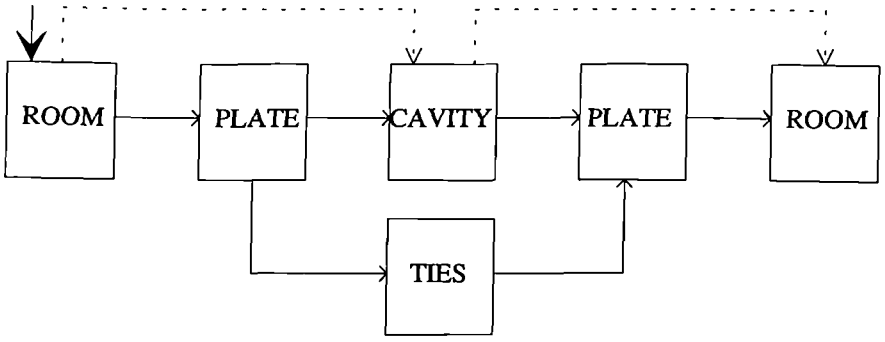

(c) 6 subsystem model of two rooms separated by a double wall with point connecting ties. (Crocker, Bhattacharya and Price)

Figure 2.5 SEA models and sound transmission paths for double walls studied by previous authors. (____) resonant transmission paths (- - -) non resonant transmission paths. (➔) source

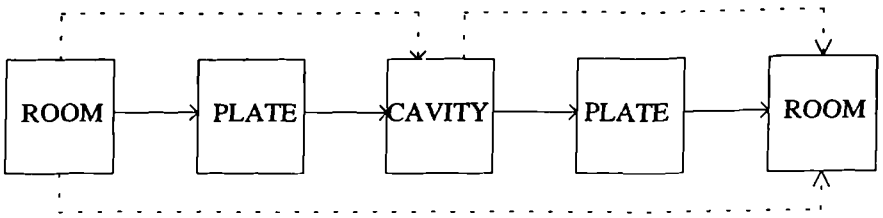

(d) 5 subsystem model of two rooms separated by a double wall with an additional non-resonant path from room to room. (Ohta *et al*)

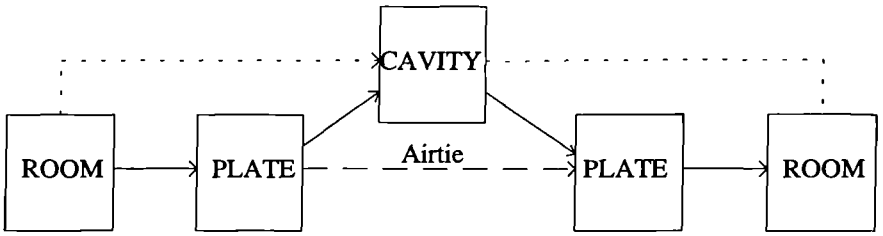

(e) 5 subsystem model of two rooms separated by a cavity wall with an 'airtie' coupling path. (Craik and Wilson)

(f) Multi subsystem model of two rooms separated by a diaphramg wall with a line connecting cross rib. (Gibbs and Sullivan)

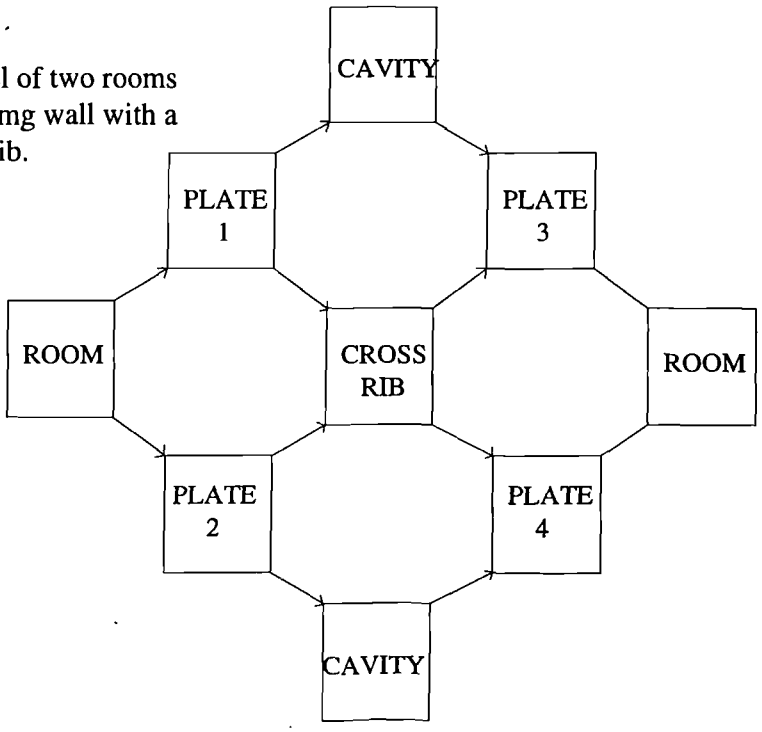

Figure 2.5(cont.) SEA models and sound transmission paths for double walls studied by previous authors. (____) resonant transmission paths (- - -) non resonant transmission paths. (➔) source

Brekke [50] also investigated double walls using SEA and gave an empirical term for the stiffness of the air in the cavity which he believed would account for the omission of the cavity depth in Price and Crocker's theory. But this was only useful for predicting airborne performance and not for when structural coupling was present. Brekke also used SEA for triple walls consisting of three plates and two cavities.

Elmallawany [52] carried out a comparison of SEA and classical theories for sound transmission through double walls. Generally it was found that the SEA model coped adequately well when compared with the measured data. Previous authors had stated concerns over the first cross cavity resonance and that the depth of the cavity was not taken into account in Price and Crocker's SEA model [49]. However, Elmallawany showed that even without structural coupling in the double wall, causing the cavity to be a more dominant path, the reduction of sound transmission loss due the cavity resonance of the air was not "remarkable" when compared with the computed SEA results. Hence the fears of not including the depth in the SEA model and predicting this resonance were unfounded.

Craik [9] carried out extensive experiments on real walls to compare with SEA models. An expression was presented that allowed the coupling across the wall ties to be included in an SEA model. The ties were not modelled as subsystems.

Ohta *et al* [53] also studied sound transmission through double walls using SEA. From past work by previous authors it was found that there was a discrepancy at low frequencies between the measured and predicted results. They assumed that this was due to the omission of the non-resonant path from the source room through the double wall to the receiving room, shown in Fig 2.5d. They included this path at low and mid frequencies and found good comparison. Interestingly they did not show a comparison between their revised SEA model results and the predicted results without this path. From work carried out in this study it may be possible to include this path at low frequencies below the MSM but thereafter this path is extremely weak and would not alleviate the problems associated with the mid frequencies.

Craik and Wilson [10] produced an expression to account for the coupling across the

cavity by the air between the two plates of a cavity wall which would include a term for the cavity depth, shown in Fig 2.5e. This "airtie" expression was calculated by replacing the wall tie stiffness term with the air stiffness term.

Further discussion of Wilson's work may also be found in Craik [13]. Wilson [8] also studied structural sound transmission through double walls using wave models which could then be inserted into SEA models. The walls under study were cavity walls as found in the external walls of domestic construction. The transmission coefficient for structural line connections between the cavity walls were calculated from the flexural wave motion of the cavity wall plates. His work was used as a foundation for this study to apply SEA models to lightweight parallel plates.

Sullivan [54] studied sound transmission through diaphragm walls using SEA for the purpose of analysing the various transmission paths and material characteristics. The cross-ribs of the diaphragm walls were at a depth which could support modal behaviour. The SEA model is shown in Fig 2.5f. A flexural wave model and a full wave model for the structural sound transmission path were compared. It was found that the energy transmission was dominated by the cross-ribs and that the cavity path could be neglected up to 1250Hz for the size of wall studied. Good agreement was found between the measured and predicted data. Further discussion may be found on this research by Sullivan and Gibbs [55] and Craik [13].

The above mentioned SEA theories have modelled either lightweight double walls or masonry cavity walls/diaphragm walls. The theories for lightweight walls have either ignored the structural path or avoided dividing the system down into further subsystems or input terms to assist the agreement. The theories by Wilson and Sullivan have used wave models to assist in predicting the structural sound transmission path for a line connection but these were for heavy masonry constructions.

These theories have shown that SEA is the most promising approach to study double walls. Due to the number of components and variables within a double wall SEA can take account of these factors and any changes made to them. SEA is therefore adopted in this work to study sound transmission through double walls.

2.5 Basic theory of statistical energy analysis

Before developing the SEA model the underlying principles are described so that the process of development can be put in context. This section describes the basic theory of statistical energy analysis (SEA) and how this is used in SEA system models with regards to predicting sound transmission through lightweight double walls.

Lyon *et al* [12] describes SEA as a procedure for calculating the power flow and storage of energy in a complex system. As mentioned in section 2.3 the system may be broken down into subsystems. Power flows through a system from a subsystem of high modal energy to a subsystem of low modal energy. The power into a subsystem, W_{in}, must equal the power out of a subsystem. Fig 2.6 shows a typical representation of a subsystem. The power flowing between subsystems or energy lost due to coupling between elements must be calculated. This is termed the coupling loss factor (CLF). This is defined as the fraction of energy transmitted from subsystem i to subsystem j per radian cycle, η_{ij}. The power flowing from subsystem i to subsystem j may be given by [11],

$$W_{ij}=E_i\omega\eta_{ij} \tag{2.1}$$

where E_i is the energy in subsystem i. In addition to the CLF there is also a dissipation of power from each subsystem. This energy loss may be dissipated as heat within the subsystem. This dissipated energy is termed the internal loss factor (ILF) and is defined as the fraction of energy which is dissipated as heat within subsystem i per radian cycle, η_{id}. The power dissipated in subsystem i of Fig 2.6 may be given as [11],

$$W_{id}=E_i\omega\eta_{id} \tag{2.2}$$

The CLF's and the ILF of a particular subsystem i may be summed to give a subsystems total loss factor TLF, η_i. The total power loss from subsystem i may be given as,

$$W_i=E_i\omega\eta_i \tag{2.3}$$

where η_i may be given by,

$$\eta_i = \sum_{i=1, i=j}^{n} \eta_{ij} + \eta_{id} \tag{2.4}$$

and is defined as the fraction of energy which is lost from the subsystem in one radian cycle and is either dissipated within the subsystem or transmitted to other subsystems

Three subsystem SEA model

Fig 2.7 shows a three subsystem SEA model for two rooms separated by a wall as described by Crocker and Price [48]. There are resonant transmission paths from *source room to wall*, W_{12}, and *wall to receiving room*, W_{23} and a non resonant transmission path *source room to receiving room*, W_{13}. In addition to coupling between the source room and the wall there is also coupling between the wall back to the source room, W_{21}. Although the effect of this coupling may perhaps be small it is included in the model for completeness. The same applies for the receiving room to the wall, W_{32} and for the receiving room to the source room, W_{31}. These minor transmission paths were not included in the Crocker and Price model. The power balance equation for subsystems 1, 2 and 3 may be given as,

$$W_{in} + W_{31} + W_{21} = W_{12} + W_{13} + W_{1d} \tag{2.5}$$

$$W_{12} + W_{32} = W_{21} + W_{23} + W_{2d} \tag{2.6}$$

$$W_{13} + W_{23} = W_{31} + W_{32} + W_{3d} \tag{2.7}$$

The energy ratio for this model due to direct resonant transmission path can be given by [13],

$$\frac{E_1}{E_3} = \frac{\eta_2 \eta_3 V_3}{\eta_{12} \eta_{23} V_1} \tag{2.8}$$

giving a level difference, D, as [13],

$$D = 10 \log \frac{\eta_2 \eta_3 V_3}{\eta_{12} \eta_{23} V_3} \tag{2.9}$$

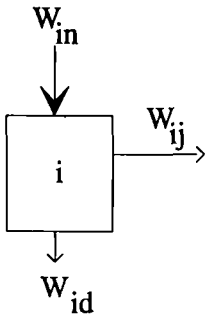

Figure 2.6 Typical SEA subsystem

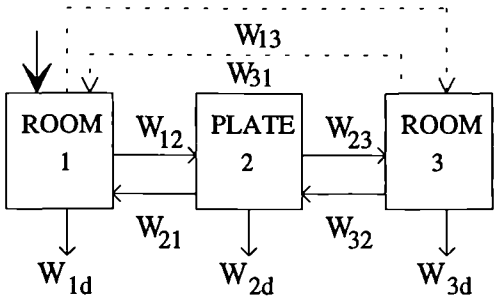

Figure 2.7 Three subsystem model

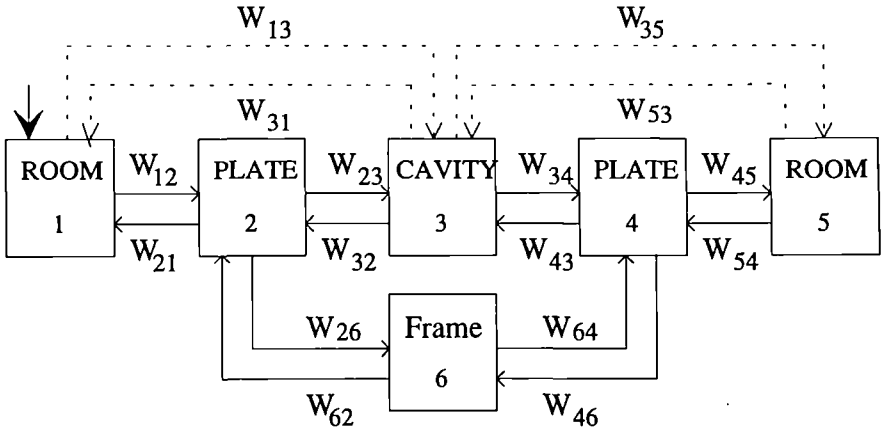

Figure 2.8 Six subsystem model (W_{nd} not shown for clarity)

SEA models with n subsystems

Real double wall structures contain far more than six subsystems and it is simpler to write the power balance equations in a matrix form. For general systems with n subsystems the power balance matrix may be written as,

$$\begin{bmatrix} \eta_1 & \eta_{21} & \eta_{31} & \cdots & \eta_{n1} \\ \eta_{12} & \eta_2 & \eta_{32} & \cdots & \eta_{n2} \\ \eta_{13} & \eta_{23} & \eta_3 & \cdots & \eta_{n3} \\ \cdots & \cdots & \cdots & \cdots & \cdots \\ \eta_{1n} & \eta_{2n} & \eta_{3n} & \cdots & \eta_n \end{bmatrix} \begin{bmatrix} E_1 \\ E_2 \\ E_3 \\ \cdots \\ E_n \end{bmatrix} = \begin{bmatrix} -W_1/\omega \\ -W_2/\omega \\ -W_3/\omega \\ \cdots \\ -W_n/\omega \end{bmatrix} \tag{2.10}$$

This may be solved numerically (e.g. Gaussian elimination) to obtain the energy in each subsystem for given loss factors and power inputs.

The equation for the level difference for any path can also be written from any number of subsystems so that eqn (2.9) becomes,

$$D_{1-2\ldots n} = 10 \log \frac{\eta_2 \eta_3 \eta_4 \cdots \eta_n V_n}{\eta_{12} \eta_{23} \eta_{34} \cdots \eta_{n-1n} V_1} \tag{2.11}$$

For all SEA models the various elements of the structure such as plates, rooms, cavities and frame all have their own expressions for modal density and energy. The following section outlines the basic theory for these factors.

Subsystem energy and modal density

The energy in a room, E_r, of volume V, is related to the mean square sound pressure, p^2, through [11],

$$E_r = \frac{p^2 V}{\rho c^2} \tag{2.12}$$

The energy in a structure, E_s, is stored in both kinetic and potential energy. The total energy can be obtained from twice the kinetic energy, as the potential and kinetic energy are equal. This is related to the mean square velocity, v^2, on a structure of mass, m, by,

$$E_s = mv^2 \tag{2.13}$$

The modal density of a room, n_r (modes/Hz), of volume V is given by [59],

$$n_r(f) = \frac{4\pi f^2 V}{c^3} + \frac{\pi f S}{2c^2} + \frac{L}{8c} \tag{2.14}$$

where L is the total length of all the edges in the room and S is the total surface area of the room.

Due to the cavity depth being small in comparison with the other two dimensions, modal behaviour occurs in only two directions. Eqn(5.14) for rooms is for three dimensions and cannot be used for two dimensional cavities. Price and Crocker [49] suggested an expression for the modal density of a cavity, n_c, below the first cross cavity resonance f_x,

$$n_c = \frac{S_c f}{c^2} \tag{2.15}$$

where S_c represents the cross sectional area of the cavity and the first cross cavity resonance, f_x, may be determined by,

$$f_x = \frac{c}{2l} \tag{2.16}$$

where l is the depth of the cavity. Above the first cross cavity resonance eqn(2.14) may be used for the modal density of a cavity. The modal density of bending modes on a plate is given by Lyon [11] as,

$$n_p(f) = \frac{\sqrt{3}S}{C_L h} \tag{2.17}$$

where S, h and C_L are the surface area, thickness and longitudinal wavespeed of the plate respectively. The modal density of a beam may be given by,

$$n_b(f) = \frac{3^{1/4}}{\pi} \frac{l}{\sqrt{C_L h f}} \tag{2.18}$$

where l is the length of the beam.

Coupling loss factors

The coupling loss factors (CLF's) for double walls can be divided into two groups. The first group involves the interaction between the structure and the air, such as plate to room, plate to cavity, room to room and room to cavity. The second group involves the coupling between the different structural elements such as plate to frame and plate to plate for point and line connection.

The CLF for a plate to a room involves calculating the radiation efficiency, σ, which is defined as the power radiated by a structure compared to that of a piston with the same area and the same velocity [13]. Calculating the radiation efficiency assists in determining the power radiated by the plates of a double wall.

The classical method of determining the power radiated by a wall (plate) is,

$$W_{rad} = v^2 \rho_0 c_0 S \sigma \tag{2.19}$$

The power radiated from a wall, 1, to a room, 2, in SEA notation is,

$$W_{12} = E_1 \omega \eta_{12} = \rho_s S v^2 \omega \eta_{12} \tag{2.20}$$

Equating equations 2.19 and 2.20 gives the CLF from a plate to a room as,

$$\eta_{12} = \frac{\rho_0 c_0 \sigma}{2\pi f \rho_s} \tag{2.21}$$

If part of the wall is radiating into a different subsystem, as may be found in double wall structures, then the CLF should be reduced in proportion to the ratio of the area radiating sound to the total area.

The radiation efficiency, σ, from a finite plate may be calculated by several methods. Wallace [56], Maidanik [40] and Leppington *et al* [41-43] amongst others have proposed expressions for calculating σ. For the purpose of this study σ has been calculated using Leppington *et al* [41]. The expression given by Wallace [56] is extremely complex and excessive as it calculates σ for each mode. Leppington *et al* [41] produced similar expressions to Maidanik except that a correction was made for frequencies below the critical frequency, f_c, setting Maidanik's term 'g_1 or g_2' to zero

and correcting the values at f_c. The critical frequency is the frequency at which the wavespeed in the structure and wavespeed in the air are equal. This is given by,

$$f_c = \frac{c^2\sqrt{3}}{\pi h C_L} \tag{2.22}$$

Leppington *et al* [41] provide three expressions for the radiation efficiency, σ, for frequencies below, equal to and above critical frequency, ($f < f_c, f = f_c, f > f_c$). The following expressions are given for a simply supported panel (freely hinged at its edges), which is placed in an infinite baffle and radiating into free space [41],

$$\sigma = \frac{Uc_o}{4\pi^2 f^{1/2} f_c^{1/2} S(\mu^2-1)^{1/2}}\left[\ln\left[\frac{\mu+1}{\mu-1}\right]+\frac{2\mu}{\mu^2-1}\right] \quad f<f_c \tag{2.23}$$

$$\sigma = \left[\frac{2\pi f}{c_0}\right]^{1/2} l_x^{1/2}\left[0.5-0.15\frac{l_x}{l_y}\right] \quad f=f_c \tag{2.24}$$

$$\sigma = \left[1-\frac{f_c}{f}\right]^{-1/2} \quad f>f_c \tag{2.25}$$

where $\mu=(f_c/f)^{1/2}$, l_x and l_y are the plate dimensions ($l_x \leq l_y$), and U is the perimeter length of the radiating area.

However, most real edges are not simply supported but are clamped and this increases the radiation below f_c [40],[42]. From experimental work by Heron [57] and later theoretical work by Leppington *et al* [42] for most real edges the radiation efficiency will be increased by 3dB or a multiplier of 2, where there is some clamping. Also most walls and floors are not in the same plane as the baffle but are surrounded by other walls and floors perpendicular to the radiating surface. This further increases the radiation efficiency below f_c by a multiplier of 2, or 3dB [43]

The increased radiation for real edges and perpendicular baffles or other structures is equivalent to a multiplier of 4 and a sharp transition at the critical frequency occurs. To avoid this and enable a smooth transition for σ Leppington *et al*[58] suggest a

correction factor to be applied below the critical frequency, which is given as [13],

$$m-(m-1)\left[\frac{f}{f_c}\right]^4 \tag{2.26}$$

where m is the multiplier. Fig 2.9 provides a summary of the radiation from a plate with different boundary conditions and the multiplier used below the critical frequency.

Equation (2.21) and the above expressions for radiation efficiency may also be used for calculating the CLF from a plate to a cavity. Price and Crocker [49] amongst others also suggested that the radiation efficiency should be doubled due to the effect of a perpendicular baffle.

The CLF from a room, 1, to a plate, 2, may be calculated using the consistency relationship [11] which is valid for all CLF's,

$$n_1\eta_{12} = n_2\eta_{21} \tag{2.27}$$

where n is the subsystem modal density. Taking the first term for modal density of a room from eqn(2.14) and the modal density of a plate, eqn(2.17), the CLF from a room to a plate may be given as,

$$\eta_{21}=\frac{\rho_0 c_0^2 S f_{c2}\sigma}{8\pi V_1 \rho_{s2} f^3} \tag{2.28}$$

The CLF for transmission from a cavity to a plate may be found using the consistency relationship but using the modal density for a cavity, where the frequencies of interest are below f_x, and the modal density for a room, for frequencies above f_x. The CLF for transmission from a cavity, 2, to a plate, 1, for frequencies below f_x is given as,

$$\eta_{21} = \frac{\rho_0 c_o f_{c1}\sigma_1}{4\pi f^2 \rho_{s1}} \tag{2.29}$$

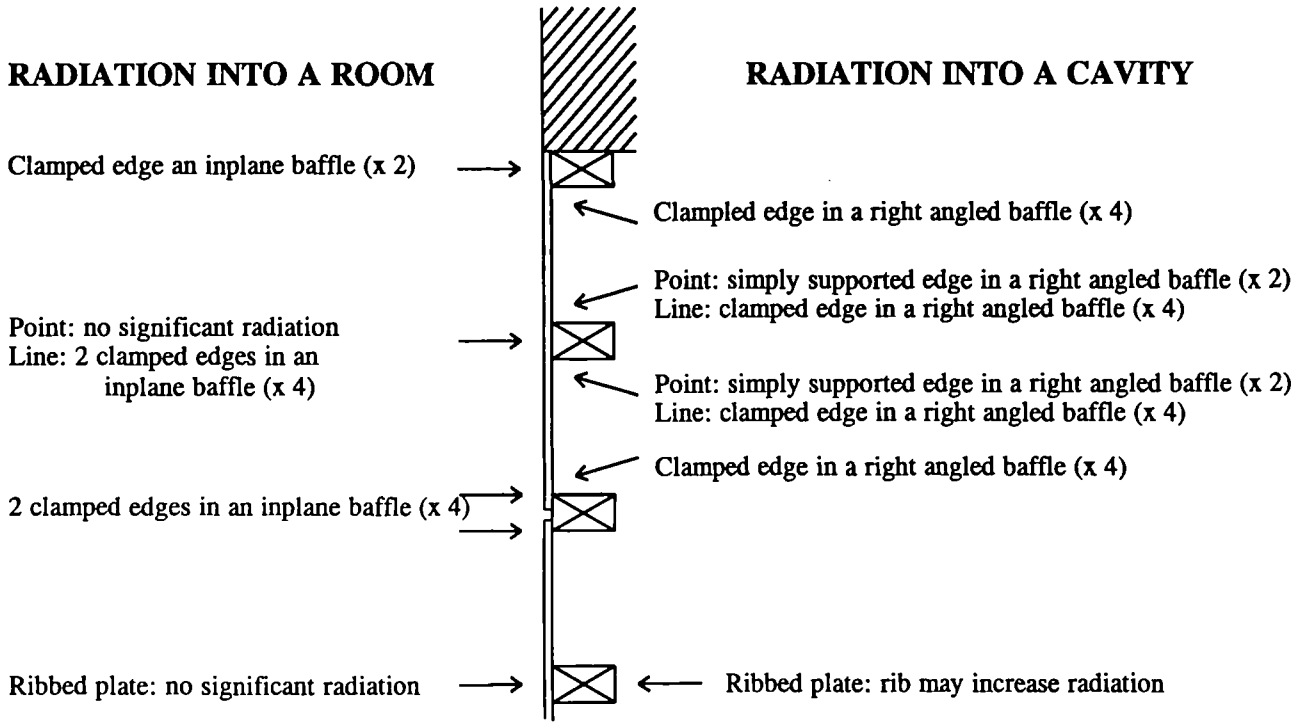

Figure 2.9 Radiation from a plate with different boundary conditions and the multiplier used below the critical frequency.

The room to room CLF for non resonant transmission or mass law coupling is related to the transmission coefficient, τ_{rr}. At all angles of incidence below f_c the free bending waves on the wall play no part in this mechanism of transmission for an airborne source being incident on the wall. The structural subsystem or wall, is effectively bypassed and the two rooms are coupled directly. Transmission associated with this motion is called forced motion. The power transmitted is given by,

$$W_{trans} = W_{inc}\tau_{rr} = \frac{Ec_0S}{4V}\tau_{rr} \tag{2.30}$$

where S is the area of the wall through which the sound is passing and V is the volume of the source room. Equating eqn(2.30) with eqn(2.1) the CLF between any rooms 1 and 2 may be given by,

$$\eta_{12} = \frac{c_0 S\tau_{12}}{8\pi f V_1} \tag{2.31}$$

This equation may also be used for calculating the CLF from a room to a cavity. However, for calculating the CLF from a cavity to a room requires the modal density of cavity for frequencies below f_x. Taking the first term of eqn(2.14), the modal density of a cavity, eqn(2.15), and using the consistency relationship, eqn(2.27), gives the CLF from a cavity, 1, to a room, 2, as [13],

$$\eta_{12} = \frac{\tau_{12}}{4\pi} \tag{2.32}$$

The non resonant transmission coefficient used in this study is that given by Leppington *et al* [43],

$$\tau = \left[\frac{\rho_0 c_0}{\pi f \rho_s (1-f^2/f_c^2)}\right]^2 \ln\left[\frac{2\pi f\sqrt{S}}{c_0}\right] + 0.160 + U(l_x,l_y) + \frac{1}{4\mu^6}\left[(2\mu^2-1)(\mu^2+1)^2\ln(\mu^2-1) + (2\mu^2+1)(\mu^2-1)^2\ln(\mu^2+1) - 4\mu^2 - 8\mu^6\ln(\mu)\right] \tag{2.33}$$

where $\mu=(f_c/f)^{1/2}$ and $U(l_x,l_y)$ is a function of shape and can be ignored for normal shaped structures (where $0.1 < l_x/l_y < 10$).

There are principally two types of CLF for structure borne sound transmission used in this study. These are CLF's for point or line connection. The CLF for point connection is calculated using mobility functions. The CLF between any two subsystems connected by an infinitely stiff connection, can be given by [13],

$$\eta_{12} = \frac{N\,Re(Y_2)}{\omega m_1 |Y_1 + Y_2|^2} \tag{2.34}$$

where N is the number of point connections, m_1 is the mass of the source subsystem and Y_1 and Y_2 are the mobilities of the source and receiving subsystems respectively. This can be used to calculate the CLF from plate to plate, plate to frame or frame to plate in double wall structures where the frame is modelled as a beam. The mobility of a plate excited by a point source at its centre, far from the edge is given by [44],

$$Y_{plate} = \frac{1}{2.3\rho_s C_L h} \tag{2.35}$$

where ρ_s, C_L and h are the plate surface density, longitudinal wavespeed and thickness. The point mobility of a beam excited far from an edge is given as [44],

$$Y_{beam} = \frac{1}{2.67\rho S\sqrt{C_L h f}(1+i)} \tag{2.36}$$

where ρ, S, h and C_L are density, cross sectional area, thickness and longitudinal wavespeed of the beam respectively. Further discussion of point connections for parallel plate structures is given in Chapter 4.

The CLF for line connected plate structures is related to the transmission coefficient, τ, where this is defined as,

$$\tau = \frac{Power\ transmitted}{Power\ incident} \tag{2.37}$$

The power transmitted from plate 1 to plate 2 across a structural joint with length L_{12} is [11],

$$W_{12} = \frac{E_1 c_{g1} L_{12} \tau_{12}}{\pi S_1} = E_1 \omega \eta_{12} \tag{2.38}$$

giving the general expression for the CLF as,

$$\eta_{12} = \frac{c_g L_{12} \tau_{12}}{2\pi^2 f S_1} \tag{2.39}$$

where S_1 is the surface area of the source plate, L_{12} is the joint length and c_g is the group velocity. The group velocity is the speed at which energy is transported across a plate and is the same as the phase velocity for longitudinal and transverse waves and is twice the phase velocity, $2c_B$, for bending waves on thin plates, where c_B is given by,

$$c_B = \sqrt{1.8 h c_L f} \tag{2.40}$$

Chapter 5 in this study discusses in more detail the structural coupling between parallel plates for a line connection.

Total loss factors

The total loss factor (TLF) may be calculated from the sum of the coupling loss factors plus the internal loss factor (ILF). For all subsystems the TLF is related to the reverberation time T_{60} by,

$$\eta = \frac{2.2}{f T_{60}} \tag{2.41}$$

For rooms it is difficult to separate the total loss factor from the internal loss factor and measured data is usually used. In this study all the room TLF's were measured. However, the T_{60} can be predicted from [59],

$$T_{60} = \frac{0.161 V}{\Sigma S \alpha} \tag{2.42}$$

where S is the surface area of a given material present in the room, α is the absorption coefficient of that material and V is the volume of the room. The TLF of a cavity can be given by [49],

$$\eta_c = \frac{0.375 A c \alpha}{V_c \omega} \tag{2.43}$$

where A is the surface area of the edges of the cavity. For structures where possible the TLF has been calculated by summing the CLF's plus the ILF. Where these could not be predicted as in the case of some of the chamber ceilings an approximation may be used [13],

$$\eta = \frac{1}{\sqrt{f}} + 0.015 \tag{2.44}$$

Relationship between energy and sound pressure levels and acceleration levels

The measure of how much sound is present in a subsystem is the energy in that subsystem. In classical acoustics the noise level in a room would be described by the sound pressure (level), L_p, and the vibration of a wall by the velocity (level), L_v or acceleration level L_a. Using energy can either be used in absolute units in Joules or can be measured in dB. It is usual to use 10^{-12} J as the reference so that the energy level, L_e, is [13],

$$L_e = 10 \log \left(\frac{E}{10^{-12}} \right) \tag{2.45}$$

The energy level in a room is then related to the sound pressure level, L_p, by [13],

$$L_e = L_p + 10 \log (V) - 25.4 \tag{2.46}$$

where V is the volume of the room (m^3). The energy level in a wall may be realted to the wall mass, m, and the velocity level or acceleration level given by [13],

$$L_v = L_e - 10 \log m \tag{2.47}$$

or

$$L_a = L_e - 10 \log m + 20 \log \omega \tag{2.48}$$

where L_v and L_a are the velocity and acceleration level of the wall in dB re 10^{-6} m/s and $10^{-6} m/s^2$ respectively.

2.6 Conclusions

This chapter presented past work by previous authors on double walls. It was found that existing classical theories could not cope with any changes to parameters of the structure or analyse the contributions from specific paths. A review of SEA for double walls was also discussed and its development by various authors in tackling the various sound transmission paths. Some of these authors included the non-resonant path through the entire structure over the complete frequency range. However, this path is extremely weak at higher frequencies and is not important. Price and Crocker's work did not deal with real walls and the paper written with Bhattacharya had a 6dB adjustment which could not be justified other than to produce good agreement between the predicted and measured data. The theory necessary to calculate the coupling loss factors for a general model was discussed inluding the coupling loss factors specific to double walls. The final section showed how the total loss factors of structures, rooms and cavities are determined.

Further work is required to predict sound transmission through double walls using SEA models where the application is to real walls incorporating structural frames and cavities. In addition these models must be able to predict variations to the components within the structure and analyse the contributions from the various transmission paths.

Chapter 3

Experimental Facilities and Measurement Techniques

3.1 Introduction

This chapters describes the measurement facilities, test structures and equipment used in carrying out the measurements and determining the material properties. It also describes the calibration of microphones and accelerometers and the accuracy of the measured results. During the period of this research over forty different test structures have been built and tested. This chapter also describes some of the principle test structures and Table 3.1 lists all the test structures built.

3.2 Measurement facilities and test structures

A large majority of the measurements performed in this work were made on lightweight double leaf plasterboard partitions built in a transmission suite. The horizontal transmission suite used for these partitions is shown in Fig 3.1. An example of one of the test walls built is shown in Fig 3.2. The horizontal transmission suite consisted of two rooms (chambers) that were structurally isolated from each other. Both rooms had a common opening measuring 4.0x3.0m where the test walls were constructed. The smaller of the two rooms measuring 6.8x4.0x3.0m was used as the source room for airborne level difference measurements. When testing partition walls in the early period of this work a concrete block wall was built into the source chamber reducing the length of the room to 6m. The second room measuring 7.0x6.0x5.0m was used as the receiving room for the above experiments.

The floors and ceilings of the chambers were made from 0.2m thick in-situ concrete which had a measured longitudinal wavespeed of 3250m/s and a density of 2400Kg/m^3. The walls of the chambers were built from 0.22m thick brickwork with a measured

Vertical transmission suite *(common opening 3.2x3.6m)*
150mm built-in timber floor structure (without absorption)

Horizontal transmission suite *(common opening 3.0x4.0m)*
150mm chipboard / plasterboard studwall (without absorption)
100mm line connected plasterboard studwall (with absorption)
100mm point connected plasterboard studwall (with absorption)
100mm point connected plasterboard studwall (without absorption)
50mm point connected plasterboard studwall (with absorption)
50mm point connected plasterboard studwall (without absorption)
50x50mm frame ribbed plasterboard wall
18mm chipboard wall

Horizontal transmission suite *(common opening 1.7x1.7m)*
single leaf12.5mm plasterboard wall (perimeter frame only)
single leaf 12.5mm plasterboard wall (perimeter frame + 1 rib)
single leaf 12.5mm plasterboard wall (perimeter frame + 3 ribs)
double leaf 12.5mm plasterboard wall (perimeter frame only)
double leaf 12.5mm plasterboard wall (perimeter frame + 1 rib)
double leaf 12.5mm plasterboard wall (perimeter frame + 3 ribs)

Test cavity structure *(1.9x0.96m with varying depth)*
150mm floor cavity, 100mm floor cavity, 50mm floor cavity,
25mm floor cavity, 50mm floor cavity (with absorption),
25mm floor cavity (with absorption)

Freely suspended plasterboard plate double wall structures *(with timber frame)*
point connected two plate structure (frame 45x75mm)

line connected 'H' plate structure (1,2,3,4) 200,100 and 50mm depth frame
line connected plate structure (1,3,4) 200,100 and 50mm depth frame
line connected plate structure (1,2,4) 200,100 and 50mm depth frame
line connected plate structure (1,2,3) 200, 100 and 50mm depth frame
line connected plate structure (1,3) 200, 100 and 50mm depth frame
line connected plate structure (1,4) 200,100 and 50mm depth frame

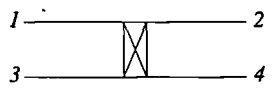

Table 3.1 Structures tested for sound transmission through lightweight parallel plates.

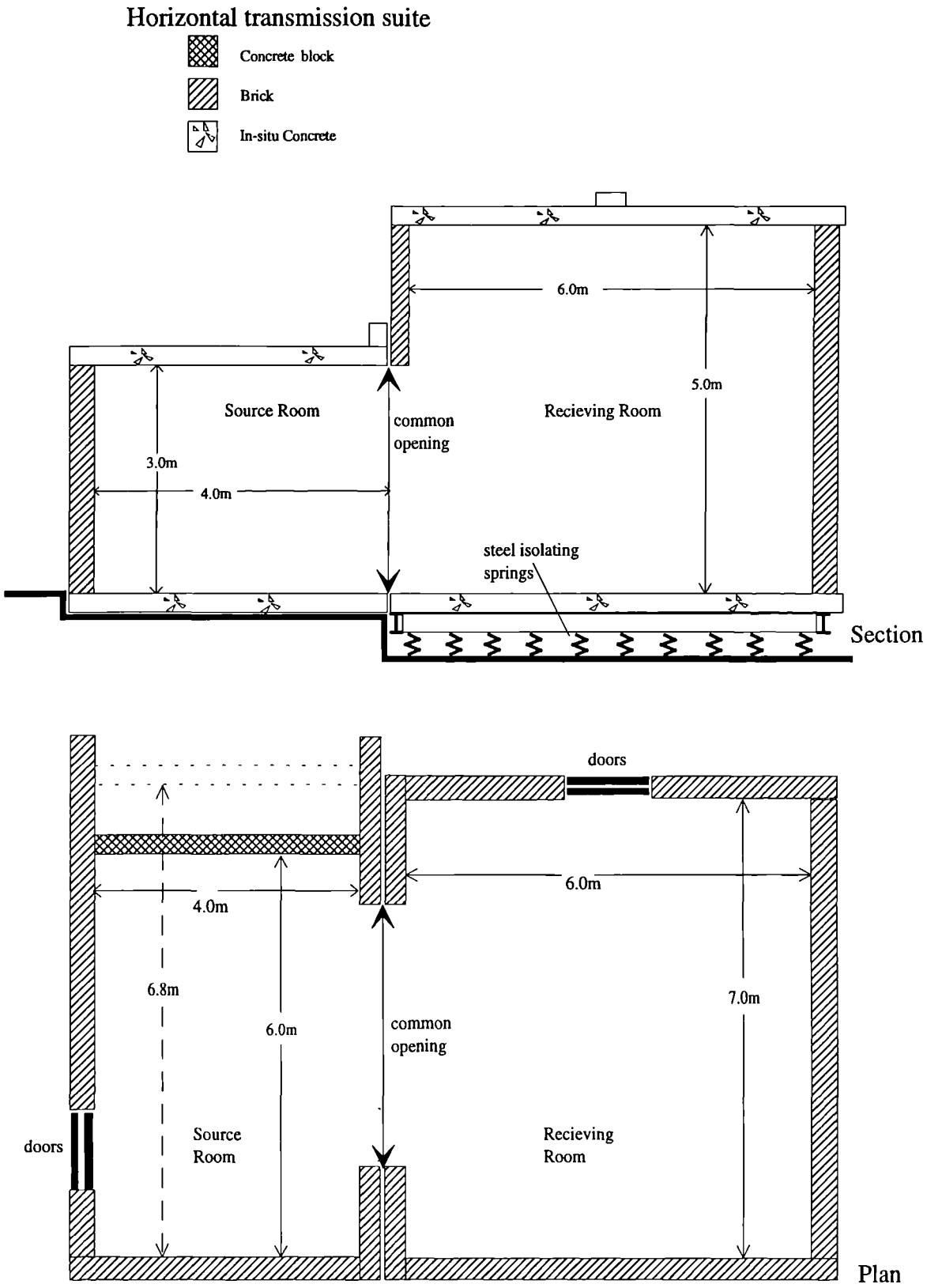

Figure 3.1 Section and plan of horizontal transmission suite.

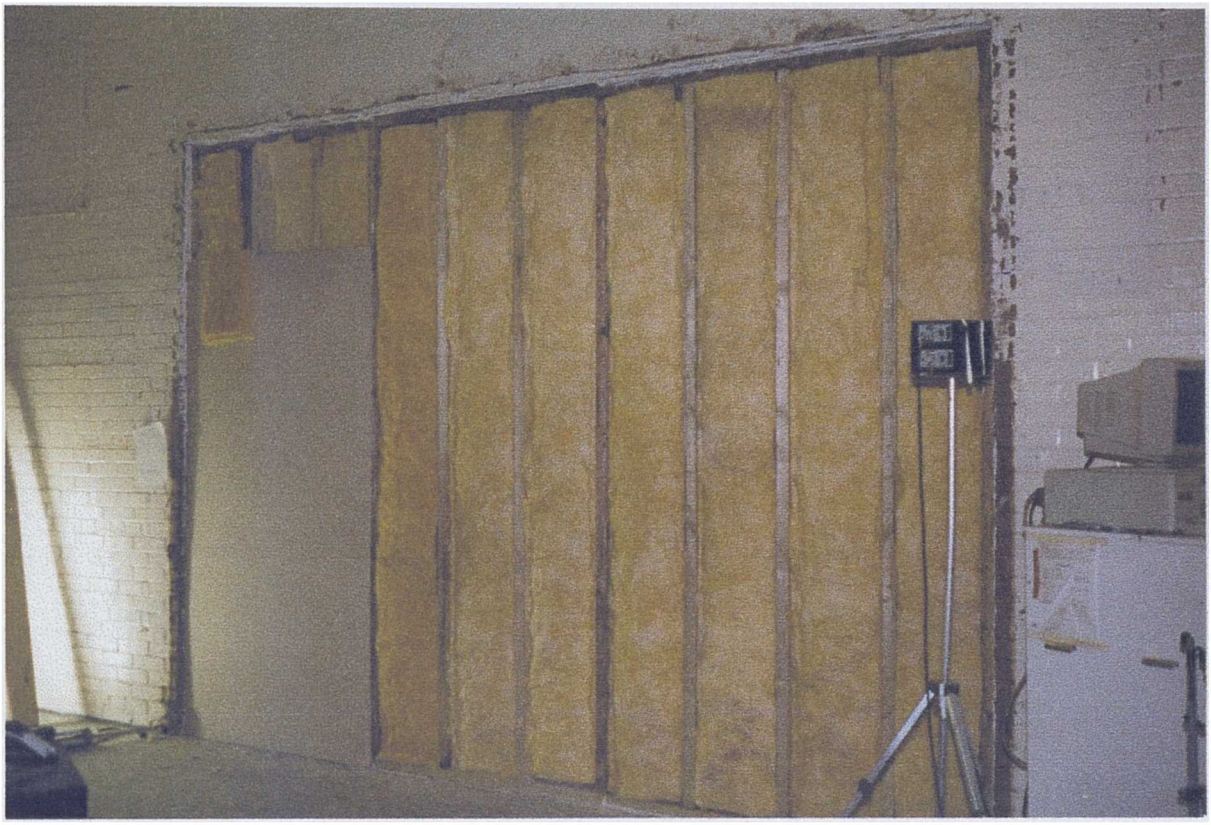

Figure 3.2 Photograph showing one of the test partitions being constructed in the common opening in the horizontal transmission suite.
(The wall shown is the 50mm insulated stud partition with the photograph taken in the receiving room at the doors.)

longitudinal wavespeed of 2130m/s and a density of 1685 Kg/m^3. The walls and ceilings were painted with a cement paint to seal the pores in the brick and concrete and reduce absorption in the room.

The two chambers were structurally isolated from one another which assisted in preventing flanking transmission from the structure of one room to the next. The larger chamber, the receiving room, was built on springs and a 15mm gap between the walls of the two chambers was filled with a mastic seal which maintained the isolation at the perimeter of the common opening. However, the structures tested in the common opening were built on one side of the opening as is shown in Fig 3.3. The plasterboard double leaf lightweight partitions were mounted on a frame which was fixed to the perimeter of the common opening in the receiving room. This meant that the structure of the receiving chamber would still slightly affect the performance of the wall. Some of these effects are discussed in more detail by Craik [13].

One of the other structures to which this research on lightweight parallel plates is applicable is that of timber floors. Tests were carried out in a vertical transmission suite where a timber floor was constructed between the rooms in a common opening as shown in Fig 3.4. A variety of acoustic tests were carried out including airborne sound level difference, structure borne sound level difference, airborne to structure and structure to airborne.

The upper chamber was separated from the lower chamber by a common concrete ring beam creating a common opening and which could support structures such as timber joists to concrete floor slabs. The 50x150mm timber floor joists could have been supported at either end by the concrete ring beam. However, it was thought that if the joists could be supported on one end by a continuous wall, linking the upper and lower chambers, then the effect of flanking transmission could also be included in this study. Therefore a 250mm wide cavity wall was constructed, linking the upper and lower chambers, to which the timber joists were built into the inner leaf, as shown in Fig 3.4 and Fig 3.5.

Horizontal transmission suite

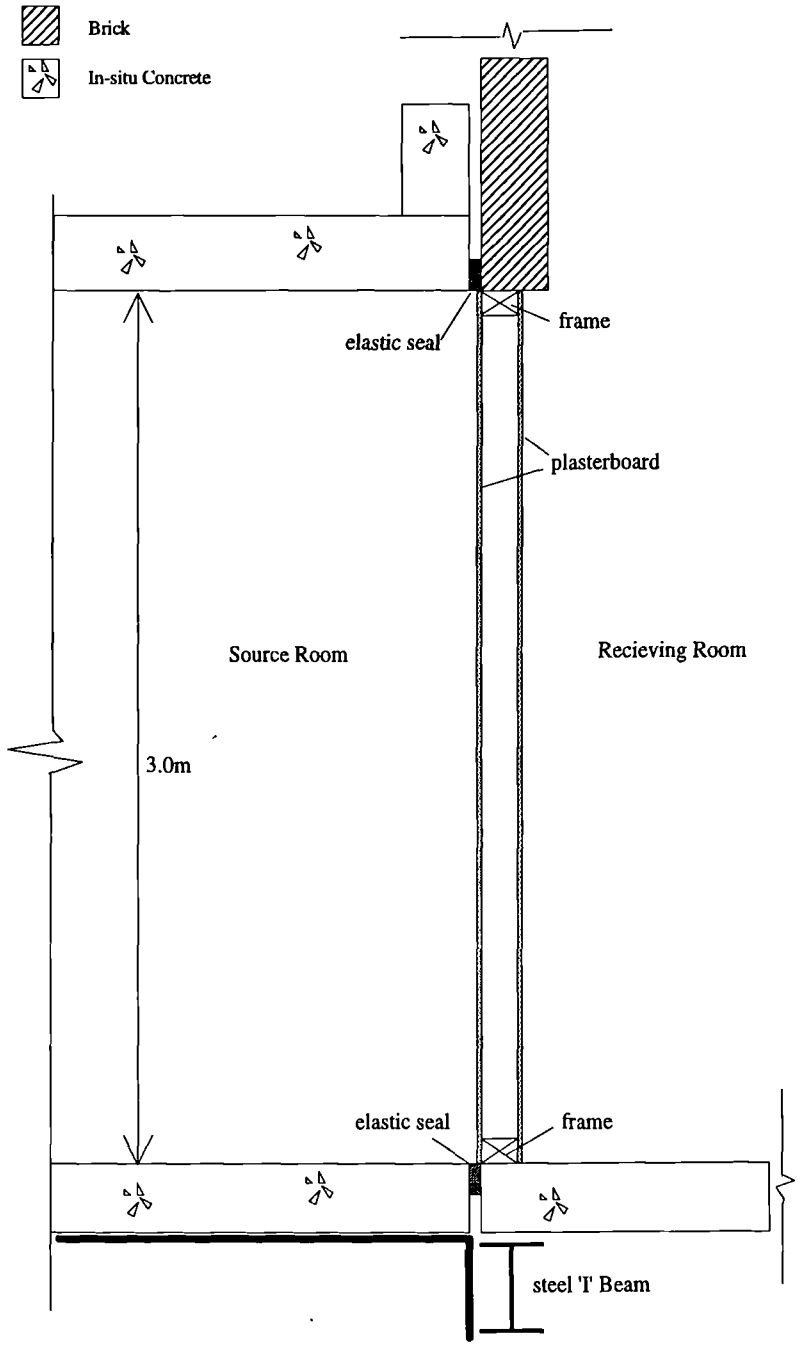

Figure 3.3 Section through common opening where the test partition is mounted on the recieving room side.

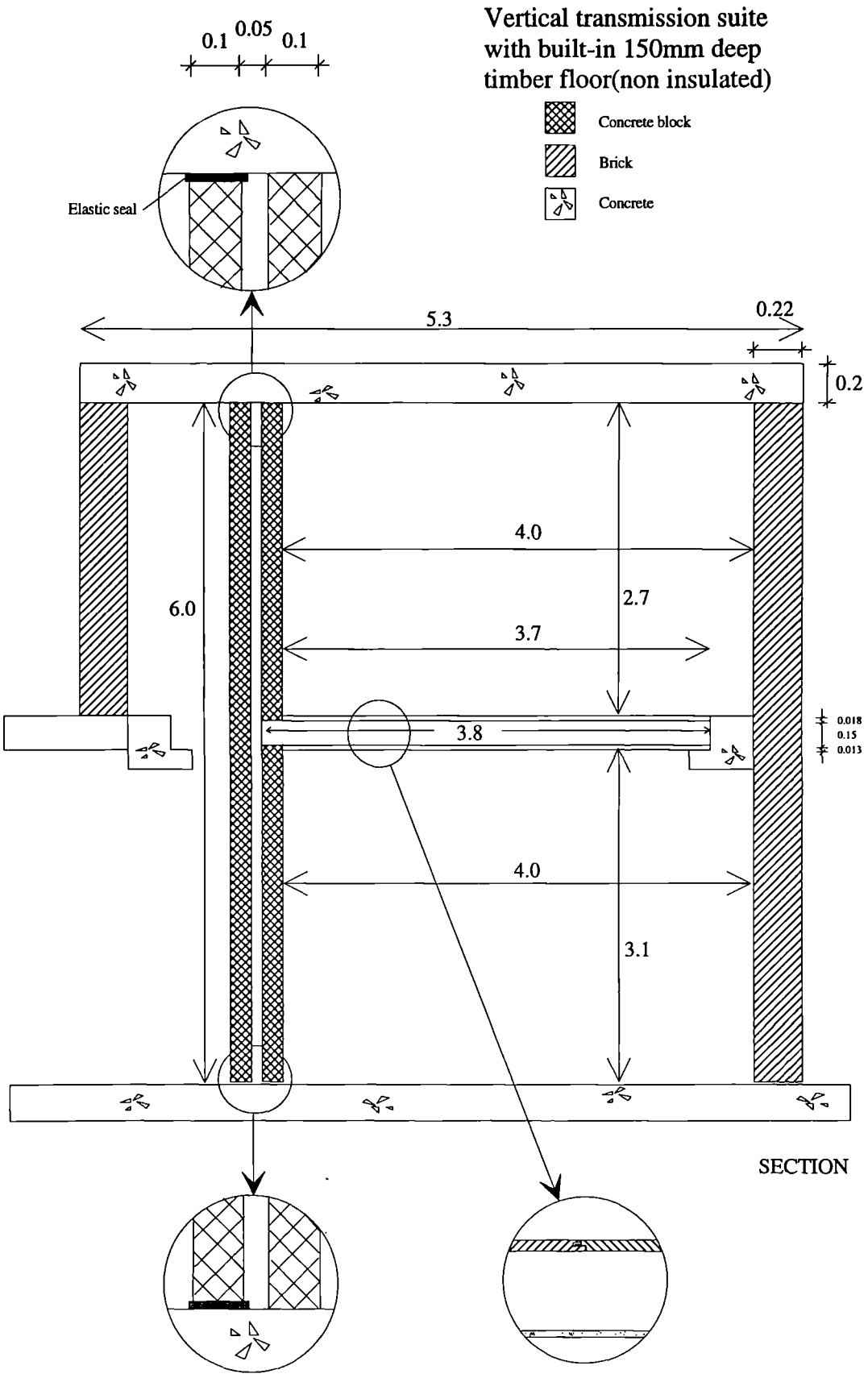

Figure 3.4 Section through the vertical transmission suite and timber floor built in to the common opening.

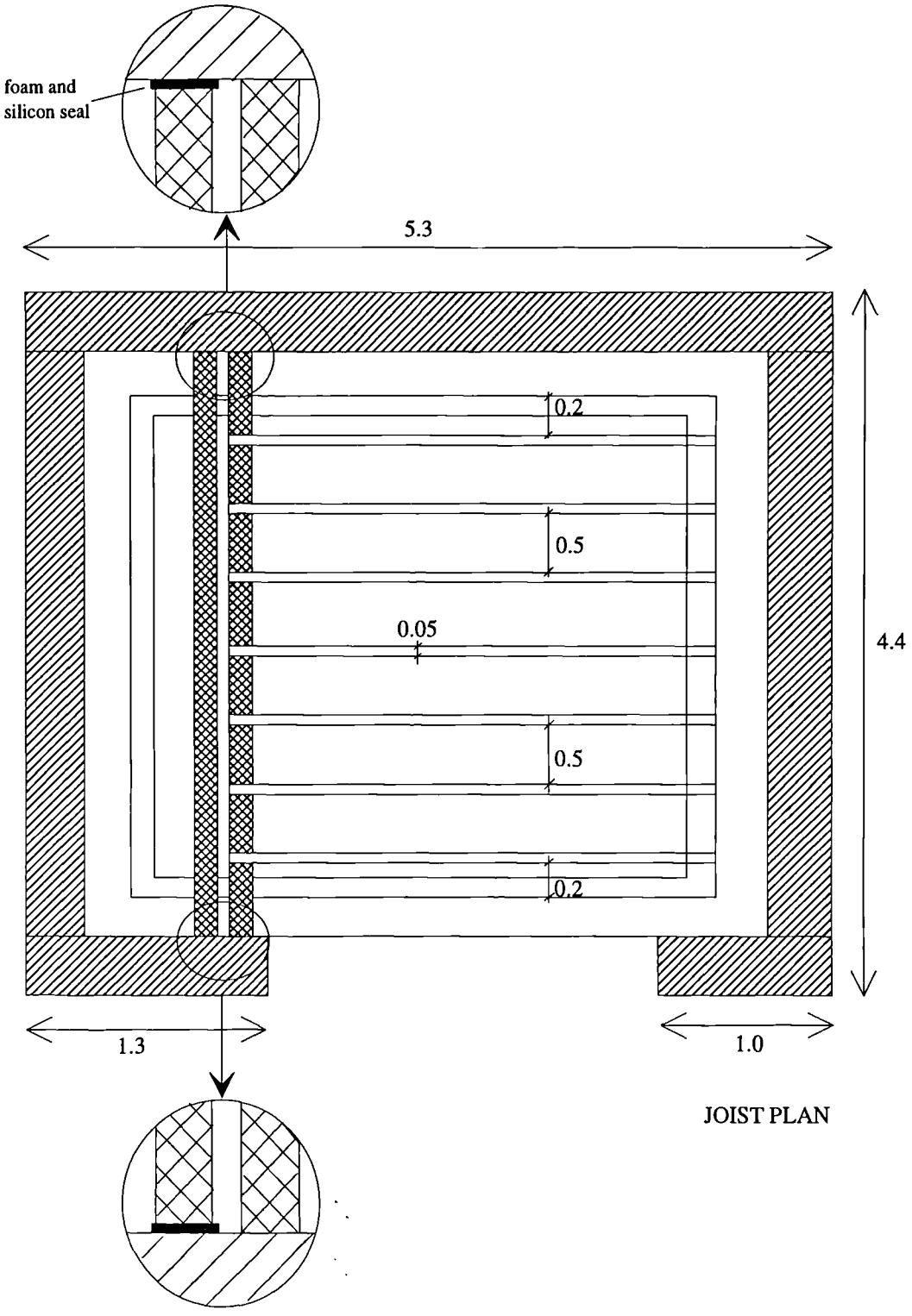

Figure 3.5 Plan of common opening in vertical transmission suite showing cavity wall and built-in joists.

The cavity wall was composed of a 100mm thick dense concrete block inner leaf mortared and sealed to the floor, ceiling and surrounding walls at its edges. The outer leaf of the cavity wall was also made up of 100mm dense concrete blocks but was sealed at its edges by a continuous 100mm foam layer and elastic mastic seal. It was only structurally connected to the inner leaf by a series of butterfly steel wall ties at 600x900mm spacings horizontally and vertically. The empty cavity formed between the inner and outer leafs was 50mm deep. The dense concrete blocks had a measured longitudinal wavespeed of 2020m/s and a density of 1836Kg/m^3. The cavity wall was painted with a cement compound paint to seal the pores in the concrete blocks and reduce the absorption.

The opposite ends of the 50x150mm timber joists, which spanned 3.8m, were supported on the concrete ring beam and had small timber wedges between them to maintain their spacing. The majority of the seven timber joists were at 500mm centres which in turn supported an 18mm thick chipboard floor and a 12.5mm thick plasterboard ceiling. The 0.6m wide tongue and groove chipboard floor panels were connected by screws at 300mm centres to the joists. The 1.2m wide plasterboard sheets were connected at 150mm centres by nails. Figs 3.6 and 3.7 show the chipboard and plasterboard layout.

The dimensions of the upper chamber were 4.0x4.0x2.7m and the lower chamber were 4.0x4.0x3.1m. The surrounding walls of the upper and lower chambers were primarily made up of 0.22m thick brickwork and the ceiling and floors were 0.2m thick in-situ concrete with similar material properties to those of the horizontal transmission suite mentioned previously.

Due to the interaction that occurs between the test wall and chambers, the chamber structures such as floor, walls and ceiling were included in the SEA models that were used to compute the overall sound transmission. The breakdown of these structures into SEA subsystems is discussed further in Chapter 8.

As will be discussed in later chapters, the structural sound transmission through the supporting frame, whether a partition or floor, plays an important role in the overall sound transmission through lightweight parallel plates. In the course of this work a major

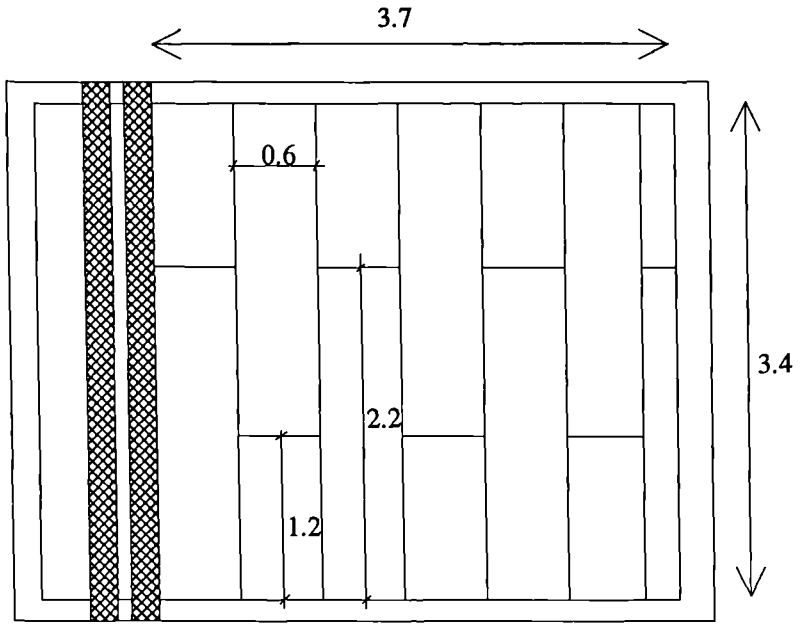

Figure 3.6 Plan of 18mm thick chipboard floor panels for the 150mm timber floor.

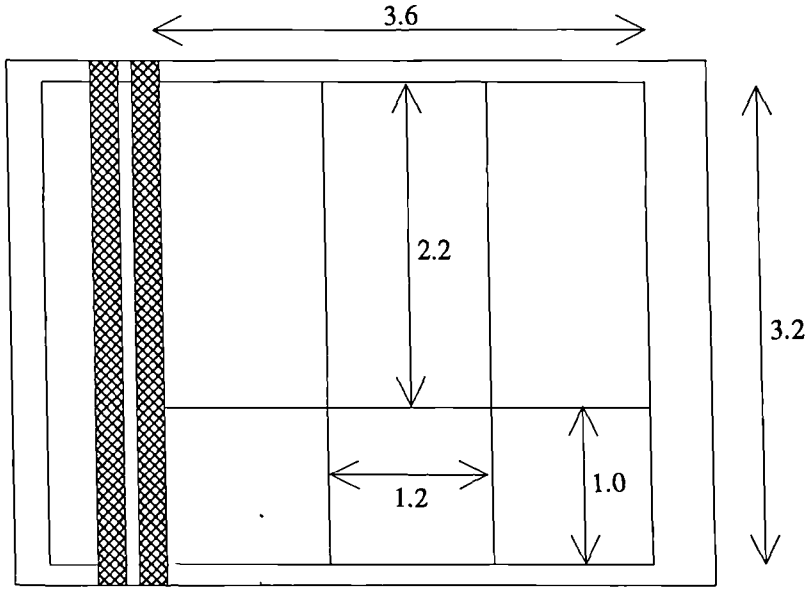

Figure 3.7 Plan of 12.5mm thick plasterboard ceiling panels.

part of the research has been to develop prediction models for sound transmission through point and line connected structures. Measurements were carried out on various small parallel plate lightweight structures, freely suspended in an anechoic chamber. By suspending these small sections of lightweight partition, the structural sound transmission path through the frame could be analysed in more detail with no flanking or other influences from surrounding structures if built into a transmission suite. Also by measuring in an anechoic chamber any effects of reflections from surrounding surfaces could be greatly reduced. Fig 3.8 shows a typical test structure in an anechoic chamber. Chapter 6 explains in more detail the varieties of structures tested and gives the results for the measured and predicted data.

The construction of lightweight partitions or timber floors requires a structural frame, studs or joists, at regular spacings which couple the parallel plates. As a result of these regular spacings and offset between the parallel plates, equal to the depth of the frame, large voids or cavities are created. These cavities play a crucial role in the non-resonant transmission path through these structures. Consequently tests were carried out on a separate test structure to analyse sound transmission into cavities.

Figs 3.9 and 3.10 show the cavity test structure. It was constructed of dense concrete blocks which formed the base and walls of the cavity which was mounted on one of the test chamber floors. A plasterboard sheet was then laid inside the cavity structure to provide a flush flat finish. A second plasterboard plate of slightly larger dimensions was then placed on top of the cavity, supported at its edges on the concrete blocks and sealed with mortar. Once the top plasterboard sheet was installed this sealed inside the cavity a microphone, B&K type 4190, which was pre-calibrated. Using thin wires, which were inserted through minute holes in the wall edges, the microphone could be moved around within the cavity to obtain individual measurements for various locations within the cavity to achieve a mean value. The holes were sealed before taking measurements.

This test cavity structure could have its depth varied by increasing or decreasing the height of the perimeter walls. The depths varied from 25mm to 150mm and were tested with and without absorption. The length and width of the cavity were 1.9mx0.96m as shown in Fig 3.9.

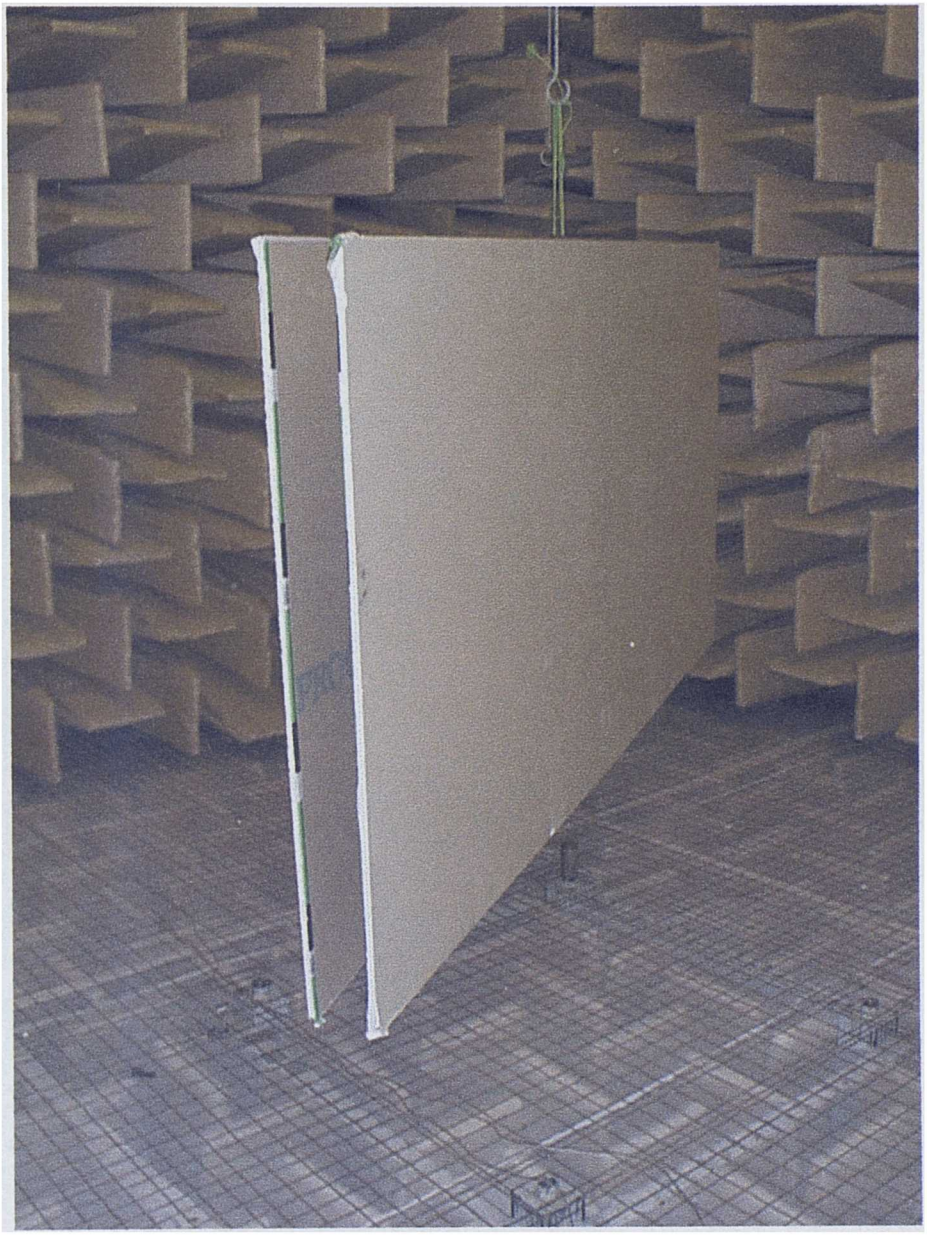

Figure 3.8 Photograph showing one of the freely suspended test structures in the anechoic chamber.

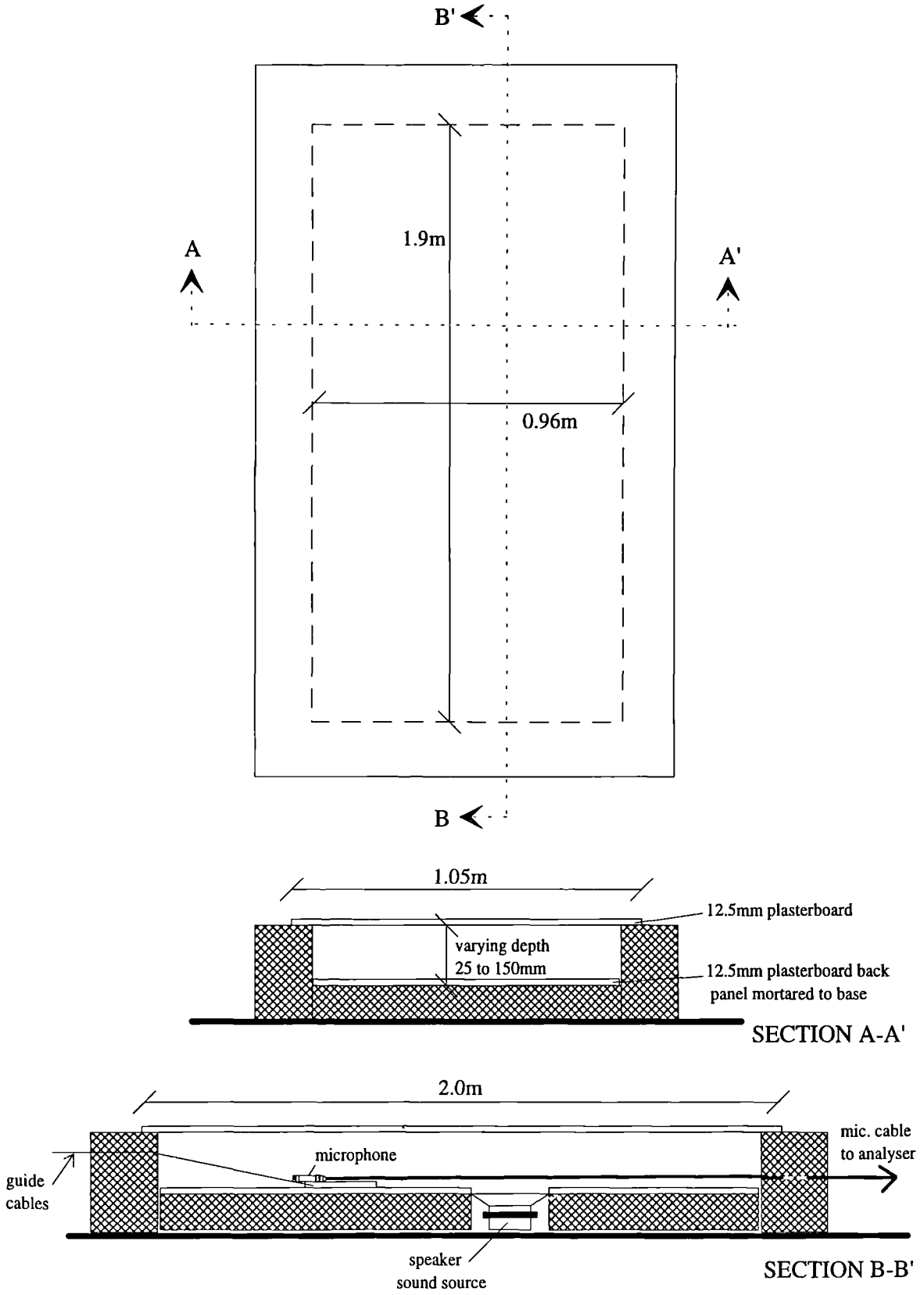

Figure 3.9 Sections and plan of cavity test structure with built-in speaker and microphone.

Figure 3.10 Photograph showing the cavity test structure. (The cavity shown is the 25mm non insulated cavity prior to the top plasterboard plate being mounted. The circle in the left of centre is the built-in speaker.)

3.3 Measurement of density

The material used in the test structures for this study include timber, brick, concrete (block and in-situ), aluminium and plasterboard. Determining the density of the materials used in the test structures was found by measuring a sample volume, V, of the materials and then weighing them on electronic scales to find the mass, m. By dividing the mass by the known volume the density, ρ, could be determined, as given by,

$$\rho = \frac{m}{V} \tag{3.1}$$

In the case of the horizontal and vertical transmission suites these had previously been constructed prior to this work. Hence, the design densities given by the architect drawings were used. Although these may not give a completely reliable measure of density of the material, the accuracy should be within 10% [8]. The design values of density were used for the chamber walls, ceilings and floors which formed flanking paths. However, these tended to be less important, so any error in the prediction from these paths would be small.

3.4 Measurement of longitudinal wavespeed

Young's modulus, E, of a material is required for many calculations and may be computed from the longitudinal wavespeed, C_L. The relationship between the density and longitudinal wavespeed to determine the Young's modulus is given by [44],

$$E = \rho C_L^2 \tag{3.2}$$

for a beam and for a plate may be given as [44],

$$E = \rho C_L^2(1-\mu^2) \tag{3.3}$$

where μ is Poisson's ratio and ρ is the density.

Fig 3.11 shows the method that was adopted in this work for measuring the longitudinal wavespeed of plasterboard, for example. The simplest way to excite a longitudinal wave on a structure is to strike it on an edge with a plastic headed hammer. Two accelerometers, B&K type 4500, were mounted on their sides onto the test material at

a measured distance, each connected to a charge amp, B&K type 2635, and then fed into a two channel oscilloscope. As the longitudinal wave passes the first and second accelerometer the oscilloscope records when the waves pass and the time interval between each. Then dividing the known distance by the time interval will determine C_L.

As the edges of the test chamber walls were not exposed it was necessary to excite the longitudinal waves indirectly. Fig 3.12 shows the method of determining the longitudinal wavespeed if the edge of the test material is not exposed. A force transducer was mounted on the tip of a plastic headed hammer to record when the waves were generated. An accelerometer mounted on the side was used to detect the arrival of the waves on the wall. The signal from both the hammer transducer and the mounted accelerometer are stored on an oscilloscope to determine the transit time. If the distance between the source hammer and receiving accelerometer is known then dividing this by the transit time will determine C_L.

The plasterboard double leaf partitions are supported by a structural timber or aluminium frame. The sizes of a timber partition in depth and width may vary from 25mm to 200mm. Due to these small dimension of the timber frame and timber's unique orthotropic properties, which are discussed further in chapter 6, the standard method of measuring the longitudinal wavespeed as shown in Fig 3.11 could not be used at all times. The timber longitudinal wavespeed varies in three dimensions, axial, tangential and radial, due to the direction of grain and plane under study. Only the axial direction may be measured using the method shown in Fig 3.11. The timber frames tested were generally varying in length, the axial direction, from 1.2m to 3.6m. The tangential and radial dimensions of the timber frames, which represented the depth and width were generally much smaller as described above. The measurement of the longitudinal wavespeed in these two directions required the use of a Terratest, see Fig 3.13. This provides a fast pulse source signal transmitted through a metal plate into the short measured timber section and then received by a second metal plate. Both plates are attached with beeswax. The source and transmitted signals are fed into a dual channel oscilloscope which can determine the time interval. Dividing the known distance between the plates by the time interval will allow the longitudinal wavespeed to be determined.

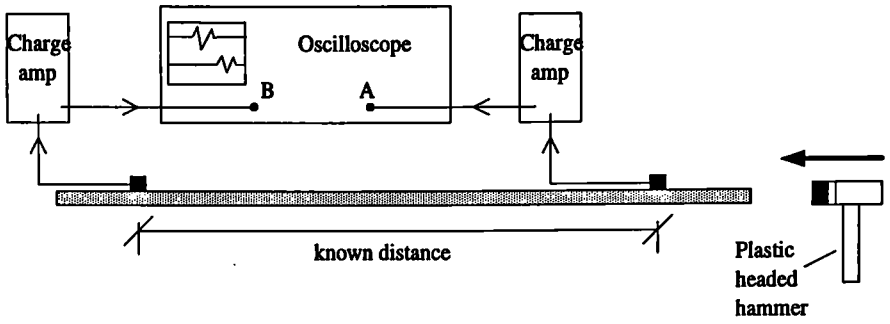

Figure 3.11 Measurement of longitudinal wavespeed

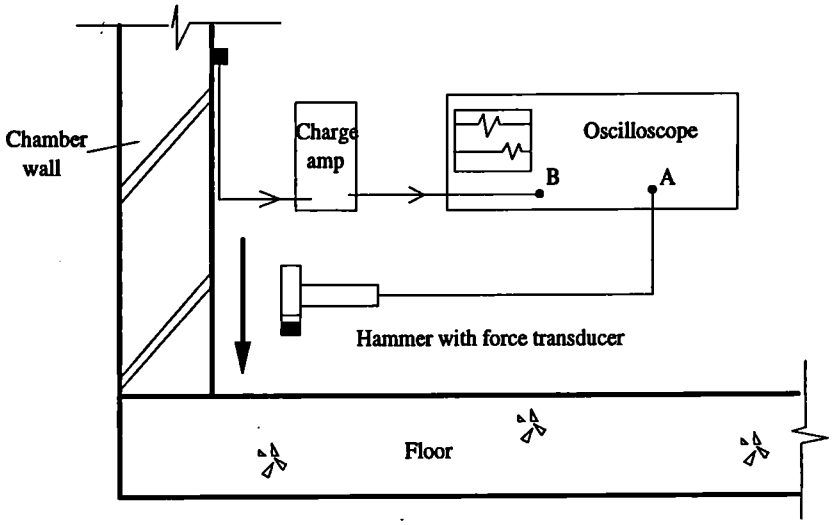

Figure 3.12 Measurement of longitudinal wavespeed when edge of structure not exposed.

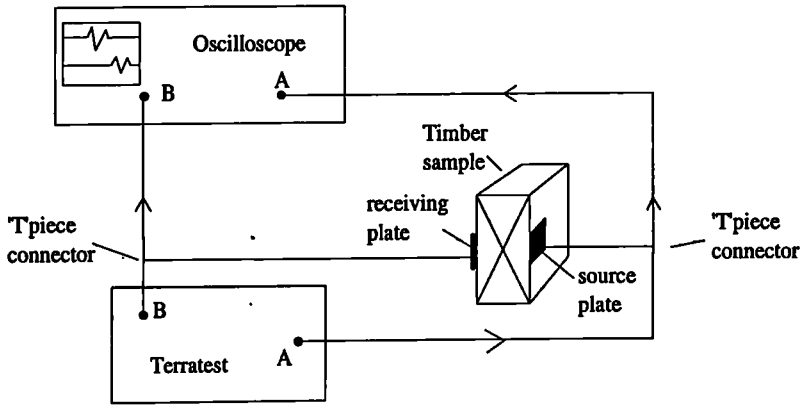

Figure 3.13 Measurement of tangential and radial longitudinal wavespeed using the Terratest.

3.5 Measurement of damping

The total loss factor, η, was required for subsystems such as rooms, cavities and plates so that it could be inserted into the SEA models. Each type of subsystem required a different technique for measuring the damping. The most common measure of damping in building acoustics is the reverberation time, which is the time for the energy to decay by 60dB once a steady state source has been stopped. The reverberation time, T, and the total loss factor are related by,

$$\eta = \frac{\ln(10^6)}{2\pi f T} = \frac{2.2}{fT} \tag{3.4}$$

The reverberation time for a room was measured using a Nortronics Type 823 analyser, a B&K speaker and a 1/2" B&K type 4190 microphone. The Nortronics generates noise at third octaves which is cut off and then records the decay of sound pressure in the room. It calculates the reverberation time from the first 30dB and first 15dB of usable decay, normalised to 60dB range. Measurements were made between 50Hz to 6300Hz over at least 6 positions.

For cavities this method can also be used but due to the small volume of some of the cavities tested the reverberation time was very short and the reverberation time fell below the cut off filter of the Nortronics. An example of the difference in reverberation time between a room and a cavity is shown in Fig 3.14.

To measure the cavity reverberation time a MLSSA, Maximum-Length Sequence System Analyser, was used which could measure as low as 0.01 seconds and store the reverberation time on a desk top computer. Both the microphone and speaker were pre-calibrated and built into the cavity as shown in Fig 3.9. The results were averaged over 40 time samples for each position of the microphone and at least six positions were recorded. Due to the small size of the speaker in the cavity its operative range at the low frequencies was restricted and so the frequency range recorded was between 100Hz and 5000Hz.

However it must be stated that using the MLSSA technique may not always be possible.

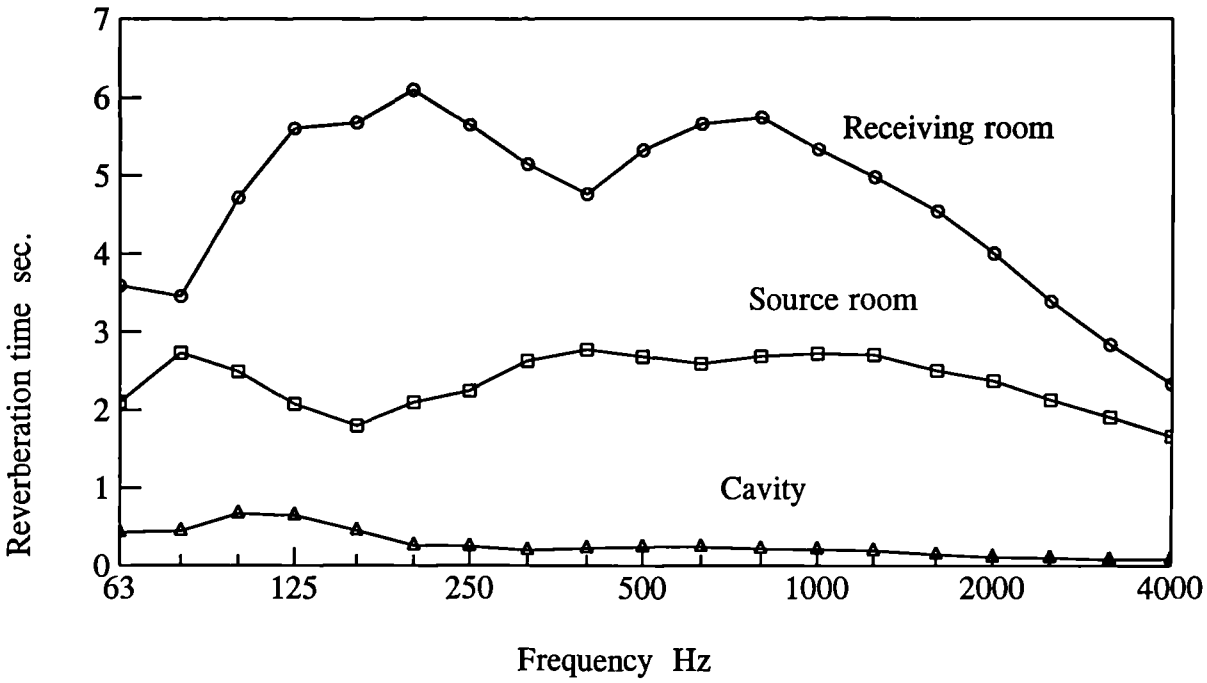

Figure 3.14 Comparison of reverberation time between test chambers and a cavity. Volumes - (O) 210m^3, (□) 72m^3, (Δ) 0.18m^3.

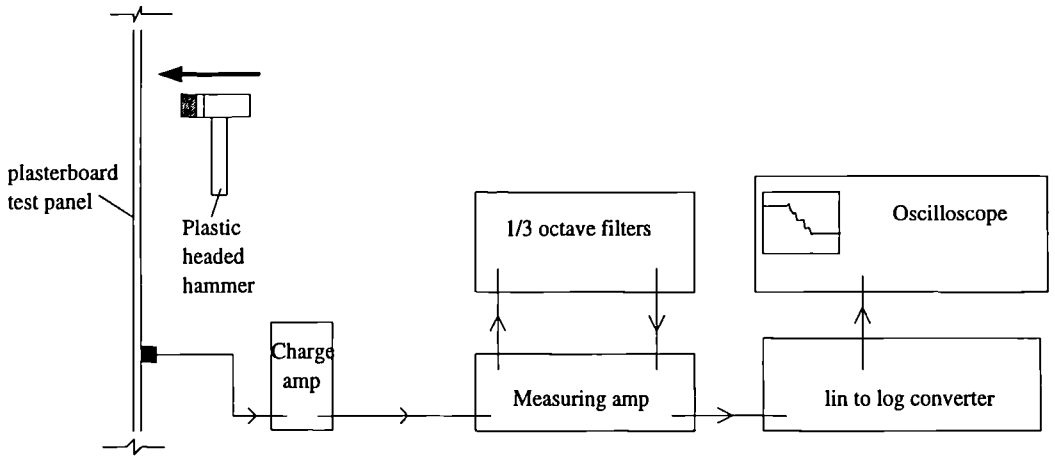

Figure 3.15 Measurement of structural damping

It was found that when measuring the reverberation time on cavities with absorption present the reverberation time was extremely short and sometimes fell below the cut off filter for the MLSSA. These measurements are discussed in more detail in Chapter 7.

For structures, an accelerometer is used instead of a microphone to detect the decay. Due to the short decay the equipment shown in Fig 3.15 was used, following a procedure given by Craik [60]. The accelerometer was attached to the structure by beeswax and using a single blow from a plastic-headed hammer to excite the subsystem the decay was detected by the accelerometer. To avoid nearfield effects care was taken not to strike the structure too close to the accelerometer. The signal from the accelerometer was fed into a measuring amplifier and passed through a set of third octave filters. Taking the rms value this was then converted into a logarithmic signal and fed to an oscilloscope. This allows a straight line decay to be displayed, stored on the oscilloscope and calibrated in dB along its vertical axis. The slope of the decay was measured and knowing the time base on the oscilloscope, it was possible to determine the reverberation time for the structure to find the total loss factor, TLF, using eqn(2.41).

Fig 3.16 shows the measured and predicted TLF for a plasterboard panel in a wall. As can be seen there is good agreement. Where there was no absorption touching the plates the predicted TLF of the plates was used for ease. But when absorption was present the measured TLF was used.

This technique was also used to find the internal loss factor of the plate materials, chipboard and plasterboard, used in this study. Fig 3.17 shows the measured and predicted internal loss factor for freely suspended chipboard and plasterboard plates. The measured ILF for both materials increases in value slightly at the higher frequencies due to the critical frequency, where the critical frequency for chipboard is approximately 2000Hz and is 3150Hz for plasterboard. The internal loss factor for both materials was generally quite constant and these could be inserted into the full SEA models, discussed in later chapters, using the absolute units 0.01 for plasterboard and 0.018 for chipboard, (100dB and 102.55dB re 10^{-12}). Measurements were made at six positions between 50Hz to 6300Hz on each test structure.

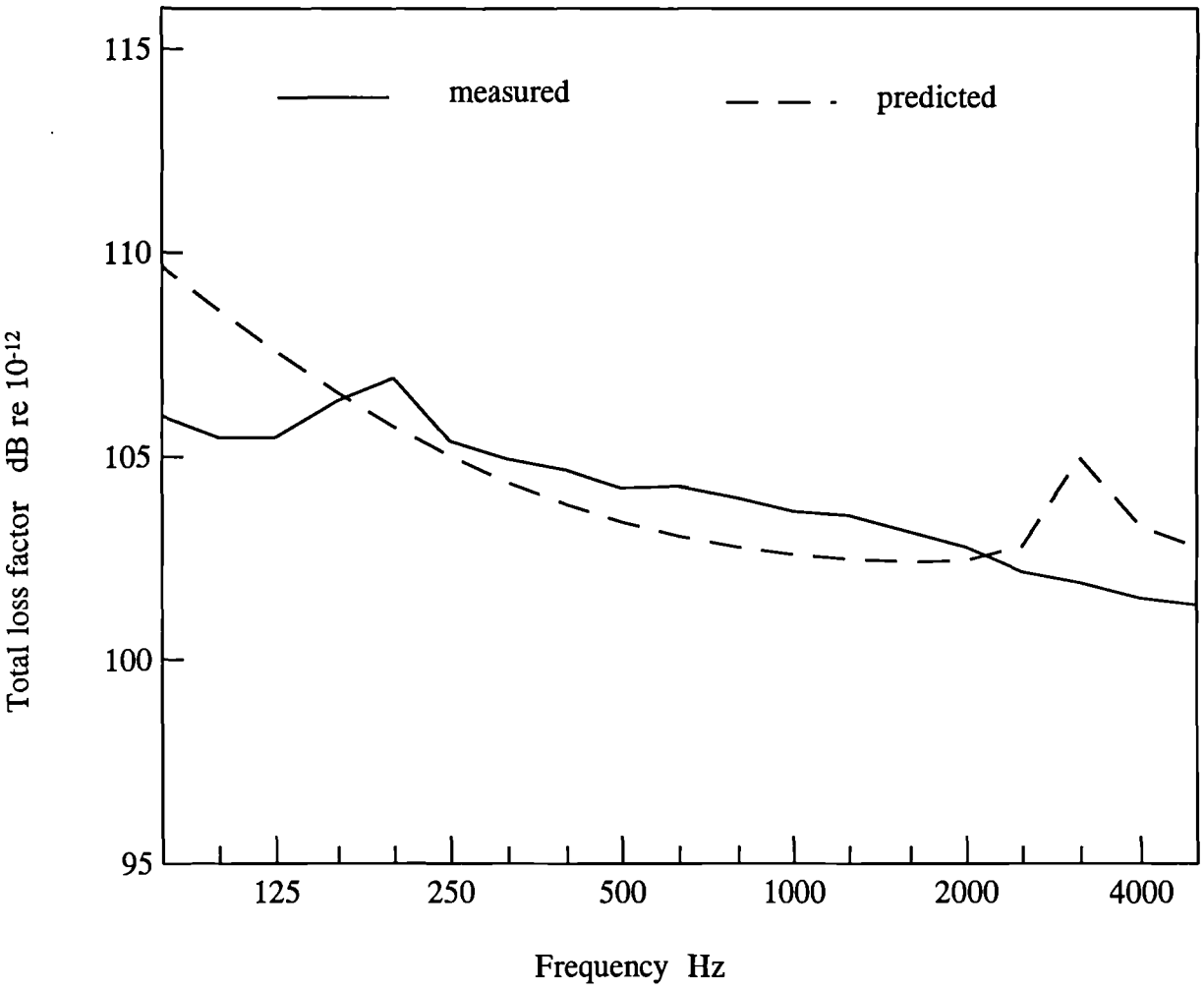

Figure 3.16 Measured and predicted TLF for a plasterboard panel in the 150mm double wall with no absorption.

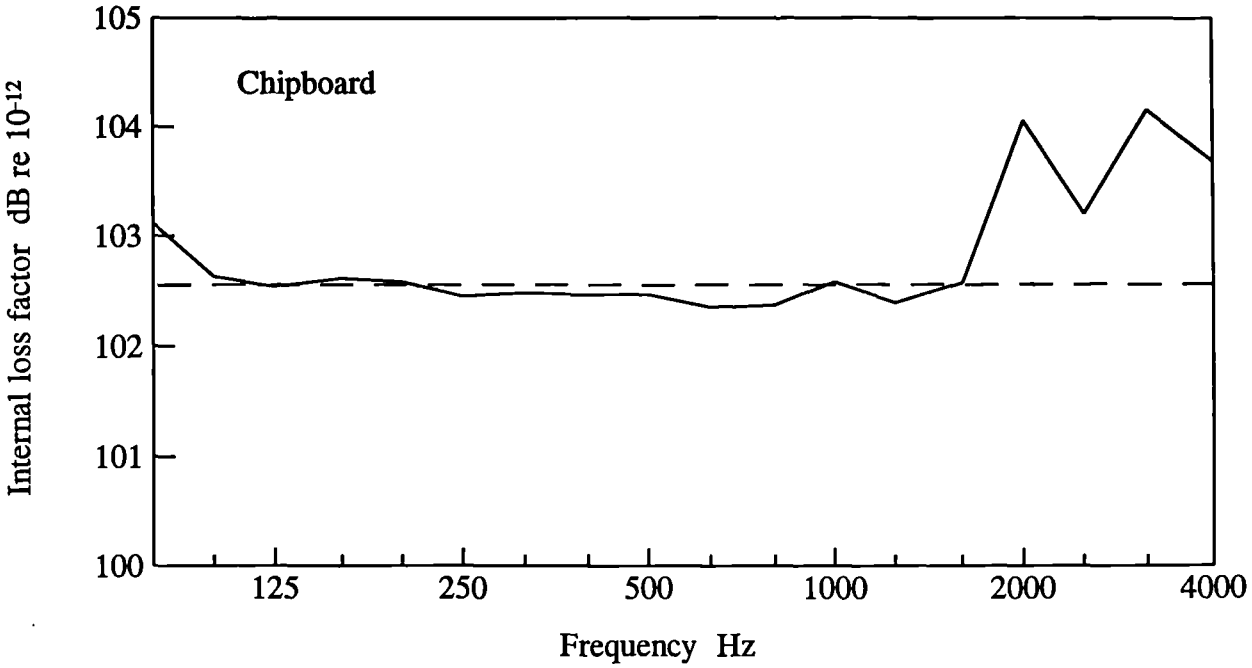

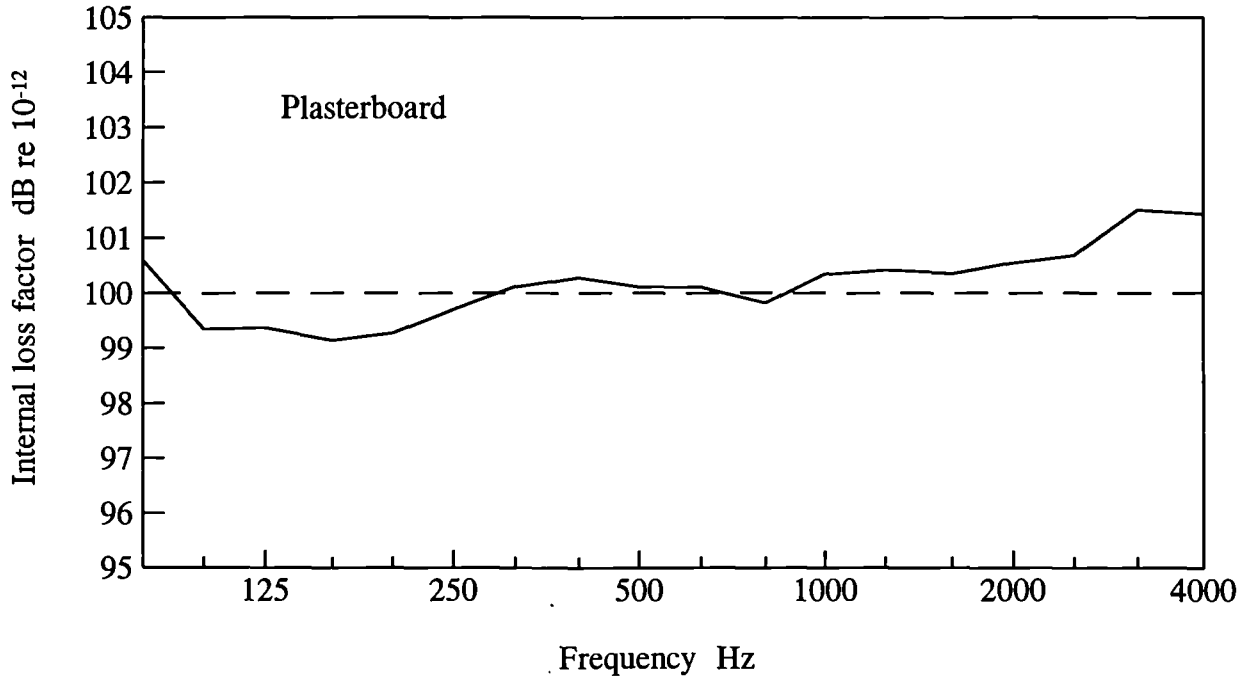

Figure 3.17 Measured and predicted internal loss factor for plates.
Plasterboard (____) measured, (- - -) predicted using 0.01.
Chipboard (____) measured, (- - -) predicted using 0.018.

3.6 Calibration

Accelerometers

The measurements performed in this study were made using B&K Type 4369 and B&K Type 4500 accelerometers with B&K Type 2635 charge amplifiers. To calibrate the accelerometers a B&K Type 4294 vibration calibrator was used that produces an acceleration of $10m/s^2$ at 159.2Hz to an accuracy of ±0.2dB.

Microphones

The airborne measurements were carried out using 1/2" B&K Type 4190 condenser microphone connected to B&K Type 2639 pre amplifiers. These were calibrated before and after each measurement using a B&K Type 4230 or B&K Type 4231 sound level calibrator. These generate a sound pressure level of 93.8dB at 1 KHz for a 1/2" microphone and calibrate to an accuracy of ±0.3dB.

3.7 Level difference and phase measurements

The majority of the experiments carried out for this work were level difference measurements. These type of measurements involved airborne level difference (the sound pressure level between two rooms), structural level difference (the difference between acceleration levels measured on two structures), room to structure and vice versa.

To undertake these tests two real time digital frequency analysers were used measuring at third octaves. For the airborne level difference measurements a loudspeaker fed with pink noise from the Nortronics Type 823 noise generator was used as the sound source. For structural level differences a plastic-headed hammer or a B&K Type 4810 shaker was used as the structure borne sound source on the structural source plate. Calibration was carried out before and after each test and for structural measurements the charge amplifiers and analysers were constantly checked to ensure that they were not overloaded by the hammer blows. In the latter stages of the tests a B&K Type 2148 portable dual channel frequency analyser was used, this being portable and lighter was easier to use than the two older and larger single channel B&K Type 2131 real time analysers.

The experimental set up for making third octave level difference measurements is shown in Fig 3.18. The source and receiving signals were fed into the two real time analysers (B&K Type 2131) connected via an IEEE bus cable to a desk top computer. This allowed simultaneous measurements to be recorded for all third octave bands. At each measurement position sixteen seconds of linear averaging was carried out and at the end of the averaging time the computer automatically read and stored the data from both the analysers. The computer calculated the mean, standard deviation and 95% confidence interval for the level difference at each frequency. The microphone or accelerometer positions were then changed and the procedure repeated until the 95% confidence interval was less than 1dB between 100Hz and 5KHz. Generally the number of measured positions for each subsystem whether a room, cavity or plate was approximately twenty.

Once a measurement was completed, the mean was recomputed to account for the effects of background noise. If the measured level was within 8dB of background noise the data was disallowed. This rarely happened during the tests for this work.

Narrowband measurements were also carried out for analysis of phase for mass-spring-mass in the plasterboard double wall structures. These were made using a B&K Type 2032 FFT dual channel analyser over a frequency range of 20Hz to 1.6KHz. At each position a linear average was taken of 400 time samples. Using two accelerometers which each had a charge amplifier the signal was fed directly into a desk top computer via an IEEE bus and stored.

3.8 Accuracy of measurements

When carrying out any experiments it is important to guage the accuracy of the data recorded. Some experiments on the partitions involved minor changes to the construction, such as changing the number of fixing nails, depth of the frame and placing absorption in the cavities. These construction alterations may only slightly affect the measured data results. Therefore in this work a high degree of accuracy was adopted. This would try to ensure that any changes measured were due to the change in construction and not statistical variations arising from the measurement procedure.

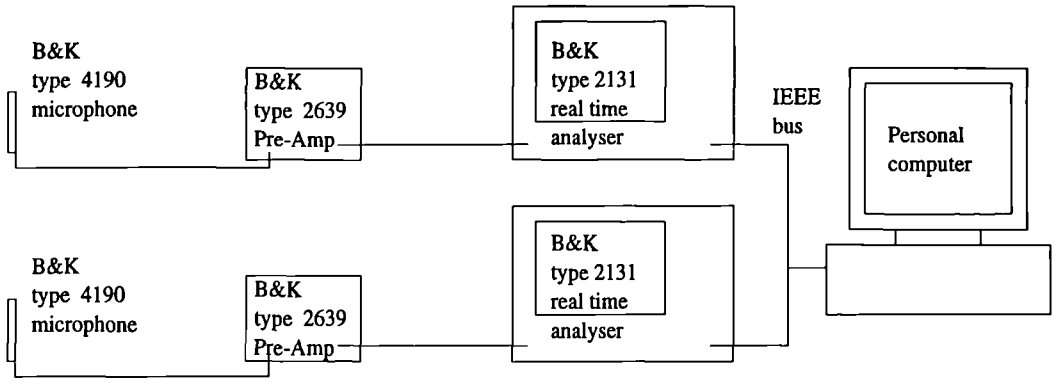

Airborne level difference equipment

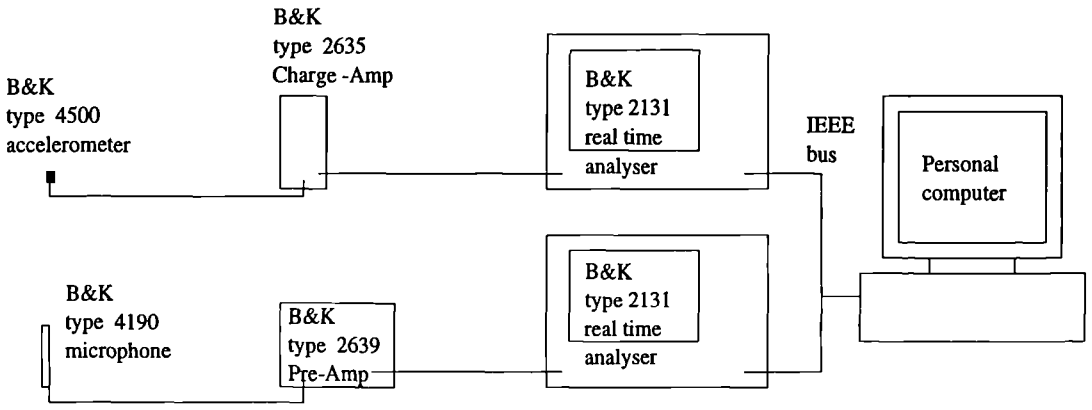

Airborne to structure (or vice versa)

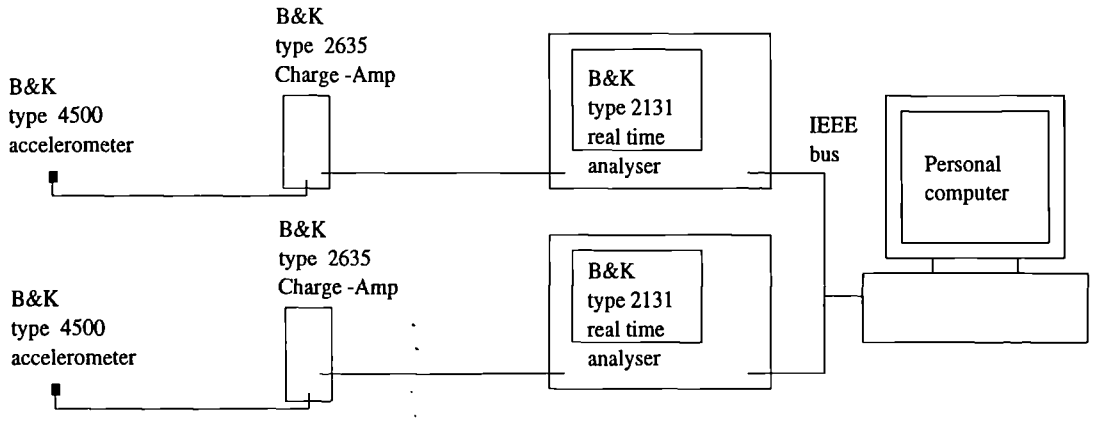

Structural level difference

Figure 3.18 Schematic of experimental set up for 1/3 octave level difference measurements

Throughout this research when measurements were carried out the standard deviation, *sd*, and 95% confidence interval were calculated as an on going process as each position's data was recorded.

To determine the accuracy it is necessary to know the distribution of the data. Craik [13], examined this problem and concluded that the 95% confidence interval and standard deviation for structural and airborne data, when in dB, could be assumed to follow a normal distribution. The following section describes the expressions for determining accuracy that were used.

The mean was calculated by converting the measured data from dB into absolute units. The mean was then calculated and converted back into dB. For a single variable measurement, x, the mean, m, of a set of, n, measurements is given by [61],

$$m = \frac{\Sigma x}{n} \tag{3.5}$$

When calculating the standard deviation, *sd*, and the 95% confidence interval it is not necessary to convert the measured data into absolute units, as these can be obtained directly from dB values [13]. The standard deviation is given by [61],

$$sd = \sqrt{\frac{\Sigma x^2 - \frac{(\Sigma x)^2}{n}}{n-1}} \tag{3.6}$$

and the 95% confidence interval is obtained using [61],

$$95\%CC = \frac{sd(dB)}{\sqrt{n}} \times t_{v,0.975} \tag{3.7}$$

$t_{v,0.975}$ is the value taken from the students t-distribution for a 95% confidence interval for a measurement with v degrees of freedom, where v is equal to n-1.

Figs 3.19 and 3.20 show the typical 95% confidence intervals for the third octave band measurements carried out for airborne level difference and structural level difference for the partition test structures.

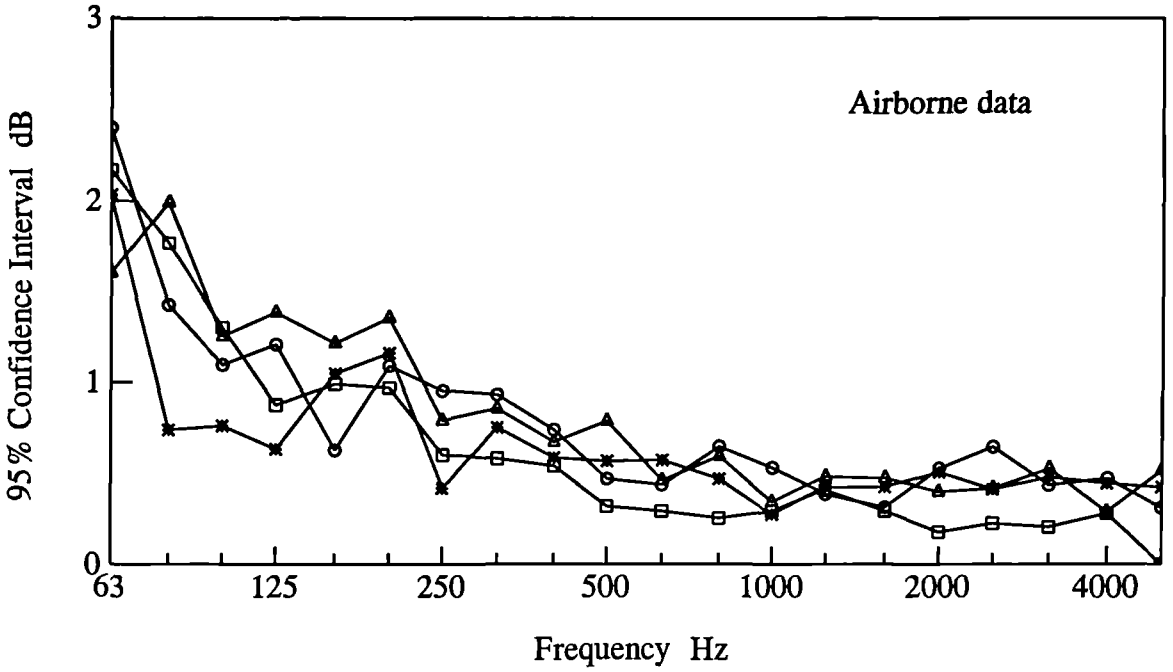

Figure 3.19 95% confidence interval for the airborne level difference for various structures tested.
Point connected partitions (□) 150mm wall, (○) 100mm wall, (Δ) line connected wall, (*) ribbed wall.

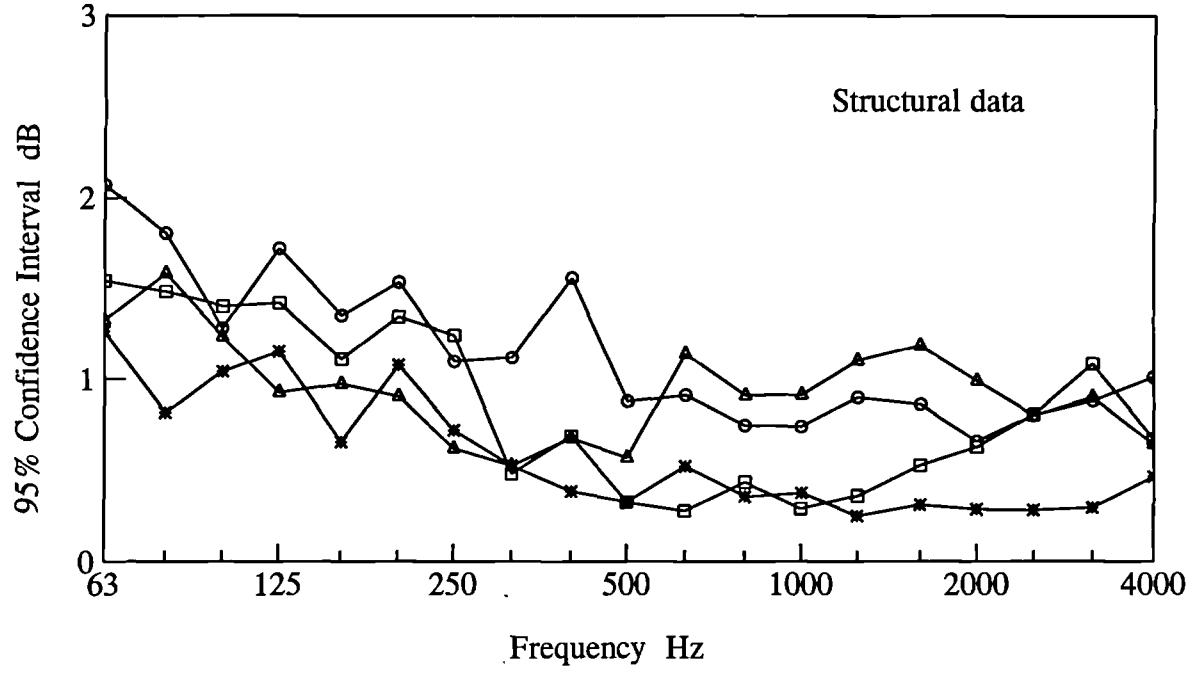

Figure 3.20 95% confidence interval for the structural level difference for various structures tested
Point connected partitions (□) 150mm wall, (○) 100mm wall, (Δ) line connected wall, (*) ribbed wall.

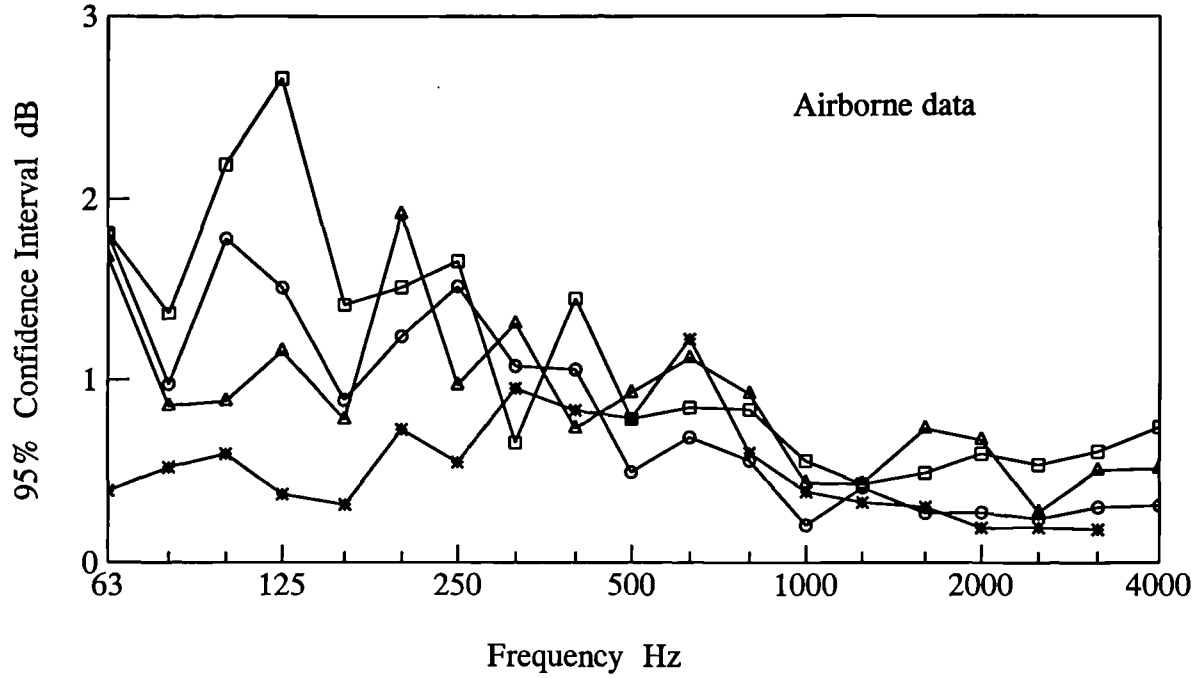

Figure 3.21 95% confidence interval for the airborne level difference for the cavity test structure with varying depth.
(□) 150mm, (○) 100mm, (Δ) 50mm, (*) 25mm.

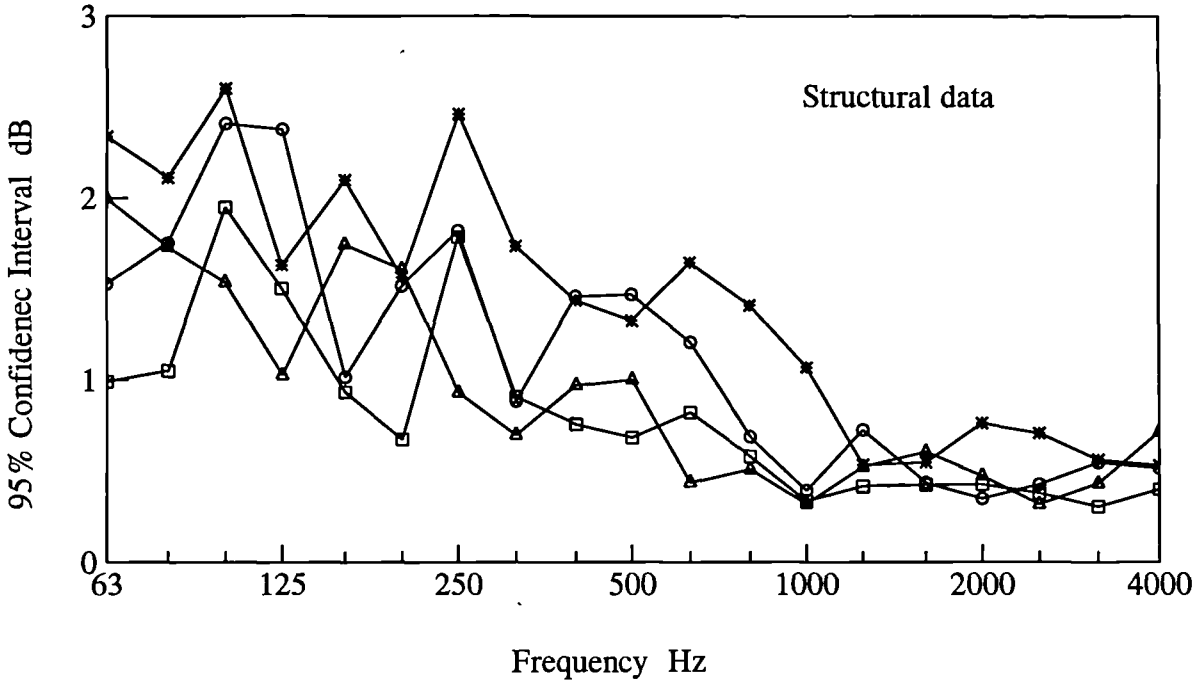

Figure 3.22 95% confidence interval for the structural level difference for various freely suspended line connected 'H' type structures with 100mm depth frame.
(□) 4 plates, 1 to 3, (○) 3 plates 1 to 3, (Δ) 1 to 2, (*) 2 plates 1 to 3.

Over most of the frequency range the 95% confidence interval was less than 1dB for the airborne data and 1.5dB for the structural data. At the low frequencies there are exceptions to this but generally these were less than 2.5dB. Figs 3.21 and 3.22 show the typical 95% confidence intervals for the 1/3 octave band measurements carried out for airborne level difference to the cavity and suspended plate structures.

The 95% confidence interval results shown are for level difference results only. The total loss factor results for both cavities and plates must also take into account variation from the mean and this is discussed in more detail in Chapter 7 and Chapter 8.

3.9 Conclusions

This chapter has described the test facilities and the principle test structures built inside them. The test structures were designed and constructed so that structural flanking could either be controlled and investigated where required, reduced to a minimum or omitted completely. By reducing or omitting the flanking transmission this helped to increase the dominance of the direct transmission paths through the test structures.

The techniques used to perform the airborne and structural measurements on the test structures were described. Through consistent monitoring and sustaining of the 95% confidence interval to be less than ± 1dB any changes to the construction of the test structures could be observed.

Methods were described of how the subsystem parameters such as damping and longitudinal wavespeed were measured and the varying techniques adopted for the orthotropic nature and size of the partition timber frames.

Chapter 4

Transmission Between Parallel Plates with Point Connection

4.1 Introduction

This chapter describes the transmission between parallel plates for different forms of point connection. The coupling between such plates may vary depending upon the type of construction. Different types of parallel plate construction can be found in domestic housing as shown in Figure 4.1. Previous work by Wilson [8] covered transmission between parallel plates for cavity walls where the thickness of the plates, made of brickwork or concrete blockwork, was greater than the depth of the cavity. However another common area where lightweight parallel plates can be found, made from plasterboard and chipboard, is in internal partitions and timber floors.

This chapter will describe the different forms of lightweight parallel plate construction, the methods of modelling the point connection and how the coupling is affected by varying the parameters within the structure. Overall sound transmission through point connected double walls, including all transmission paths, will be discussed later in Chapter 8. This chapter discusses only the structural sound transmission path for point connected plates. As will be shown in later chapters the transmission of the structure borne sound through either point or line connected parallel plates is a primary sound transmission path in buildings and thus the thrust of this thesis is concentrated in this area.

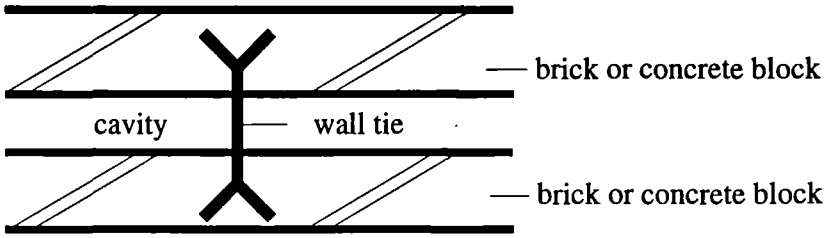

a) Cavity wall (plan view)

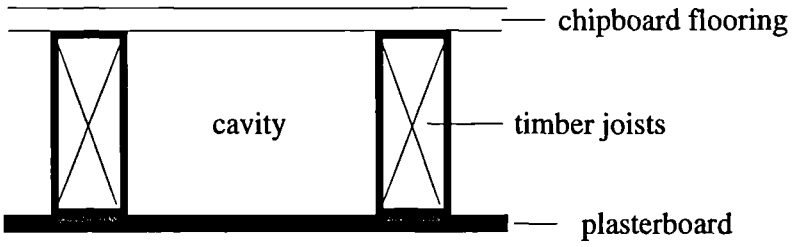

b) Timber floor (cross section view)

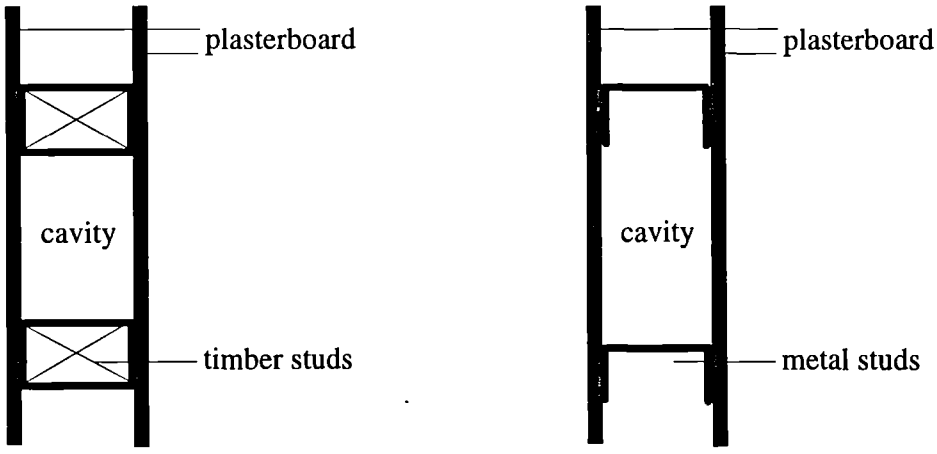

c) Internal partitions with timber or metal frames (plan view)

Figure 4.1 Types of parallel plates in housing

4.2 Types of parallel plates in housing

Different types of parallel plate structures exist in housing which can be of heavy or lightweight construction and are shown in Figure 4.1. The research carried out by Wilson [8] on point connection in cavity walls was for structures as shown in (a). This thesis will concentrate on lightweight parallel plate structures as shown in (b) and (c). The basic timber floor section shown in (b) is normally made up of a series of timber joists acting as the supporting frame connected by nails or screws to chipboard panels for the floor and plasterboard sheets for the ceiling. The internal partition (c) is formed from one or more layers of plasterboard sheet on either side of a timber stud frame also connected by screws or nails.

The average spacing of the timber joists or studs is about 450mm, depending on the span and loading. The nails or screws connecting the floor or partition panels (plates) to the frames are spaced randomly between 100 to 600mm centres. The spacing of these point connections is a principle factor in deciding whether the panels (plates) are point or line connected. Also in structures such as these the nails or screws are spaced randomly along the length of the frame and may or may not be immediately opposite each other on either side of the frame connecting the plates as shown in Figure 4.2.

Therefore this section describes the effect of the spacing of the nails or screws with regards to structure borne sound transmission.

4.3 Review of existing theory

Several authors have examined the problem of plates coupled by points and the types of structures studied are shown in Figure 4.3

Cremer, Heckl and Ungar [44] covered the basic theory relating to point acting sound bridges, (a), by using impedances of the components of the structure. From this the power transmitted from one plate to another could be found. They also studied low and high frequency models, structural parameters of the bridge between the two plates and elastic interlayers.

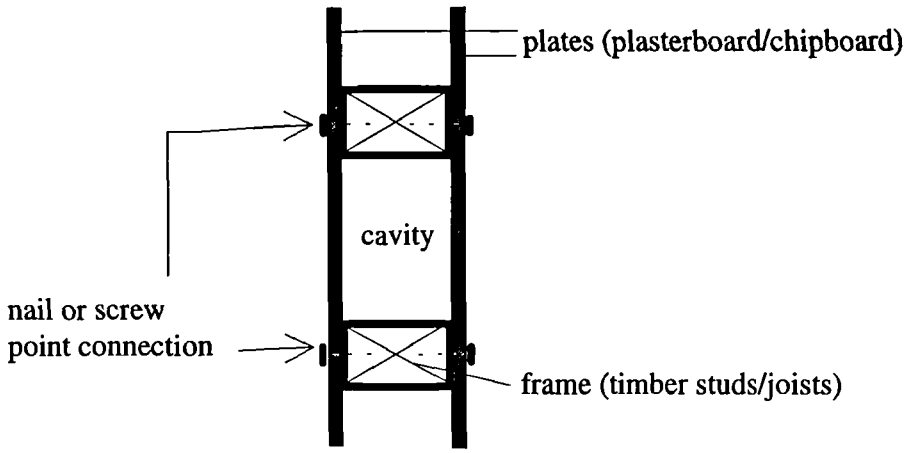

a) Typical method of connection for lightweight parallel plates

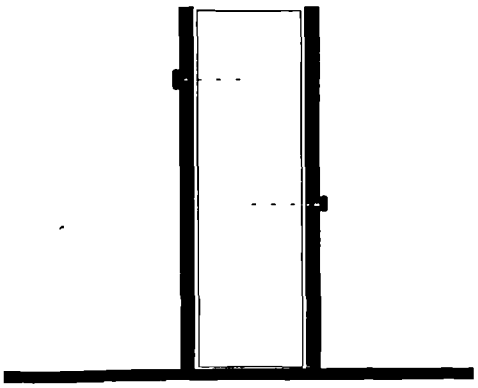

b)Plates coupled by offset point connection

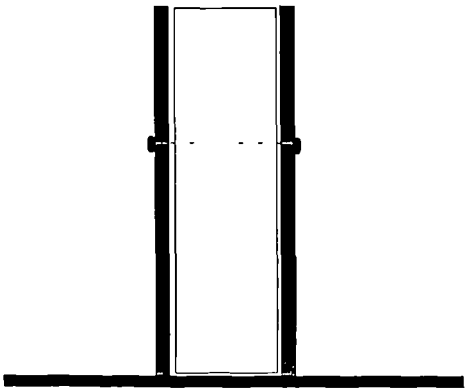

c) Plates coupled by immediate opposite point connection

Figure 4.2 Location of point connections for plate coupling

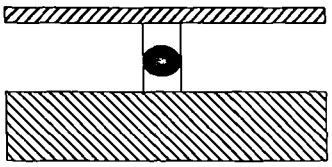

a) Point acting sound bridges
(Cremer)

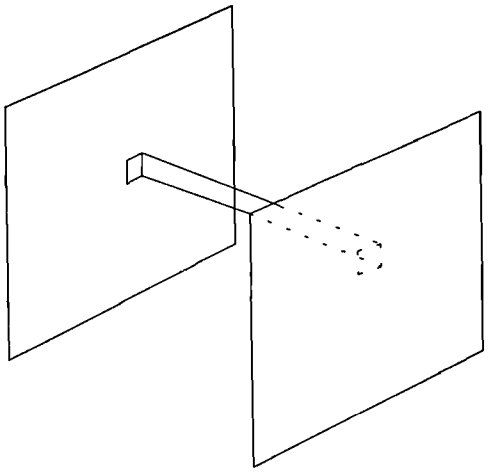

b) Plates connected by a tie beam
(Bhattacharya)

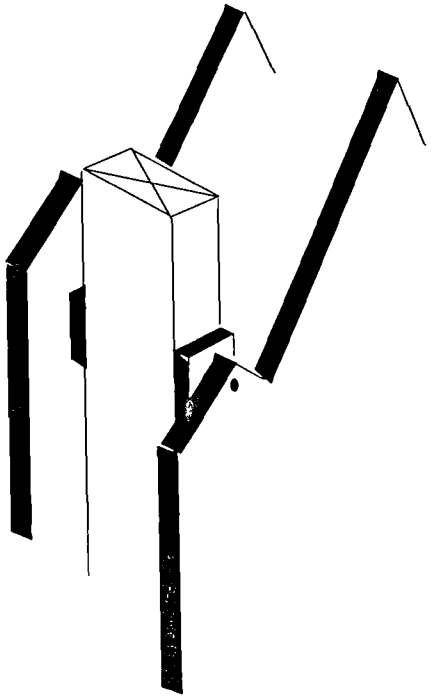

c) Point connection of stud walls
(Sharp)

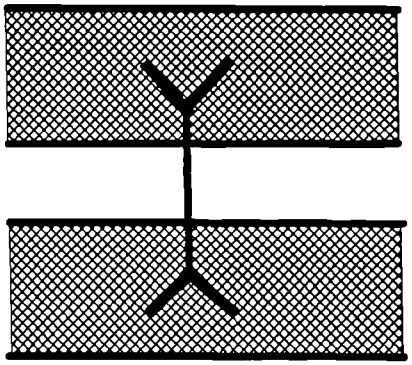

d) Cavity walls connected by wall ties
(Craik),(Wilson)

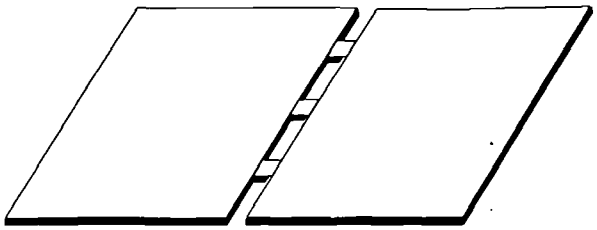

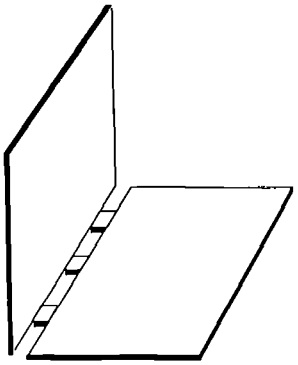

e) Point connected plates
(Bosmans and Vermeir)

Figure 4.3 Types of point connected plate structures studied by previous authors

Bhattacharya *et al* [29] modelled two large plates connected by a tie beam,(b). The majority of the research was in calculating the transmission coefficients between parallel plates coupled by a tie plate. This theory was then adapted to model parallel plates connected by a narrow tie beam. The plate to plate CLF was multiplied by the ratio of the tie width and the plate width along the junction length. This CLF could then be denoted as a plate to tie beam, and using reciprocity, tie beam to plate could also be found. They modelled the tie beam as a subsystem. However, it may not be possible to model these as a subsystem due to the lack of resonant modes. No parametric study was undertaken to see what effect varying the number of ties or varying its properties would have on the coupling.

Sharp [27] also looked at parallel plate structures and in particular stud partitions, (c). He developed an "approximate" method of calculating the overall transmission loss for point connected plates by modification of the mass law. The method of point connection used in the experiments was to mount small timber 'dabs' between plates and frame to ensure point and not line connection. However, this method is very approximate and the extra terms inserted into the equations for transmission loss are not clarified.

Craik [13] used electrical analogues to assist in the determination of point connection CLF's for plates in cavity walls connected by wall ties, (d). Due to the spacing of the ties in cavity walls each tie could be considered independent in its effect in transmission across the cavity. The CLF could be calculated for one tie and the total coupling due to all ties found by simply multiplying by the total number of ties. Also by including the mobility of the tie, (the inverse of impedance), it was possible to find the transmission across the cavity, separating the parallel plates, for different types of cavity ties. Craik also found experimentally and theoretically that the smaller the cross sectional area of the tie the lower the CLF between the two plates.

Wilson [8] carried out substantial measurements on cavity walls varying the number of ties using different designs of wall ties. Using the theory previously researched by Craik [9] an indepth analysis was undertaken resulting in full SEA models for cavity walls with point connections and showing the importance of the transmission path across the ties.

Lyon *et al* [12] and Manning [62] studied vibrational energy flow between point connected structures in the context of SEA. Both authors derived expressions for the coupling loss factor for point connected systems using a mobility function formulation. Lyon *et al* studied two different approaches for point connected structures, the wave approach and the modal approach. Structures studied include multi dimensional subsystems, multiple subsystems at a connection and multi degrees of freedom at a connection. Bosmans and Vermeir [63] more recently have also calculated the transmission between periodically coupled plates. This advanced model, based on the wave approach for elastically coupled semi-infinite plates, calculated the transmission for two plates coupled at a corner, at 90^0 to one another, and two inline plates (e). They found that to model a point connected plate junction at low frequencies by use of a continuous line junction was not always a good approximation. In addition, observations regarding the importance of the spacing and number of point connections agreed with work carried out in the early part of research for this thesis [64].

The work of Cremer *et al*, Lyon *et al*, Craik and Wilson has particular relevance to the study presented in this chapter due to their study of coupling using impedance models. However, none of these authors have carried out a parametric study of the structure and only Craik and Wilson have studied real walls and these were cavity walls, with no connecting frame.

4.4 Theory for coupling of parallel plates at points

In the work by Craik and Wilson [10] coupling loss factors were derived using mobility functions for point connection between two leaves of a cavity wall due to the presence of wall ties. A variety of wall ties were studied with varying degrees of stiffness. In the context of this work the points of connection are formed by screws or nails which are considerably smaller and stiffer than wall ties and are regarded as being infinitely stiff and extremely short in length. Results will be shown later in this chapter to support this assumption. The spacing of the wall ties in cavity walls is quite even over the surface area of the wall, but in lightweight partitions or timber floors the points of connection are concentrated in a specific axial direction where the frame is connected to the plates.

A primary concern when calculating the sound transmission for such structures is when is the connection a point or a line. The spacing of the nails or screws may vary due to the designs and thus the points of contact coupling the plates to the frame may be closer together or further apart. In addition as frequency increases so the plate bending wavelength decreases and thus the frequency range under study is important in terms of whether the structure is line or point connected.

Figure 4.4 shows the boundaries for point and line connection with varying bending wavelength and constant nail spacing. At low frequencies where the bending wavelength is large in comparison with the spacing between the points of connection coupling between the plates may be modelled as a line connection. At higher frequencies where the bending wavelength is small in comparison to the connection spacing the coupling between the plates can be modelled by considering them as independent points. The transition is taken in this work to be where the spacing is ($\lambda_b/2$) which agrees with experimental data and the predicted frequency when this occurs may be given by,

$$f_p = \frac{1.8hC_L}{(2s)^2} \tag{4.1}$$

where h, C_L and s are the plate thickness, longitudinal wavespeed and spacing of the point connections. The addition of more point connections will change the transition frequency f_p where the first half bending wavelength is equal to the spacing between the fixture points, as shown in Figure 4.5. As the spacing distance s and the first half bending wavelength are halved the transition frequency f_p, where the structure changes from being modelled as a line to a point, increases by a factor of 4.

The following section describes the theory of point connection for a timber stud partition with offset or opposite point connections.

Offset point connection

The structure consists of two plates connected to a timber frame by nails and screws and is shown in Figure 4.6. Figure 4.6 also shows the electrical analogue (c) for this structure and the SEA model (d) for the two plates coupled to a beam with offset point connection. In this structure the nails or screws are regarded as offset and not

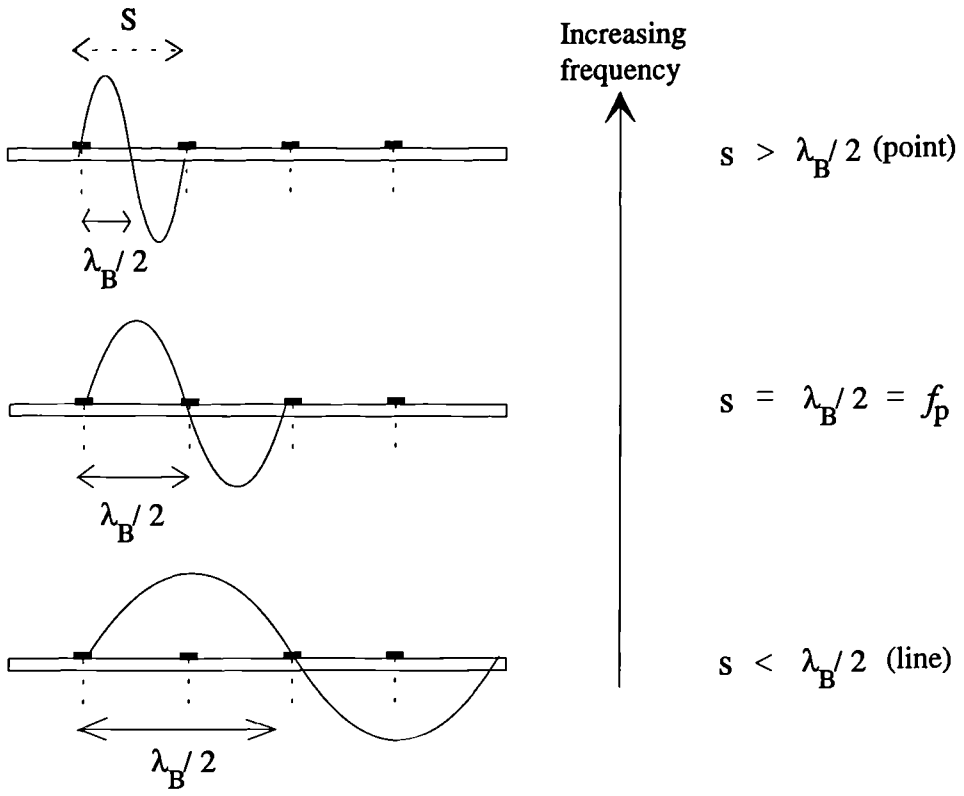

Figure 4.4 Modelling point and line connection with fixed nail spacing and variation in frequency.

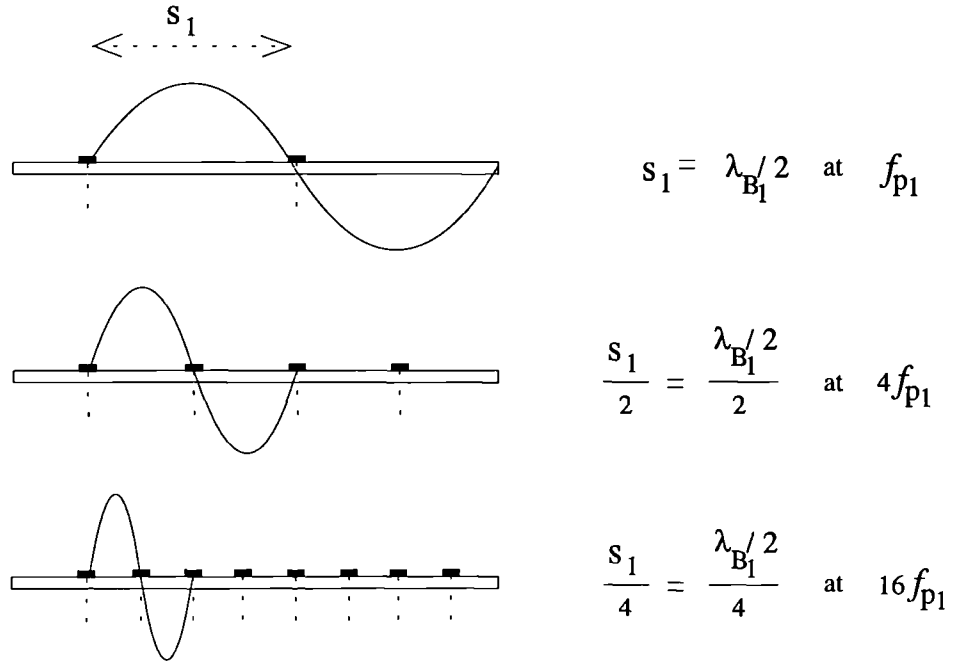

Figure 4.5 Variation of the transition frequency with increasing point connections.

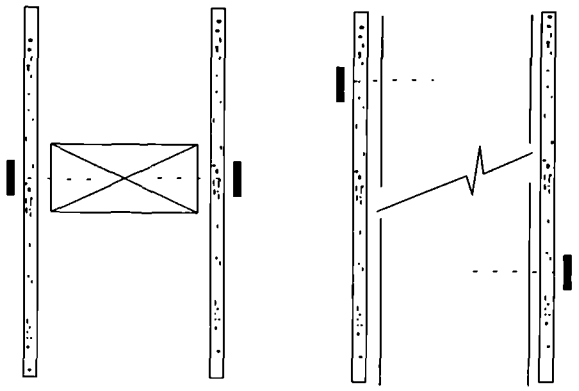

(a) (b)

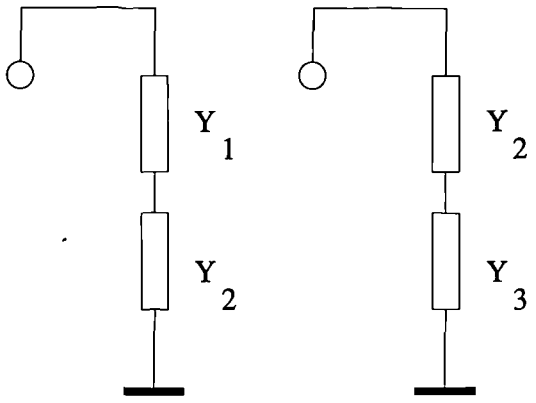

(c)

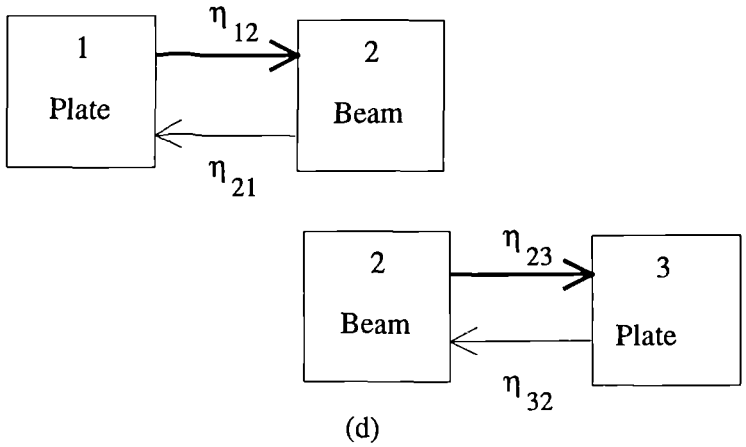

(d)

Figure 4.6 Offset point connections (a) plan, (b) section, (c) electrical circuit analogue, (d) SEA model.

immediately opposite each other and therefore act independently. The mobilities of the two plates and frame are Y_1, Y_3 and Y_2.

The CLF between two subsystems connected by an infinitely stiff connection, can be given by,

$$\eta_{12} = \frac{N \quad Re(Y_2)}{\omega m_1 |Y_1 + Y_2|^2} \tag{4.2}$$

where N is the number of point connections, m_1 is the mass of the source subsystem and Y_1 and Y_2 are the mobilities of the source and receiving subsystems respectively. This can be used to calculate the coupling from a plate to plate, plate to beam or beam to plate. The mobility of a plate at its centre is given by [44],

$$Y_p = \frac{1}{2.3 \rho_s C_L h} \tag{4.3}$$

and the mobility of a beam is [44],

$$Y_b = \frac{1}{2.67 \rho S \sqrt{C_L h f}(1+i)} \tag{4.4}$$

where ρ is the beam density, S is the beam's cross sectional area, C_L is the longitudinal wavespeed and h is the beam depth. Some previous authors have taken the mobility of a plate at its edge which is given by [44],

$$Y_{p(edge)} = \frac{8Y_p}{2.3} \tag{4.5}$$

but for the purpose of the structures studied in this work Equation 4.3 is used.

Immediately opposite point connections

In some cases the structure may be constructed so that the point connections may be immediately opposite each other.

Such a structure is shown in Figure 4.7, including the electrical circuit analogue (c), and the SEA model (d). In this structure coupling can occur between the source plate and beam, and also directly from the source plate to the receiving plate. Thus the CLF is

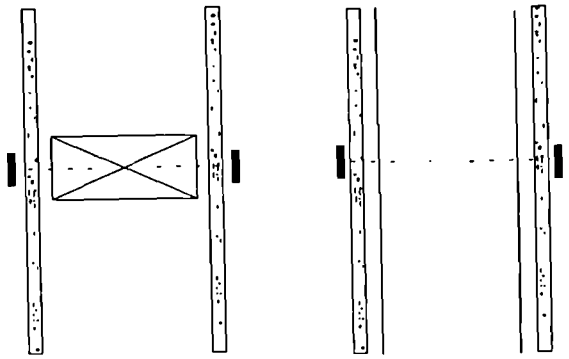

(a) (b)

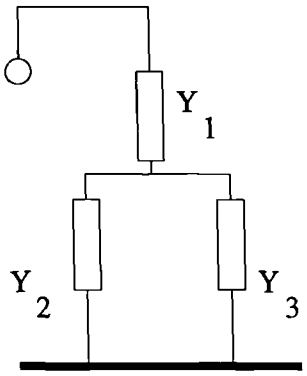

(c)

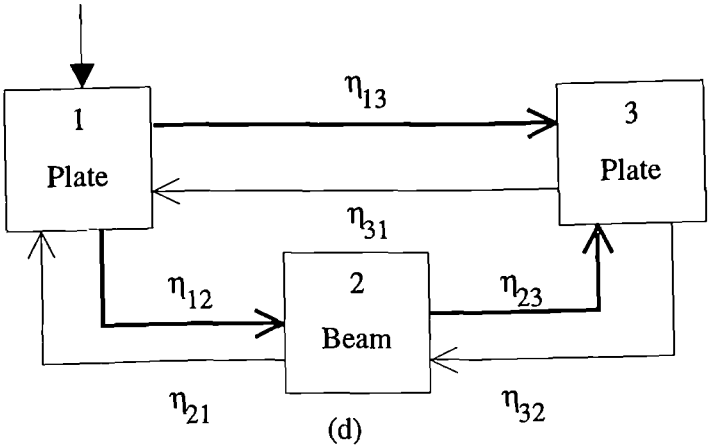

(d)

Figure 4.7 Immediatly opposite point connections (a) plan, (b) section, (c) electrical circuit analogue, (d) SEA model.

affected by the mobility of the beam Y_2 and the mobility of the receiving plate Y_3 and together their mobilities can be represented by Y_e. Thus the total mobility of the receiving plate and beam, Y_e, is given by,

$$\frac{1}{Y_e}=\frac{1}{Y_2}+\frac{1}{Y_3} \tag{4.6}$$

The velocity at the connection point, v_1 is given by,

$$\frac{v_1}{v_0}=\frac{Y_e}{Y_1+Y_e} \tag{4.7}$$

The power transmitted to subsystem (3), plate, or subsystem (2), beam, may be written as,

$$W_{13}=Re\left(\frac{v_2}{Y_3}(v_2^*)\right)=Re\left(\frac{1}{Y_3}\left[\frac{v_0Y_e}{Y_1+Y_e}\right]\left[\frac{v_0Y_e}{Y_1+Y_e}\right]^*\right)=Re\left(\frac{1}{Y_3}\left|\frac{v_0Y_e}{Y_1+Y_e}\right|^2\right) \tag{4.8}$$

Equating Equation 4.8 and the standard equation for power transmitted between two subsystems given by,

$$W_{13}=E_1\omega\eta_{13} \tag{4.9}$$

the coupling loss factor between the source plate and the receiving plate for N number of point connections is given as,

$$\eta_{13}=\frac{N}{m_1\omega}Re\left(\frac{1}{Y_3}\right)\frac{|Y_e|^2}{|Y_1+Y_e|^2} \tag{4.10}$$

4.5 Parametric study of point connected plates

This section describes the predicted changes to the structure borne sound transmission by varying the construction and material parameters for two lightweight parallel plates connected by point connection to a beam (frame).

The SEA model of the system was shown previously in Figure 4.6 and the structure studied is shown in Figure 4.8. There are three subsystems involved, the source plate, the beam and receiving plate. There are four coupling loss factors η_{12}, η_{23} and the reciprocal η_{21} and η_{32}. Each of the subsystems also has an internal loss factor η_{id}. Typical values of the principle material properties of the subsystems are shown in Table 4.1.

Whilst there may be only three subsystems in this SEA model there are a number of parameters which may vary depending on the materials used and the construction. These include:-

- the number of point connections
- the value of the tie stiffness
- the material properties of the beam
- and whether the point connections are offset or opposite.

This section describes each of these parameters using a theoretical SEA model for point connected plates. The subsequent section, section 4.6, compares measured and predicted results for a similar type of structure.

Varying the number of point connections

Using Equation 4.2 it is possible to calculate the change to the coupling loss factor as the number of point connections is varied. Figure 4.9 shows the coupling loss factor from plate to beam and beam to plate with varying number of point connections. It is noticeable that the beam to plate CLF is higher than the plate to beam CLF across the frequency range. This is due to the low impedance of the plate in comparison to the impedance of the beam. The high value for the CLF from the beam to the plate suggests that there is equipartition of modal energy.

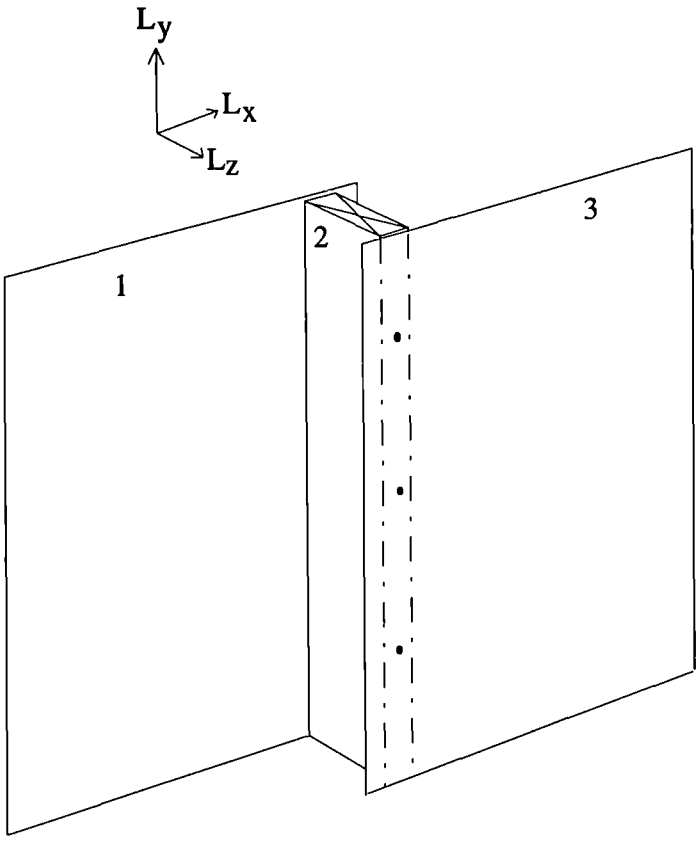

Figure 4.8 Schematic of structure with point connection

Subsystem	Dimensions (m)			Material properties				
	L_x	L_y	L_z	ρ (kg/m^3)	E_a (N/m^2)	E_r (N/m^2)	μ	η_i (ILF)
Plate 1	1.2	1.2	0.0125	793	2.31×10^9	-	0.2	0.01
Frame 2	0.05	1.2	0.1	475	8.21×10^9	1.51×10^8	0.3	0.015
Plate 3	1.2	1.2	0.0125	793	2.31×10^9	-	0.2	0.01

Table 4.1 Material properties of plasterboard plates and timber frame for point connected test structure.

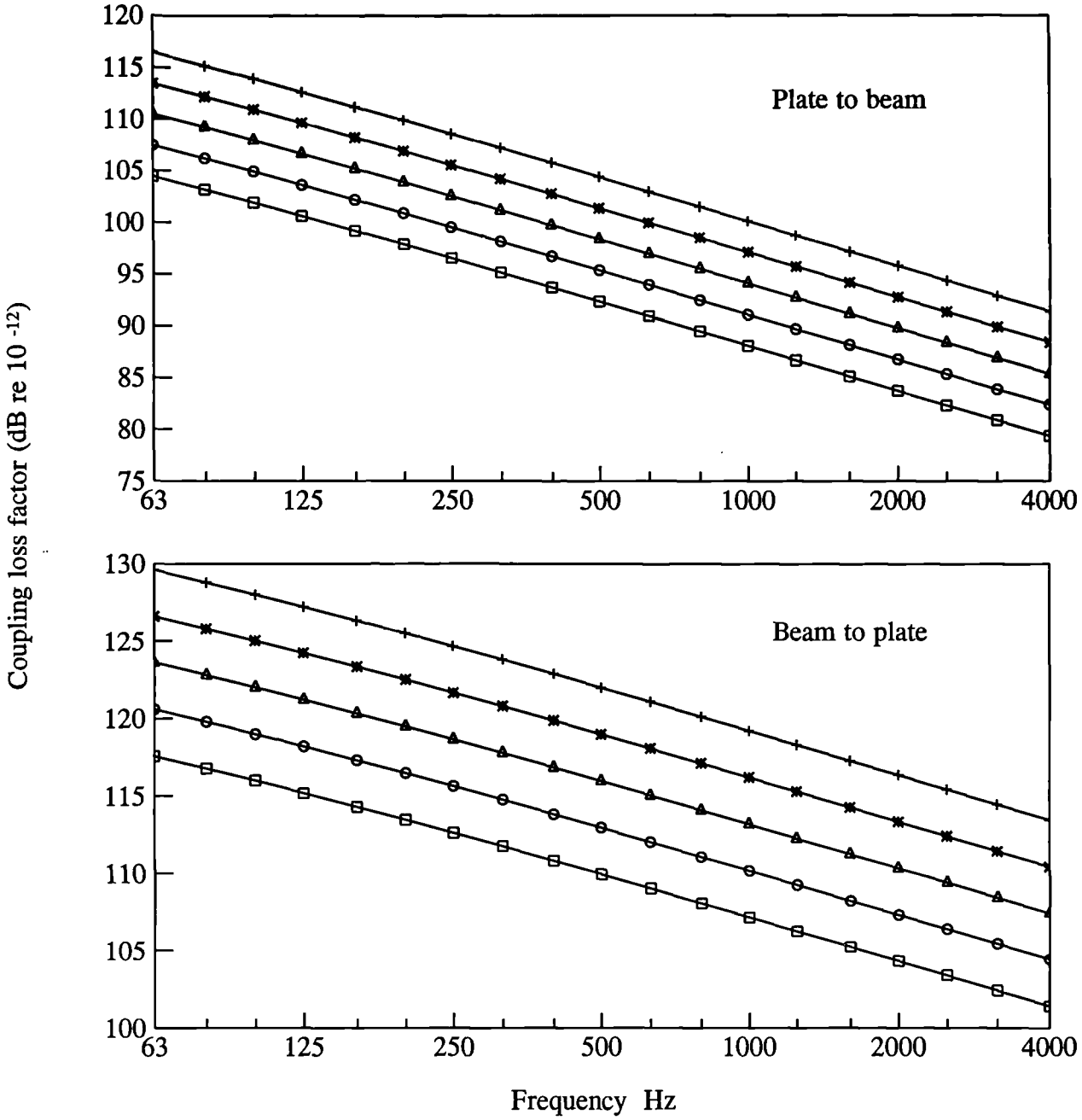

Figure 4.9 Predicted coupling loss factor for plate to beam and beam to plate with varying number of point connections.

Equipartition is where both subsystems have the same modal energy and there is no net power flow between them. As a result, at the low frequencies where the coupling is very strong, the predicted level difference would be unchanged by any increase in the coupling. This is shown in Fig 4.10. As can be seen the level difference at the low frequencies is tending to zero for all number of point connections.

The effect of varying the number of point connections on either side of the frame (beam) connecting the plates can be seen in Figure 4.10, which shows the predicted acceleration level difference between the source and receiving plates. As the frequency increases so the level difference becomes greater and as more point connections are added the level difference becomes smaller with increased coupling.

Varying the stiffness of the ties

There are two methods of point fixture from the plates to the beam either using nails or screws. Generally these two forms of fixture are made of steel or steel alloy which are small in length, about 40mm, and with diameter of several millimetres. Due to their size and separation distance between plate and beam, which is no more than 2mm they can be regarded as being infinitely stiff and extremely short. If the worst case limit was evaluated for a tie of length 2mm and a diameter of 1mm then the tie stiffness, k_t, would be $8.25\text{x}10^7\text{N/m}^2$ computed from [8],

$$k_t = \frac{ES}{L} \tag{4.11}$$

where E, S and L are the Young's modulus, cross sectional area and length of the ties respectively, where the value of E for steel is $2.1\text{x}10^{11}$ N/m^2. Using this value for k_t it is possible to calculate the effect of tie stiffness on the CLF given by [8],

$$\eta_{12} = \frac{N \;\; Re(Y_2)}{\omega m_1 \left| Y_1 + Y_2 + \frac{\omega}{k_t} \right|^2} \tag{4.12}$$

Figure 4.11 shows the acceleration level difference between two point connected plates where the value of k_t is varied from $1\text{x}10^{10}\text{N/m}^2$ to $5\text{x}10^7\text{N/m}^2$. As can be seen in Figure

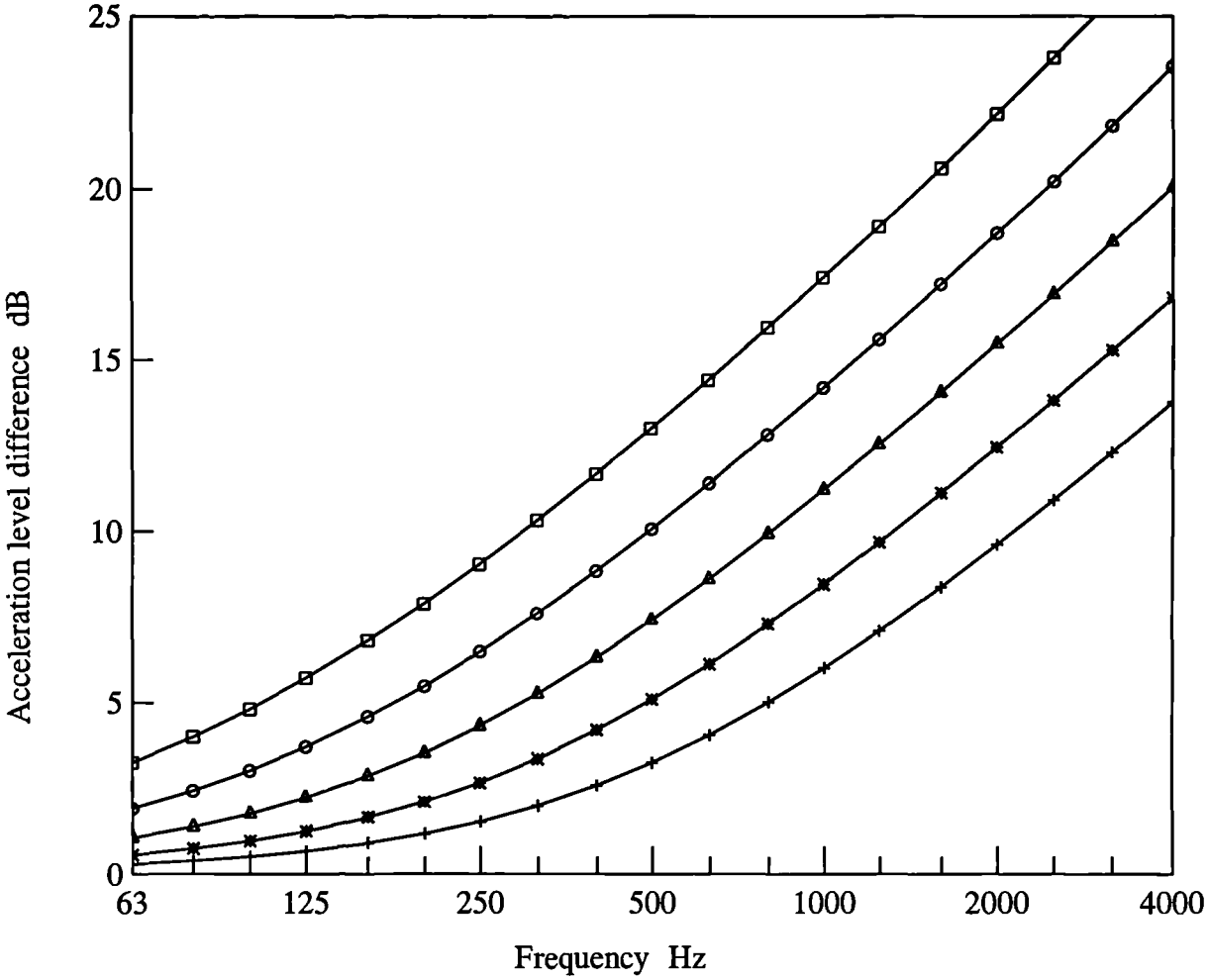

Figure 4.10 Predicted acceleration level difference between the source and receiving plates with varying number of point connections on each plate.

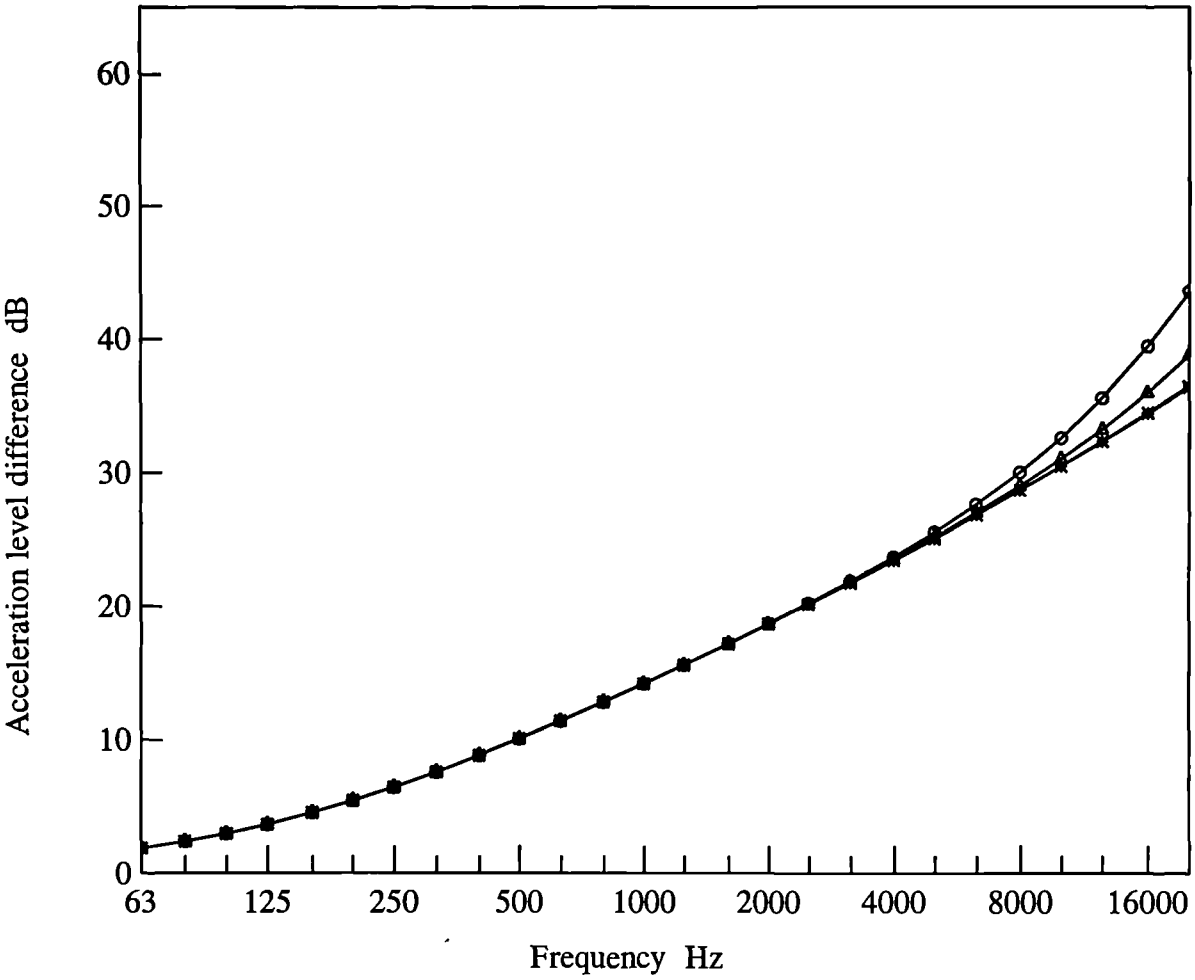

Tie stiffness values (N/m^2)

$1x10^{10}$
$5x10^{9}$
$1x10^{9}$
$5x10^{8}$
$1x10^{8}$
$5x10^{7}$

Figure 4.11 Predicted acceleration level difference between two point connected plates with varying stiffness values.

4.11 the tie stiffness lower limit only slightly affects the transmission at very high frequencies, however this is out with the frequency range of importance in sound transmission in buildings, which is 63Hz to 5KHz. Therefore it is reasonable to assume for this work that the point connections can be regarded as infinitely stiff.

Varying the properties of the beam

The key properties of the beam which can affect the transmission between the two plates are the beam depth, width, density, and Young's modulus. The plate damping may also be a variable factor but for this work the measured values were always used and are shown in Table 4.1.

The depth of a timber stud partition can vary from 50mm to 200mm. Figures 4.12 and 4.13 show the predicted acceleration level difference for two point connected plates where the depth or width of the beam is varied.

As the parameters are increased so the impedance of the beam becomes greater and the coupling loss factor decreases resulting in weaker transmission. Noticeably as these values increase by the same increment the marginal weakening in coupling decreases each time.

Figures 4.14 and 4.15 show the change in level difference as the density and Young's modulus are changed. Increasing these parameters increases the acceleration level difference. At the low frequencies any change in the parameters has a small effect to the acceleration level difference than at the high frequencies.

Comparison of predicted results for offset and opposite point connections

As previously discussed the point connections in lightweight parallel plates may be directly opposite or offset. The two theories presented in section 4.4 are compared in Figure 4.16. As expected the opposite point connection theory shows stronger coupling between the parallel plates and a lower acceleration level difference than the predicted offset results. However, the increase in coupling from offset to opposite point connection at 500Hz is only 0.8dB, which is an insignificant increase in transmission.

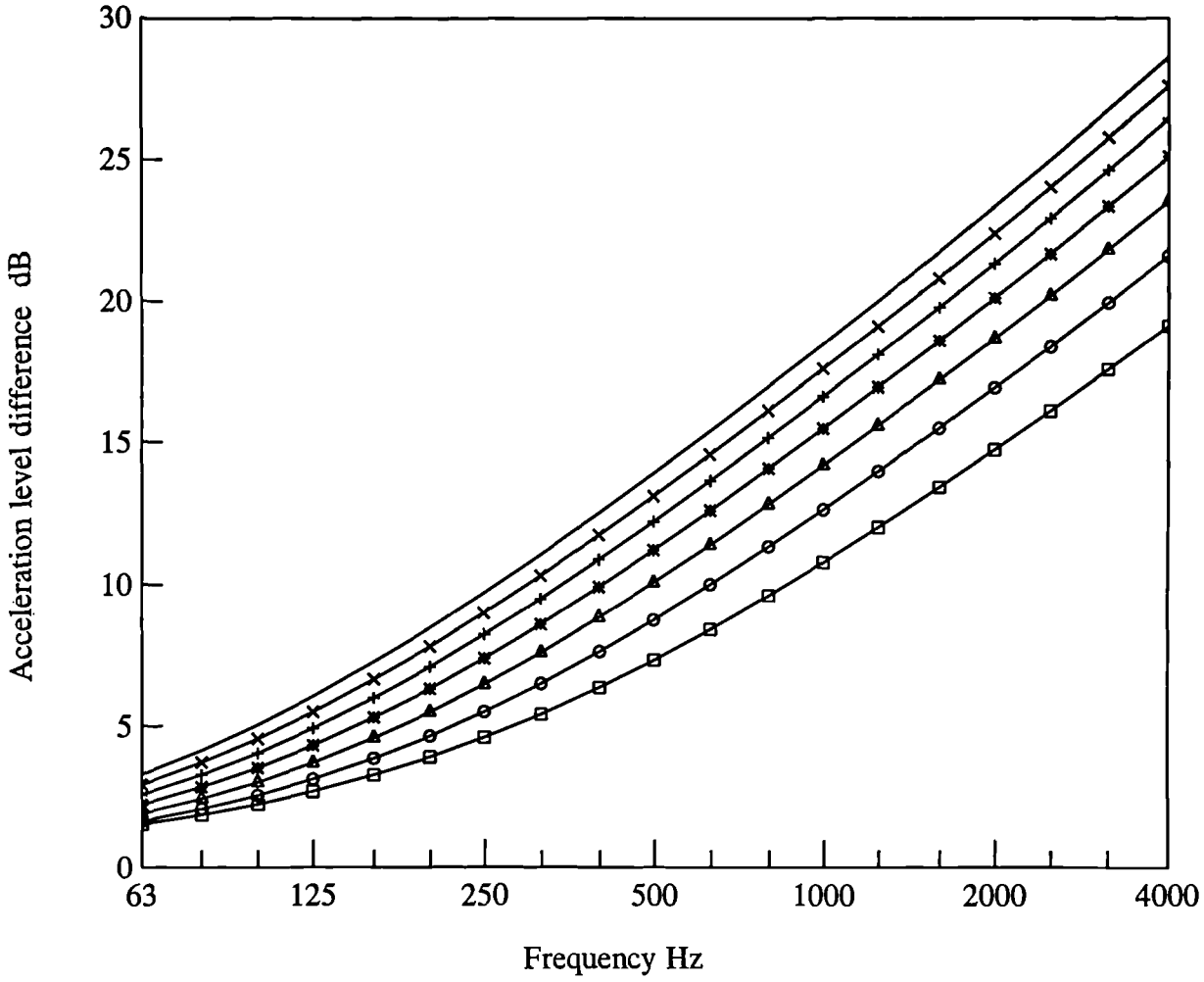

Figure 4.12 Predicted acceleration level difference for two point connected plates with varying depth.

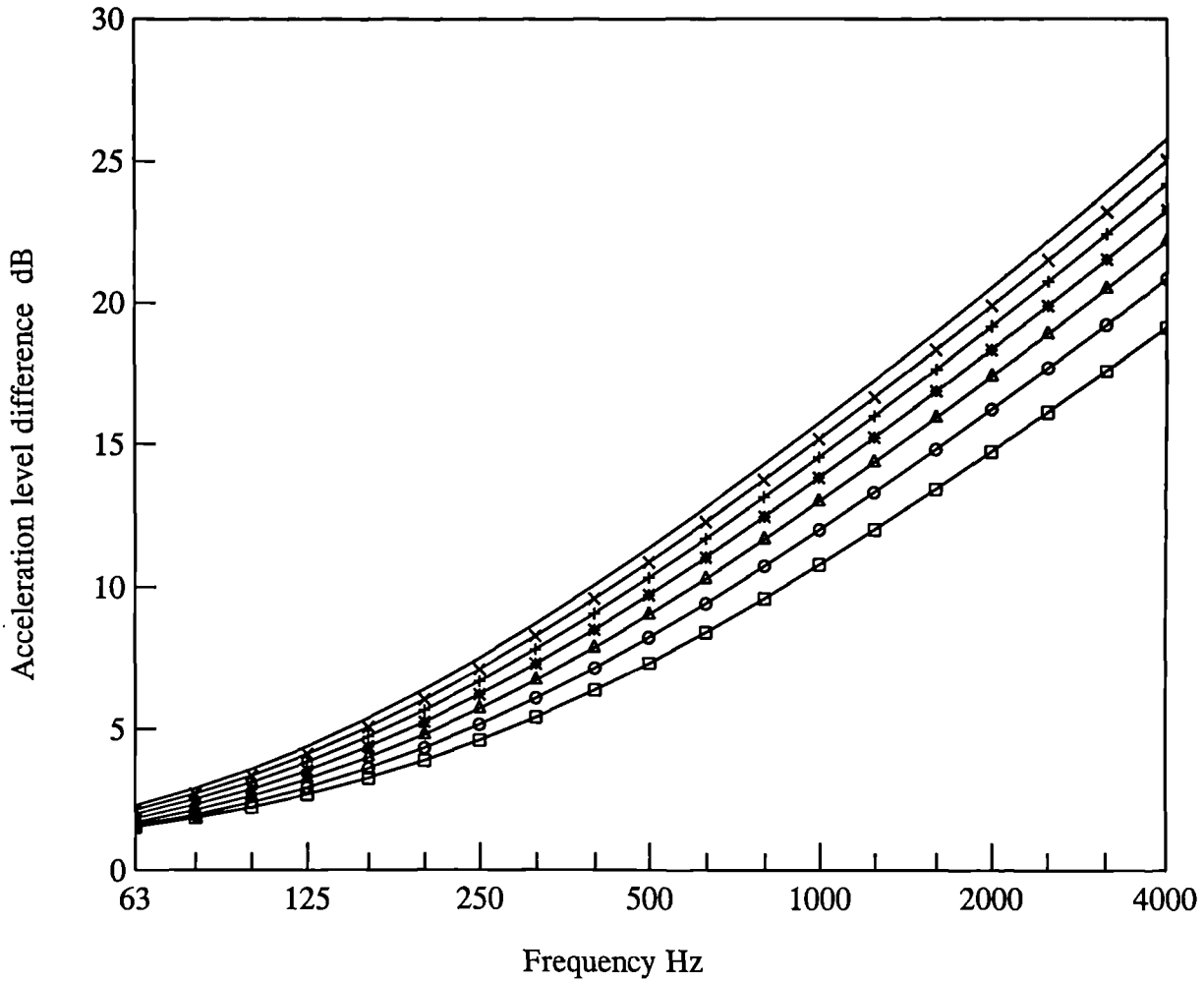

Figure 4.13 Predicted acceleration level difference for two point connected plates with varying width.

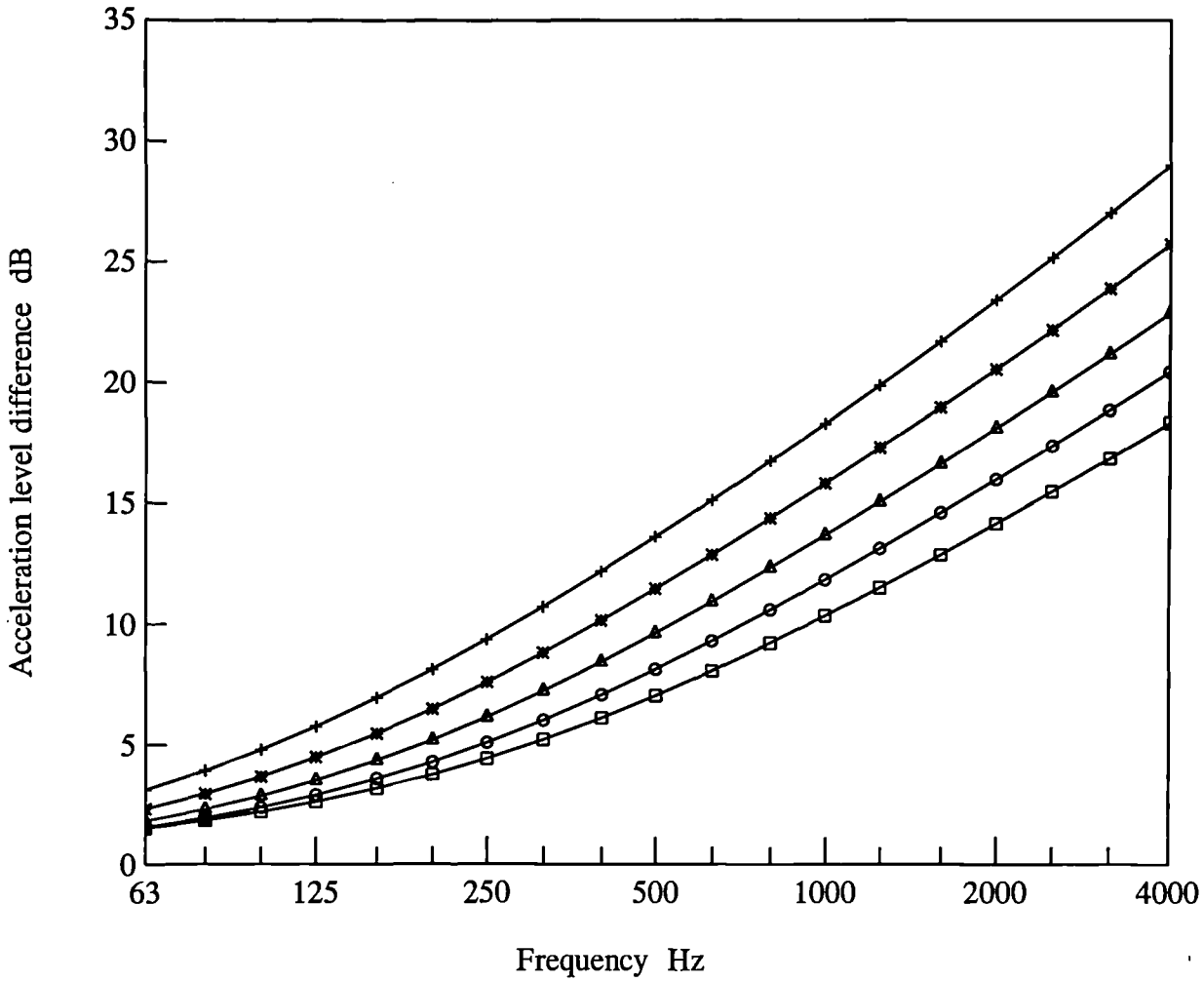

Figure 4.14 Predicted acceleration level difference for two point connected plates with varying beam density.

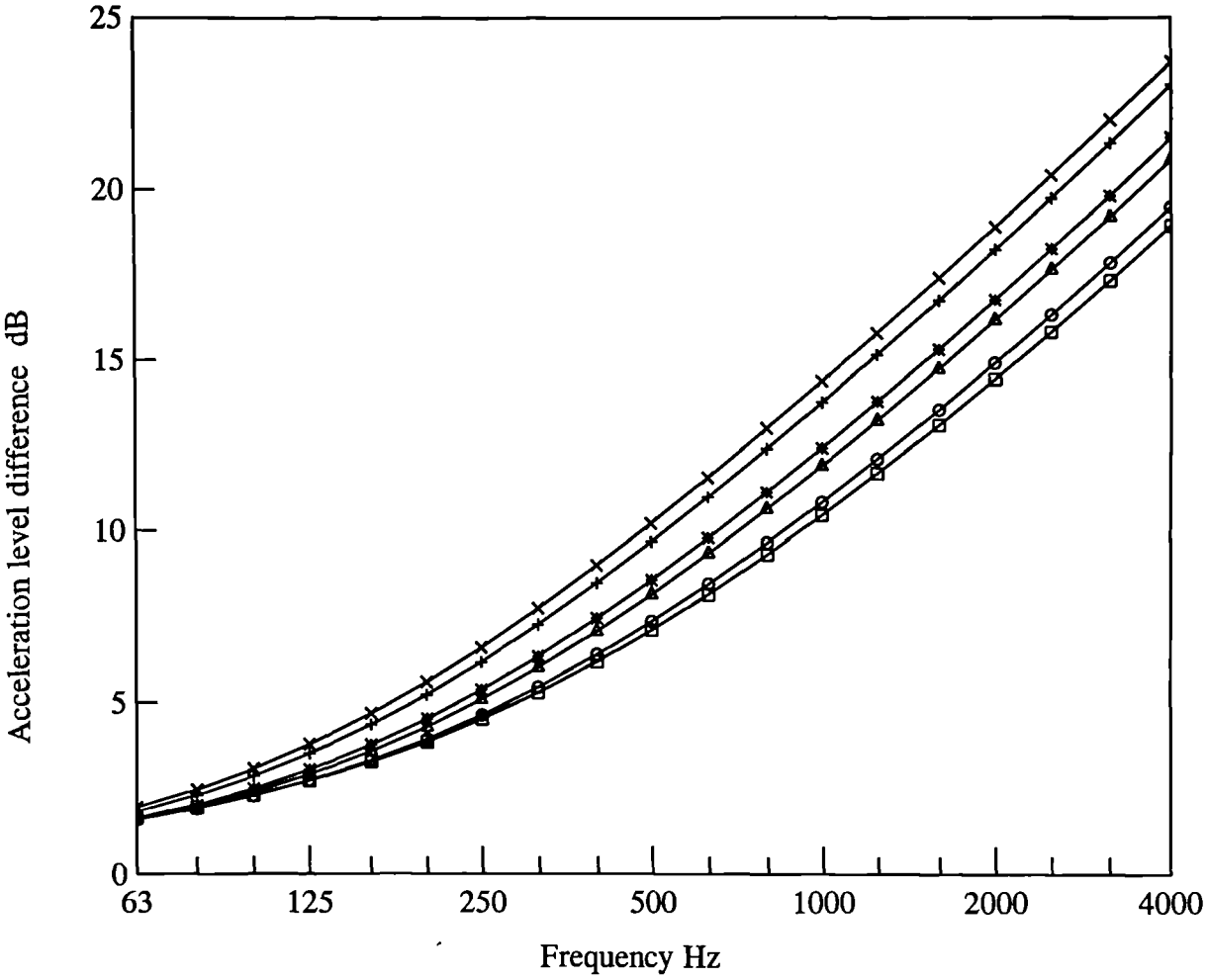

Figure 4.15 Predicted acceleration level difference for two point connected plates with varying beam Young modulus.

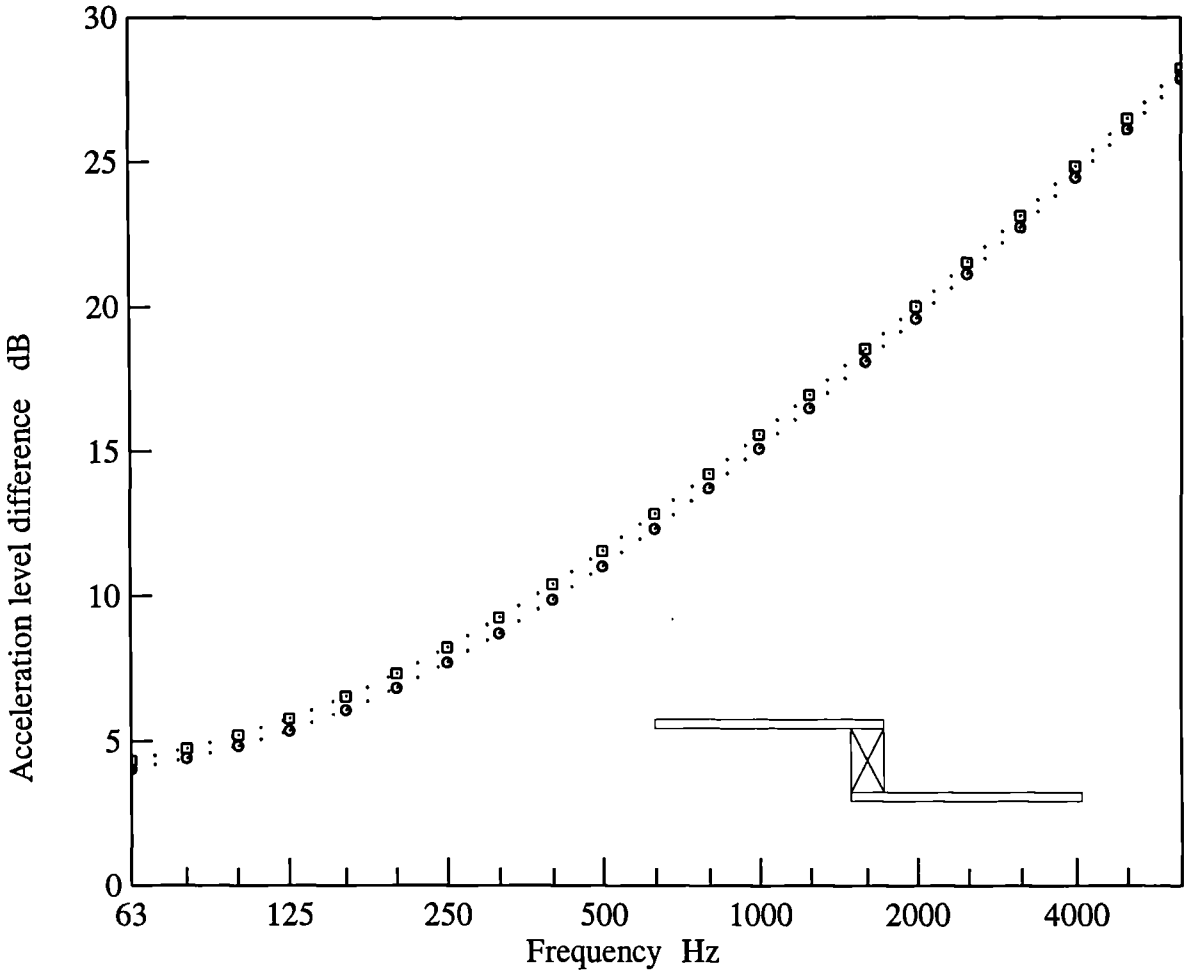

. . □ . . . . . predicted offset
. . o . . . . . predicted opposite

Figure 4.16 Comparison of predicted acceleration level difference for opposite and offset point connections.

4.6 Comparison of measured and predicted results for point coupled plates

This section compares measured and predicted results for the test structure shown in Figure 4.17. using the previous theory for offset point connected plates. Chapter 8 describes the measured and predicted results for point connected full scale double walls.

The test structure was suspended in an anechoic chamber to reduce sound being radiated from any surrounding surfaces. The SEA model of the test structure is similar to that shown in Figure 4.6 using offset point connections. Structure borne excitation was by an acoustic hammer on the source plate (subsystem 1) and the acceleration level difference was measured between the two plates (subsystems 1 and 3). The points of fixture connecting the plates to the beam were 30mm steel screws and the subsystem material properties are shown in Table 4.2.

Comparison of offset and opposite point coupling

Measurements were carried out on the test structure shown in Figure 4.17, to compare offset and opposite point connections, using 8 screws coupling each plate to the beam. The measured and predicted results for these two methods of coupling are shown in Figure 4.18 and the material properties in Table 4.2.

In the frequency range 200Hz to 500Hz there is a slight difference in the measured results. This may be due to several factors including the cut of the grain in the timber, the presence of knots and flaws in the beam where the point connections are attached, and the orthotropic properties of the wood. There is generally good agreement between the measured and predicted results. As was shown in Fig 4.16 there is very little difference between the predicted offset and opposite point connection transmission loss and the measured results shown in Fig 4.18 support this.

Number of point connections

A test was carried out by varying the number of point connections on the test structure shown in Figure 4.17 for 3,7 and 15 screws coupling each plate to the beam. As more screws are added along a finite length so the spacing between each point will decrease.

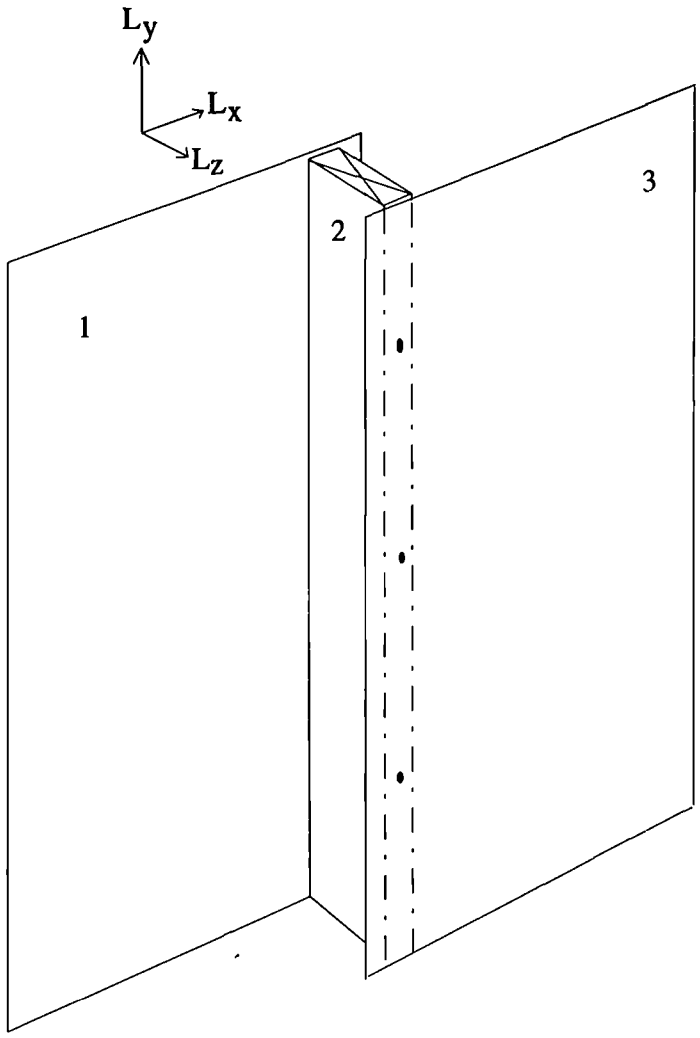

Figure 4.17 Schematic of test structure with point connection

Subsystem	Dimensions (m)			Material properties				
	L_x	L_y	L_z	ρ (kg/m^3)	E_a (N/m^2)	E_r (N/m^2)	μ	η_i (ILF)
Plate 1	1.17	2.4	0.009	801	2.31×10^9	-	0.2	0.01
Frame 2	0.045	2.4	0.075	475	8.21×10^9	1.51×10^8	0.3	0.015
Plate 3	1.17	2.4	0.0125	793	2.31×10^9	-	0.2	0.01

Table 4.2 Material properties of plasterboard plates and timber frame for point connected test structure.

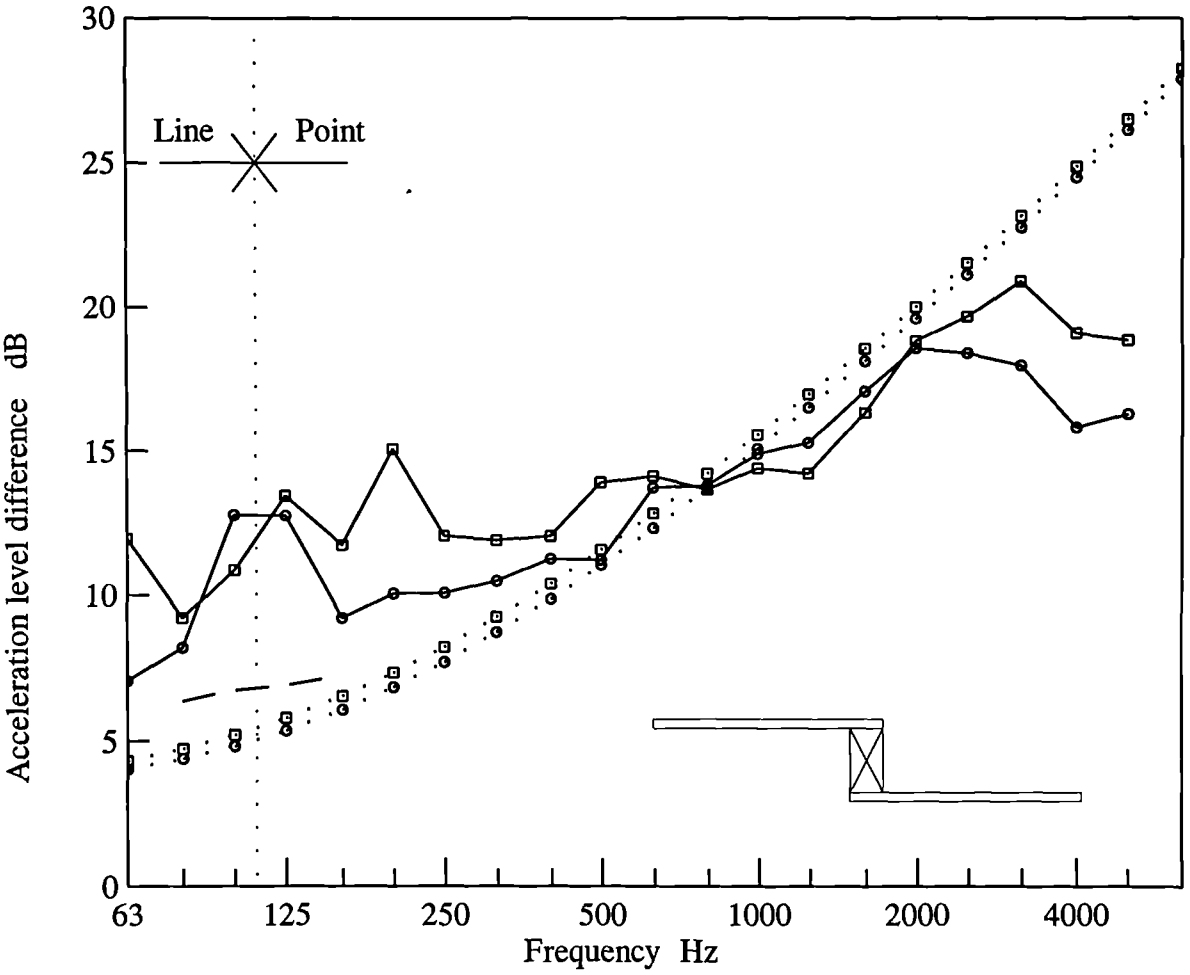

predicted offset
predicted opposite
measured offset
measured opposite

transition frequency
predicted line model

Figure 4.18 Comparison of measured and predicted acceleration level difference for opposite and offset point connections.

Figure 4.19 shows the measured results of varying the number of screws attaching the plates to the beam. As the number of screws increase so the coupling and transmission increases resulting in a reduced level difference between the plates.

A comparison of the measured and predicted acceleration level difference is shown in Figure 4.20. For a 2.4m length junction with 3 screws equally positioned at 600mm centres the first half bending wavelength would fit between the points at a frequency of 28Hz. This is out with the frequency range of interest. However, if the distance between the point connections was halved by adding more screws, (to 7), the first half bending wavelength would fit between the fixture points at 112Hz and for 15 screws to 448Hz.

At frequencies below f_p the junction behaves as a line connection, and above this frequency it behaves as a series of points. The total loss factor of the plates was calculated by measuring the internal loss factor of the plates and adding the coupling loss factors. Figure 4.20 shows good agreement between the measured and predicted results.

4.7 Discussion

The construction of internal partitions and timber floors in the U.K. are subject to the Building Regulations[1,2] and the British Standards. In the design of such structures factors to be considered include strength and stability, load and span, fire resistance and fire protection, handling requirements, service penetrations and sound insulation. The spacing of point connection fixtures is stipulated in the British Standards [16,17] primarily for strength and stability factors but no mention is made of the effect to sound insulation.

The spacings distances, for nails conforming to BS 1202 [65] and screws conforming to BS 1210 [66], in such structures are specified as 'maximum' spacings. BS 5234 Code of Practice for *'Dry lining partitioning using gypsum plasterboard'* [16] specifies that the maximum distance for nails should be 150mm and for screws 300mm. The primary reason for the nails being closer together is because the nails have a weaker mechanical coupling to the frame than the screws.

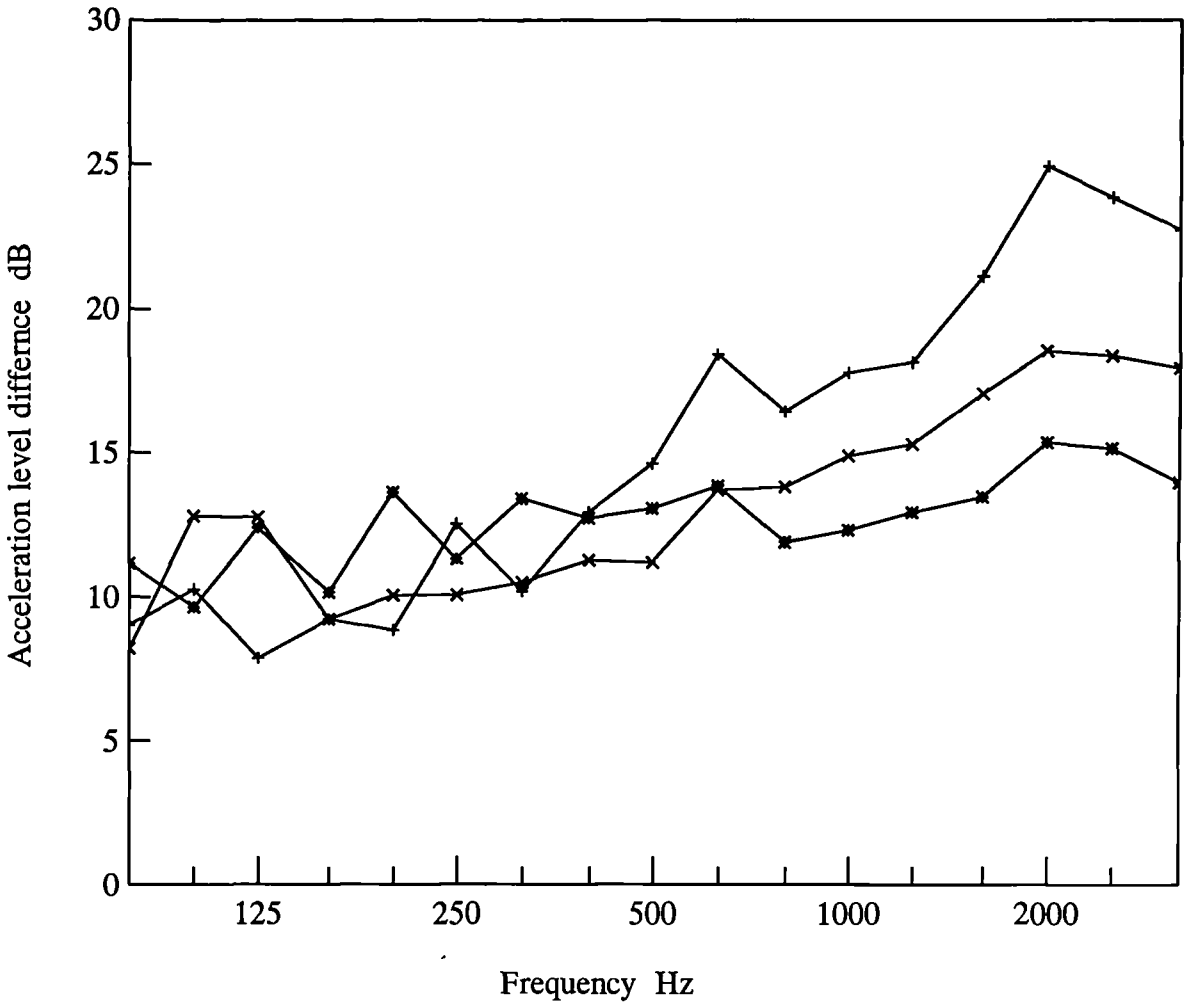

Figure 4.19 Measured acceleration level difference between two point connected plates with varying number of fixture points.

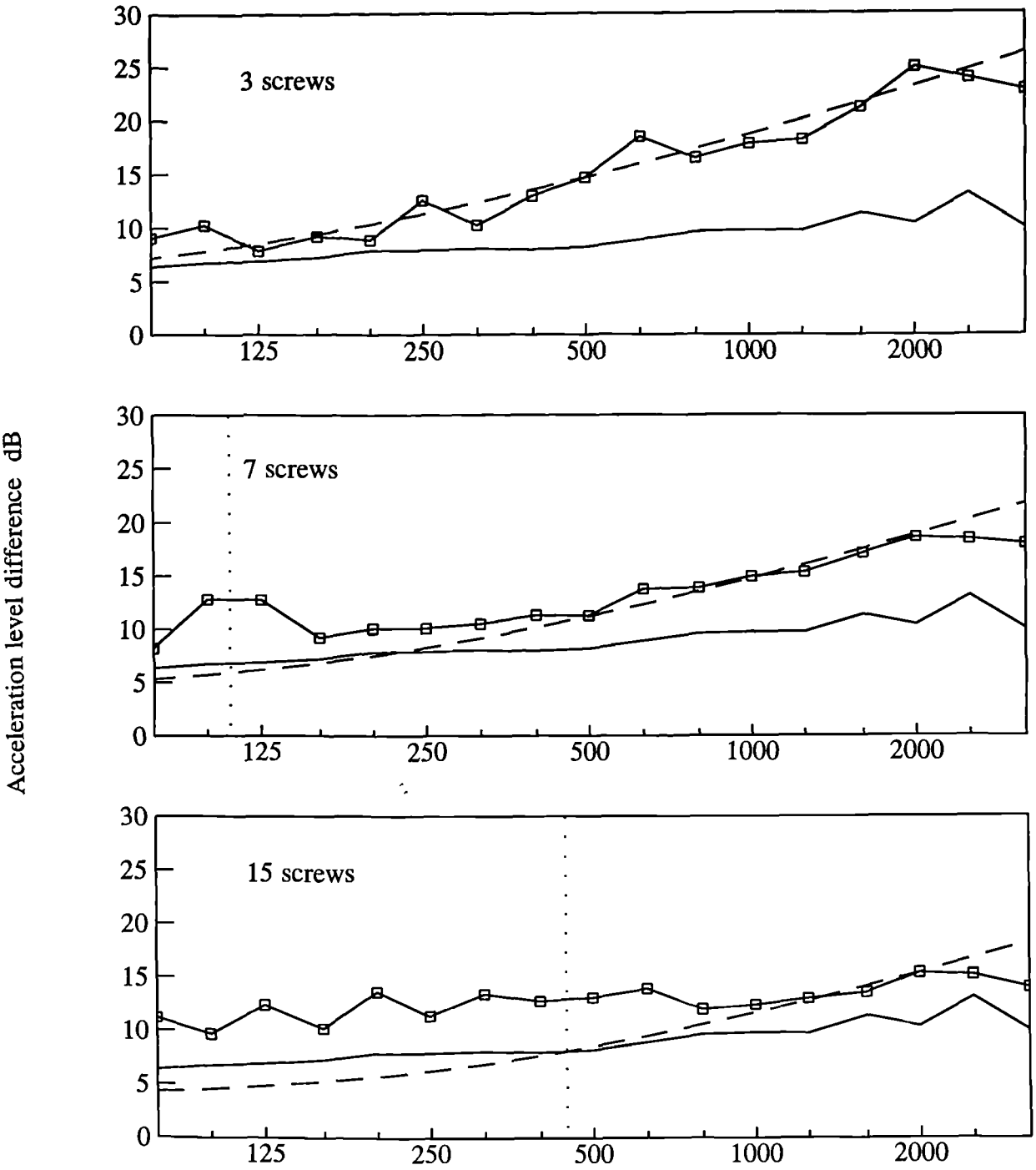

Figure 4.20 Comparison of measured and predicted acceleration level difference for two plates coupled with varying number of point connections

For a nail spacing of 150mm or a screw spacing of 300mm in a standard plasterboard partition the first half bending wavelength will fit between the points of contact at 425Hz and 106Hz respectively. Subsequently using nails rather than screws in drywall partitions will increase the transition frequency f_p and thus the behaviour of the connection will be similar to a line over a larger frequency range. This can only result in stronger sound transmission through the structural path and overall increase sound transmission to the receiving room and reduce the sound insulation properties of the wall. Although the screws specified in BS 1210 will be of a slightly increased diameter than nails, as has been shown in the parametric study of tie stiffness this increase will not affect the acceleration level difference between two plates. Hence the use of screws at larger spacings would be a more preferable option for reducing sound transmission.

In the case of timber floors BS 8103 [67] specifies smaller spacing of nails than screws. The spacing of nails and screws for plywood flooring to the joists is 150mm and 300mm respectively. For plasterboard ceilings fastened to the underside of the joists the nail spacing should be a maximum of 150mm and 230mm for screws. The closer spacing of the nails for 22mm thick plywood boards with a longitudinal wavespeed of 2134m/s will result in a transition frequency between line and point connection at approximately 720Hz in comparison to 180Hz for screw fixings. Thus the behaviour of the connection will be similar to a line for an even greater frequency range for nail fixings.

Although regulations clearly specify the fixing spacing unfortunately the difference between what is specified and what is constructed on site can be quite large.

4.8 Conclusions

The predicted results using the offset point theory has shown to give good agreement with the measured results. The measured results suggest the transition frequency f_p, where connection behaviour changes from a line to a point, can be approximated to $\lambda_b/2$. Increasing the depth or width of the frame will result in weaker sound transmission through the frame. Due to design restrictions it may be easier to increase the width of the frame to reduce sound transmission in the structural paths than to increase the depth and reduce the overall dimensions of the rooms by increasing the thickness of the walls.

The point connections which couple the plates to the frame may be regarded as infinitely stiff and infinitely short. The use of offset or opposite point connections in a partition appears to make very little difference to the structural sound transmission path across a timber frame. A suggestion of further work in this area would be to carry out tests on offset or opposite point connections using an isotropic material such as steel.

Increasing the number of point connections can increase the sound transmission by 3dB per doubling of connections. Also changing the spacing of the fixings will result in the structure behaving similar to a line connection for a greater frequency range which can only reduce the overall sound insulation of the structure.

Chapter 5

Transmission Between Parallel Plates with Line Connection

5.1 Introduction

This chapter examines the transmission that occurs in another important group of joints in parallel plate structures, that of line connected parallel plates. These structures are formed from two parallel plates coupled by a frame or bridging element which can allow the transmission of structure borne sound between the two plates. In buildings these are found where there is a continuous line connection perpendicular to two plates, of which the fixing may be by glue or screws/nails such as in stud partitions and timber floors. Although the fixings may be by screws or nails, as mentioned previously in chapter 4, if the bending wavelengths of the plates are larger than the spacing of the points then it may be assumed that a line connection is formed.

Other structures to which this work is applicable include aerospace and flight vehicles, both fixed wing and rotary wing. The close spacing of rivets in such structures, which may be spaced from 10mm to 30mm, results in a 'weld' like line connection coupling the plates.

In the case of partitions, as shown in Fig 5.1, the lightweight parallel plate structure presents a variety of interesting structure configurations to be studied. Apart from the 'H' shape structure, there are the jambs where the partitions connect to doors and windows and coupling to masonry walls. For these types of structures some of the plates may be omitted and this must be accounted for when considering the development of any theory.

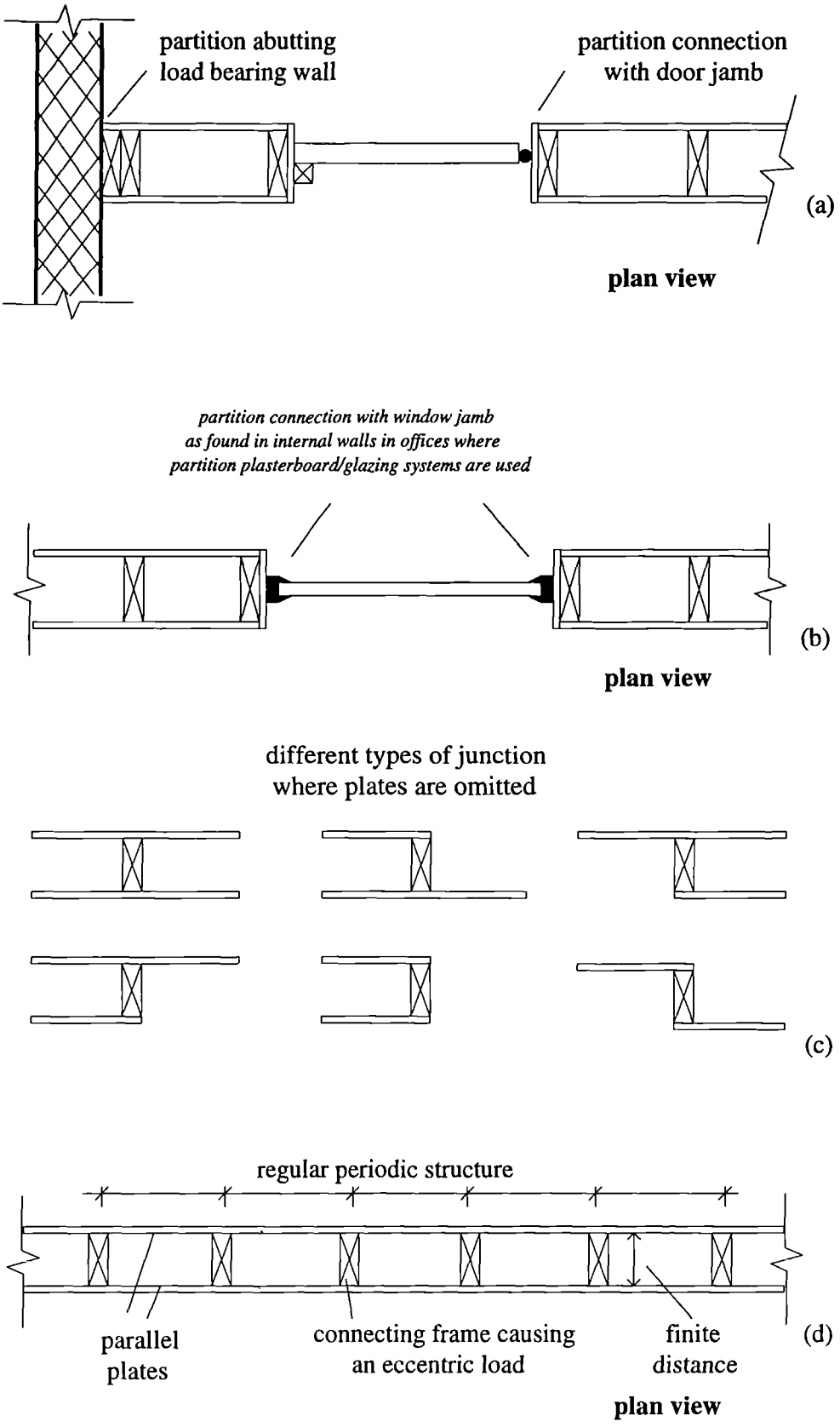

Figure 5.1 Different structure configurations for lightweight parallel plates

The frame in plasterboard partitions is generally the principle structural support and as such it can create an eccentric mass attached to the plates. The fact that the frame studs must be attached at regular centres of 400 to 600mm results in a periodic structure with multiple plates and ribs (frames).

This chapter is divided into three sections. The first section reviews existing work carried out by previous authors which is relevant to parallel plate structures with a line connection.

Section two describes two theoretical models to predict line connection between parallel plates. Both models use wave theory and analyse bending, longitudinal and transverse wave motion for random incidence. The first model assumes the frame connecting element to be a beam and the second model assumes the frame to be a finite plate. A third model is also briefly presented in section two which involves modelling the frame as an SEA subsystem and divides the 'H' structure into two 'T' junctions.

Section three compares the various theoretical models discussed in section two and presents a parametric study where the frame is modelled as a finite plate.

Detailed measured and predicted results for standard 'H' joint structures are shown in chapter 6, when the effects of omitting various plates and changing the finite distance between the parallel plates are also discussed.

5.2 Review of Existing Theory

The prediction of structure borne sound transmission for line connected semi-infinite plate structures has been studied by numerous authors. Whilst some authors have concentrated on complex cross junctions and the behaviour of bending and longitudinal wave motion and the application of such studies to other structures, very few authors have studied structure borne sound transmission between parallel plates (double walls). This section is divided into two parts, past work relating to the basic theory and past work which is specific to double walls.

Previous work by past authors on line connection

The following section describes the principal work by previous authors regarding general wave model studies. Although these works are not specifically on double walls the theory and findings are relevant to this study and are given due mention.

Cremer, Heckl and Ungar [44] were the principle authors in the advancing of studies for line connected semi-infinite plate structures and investigated bending and longitudinal wave transmission. The structures studied included inline plates and 'L' junctions as shown Figs 5.2 to 5.5. The effects of blocking masses, eccentric ribs or masses were also studied. Ungar [68] described in detail the transmission of flexural waves through a reinforcing beam attached to plates as would be found in flight vehicle structures and the importance of the beam's torsional and flexural properties. Both Cremer's early work [69] and Ungar's work investigated infinite and semi-infinite plate/beam systems showing the effect of the coincidence phenomena, which causes an unattenuated propagation of plane bending waves when impinging at certain angles on the beam. In the case of Heckl's work [70] this was extended to consider finite plate/beam systems and in more detail, random incidence.

Cremer, in chapter 5 of Cremer *et al* [44], describes the importance of the coupling between bending and longitudinal waves with regard to eccentric and non-eccentric blocking masses. From previous work by Muller [71], and electrical circuit analogues by Wigge [72] equations were given for the transmission and attenuation of longitudinal waves particularly for "longitudinal periodic systems" where a beam has periodic changes in the cross section. The theory presented for the attenuation of bending waves was found to be in good agreement with measured data after the first blocking mass. However the acceleration levels measured and predicted after subsequent blocking masses did not compare as well and it was found that the flanking paths, consisting of secondary longitudinal waves which in turn convert into tertiary bending waves, dominate the acceleration levels produced after these subsequent masses.

In the case of two dimensional configurations such as plates the agreement between the idealised one dimensional beam analysis results and measured results was much worse due to the waves impinging at the junction at oblique angles. Cremer *et al* [44] also

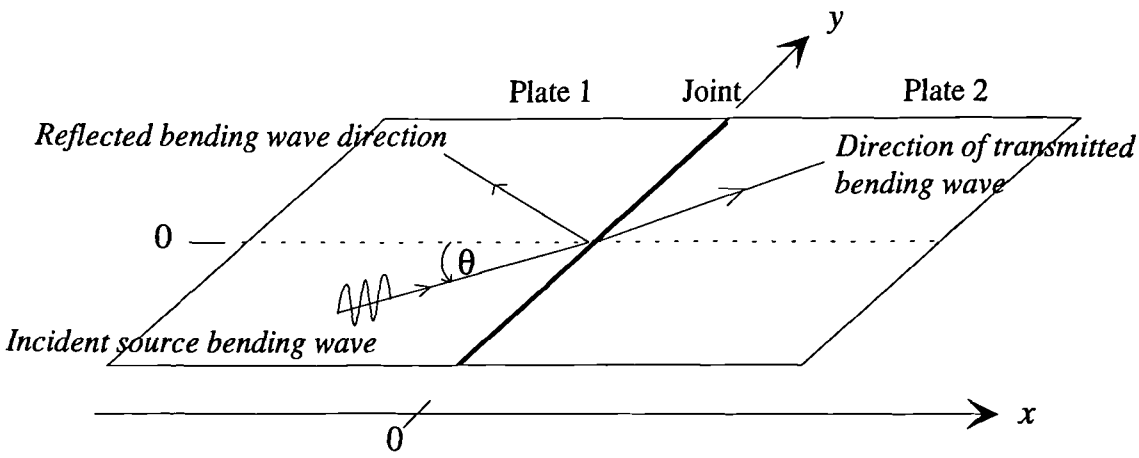

Figure 5.2 Bending wave incident at a joint between two inline plates showing the reflected and transmitted bending waves.

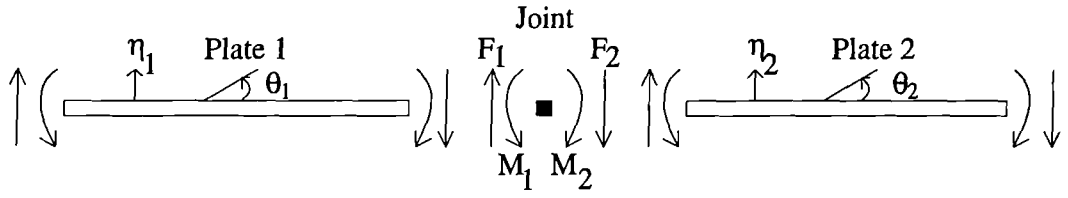

Figure 5.3 Plate configuration and resultant moments and forces for structure in figure 5.2.

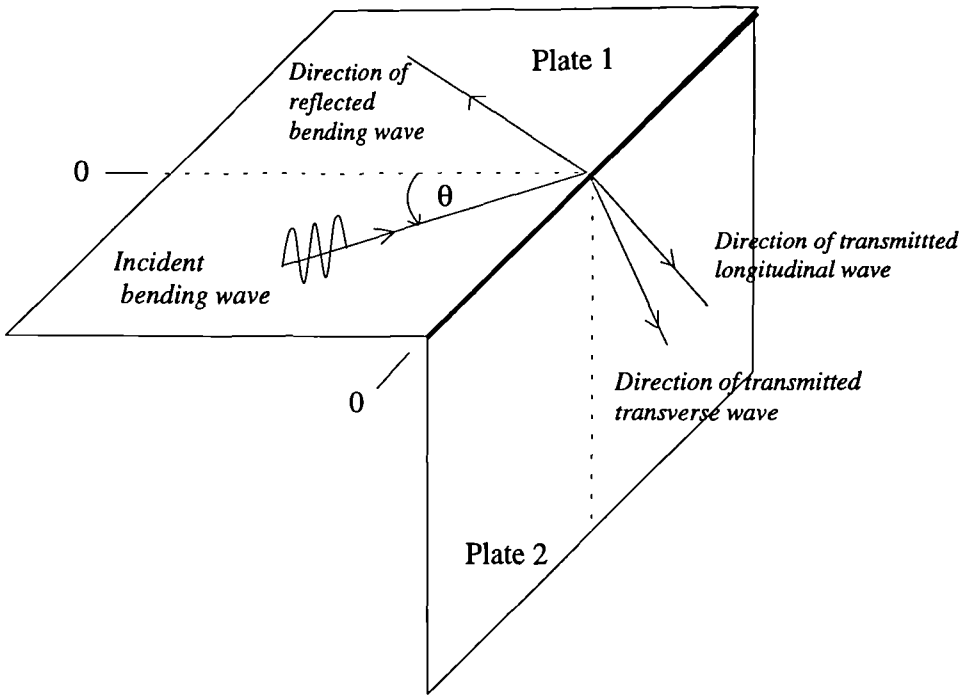

Figure 5.4 Transfer from a bending wave to inplane waves at a corner junction.

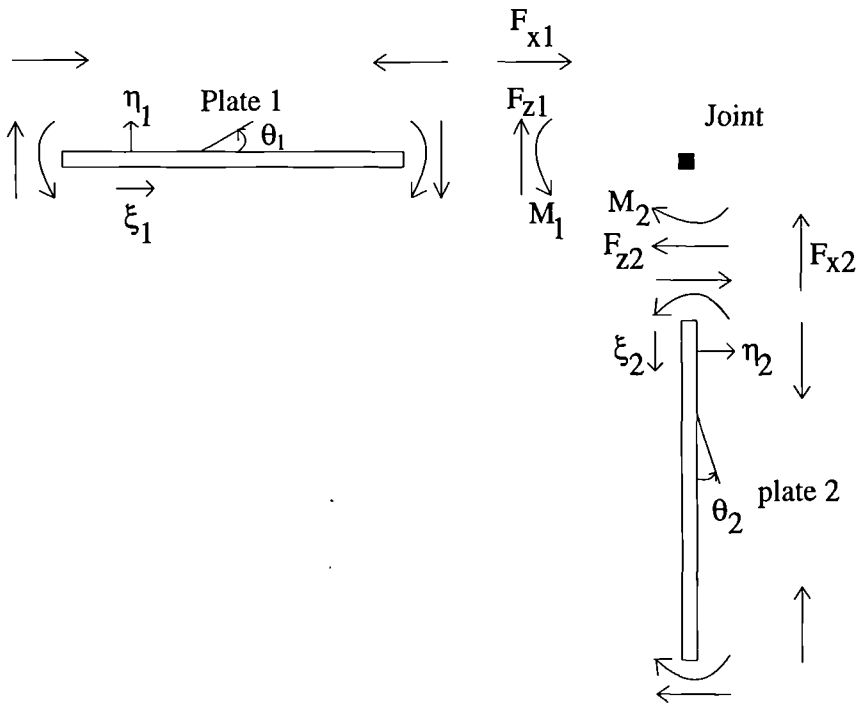

Figure 5.5 Plate configuration and resultant moments and forces for structure in figure 5.4.

therefore described in detail the important effects of oblique incidence (random incidence) for a plate with a reinforcing beam.

Zabarov [73] investigated the transmission of sound through a double wall joined at its edges. Using a wave model approach expressions were given for the transmission of flexural waves from one plate to the other. It was found that when the panels have a larger flexural stiffness than the ribbing the bending waves play a principle role in the transmission of sound through the ribbing. If however the ribbing has a higher flexural stiffness than the plates then the transmission of sound cannot be accounted for without due allowance for longitudinal wave motion in the panels. Furthermore Zabarov suggests any steps taken to enhance the sound proofing of such walls should be aimed at reducing flexural *and* longitudinal wave motion in the panels. However, Zabarov did not investigate these assumptions further and his work was only on flexural waves.

Mead [74] carried out detailed analysis of wave propagation and attenuation in periodic systems(structures). One of the types of structure studied, which is used in aeroplane tailplanes and fins, is the rib-skin structure. Mead found that waves can propagate through periodic systems only in particular frequency zones. The bounding frequencies for these zones are obtained in terms of the natural frequencies of the elements of the system, particularly when these systems are symmetrical. The system wave motions were studied which were developed into a matrix form to study the reflection of waves from boundaries.

Budrin and Nikiforou [75] considered normal incidence transmission at cross joints where wave transformation takes place, when an incident bending wave excites transmitted and reflected longitudinal waves and vice versa. Kihlman [45] investigated cross joints to include solutions for random incidence which required the inclusion of transverse waves. This work was significant in proving the importance of inplane waves (longitudinal and transverse) in structure borne sound transmission. Although Zabarov had stated that longitudinal waves were important in the study of structure borne sound, he did not provide theory to back this statement. Kihlman however did provide theory to support this argument. Kihlman [76] then presented further results to confirm that for certain plate configurations the inclusion of longitudinal and transverse waves was

essential. Gibbs and Gilford [77] used SEA to compare predictions of the wave models by Cremer and Kihlman with measurements on 1/4 scale cross and tee junctions of finite concrete plates, as shown in Fig 5.6. Craven and Gibbs [78] presented a "new approach" inspired by the progress in computing facilities at that time to provide solutions, involving bending and inplane waves at random incidence on a cross joint, for several plates of unequal thickness and composition. This approach to investigating various parameters of the structure is carried out in this work and results are shown in Chapter 6.

Craik expanded the application of these works by investigating structure borne sound transmission through an entire building, composed of multiple plates and multiple junctions. This work was then further enhanced by Craik and Thanacanamootoo [79] by the inclusion of longitudinal and transverse waves, to compare with the previous works experimental data. They found for walls and floors close to the source plate (i.e. within four structural joints), the inclusion of inplane waves was not significant. However, at greater distances a significant part of the bending wave energy was due to energy carried by inplane waves and transferring to bending waves at plate junctions. They also found that equi-partition of energy occurred between longitudinal and transverse waves and therefore they could be modelled as a single 'inplane wave' subsystem in an SEA model. The importance of inplane waves found by Craik *et al* and Craven and Gibbs gives further cause for their inclusion in this particular work.

Fig 5.7 shows the reflected and transmitted inplane waves for plates 1 and 3 at a cross joint which was studied by authors such as Kihlman [45], Craven and Gibbs [78] and Craik and Thanacanamootoo [79].

Recently more complicated structures outside the building envelope has included research by Langley and Heron [47] on multi-plate and random angle junctions. Here the plates are attached at various angles to a central beam element by a line connection.

Bosmans and Vermeir [63] studied transmission between periodically coupled plates. Using an advanced wave approach they found that at low frequencies, despite the bending wavelength being considerably larger than the point spacing, that a continuous

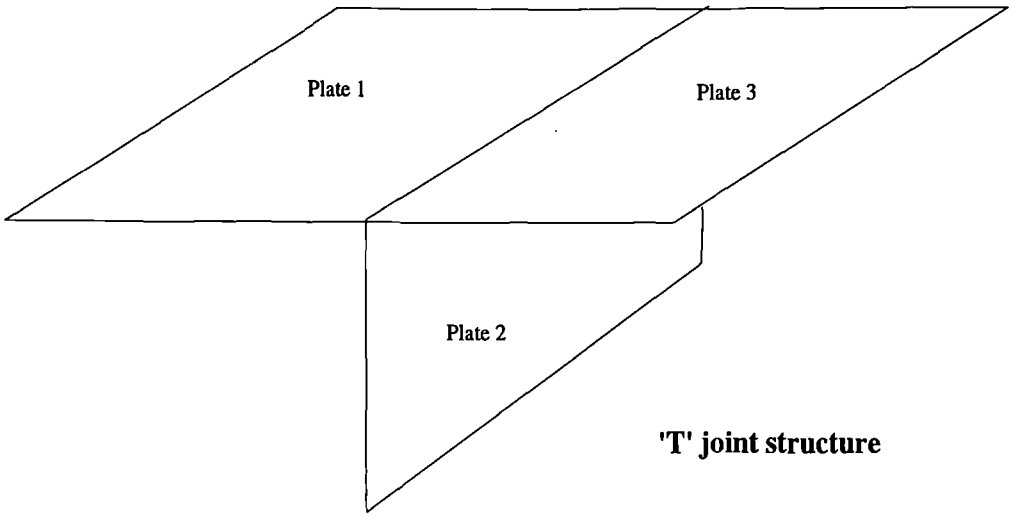

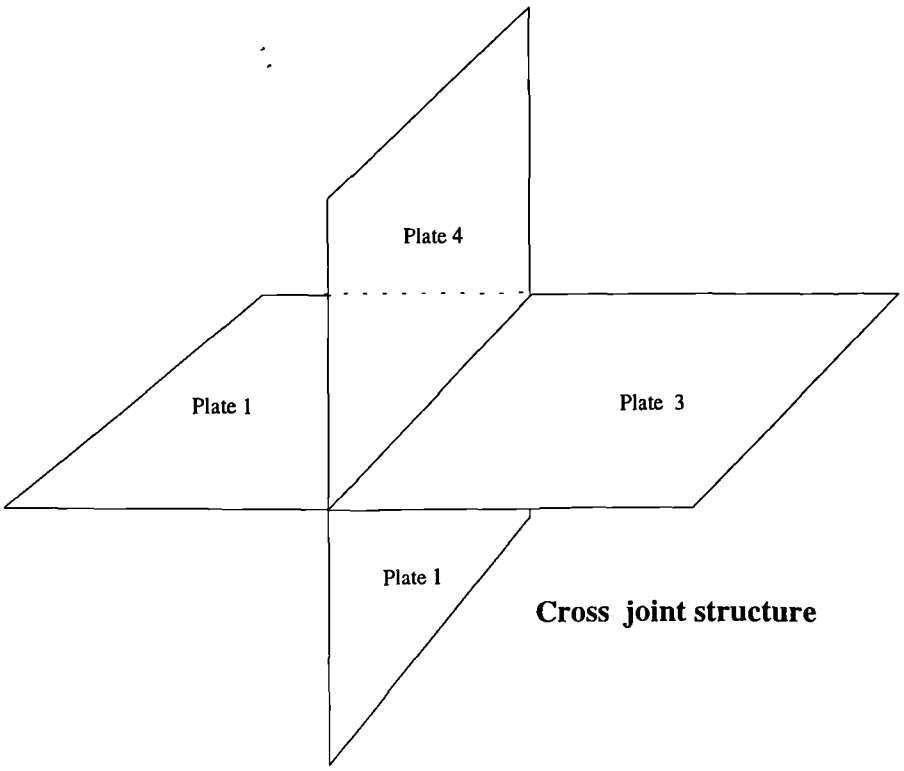

Figure 5.6 'T' and cross joint structures studied by Kihlman, Craven and Gibbs and Craik.

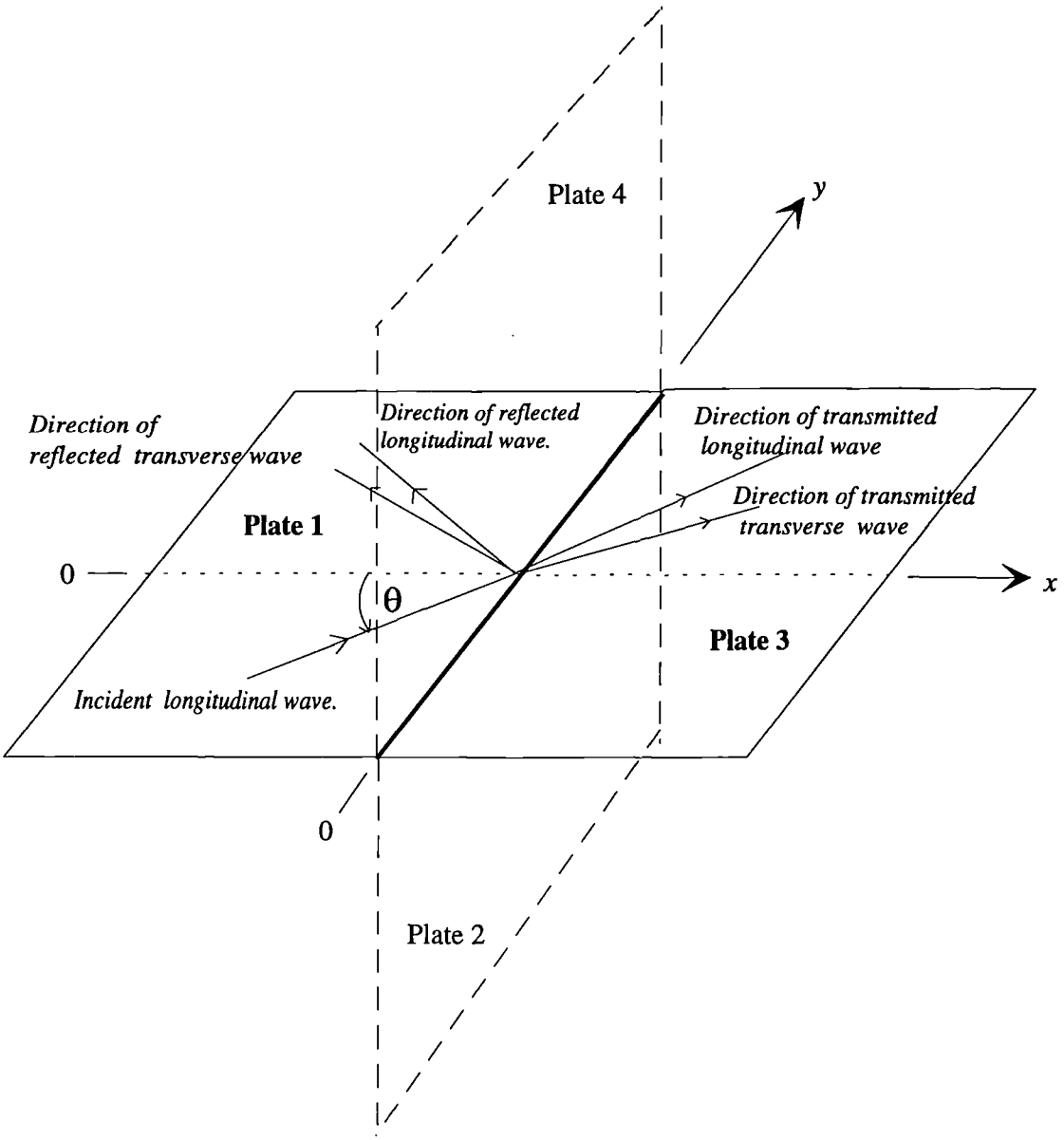

Figure 5.7 In plane waves on plates 1 and 3 for a cross joint due to an incident longitudinal wave.

line junction does not always represent a good approximation. This finding is not accepted by the work carried out in this study and results are shown in Chapter 6 to support this. Different approaches have been studied by previous authors where the mobilities of the various elements of the structure have been incorporated into an electrical analogue [80], [81], [82], and [83]. These provide a fast and straightforward technique which can yield reliable results for some structures. But as this chapter deals specifically with wave models and these works have been described in detail by many previous authors they are not covered in more detail here.

Previous work on line connection specific to double walls

Fig 5.8 shows the types of parallel plate structures studied by previous authors. Bhattacharya, Mulholland and Crocker [29] examined transmission through double panels connected with a tie plate. The research carried out by these authors and in particular Bhattacharya [51] whose thesis much of the above mentioned paper is written from, was and is to date one of the most comprehensive studies undertaken on double walls and the transmission of sound through structural junctions connecting parallel plates. The structure consisted of two parallel plates connected by a tie plate. The two connection points where the tie plate connected to the top and bottom parallel plates by a finite distance, the tie plate's length, divided the structure into two junctions I and II. Using a wave model approach firstly for a normal incident bending wave at junction I solutions were produced for the secondary flexural and longitudinal waves on the tie plate. Of these two waves the longitudinal wave was found to dominate the generation of tertiary bending waves on the bottom parallel plate. As the secondary bending wave on the tie plate was found to produce a tertiary longitudinal wave of small amplitude in the bottom parallel plate. As the secondary longitudinal wave on the tie plate transports energy at a faster rate and reconverts to a tertiary bending wave on the second parallel plate this results in the radiation of noise of which its contribution is appreciable. Secondly the wave model approach was expanded to account for random incidence at the junctions and full inclusion of longitudinal and transverse shear waves. Due to the complexity of the random incidence model only a detailed analysis was carried out for normal incidence. However the authors stated that the extent of the inplane waves influence would be dependant upon the physical parameters of the plates.

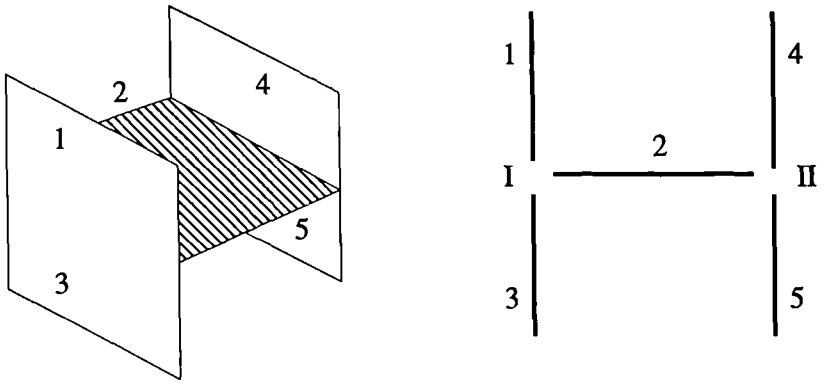

(a) Bhattacharya, Mulholland and Crocker

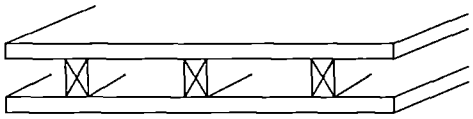

(b) Lin and Garrelick, Sharp and Gu and Wang

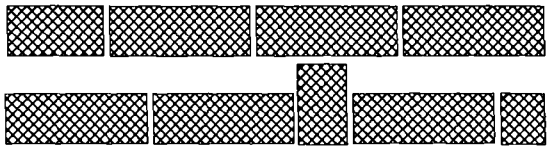

(c) Wilson

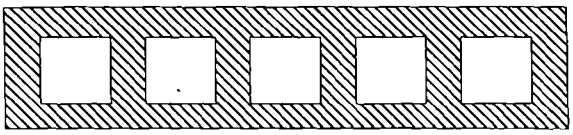

(d) Sullivan

Figure 5.8 Types of parallel plate structures studied by previous authors

Lin and Garrelick [32] examined transmission through two infinite parallel plates with multiple tie plates at periodic spacings. Comparing sound transmission paths through the cavity and structurally through the tie plates, they found the structural path was dominant when the structural wavelength of the bending waves on the plates was a multiple of the bridge spacing. However, this finding was based on a comparison of two graphs. When structural bridges are inserted into the cavity between the parallel plates the behaviour of the plates, cavity and frame are changed. The plates are divided into smaller plates and this was not included in their study.

Sharp [27] produced an expression, based on impedances, for transmission through rigid line connections between the leaves of a double wall. Using this expression and an 'approximate' expression for the transmission of sound through a structurally isolated wall, it was possible to predict the wall's airborne performance. Gu and Wang [33] modified Sharp's expression to account for resilient line connections. However both these theories are impedance models and are limited to transmission of bending waves which are normally incident on the joint. However, real walls have waves at all angle of incidence and therefore a random incident solution is required.

Wilson [8] investigated sound transmission for line connection in cavity walls. Using simple bending wave transmission, which then provided solutions in the form of coupling loss factors, excellent agreement was found between the measured and predicted results. The connecting line bridge between the cavity wall plates was assumed to be inertialess, as shown in Fig 5.9 and 5.10. Furthermore theoretical and measured results were shown for line connected parallel plates where plates were omitted and plate material properties were dissimilar. Sullivan and Gibbs [55] also examined the transmission of energy in cavity walls, between the leaves of diaphram walls. A flexural and full wave model were compared. Whilst resonances were predicted in the cross ribs they were not found in measurements. The number of cross ribs dominated the transmission of energy between the leaves. SEA models were compared with field measurements and good agreement was found. Variation to the material or geometry altered the transmission loss by no more than 2dB.

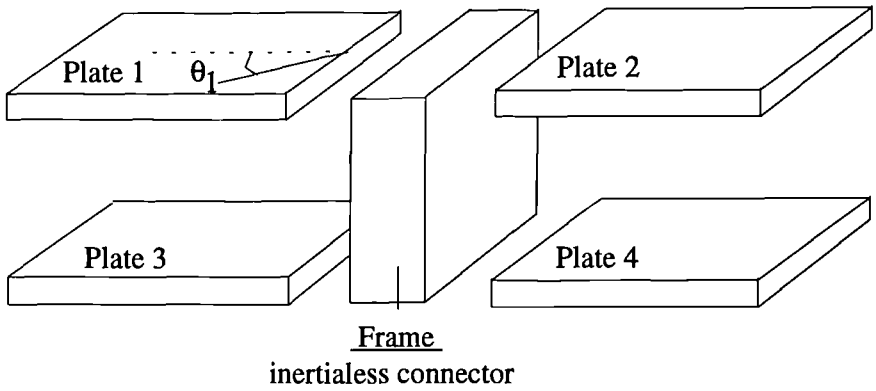

Figure 5.9 Structure configuration for parallel plates and frame with an inertialess connector. (Craik andWilson).

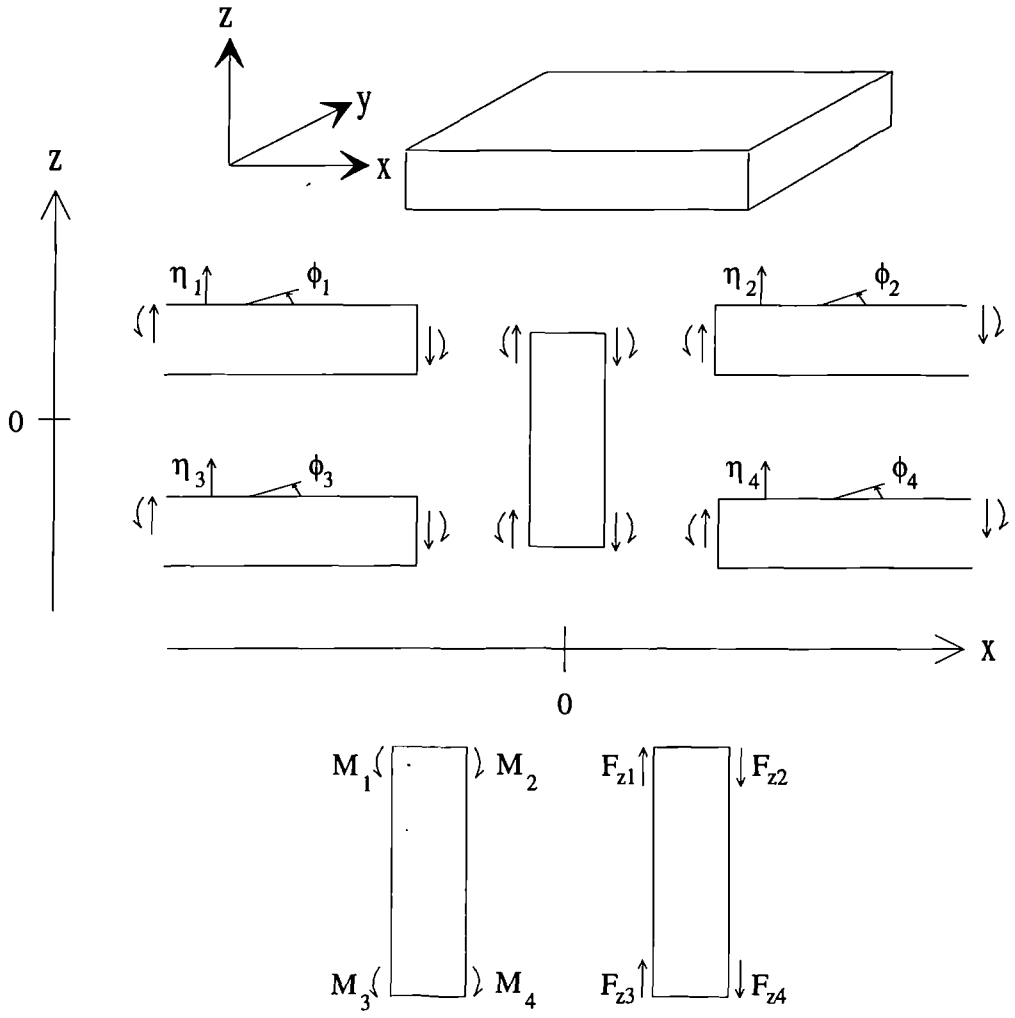

Figure 5.10 Displacement (η), slope (ϕ),moments (M)and forces (F)for parallel plates and frame for flexural motion only.

Discussion

Most of the previous works directly relevant to parallel plates have studied flexural wave motion with only Bhattacharya *et al* [29] and Sullivan and Gibbs [55] detailing the theory for inplane wave motion. Bhattacharya studied partition walls but the transmission as a result of incident inplane waves was not included and no detailed analysis, such as a parametric study, was undertaken on the finite frame element.

In the study of cavity walls, by Wilson [8], the plate thickness was twice the line bridge depth, but in lightweight parallel plates the line bridge depth may be as much as twenty times the plate thickness. The studies by Sullivan [54] which covered similar materials as that of Wilson, brick and concrete, but with a wider cavity found little change to the transmission loss by varying the material or geometry. Both in Wilson's and Sullivan's work the material of the cross rib was inertialess, but in lightweight partitions this cannot be assumed.

This following section attempts to build on these works by the inclusion of inplane waves for lightweight parallel plate structures including incident longitudinal and transverse waves. In addition, two different theoretical models are presented where the frame is modelled as a beam and as a finite plate. The finite nature of the connecting plate (frame) and that the frame material in real partitions is dissimilar to the plates, is analysed through a parametric study of the plate model presented in section 5.4 of this work.

The good comparison between the measured and predicted results in Wilson's work was a stimulus for the advancement of this thesis to then investigate lightweight parallel plates where the connecting line bridge cannot be assumed to be inertialess.

5.3 Theory for parallel plates connected along a line

This section describes the theoretical models for sound transmission through lightweight parallel plates. Principally two models are presented. The first models the frame as a beam with mass and inertia and the second model assumes the frame to be a finite plate.

5.3.1 *Background wave theory*

The properties of waves on plates and beams can be found by considering the action of moments and forces on an element of the beam or plate. The interaction of the moments and forces leads to an equation known as the wave equation from which acoustical properties, such as wavespeed, can be found. A full derivation of the wave equation may be found in Cremer *et al* [44]. The equation of motion for bending waves on any thin plate may be written as [44],

$$\frac{B_j}{\rho_{s_j}}\nabla^4\gamma_j+\frac{\partial^2\gamma_j}{\partial t^2}=0 \tag{5.1}$$

where ρ_s is the surface density, γ is the flexural displacement and B is the bending stiffness given by [44],

$$B_j=\frac{E_j h_j^3}{12(1-\mu_j^2)} \tag{5.2}$$

where E is Young's Modulus, h is the thickness and μ is the Poisson ratio.

Fig 5.11 shows a source bending wave incident at an angle θ, (relative to the normal), at a plate edge parallel to the y-axis, which is travelling in a positive x and y direction, and which may be written as [44],

$$\gamma_0=T_{B0}e^{-ik_{B0}\cos\theta_{B0}x}e^{-ik_{B0}\sin\theta_{B0}y}e^{i\omega t} \tag{5.3}$$

where T_{B0} represents the incident wave amplitude. All secondary waves produced by this primary wave will have the same spacial dependence in the y direction and the same time dependence. For simplicity the terms relating to y and t are not included hereafter.

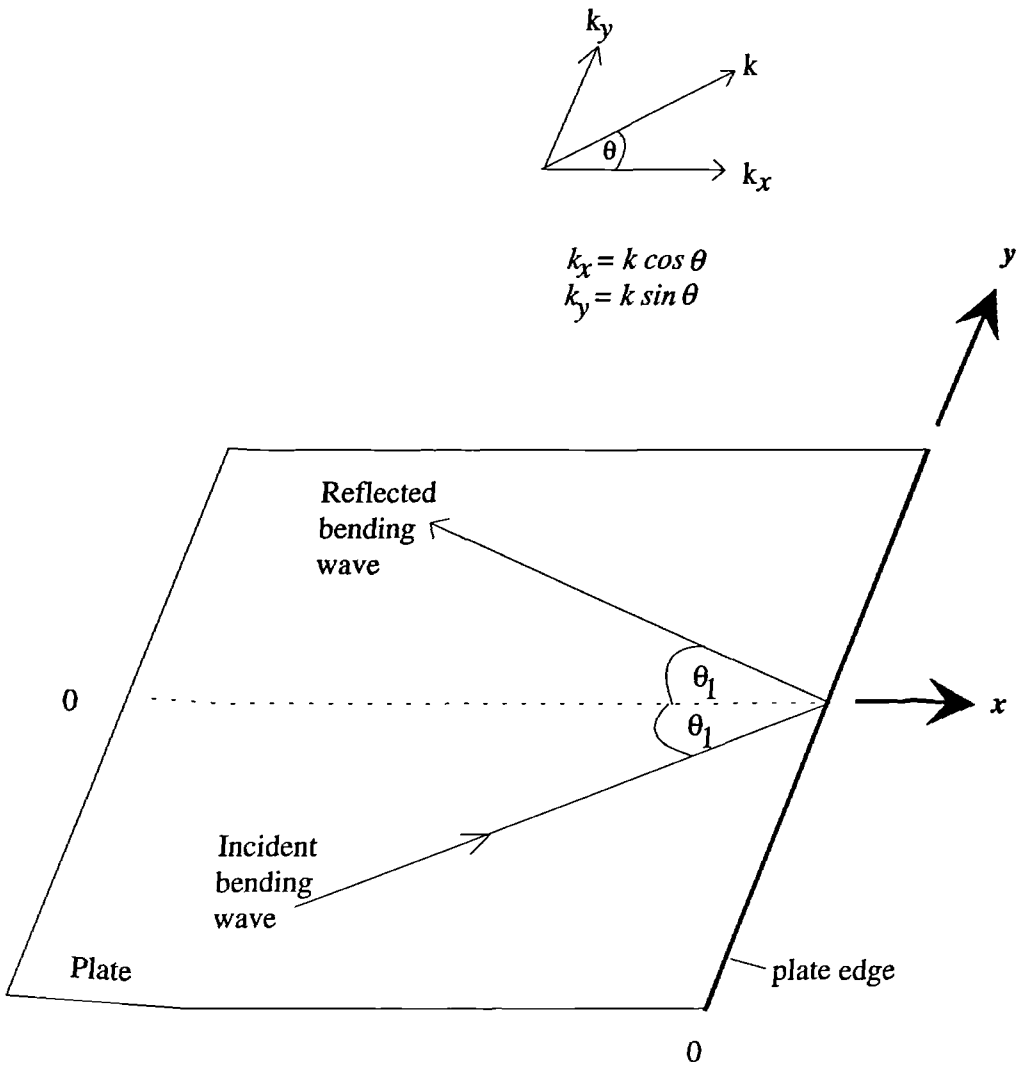

Figure 5.11 Source and reflected bending waves at a plate edge

As a result of an incident bending wave at the plate edge a reflected bending wave with amplitude T_{B1} and a nearfield wave with amplitude T_{n1} both travelling in the negative x-direction will occur. The amplitude of the nearfield wave decays rapidly with distance and hence only occurs in the "nearfield" of the joint. Hence the total displacement on plate 1, γ_1, may be given as [44],

$$\gamma_1 = T_{B0} e^{-ik_{B0}\cos\theta_{B0}x} + T_{B1} e^{ik_{B1}\cos\theta_{B1}x} + T_{n1} e^{k_{n1}x} \tag{5.4}$$

where k_B is the bending wavenumber given by [44],

$$k_B = \omega^{1/2}\left[\frac{\rho_s}{B}\right]^{1/4} \tag{5.5}$$

In eqn(5.4) the (-) sign represents a wave travelling in a positive direction and the (+) sign is for a wave travelling in a negative direction. The nearfield wavenumber, k_n, has similar sign convention for direction of propagation and is given by [44],

$$k_n = \sqrt{k_B^2(1+\sin^2\theta)} \tag{5.6}$$

At a plate edge the slope or angular displacement may be given by [44],

$$\phi_j = \frac{\partial\gamma}{\partial x} \tag{5.7}$$

The bending moment acting on the plate edge due to a wave may be given by [44],

$$M_j = -B\left[\frac{\partial^2\gamma_j}{\partial x^2} + \mu_j\frac{\partial^2\gamma_j}{\partial y^2}\right] \tag{5.8}$$

The forces at a plate edge are composed of a shear force and a force that resists twisting at the boundary and may be given by [44],

$$F_j = B_j\left[\frac{\partial^3\gamma_j}{\partial x^3} + (2-\mu_j)\frac{\partial^3\gamma_j}{\partial x\partial y^2}\right] \tag{5.9}$$

These equations are used when computing the amplitude of the reflected waves. As described in section 5.2, previous authors have shown that inplane waves can play an important role in structure borne sound transmission. The term inplane waves includes longitudinal and transverse wave motion.

Unlike bending waves whose particle motion is perpendicular to the direction of wave propagation, the particle motion for inplane waves is in the same plane. For longitudinal waves the particle motion is in the same direction as the direction of wave propagation and for transverse waves the particle motion is perpendicular to the direction of wave propagation but in the same plane, as shown in Fig 5.12.

The equations of motion for inplane waves are [47],

$$\frac{E_j}{(1-\mu_j^2)}\left(\frac{\partial^2\xi_j}{\partial x^2}+\mu_j\frac{\partial^2\zeta_j}{\partial x\partial y}\right)+\frac{E_j}{2(1+\mu_j)}\left(\frac{\partial^2\xi_j}{\partial y^2}+\frac{\partial^2\zeta_j}{\partial x\partial y}\right)-\rho_j\frac{\partial^2\xi_j}{\partial t^2}=0 \qquad (5.10)$$

$$\frac{E_j}{(1-\mu_j^2)}\left(\frac{\partial^2\zeta_j}{\partial y^2}+\mu_j\frac{\partial^2\xi_j}{\partial x\partial y}\right)+\frac{E_j}{2(1+\mu_j)}\left(\frac{\partial^2\zeta_j}{\partial x^2}+\frac{\partial^2\xi_j}{\partial x\partial y}\right)-\rho_j\frac{\partial^2\zeta_j}{\partial t^2}=0 \qquad (5.11)$$

A full derivation of the inplane equations of motion may be found in Ashton and Whitney [84]. There are two principle equations which are used to describe the inplane forces in the x and y directions and may be given as [47],

$$F_{xj}=-\frac{E_j h_j}{1-\mu_j^2}\left(\frac{\partial\xi_j}{\partial x}+\mu_j\frac{\partial\zeta_j}{\partial y}\right) \qquad (5.12)$$

and

$$F_{yj}=-\frac{E_j h_j}{2(1+\mu_j)}\left(\frac{\partial\xi_j}{\partial y}+\frac{\partial\zeta_j}{\partial x}\right) \qquad (5.13)$$

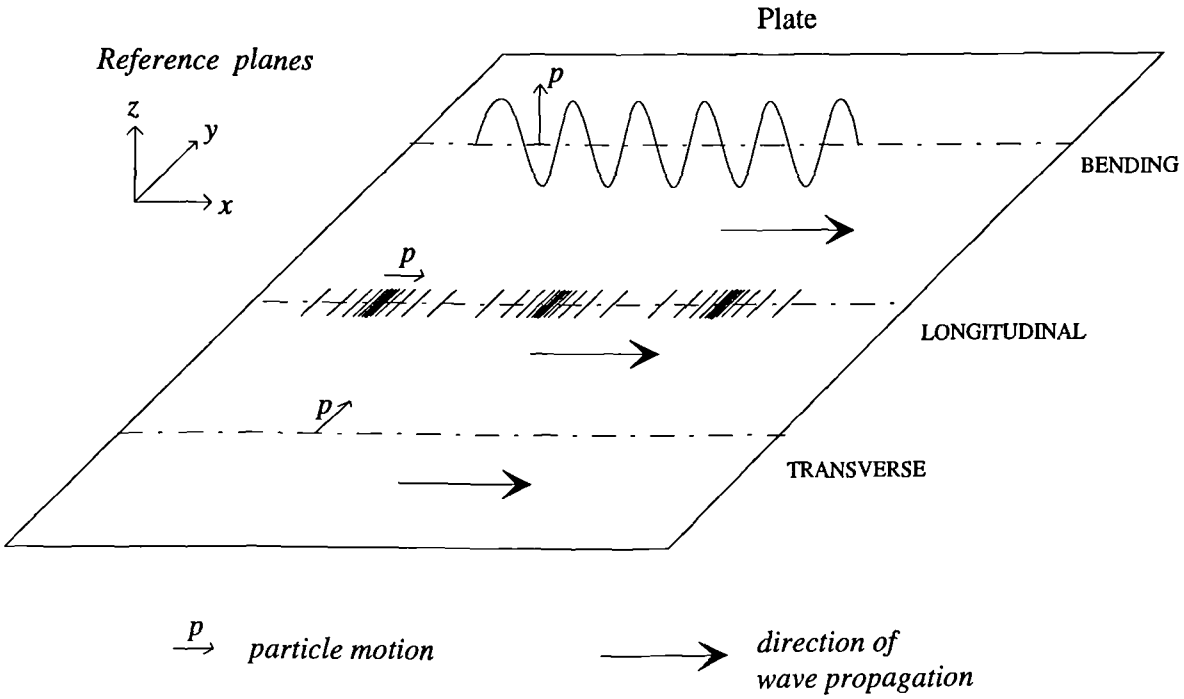

Figure 5.12 Particle motion and direction of wave propagation for bending, longitudinal and transverse waves.

Fig 5.13 shows a plate with an incident longitudinal wave in the x-direction which may be given as [85],

$$\xi_{L0}=T_{L0}\cos\theta_{L0}e^{-ik_{L0}\cos\theta_{L0}x}e^{-ik_{L0}\sin\theta_{L0}y}e^{i\omega t} \tag{5.14}$$

The displacement for an incident transverse wave in the x-direction may be given by [85],

$$\xi_{T0}=T_{T0}\cos(\theta_{T0}+\frac{\pi}{2})e^{-ik_{T0}\cos\theta_{T0}x}e^{-ik_{T0}\sin\theta_{T0}y}e^{i\omega t} \tag{5.15}$$

where the $\pi/2$ terms occur due to the particle motion of transverse waves being perpendicular to the direction of wave propagation. The longitudinal and transverse wavenumbers k_L and k_T may be given by [47],

$$k_L^2=\frac{\omega^2(1-\mu^2)\rho}{E} \qquad k_T^2=\frac{\omega^2 2(1+\mu)\rho}{E} \tag{5.16a,b}$$

For inplane waves the displacement in the x-direction, ξ_1, consists of components of reflected longitudinal and transverse waves together with components of the incident wave which may be given as,

$$\begin{aligned}\xi_1 = {} & T_{L0}\cos\theta_{L0}e^{-ik_{L0}\cos\theta_{L0}x}+T_{T0}\cos(\theta_{T0}+\frac{\pi}{2})e^{-ik_{T0}\cos\theta_{T0}x} \\ & +T_{L1}\cos\theta_{L1}e^{ik_{L1}\cos\theta L1x}+T_{T1}\cos(\theta_{T1}+\frac{\pi}{2})e^{ik_{T1}\cos\theta_{T1}x}\end{aligned} \tag{5.17}$$

where the incident transverse component, T_{T0}, is omitted for an incident bending or longitudinal wave and similarly the incident longitudinal component, T_{L0}, is omitted for an incident bending or transverse wave. Similarly the total displacement in the y-direction, ζ_1, for plate 1 may be given by,

$$\begin{aligned}\zeta_1 = {} & T_{L0}\sin\theta_{L0}e^{-ik_{L0}\cos\theta_{L0}x}+T_{T0}\sin(\theta_{T0}+\frac{\pi}{2})e^{-ik_{T0}\cos\theta_{T0}x} \\ & +T_{L1}\sin\theta_{L1}e^{ik_{L1}\cos\theta_{L1}x}+T_{T1}\sin(\theta_{T1}+\frac{\pi}{2})e^{ik_{T1}\cos\theta_{T1}x}\end{aligned} \tag{5.18}$$

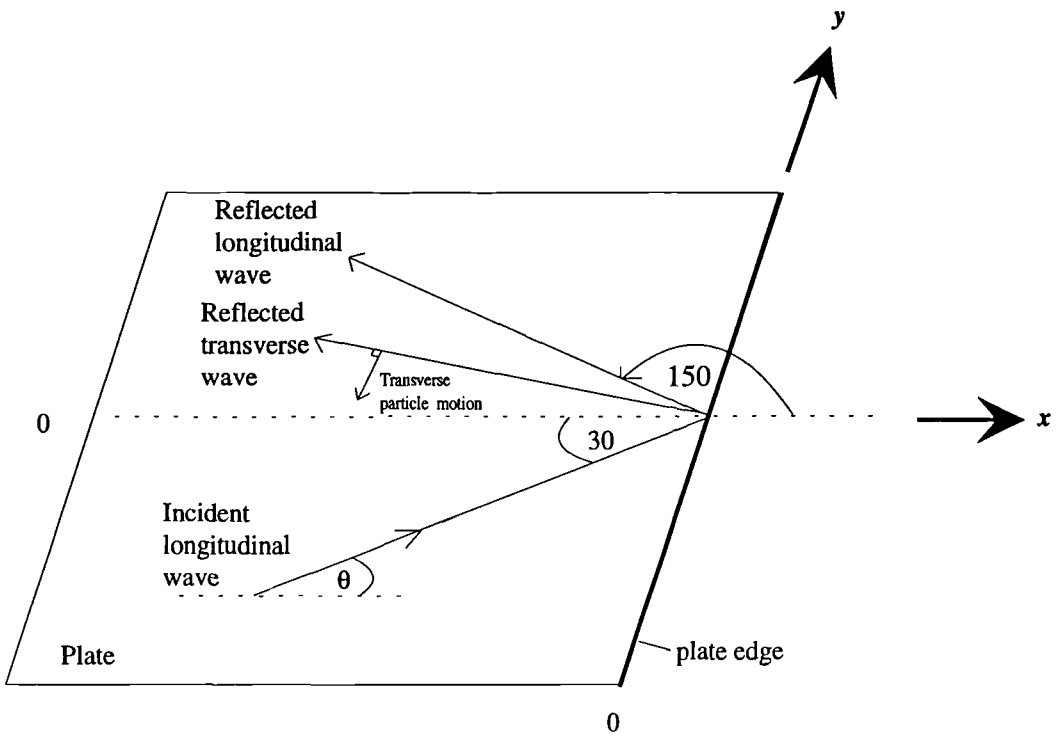

Figure 5.13 Resultant reflected longitudinal and transverse waves due to an incident longitudinal wave at a plate edge.

For an incident transverse wave the incident longitudinal component, T_{L0}, would be set to zero and for an incident bending or longitudinal wave the transverse incident component, T_{T0}, would be set to zero.

The angles of transmission of any wave on any plate, θ_j, with wavenumber k_j is related to the angle of incidence of the incident wave θ_0 (with wavenumber k_0) through Snell's Law giving,

$$k_0 \sin\theta_0 = k_j \sin\theta_j \tag{5.19}$$

The relationship between k_L and k_T may be determined from eqns(5.14a,b) given by,

$$k_T = k_L \sqrt{\frac{2}{1-\mu}} \tag{5.20}$$

5.3.2 *Modelling the frame as a beam*

The frame element in plasterboard partitions is not normally made of the same material as the plates. The most common material used for the structural frame of partitions is softwood timber. In partitions constructed for offices the frame material is a mild steel alloy. The standard term in construction for the structural frame in partitions is 'stud'.

This section details the theory where the frame is modelled as a beam and Fig 5.14 shows the coordinate system. This allows the material properties of the frame, such as density, longitudinal wavespeed and bending stiffness to be included. Eqn(5.4) described the total flexural displacement on plate 1 for an incident bending wave at a joint. In addition to the reflected wave on plate 1, the incident wave also generates three pairs of transmitted travelling and nearfield waves on the remaining three plates. As a result the flexural displacement on these three plates may be written as [44],

$$\begin{aligned} \gamma_2 &= T_{B2} e^{-ik_{B2}\cos\theta_{B2}x} + T_{n2} e^{-k_{n2}x} \\ \gamma_3 &= T_{B3} e^{ik_{B3}\cos\theta_{B3}x} + T_{n3} e^{k_{n3}x} \\ \gamma_4 &= T_{B4} e^{-ik_{B4}\cos\theta_{B4}x} + T_{n4} e^{-k_{n4}x} \end{aligned} \tag{5.21a,b,c}$$

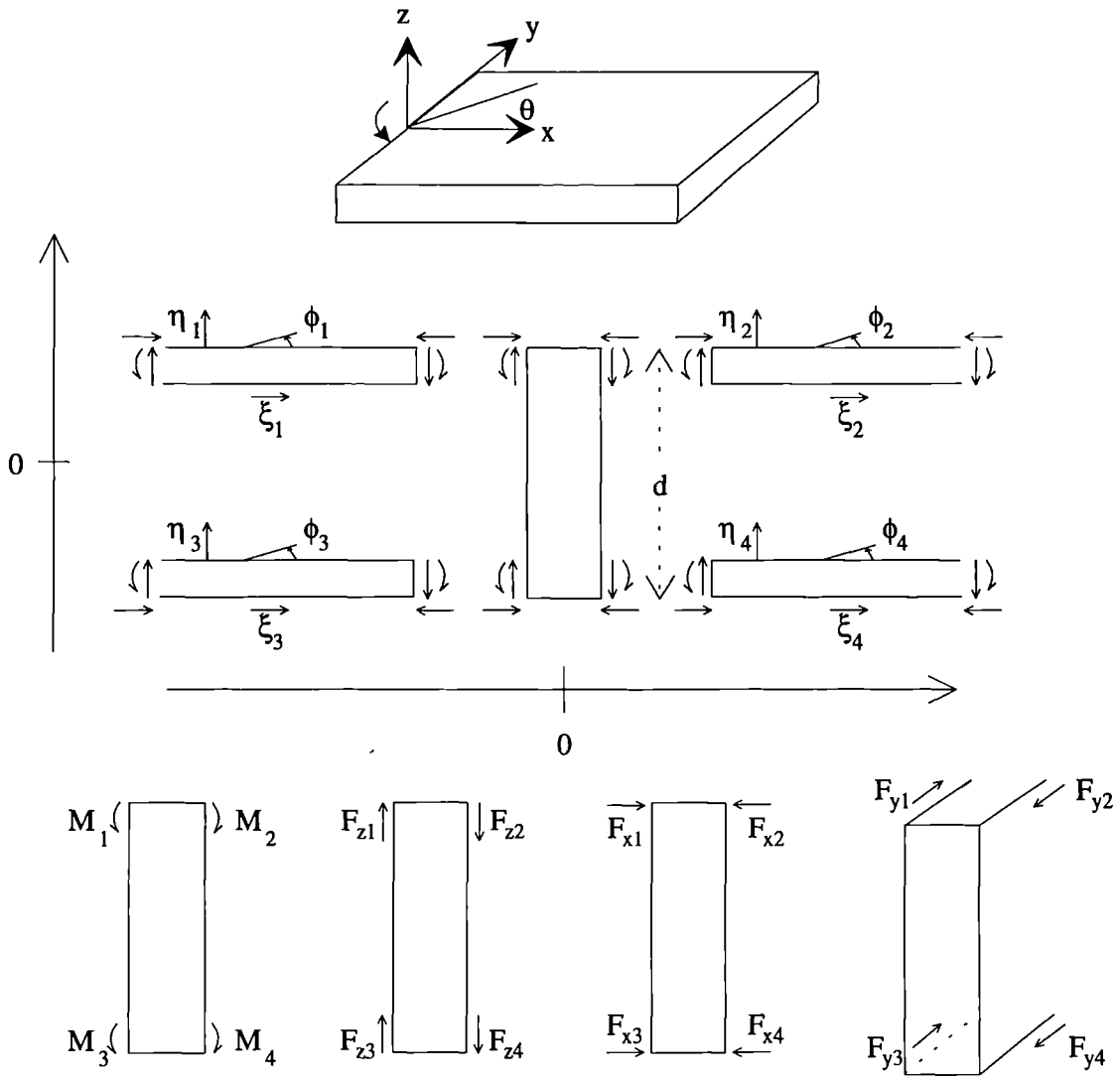

Figure 5.14 Structure configuration for parallel plates when modelling the frame as a beam.

The boundary conditions for parallel plates connected by a beam may be given as,

(i) Continuity of displacement across the joint,

(ii) Preservation of right angles between the plates and the frame,

(iii) Sum of the bending moments about the y-axis is zero,

(iv) Sum of the forces in the x, y and z directions is zero.

Due to the structure being able to support bending, longitudinal and transverse waves the following equations as determined within the boundary conditions and are written in full, including terms for incident bending, longitudinal or transverse waves, which are enclosed in square brackets ([]). This allows all incident waves to be considered. If there is an incident bending wave, for example, then all terms with T_{L0} and T_{T0} should be omitted or set to zero.

At the junction, $x = 0$, the flexural displacement of all four plates must be equal and are given as,

$$\gamma_1=\gamma_2 \quad \gamma_1=\gamma_3 \quad \gamma_1=\gamma_4 \tag{5.22a,b,c}$$

and these may be written as,

$$T_{B1}+T_{n1}-T_{B2}-T_{n2}=[-T_{B0}] \tag{5.23}$$

$$T_{B1}+T_{n1}-T_{B3}-T_{n3}=[-T_{B0}] \tag{5.24}$$

$$T_{B1}+T_{n1}-T_{B4}-T_{n4}=[-T_{B0}] \tag{5.25}$$

To simplify the number of terms in the equations presented all the waves are written in terms of angles between 0 to $\pi/2$. Also the reflected angles on plate 1 are given in relation to the incident wave angle as the angles are equal, relative to the normal. As shown in Fig 5.13 an incident longitudinal wave, $T_{L0}\cos\theta_{L1}$, arriving at the plate edge relative to the normal at 30°, θ_{L1}, will result in a reflected longitudinal wave at 150° which may be written in terms of the incident wave as $-T_{L1}\cos\theta_{L1}$. Equations (5.17) and (5.18) expressed the inplane displacement in the x and y-directions on plate 1 and these

may be simplified to give,

$$\xi_1 = T_{L0}\cos\theta_{L1} - T_{L1}\cos\theta_{L1} - T_{T1}\sin\theta_{T1} - T_{T0}\sin\theta_{T1} \tag{5.26}$$

$$\zeta_1 = T_{L0}\sin\theta_{L1} + T_{L1}\sin\theta_{L1} - T_{T1}\cos\theta_{T1} + T_{T0}\cos\theta_{T1} \tag{5.27}$$

From the simplified assumption that there is no displacement at the joint the continuity of displacement requires that the inplane displacement in the x-direction is given as,

$$\xi_1 = \xi_2 \quad \xi_3 = \xi_1 + \phi_1 d \quad \xi_3 = \xi_4 \tag{5.28a,b,c}$$

which may be written as,

$$\begin{aligned} -T_{L1}\cos\theta_{L1} - T_{T1}\sin\theta_{T1} - T_{L2}\cos\theta_{L2} + T_{T2}\sin\theta_{T2} &= [-T_{L0}\cos\theta_{L1}] \\ &= [T_{T0}\sin\theta_{T1}] \end{aligned} \tag{5.29}$$

$$\begin{aligned} -T_{L1}\sin\theta_{L1} - T_{T1}\sin_{T1} + T_{L3}\cos\theta_{L3} + T_{T3}\sin\theta_{T3} + (ik_{B1}\cos\theta_{B1}T_{B1} + k_{n1}T_{n1})d & \\ = [idk_{B1}\cos\theta_{B1}T_{B0}] & \\ = [-T_{L0}\cos\theta_{L1}] & \\ = [T_{T0}\sin\theta_{T1}] & \end{aligned} \tag{5.30}$$

$$-T_{L3}\cos\theta_{L3} - T_{T3}\sin\theta_{T3} - T_{L4}\cos\theta_{L4} + T_{T4}\sin\theta_{T4} = 0 \tag{5.31}$$

The inplane displacement in the y-direction is given as,

$$\zeta_1 = \zeta_2 \quad \zeta_1 = \zeta_3 \quad \zeta_1 = \zeta_4 \tag{5.32a,b,c}$$

and may be written as,

$$\begin{aligned} T_{L1}\sin\theta_{L1} - T_{T1}\cos\theta_{T1} - T_{L2}\sin\theta_{L2} - T_{T2}\cos\theta_{T2} &= [-T_{L0}\sin\theta_{L1}] \\ &= [-T_{T0}\cos\theta_{T0}] \end{aligned} \tag{5.33}$$

$$\begin{aligned} T_{L1}\sin\theta_{L1} - T_{T1}\cos\theta_{T1} - T_{L3}\sin\theta_{L3} + T_{T3}\cos\theta_{T3} &= [-T_{L0}\sin\theta_{L1}] \\ &= [-T_{T0}\cos\theta_{T1}] \end{aligned} \tag{5.34}$$

$$\begin{aligned} T_{L1}\sin\theta_{L1} - T_{T1}\cos\theta_{T1} - T_{L4}\sin\theta_{L4} - T_{T4}\cos\theta_{T4} &= [-T_{L0}\sin\theta_{L1}] \\ &= [-T_{T0}\cos\theta_{T1}] \end{aligned} \tag{5.35}$$

The preservation of angles for plates 1, 2, 3 and 4 is given by,

$$\phi_1=\phi_2 \quad \phi_1=\phi_3 \quad \phi_1=\phi_4 \tag{5.36a,b,c}$$

and may be written as,

$$ik_{B1}\cos\theta_{B1}T_{B1}+k_{n1}T_{n1}+ik_{B2}\cos\theta_{B2}T_{B2}+k_{n2}T_{n2}=[ik_{B1}\cos\theta_{B1}T_{B0}] \tag{5.37}$$

$$ik_{B1}\cos\theta_{B1}T_{B1}+k_{n1}T_{n1}-ik_{B3}\cos\theta_{B3}T_{B3}-k_{n3}T_{n3}=[ik_{B1}\cos\theta_{B1}T_{B0}] \tag{5.38}$$

$$ik_{B1}\cos\theta_{B1}T_{B1}+k_{n1}T_{n1}+ik_{B4}\cos\theta_{B4}T_{B4}+k_{n4}T_{n4}=[ik_{B1}\cos\theta_{B1}T_{B0}] \tag{5.39}$$

It is assumed that the plates (1, 2, 3, and 4) meet at the centre of the beam and that therefore the width of the beam, *b*, can be ignored. If this assumption was not made then shear forces acting on either side of the beam width would have to be included as was the case in Steel's work [86] on beam and plate junctions. But in this work the beam is assumed to be thin. Using the notation shown in Fig 5.14 the sum of the moments is given as

$$M_1-M_2+M_3-M_4-F_{x1}\frac{d}{2}+F_{x2}\frac{d}{2}+F_{x3}\frac{d}{2}-F_{x4}\frac{d}{2}=M^{\diamond} \tag{5.40}$$

The symbol $\diamond$ is used to denote terms relating to the beam (frame). The right hand side term $M^{\diamond}$ is the resistance of the beam and is given by [44],

$$M^{\diamond}=-\omega^2\ominus\phi_1-\frac{G\partial^2\phi_1}{\partial y^2} \tag{5.41}$$

where *G* is the torsional stiffness given by,

$$G=\frac{E}{2(1+\mu)}\left(\frac{b^3d}{3}\right) \tag{5.42}$$

and $\ominus$ is the rotary inertia given by,

$$\ominus=\left(\frac{b^2+d^2}{12}\right)bd\rho_l \tag{5.43}$$

where *b*, *d*, *E*, μ and ρ_l are the width, depth, Young's modulus, Poisson ratio and density per unit length of the beam respectively. Using eqns(5.8) and (5.12) to determine the plate moments and inplane forces eqn(5.40) may be written as,

$$
\begin{aligned}
&T_{B1}(B_1k_{B1}^2(\cos^2\theta_1+\mu_1\sin^2\theta_1)+ik_{B1}\cos\theta_1(\omega^2\Theta-Gk_{B1}^2\sin^2\theta))\\
&\quad-T_{n1}(B_1(K_{n1}^2-\mu_1k_{B1}^2\sin^2\theta_1)+k_{n1}(\omega^2\Theta-Gk_{B1}^2\sin^2\theta_{B1}))\\
&-T_{B2}(B_2k_{B2}^2(\cos^2\theta_2+\mu_2\sin^2\theta_2))+T_{n2}(B_2(k_{n2}^2-\mu_2k_{B2}^2\sin^2\theta_2))\\
&+T_{B3}(B_3k_{B3}^2(\cos^2\theta_3+\mu_3\sin^2\theta_3))-T_{n3}(B_3(k_{n3}-\mu_3k_{B3}^2\sin^2\theta_3))\\
&-T_{B4}(B_4k_{B4}^2(\cos^2\theta_4+\mu_4\sin^2\theta_4))+T_{n4}(B_4(k_{n4}^2-\mu_4k_{B4}^2\sin^2\theta_4))\\
&-T_{L1}\frac{d}{2}\left(\frac{ik_{L1}E_1h_1}{1-\mu_1^2}\right)(\cos^2\theta_1+\mu_1\sin^2\theta_1)-T_{T1}\frac{d}{2}\left(\frac{ik_{T1}E_1h_1}{1-\mu_1^2}\right)(\cos\theta_1\sin\theta_1(1-\mu_1))\\
&+T_{L2}\frac{d}{2}\left(\frac{ik_{L2}E_2h_2}{1-\mu_2^2}\right)(\cos^2\theta_2+\mu_2\sin^2\theta_2)-T_{T2}\frac{d}{2}\left(\frac{ik_{T2}E_2h_2}{1-\mu_2^2}\right)(\cos\theta_2\sin\theta_2(1-\mu_2))\\
&+T_{L3}\frac{d}{2}\left(\frac{ik_{L3}E_3h_3}{1-\mu_3^2}\right)(\cos^2\theta_3+\mu_3\sin^2\theta_3)+T_{T3}\frac{d}{2}\left(\frac{ik_{T3}E_3h_3}{1-\mu_3^2}\right)(\cos\theta_3\sin\theta_3(1-\mu_3))\\
&-T_{L4}\frac{d}{2}\left(\frac{ik_{L4}E_4h_4}{1-\mu_4^2}\right)(\cos^2\theta_4+\mu_4\sin^2\theta_4)+T_{T4}\frac{d}{2}\left(\frac{ik_{T4}E_4h_4}{1-\mu_4^2}\right)(\cos\theta_4\sin\theta_4(1-\mu_4))
\end{aligned}
\tag{5.44}
$$

$$
\begin{aligned}
&= [-T_{B0}(B_1k_{B1}(\cos^2\theta_1+\mu_1\sin^2\theta_1)+ik_{B1}\cos\theta_1(\omega^2\Theta-Gk_{B1}^2\sin^2\theta_1))]\\
&= \left[T_{L0}\frac{d}{2}\left(\frac{ik_{L1}E_1h_1}{1-\mu_1^2}\right)(\cos^2\theta_1+\mu_1\sin^2\theta_1)\right]\\
&= \left[-T_{T0}\frac{d}{2}\left(\frac{ik_{T1}E_1h_1}{1-\mu_1^2}\right)(\cos\theta_1\sin\theta_1(1-\mu_1))\right]
\end{aligned}
$$

The sum of the forces in the x y and z-direction can be given by,

$$F_{z1}-F_{z2}+F_{z3}-F_{z4}=F_z^{\diamond} \tag{5.45}$$

$$F_{x1}-F_{x2}+F_{x3}-F_{x4}=F_x^{\diamond} \tag{5.46}$$

$$F_{y1}-F_{y2}+F_{y3}-F_{y4}=F_y^{\diamond} \tag{5.47}$$

The forces $F_z^{\diamond}$, $F_x^{\diamond}$ and $F_y^{\diamond}$ are the total resisting x, y and z-direction forces of the beam and are composed of an inertia term and a term relating to bending or compressional stiffness as [44],

$$F_z^{\diamond} = -B_z \frac{\partial^4 \gamma_1}{\partial y^4} - \omega^2 \rho_l \gamma_1 \tag{5.48}$$

$$F_x^{\diamond} = -B_x \frac{\partial^4 \xi_b}{\partial y^4} - \omega^2 \rho_l \xi_b \tag{5.49}$$

$$F_y^{\diamond} = -ES \frac{\partial^2 \zeta_1}{\partial y^2} - \omega^2 \rho_l \zeta_1 \tag{5.50}$$

The first term results from the bending or compression stiffness, where B_z is the bending stiffness of the beam ($Ebd^3/12$), ξ_b is the beam displacement at its centre expressed in terms of the displacement in plate 1 as ($\xi_1 + \phi d/2$), B_x is the bending stiffness of the beam ($Edb^3/12$) and S is the cross sectional area of the beam. The second terms relate to the beam's inertia force in the x, y and z-direction. Taking eqns(5.9), (5.45) and (5.48) the forces in the z-direction may be written as,

$$\begin{aligned}
&-T_{B0}\left(iBk_{BI}^3\cos\theta_1\left(\cos^2\theta_1+(2-\mu_1)\sin^2\theta_1\right)+\omega^2\rho_l-B_1k_{BI}^4\sin^4\theta_1\right)\\
&+T_{nI}\left(B_1k_{nI}(k_{nI}^2-k_{BI}^2\sin^2\theta_1)+\omega^2\rho_l-B_1k_{BI}^4\sin^4\theta_1\right)\\
&+T_{B2}\left(iB_2k_{B2}\cos\theta_2\left(\cos^2\theta_2+(2-\mu_2)\sin^2\theta_2\right)\right)-T_{n2}\left(B_2k_{n2}(k_{n2}^2-k_{B2}^2\sin^2\theta_2)\right)\\
&-T_{B3}\left(iB_3k_{B3}\cos\theta_3\left(\cos^2\theta_3+(2-\mu_3)\sin^2\theta_3\right)\right)+T_{n3}\left(B_3k_{n3}(k_{n3}^2-k_{B3}^2\sin^2\theta_3)\right)\\
&+T_{B4}\left(iB_4k_{B4}\cos\theta_4\left(\cos^2\theta_4+(2-\mu_4)\sin^2\theta_4\right)\right)-T_{n4}\left(B_4k_{n4}(k_{n4}^2-k_{B4}^2\sin^2\theta_4)\right)\\
&=\left[-T_{B0}\left(iB_1k_{BI}\cos\theta_1\left(\cos^2\theta_1+(2-\mu_1)\sin^2\theta_1\right)-\omega^2\rho_l+B_1k_{BI}^4\sin^4\theta_1\right)\right]
\end{aligned} \tag{5.51}$$

The sum of the forces in the x-direction using eqns(5.12), (5.46) and (5.49) may be written as,

$$
\begin{aligned}
&T_{L1}\left(\left(\frac{ik_{L1}E_1h_1}{1-\mu_1^2}\right)(\cos^2\theta_1+\mu_1\sin^2\theta_1)+\cos\theta_1(-\omega^2\rho_l+B_1k_{B1}^4\sin^4\theta_1)\right)\\
&+T_{T1}\left(\left(\frac{ik_{T1}E_1h_1}{1-\mu_1^2}\right)(\cos\theta_1\sin\theta_1(1-\mu_1))+\sin\theta_1(-\omega^2\rho_l+B_1k_{B1}^4\sin^4\theta_1)\right)\\
&-T_{L2}\left(\frac{ik_{L2}E_2h_2}{1-\mu_2^2}\right)(\cos^2\theta_2+\mu_2\sin^2\theta_2)+T_{T2}\left(\frac{ik_{T2}E_2h_2}{1-\mu_2^2}\right)(\cos\theta_2\sin\theta_2(1-\mu_2))\\
&+T_{L3}\left(\frac{ik_{L3}E_3h_3}{1-\mu_3^2}\right)(\cos^2\theta_3+\mu_3\sin^2\theta_3)+T_{T3}\left(\frac{ik_{T3}E_3h_3}{1-\mu_3^2}\right)(\cos\theta_3\sin\theta_3(1-\mu_3))\\
&-T_{L4}\left(\frac{ik_{L4}E_4h_4}{1-\mu_4^2}\right)(\cos^2\theta_4+\mu_4\sin^2\theta_4)+T_{T4}\left(\frac{ik_{T4}E_4h_4}{1-\mu_4^2}\right)(\cos\theta_4\sin\theta_4(1-\mu_4))\\
&+T_{B1}\left(\frac{d}{2}ik_{B1}\cos\theta_1(\omega^2\rho_l-B_1k_{B1}^4\sin\theta_1^4)\right)+T_{n1}\left(\frac{d}{2}k_{n1}(\omega^2\rho_l-B_1k_{B1}^4\sin^4\theta_1)\right)
\end{aligned}
\qquad (5.52)
$$

$$
\begin{aligned}
&=\left[-T_{L1}\left(\left(\frac{ik_{L1}E_1h_1}{1-\mu_1^2}\right)(\cos^2\theta_1+\mu_1\sin^2\theta_1)+\cos\theta_1(-\omega^2\rho_l+B_1k_{B1}^4\sin^4\theta_1\right)\right]\\
&=\left[T_{T0}\left(\left(\frac{ik_{T0}E_1h_1}{1-\mu_1^2}\right)(\cos\theta_1\sin\theta_1(1-\mu_1))+\sin\theta_1(-\omega^2\rho_l+B_1k_{B1}^4\sin^4\theta_1\right)\right]\\
&=\left[T_{B0}\left(\frac{d}{2}ik_{B1}\cos\theta_1(\omega^2\rho_l-B_1k_{B1}^4\sin^4\theta_1)\right)\right]
\end{aligned}
$$

The sum of the forces in the y-direction may be found from equating eqns(5.13), (5.47) and (5.50) to give,

$$
\begin{aligned}
&-T_{L1}\left(\left(\frac{E_1h_1}{2(1+\mu_1)}\right)(2ik_{L1}\cos\theta_1\sin\theta_1)+\sin\theta_1(\omega^2\rho_l-SEk_{L1}\sin\theta_1)\right)\\
&-T_{T1}\left(\left(\frac{E_1h_1}{2(1+\mu_1)}\right)ik_{T1}(\sin^2\theta_1-\cos^2\theta_1)+\cos\theta_1(-\omega^2\rho_l+SEk_{T1}\sin\theta_1)\right)\\
&-T_{L2}\left(\frac{E_2h_2}{2(1+\mu_2)}(2ik_{L2}\cos\theta_2\sin\theta_2)\right)+T_{T2}\left(\frac{E_2h_2}{2(1+\mu_2)}\right)ik_{T2}(\sin^2\theta_2-\cos^2\theta_2)\\
&-T_{L3}\left(\frac{E_3h_3}{2(1+\mu_3)}(2ik_{L3}\cos\theta_3\sin\theta_3)\right)-T_{T3}\left(\frac{E_3h_3}{2(1+\mu_3)}\right)ik_{T3}(\sin^2\theta_3-\cos^2\theta_3)\\
&-T_{L4}\left(\frac{E_4h_4}{2(1+\mu_4)}(2ik_{L4}\cos\theta_4\sin\theta_4)\right)+T_{T4}\left(\frac{E_4h_4}{2(1+\mu_4)}\right)ik_{T4}(\sin^2\theta_4-\cos^2\theta_4)
\end{aligned}
\qquad (5.53)
$$

$$
\begin{aligned}
&=\left[-T_{L0}\left(\left(\frac{E_1h_1}{2(1+\mu_1)}\right)(2ik_{L1}\cos\theta_1\sin\theta_1)+\sin\theta_1(-\omega^2\rho_l+SEk_{L1}\sin\theta_1)\right)\right]\\
&=\left[T_{T0}\left(\left(\frac{E_1h_1}{2(1+\mu_1)}\right)ik_{T1}(\sin^2\theta_1-\cos^2\theta_1)+\cos\theta_1(-\omega^2\rho_l+SEk_{T1}\sin\theta_1)\right)\right]
\end{aligned}
$$

The sixteen principle equations,

(5.23)	(5.24)	(5.25)	(5.29)
(5.30)	(5.31)	(5.33)	(5.34)
(5.35)	(5.37)	(5.38)	(5.39)
(5.44)	(5.51)	(5.52)	(5.53)

can be written in a matrix format and numerically solved, (e.g. Gaussian elimination), to determine the amplitude of the bending, longitudinal, transverse and nearfield waves on the four plates, given as,

T_{B1},	T_{B2},	T_{B3},	T_{B4},
T_{L1},	T_{L2},	T_{L3},	T_{L4},
T_{T1},	T_{T2},	T_{T3},	T_{T4},
T_{n1},	T_{n2},	T_{n3},	T_{n4},

Section 5.3.5 describes how the transmission coefficients and resultant coupling loss factors may be calculated for SEA applications.

5.3.3 *Modelling the frame as a plate*

An alternative method of modelling the junction is to model the frame as a plate. When the beam is substantial so that d is large but b is still small then the frame will bend along its depth so that ϕ_1 is no longer equal to ϕ_3. This could be included in the beam model by a specific fix to the appropriate equations, (see section 5.6 *Discussion*), but it is more properly incorporated into the model by modelling the element as a finite length plate.

Bhattacharya [51] and Sullivan [54] used a similar technique of modelling the connecting element as a plate. The plate configuration used is shown in Fig 5.15. Where the connecting plate, plate 5, couples the parallel plates two junctions are formed, I and II. Junction I is where plates 1, 2 and 5 are coupled and junction II is where plates 3, 4 and 5 are coupled. The requirements of continuity and equilibrium must be satisfied at both ends of the plate. Due to the finite nature of the connecting plate, plate 5, there will be waves travelling in both a positive and a negative direction. The bending displacement on plate 5 can be given by,

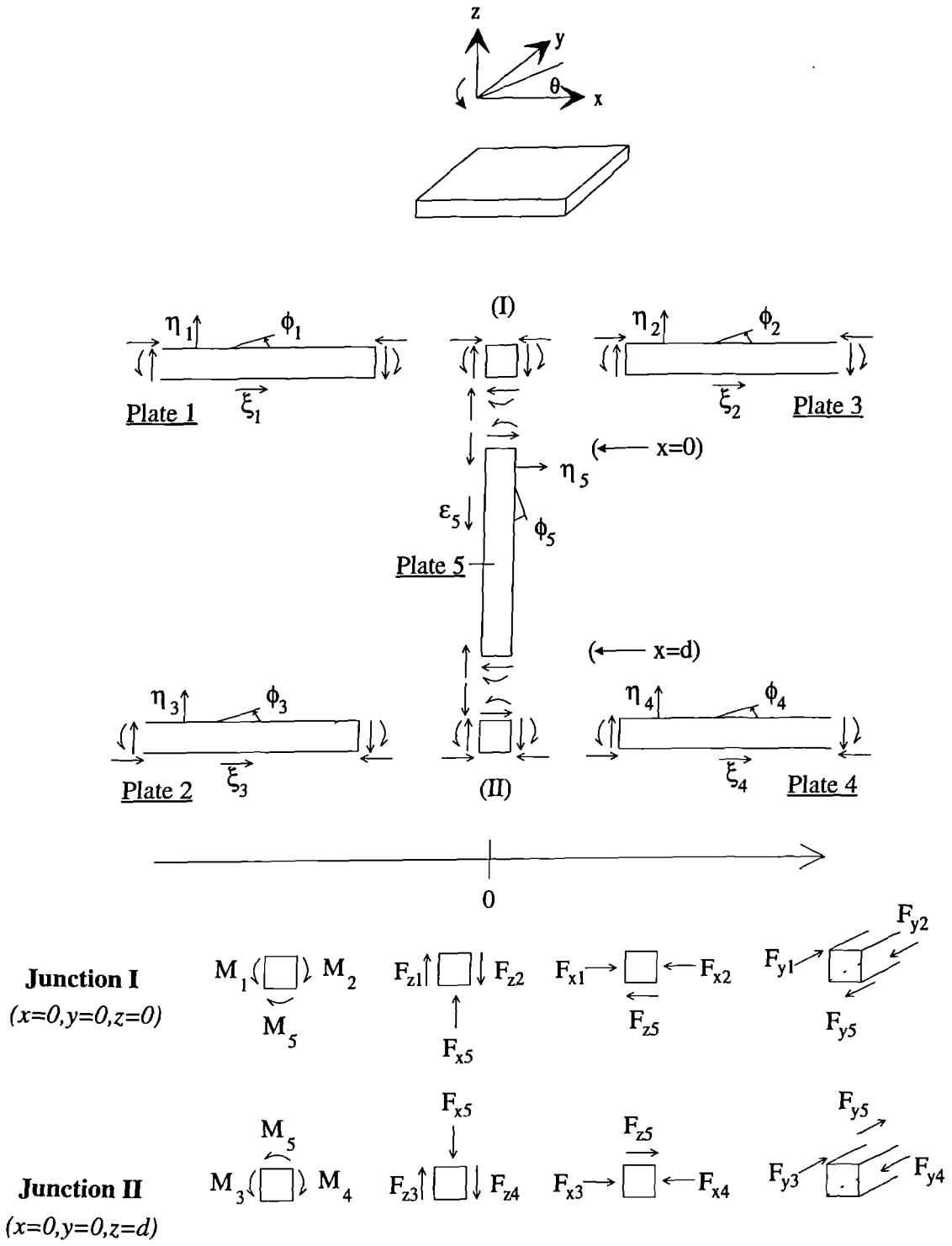

Figure 5.15 Structure configuration for plates and frame when modelling the frame as a plate.

$$\gamma_5 = T_{B5+}e^{-ik_{B5}\cos\theta_{B5}z} + T_{n5+}e^{-k_{n5}z} + T_{B5-}e^{ik_{B5}\cos\theta_{B5}(z-d)} + T_{n5-}e^{k_{n5}(z-d)} \qquad (5.54)$$

where subscript (+) refers to the amplitude of waves travelling from junction I to junction II, subscript (-) refers to the waves travelling from junction II to junction I and d is the depth of the frame and is a positive integer. Similarly the inplane displacement on plate 5 is described by,

$$\begin{aligned}\xi_5 = {} & T_{L5+}\cos\theta_{L5}e^{-ik_{L5}\cos\theta_{L5}z} - T_{T5+}\sin\theta_{T5}e^{-ik_{T5}\cos\theta_{T5}z} \\ & - T_{L5-}\cos\theta_{L5}e^{ik_{L5}\cos\theta_{L5}(z-d)} - T_{T5-}\sin\theta_{T5}^{ik_{T5}\cos\theta_{T5}(z-d)}\end{aligned} \qquad (5.55)$$

and

$$\begin{aligned}\zeta_5 = {} & T_{L5+}\sin\theta_{L5}e^{-ik_{L5}\cos\theta_{L5}z} + T_{T5+}\cos\theta_{T5}e^{-ik_{T5}\cos\theta_{T5}z} \\ & + T_{L5-}\sin\theta_{L5}e^{ik_{L5}\cos\theta_{L5}(z-d)} - T_{T5-}\cos\theta_{T5}e^{ik_{T5}\cos\theta_{T5}(z-d)}\end{aligned} \qquad (5.56)$$

JUNCTION I

The boundary conditions for junction I are similar to that described where the frame is modelled as a beam. But in the case of modelling the frame as a finite plate they must apply to both junctions, I and II. The boundary conditions are the continuity of displacement and slope and equilibrium of the moments and forces in the x, y and z directions. At junction I where (x=0, y=0 and z=0), the displacement in the z-direction is given by,

$$\gamma_1 = \gamma_2 \qquad \gamma_1 = -\xi_5 \qquad (5.57a,b)$$

and these may be written as,

$$T_{B1} + T_{n1} - T_{B2} - T_{n2} = [-T_{B0}] \qquad (5.58)$$

$$T_{B1} + T_{n1} + T_{L5+}\cos\theta_{L5} - T_{T5+}\sin\theta_{T5} - T_{L5-}\cos\theta_{L5} - T_{T5-}\sin\theta_{T5} = [-T_{B0}] \qquad (5.59)$$

The displacement in the x-direction may be given by,

$$\xi_1-\xi_2 \quad \xi_1-\gamma_5 \tag{5.60a,b}$$

which may be written as,

$$-T_{L1}\cos\theta_{L1}-T_{T1}\sin\theta_{T1}-T_{L2}\cos\theta_{L2}+T_{T2}\sin\theta_{T2}=[-T_{L0}\cos\theta_{L1}] \\ =[T_{T0}\sin\theta_{T1}] \tag{5.61}$$

$$-T_{L1}\sin\theta_{L1}-T_{T1}\sin_{T1}-T_{B5+}-T_{n5+}-T_{B5-}-T_{n5-}=[-T_{L0}\cos\theta_{L1}] \\ =[T_{T0}\sin\theta_{T1}] \tag{5.62}$$

The inplane displacement in the *y*-direction is given as,

$$\zeta_1=\zeta_2 \quad \zeta_1=\zeta_5 \tag{5.63a,b}$$

and may be written as,

$$T_{L1}\sin\theta_{L1}-T_{T1}\cos\theta_{T1}-T_{L2}\sin\theta_{L2}-T_{T2}\cos\theta_{T2}=[-T_{L0}\sin\theta_{L1}] \\ =[-T_{T0}\cos\theta_{T0}] \tag{5.64}$$

$$T_{L1}\sin\theta_{L1}-T_{T1}\cos\theta_{T1}-T_{L5+}\sin\theta_{L5}-T_{T5+}\cos\theta_{T5}-T_{L5-}\sin\theta_{L5}+T_{T5-}\cos\theta_{T5}=[-T_{L0}\sin\theta_{L1}] \\ =[-T_{T0}\cos\theta_{T1}] \tag{5.65}$$

The preservation of angles for plates 1, 2 and 5 is given by,

$$\phi_1=\phi_2 \quad \phi_1=\phi_5 \tag{5.66a,b}$$

and may be written as,

$$ik_{B1}\cos\theta_{B1}T_{B1}+k_{n1}T_{n1}+ik_{B2}\cos\theta_{B2}T_{B2}+k_{n2}T_{n2}=[ik_{B1}\cos\theta_{B1}T_{B0}] \tag{5.67}$$

$$ik_{B1}\cos\theta_{B1}T_{B1}+k_{n1}T_{n1}+ik_{B5}\cos\theta_{B5}T_{B5+}+k_{n5}T_{n5+}-ik_{B5}\cos\theta_{B5}T_{B5-}-k_{n5}T_{n5-}=[ik_{B1}\cos\theta_{B1}T_{B0}] \tag{5.68}$$

The sum of the moments is given as

$$M_1 - M_2 - M_5 = 0 \tag{5.69}$$

Using eqn(5.8) to determine the plate moments eqn(5.69) may be written as,

$$\begin{aligned} & T_{B1}(B_1 k_{B1}^2(\cos^2\theta_1 + \mu_1 \sin^2\theta_1) - T_{n1}(B_1(K_{n1}^2 - \mu_1 k_{B1}^2 \sin^2\theta_1) \\ & - T_{B2}(B_2 k_{B2}^2(\cos^2\theta_2 + \mu_2 \sin^2\theta_2)) + T_{n2}(B_2(k_{n2}^2 - \mu_2 k_{B2}^2 \sin^2\theta_2)) \\ & - T_{B5+}(B_5 k_{B5}^2(\cos^2\theta_5 + \mu_5 \sin^2\theta_5)) + T_{n5+}(B_5(k_{n5} - \mu_5 k_{B5}^2 \sin^2\theta_5)) \\ & - T_{B5-}(B_5 k_{B5}^2(\cos^2\theta_5 + \mu_5 \sin^2\theta_5)) + T_{n5-}(B_5(k_{n5}^2 - \mu_5 k_{B5}^2 \sin^2\theta_5)) \\ & = [-T_{B0}(B_1 k_{B1}(\cos^2\theta_1 + \mu_1 \sin^2\theta_1))] \end{aligned} \tag{5.70}$$

The sum of the forces in the z-direction can be given by,

$$F_{z1} - F_{z2} + F_{x5} = 0 \tag{5.71}$$

and this may be written as,

$$\begin{aligned} & -T_{B1}\left(iBk_{B1}^3 \cos\theta_1 \left(\cos^2\theta_1 + (2-\mu_1)\sin^2\theta_1\right)\right) + T_{n1}\left(B_1 k_{n1}(k_{n1}^2 - k_{B1}^2 \sin^2\theta_1)\right) \\ & + T_{B2}\left(iB_2 k_{B2}^3 \cos\theta_2 \left(\cos^2\theta_2 + (2-\mu_2)\sin^2\theta_2\right)\right) - T_{n2}\left(B_2 k_{n2}(k_{n2}^2 - k_{B2}^2 \sin^2\theta_2)\right) \\ & + T_{L5+}\left(\frac{ik_{L5}E_5 h_5}{1-\mu_5^2}\right)(\cos^2\theta_5 + \mu_5 \sin^2\theta_5) - T_{T5+}\left(\frac{ik_{T5}E_5 h_5}{1-\mu_5^2}\right)(\sin\theta_5 \cos\theta_5 (1-\mu_5)) \\ & + T_{L5-}\left(\frac{ik_{L5}E_5 h_5}{1-\mu_5^2}\right)(\cos^2\theta_5 + \mu_5 \sin^2\theta_5) + T_{T5-}\left(\frac{ik_{T5}E_5 h_5}{1-\mu_5^2}\right)(\cos\theta_5 \sin\theta_5 (1-\mu_5)) \\ & = \left[-T_{B0}(iB_1 k_{B1}^3 \cos\theta_1 (\cos^2\theta_1 + (2-\mu_1)\sin^2\theta_1))\right] \end{aligned} \tag{5.72}$$

The sum of the forces in the x-direction is given as,

$$F_{x1} - F_{x2} - F_{z5} = 0 \tag{5.73}$$

and this may be written as,

$$
\begin{aligned}
&T_{L1}\left(\frac{ik_{L1}E_1h_1}{1-\mu_1^2}\right)(\cos^2\theta_1+\mu_1\sin^2\theta_1)+T_{T1}\left(\frac{ik_{T1}E_1h_1}{1-\mu_1^2}\right)(\cos\theta_1\sin\theta_1(1-\mu_1))\\
&-T_{L2}\left(\frac{ik_{L2}E_2h_2}{1-\mu_2^2}\right)(\cos^2\theta_2+\mu_2\sin^2\theta_2)+T_{T2}\left(\frac{ik_{T2}E_2h_2}{1-\mu_2^2}\right)(\cos\theta_2\sin\theta_2(1-\mu_2))\\
&-T_{B5+}(iB_5k_{B5}^3\cos\theta_5(\cos^2\theta_5+(2-\mu_5)\sin^2\theta_5))+T_{n5+}(k_{n5}(k_{n5}^2-(2-\mu_5)k_{B5}^2\sin^2\theta_5))\\
&+T_{B5-}(iB_5k_{B5}^3\cos\theta_5(\cos^2\theta_5+(2-\mu_5)\sin^2\theta_5))-T_{n5-}(k_{n5}(k_{n5}^2-(2-\mu_5)k_{B5}^2\sin^2\theta_5))\\
&=\left[-T_{L0}\left(\frac{ik_{L1}E_1h_1}{1-\mu_1^2}\right)(\cos^2\theta_1+\mu_1\sin^2\theta_1)\right]\\
&=\left[T_{T0}\left(\frac{ik_{T1}E_1h_1}{1-\mu_1^2}\right)(\cos\theta_1\sin\theta_1(1-\mu_1))\right]
\end{aligned}
\tag{5.74}
$$

The sum of the forces in the *y*-direction may be given by,

$$
F_{y1}-F_{y2}-F_{y5}=0 \tag{5.75}
$$

and may be written as,

$$
\begin{aligned}
&-T_{L1}\left(\frac{E_1h_1}{2(1+\mu_1)}\right)(2ik_{L1}\cos\theta_1\sin\theta_1)-T_{T1}\left(\frac{E_1h_1}{2(1+\mu_1)}\right)ik_{T1}(\sin^2\theta_1-\cos^2\theta_1)\\
&-T_{L2}\left(\frac{E_2h_2}{2(1+\mu_2)}\right)(2ik_{L2}\cos\theta_2\sin\theta_2)+T_{T2}\left(\frac{E_2h_2}{2(1+\mu_2)}\right)ik_{T2}(\sin^2\theta_2-\cos^2\theta_2)\\
&-T_{L5+}\left(\frac{E_5h_5}{2(1+\mu_5)}\right)(2ik_{L5}\cos\theta_5\sin\theta_5)+T_{T5+}\left(\frac{E_5h_5}{2(1+\mu_5)}\right)ik_{T5}(\sin^2\theta_5-\cos^2\theta_5)\\
&+T_{L5-}\left(\frac{E_5h_5}{2(1+\mu_5)}\right)(2ik_{L5}\cos\theta_5\sin\theta_5)+T_{T5-}\left(\frac{E_5h_5}{2(1+\mu_5)}\right)ik_{T5}(\sin^2\theta_5-\cos^2\theta_5)\\
&=\left[-T_{L0}\left(\frac{E_1h_1}{2(1+\mu_1)}\right)(2ik_{L1}\cos\theta_1\sin\theta_1)\right]\\
&=\left[T_{T0}\left(\frac{E_1h_1}{2(1+\mu_1)}\right)ik_{T1}(\sin^2\theta_1-\cos^2\theta_1)\right]
\end{aligned}
\tag{5.76}
$$

JUNCTION II

The boundary conditions for junction II are similar to that described where the frame is modelled as a beam. At junction II where (x=0, y=0 and z=d), the displacement in the z-direction is given by,

$$\gamma_3=\gamma_4 \qquad \gamma_3=-\xi_5 \tag{5.77a,b}$$

and these may be written as,

$$T_{B3}+T_{n3}-T_{B4}-T_{n4}=0 \tag{5.78}$$

$$T_{B3}+T_{n3}+T_{L5+}\cos\theta_{L5}-T_{T5+}\sin\theta_{T5}-T_{L5-}\cos\theta_{L5}-T_{T5-}\sin\theta_{T5}=0 \tag{5.79}$$

The dislacement in the x-direction may be given by,

$$\xi_3=\xi_4 \qquad \xi_3=\gamma_5 \tag{5.80a,b}$$

which may be written as,

$$-T_{L3}\cos\theta_{L3}-T_{T3}\sin\theta_{T3}-T_{L4}\cos\theta_{L4}+T_{T4}\sin\theta_{T4}=0 \tag{5.81}$$

$$-T_{L3}\sin\theta_{L3}-T_{T3}\sin_{T3}-T_{B5+}-T_{n5+}-T_{B5-}-T_{n5-}=0 \tag{5.82}$$

The inplane displacement in the y-direction is given as,

$$\zeta_3=\zeta_4 \quad \zeta_3=\zeta_5 \tag{5.83a,b}$$

and may be written as,

$$T_{L3}\sin\theta_{L3}-T_{T3}\cos\theta_{T3}-T_{L4}\sin\theta_{L4}-T_{T4}\cos\theta_{T4}=0 \tag{5.84}$$

$$T_{L3}\sin\theta_{L3}-T_{T3}\cos\theta_{T3}-T_{L5+}\sin\theta_{L5}-T_{T5+}\cos\theta_{T5}-T_{L5-}\sin\theta_{L5}+T_{T5-}\cos\theta_{T5}=0 \tag{5.85}$$

The preservation of angles for plates 3, 4 and 5 is given by,

$$\phi_3=\phi_4 \quad \phi_3=\phi_5 \tag{5.86a,b}$$

and may be written as,

$$ik_{B3}\cos\theta_{B3}T_{B3}+k_{n3}T_{n3}+ik_{B4}\cos\theta_{B4}T_{B4}+k_{n4}T_{n4}=0 \tag{5.87}$$

$$ik_{B3}\cos\theta_{B3}T_{B3}+k_{n3}T_{n3}+ik_{B5}\cos\theta_{B5}T_{B5+}+k_{n5}T_{n5+}-ik_{B5}\cos\theta_{B5}T_{B5-}-k_{n5}T_{n5-}=0 \tag{5.88}$$

The sum of the moments is given as

$$M_3-M_4+M_5=0 \tag{5.89}$$

Using eqn(5.8) to determine the plate moments eqn(5.89) may be written as,

$$\begin{aligned}
&T_{B3}(B_3k_{B3}^2(\cos^2\theta_3+\mu_3\sin^2\theta_3)- T_{n3}(B_3(k_{n3}^2-\mu_3k_{B3}^2\sin^2\theta_3)\\
&-T_{B4}(B_4k_{B4}^2(\cos^2\theta_4+\mu_4\sin^2\theta_4))+T_{n4}(B_4(k_{n4}^2-\mu_4k_{B4}^2\sin^2\theta_4))\\
&+T_{B5+}(B_5k_{B5}^2(\cos^2\theta_5+\mu_5\sin^2\theta_5))-T_{n5+}(B_5(k_{n5}-\mu_5k_{B5}^2\sin^2\theta_5))\\
&+T_{B5-}(B_5k_{B5}^2(\cos^2\theta_5+\mu_5\sin^2\theta_5))-T_{n5-}(B_5(k_{n5}^2-\mu_5k_{B5}^2\sin^2\theta_5))\\
&=0
\end{aligned} \tag{5.90}$$

The sum of the forces in the z-direction can be given by,

$$F_{z3}-F_{z4}-F_{x5}=0 \tag{5.91}$$

and this may be written as,

$$\begin{aligned}
&-T_{B3}\left(iBk_{B3}^3\cos\theta_3\left(\cos^2\theta_3+(2-\mu_3)\sin^2\theta_3\right)\right)+T_{n3}\left(B_3k_{n3}(k_{n3}^2-k_{B3}^2\sin^2\theta_3)\right)\\
&+T_{B4}\left(iB_4k_{B4}^3\cos\theta_4\left(\cos^2\theta_4+(2-\mu_4)\sin^2\theta_4\right)\right)-T_{n4}\left(B_4k_{n4}(k_{n4}^2-k_{B4}^2\sin^2\theta_4)\right)\\
&-T_{L5+}\left(\frac{ik_{L5}E_5h_5}{1-\mu_5^2}\right)(\cos^2\theta_5+\mu_5\sin^2\theta_5)+T_{T5+}\left(\frac{ik_{T5}E_5h_5}{1-\mu_5^2}\right)(\sin\theta_5\cos\theta_5(1-\mu_5))\\
&-T_{L5-}\left(\frac{ik_{L5}E_5h_5}{1-\mu_5^2}\right)(\cos^2\theta_5+\mu_5\sin^2\theta_5)-T_{T5-}\left(\frac{ik_{T5}E_5h_5}{1-\mu_5^2}\right)(\cos\theta_5\sin\theta_5(1-\mu_5))\\
&=0
\end{aligned} \tag{5.92}$$

The sum of the forces in the x-direction is given as,

$$F_{x3}-F_{x4}+F_{z5}=0 \tag{5.93}$$

and this may be written as,

$$\begin{aligned}
&T_{L3}\left(\frac{ik_{L3}E_3h_3}{1-\mu_3^2}\right)(\cos^2\theta_3+\mu_3\sin^2\theta_3)+T_{T3}\left(\frac{ik_{T3}E_3h_3}{1-\mu_3^2}\right)(\cos\theta_3\sin\theta_3(1-\mu_3))\\
&-T_{L4}\left(\frac{ik_{L4}E_4h_4}{1-\mu_4^2}\right)(\cos^2\theta_4+\mu_4\sin^2\theta_4)+T_{T4}\left(\frac{ik_{T4}E_4h_4}{1-\mu_4^2}\right)(\cos\theta_4\sin\theta_4(1-\mu_4))\\
&+T_{B5+}(iB_5k_{B5}^3\cos\theta_5(\cos^2\theta_5+(2-\mu_5)\sin^2\theta_5))-T_{n5+}(k_{n5}(k_{n5}^2-(2-\mu_5)k_{B5}^2\sin^2\theta_5))\\
&-T_{B5-}(iB_5k_{B5}^3\cos\theta_5(\cos^2\theta_5+(2-\mu_5)\sin^2\theta_5))+T_{n5-}(k_{n5}(k_{n5}^2-(2-\mu_5)k_{B5}^2\sin^2\theta_5))\\
&=0
\end{aligned} \tag{5.94}$$

The sum of the forces in the y-direction may be given by,

$$F_{y3}-F_{y4}+F_{y5}=0 \tag{5.95}$$

and may be written as,

$$\begin{aligned}
&-T_{L3}\left(\frac{E_3h_3}{2(1+\mu_3)}\right)(2ik_{L3}\cos\theta_3\sin\theta_3)-T_{T3}\left(\frac{E_3h_3}{2(1+\mu_3)}\right)ik_{T3}(\sin^2\theta_3-\cos^2\theta_3)\\
&-T_{L4}\left(\frac{E_4h_4}{2(1+\mu_4)}\right)(2ik_{L4}\cos\theta_4\sin\theta_4)+T_{T4}\left(\frac{E_4h_4}{2(1+\mu_4)}\right)ik_{T4}(\sin^2\theta_4-\cos^2\theta_4)\\
&+T_{L5+}\left(\frac{E_5h_5}{2(1+\mu_5)}\right)(2ik_{L5}\cos\theta_5\sin\theta_5)-T_{T5+}\left(\frac{E_5h_5}{2(1+\mu_5)}\right)ik_{T5}(\sin^2\theta_5-\cos^2\theta_5)\\
&-T_{L5-}\left(\frac{E_5h_5}{2(1+\mu_5)}\right)(2ik_{L5}\cos\theta_5\sin\theta_5)-T_{T5-}\left(\frac{E_5h_5}{2(1+\mu_5)}\right)ik_{T5}(\sin^2\theta_5-\cos^2\theta_5)\\
&=0
\end{aligned} \tag{5.96}$$

When modelling the frame as a plate, plate 5, due to waves travelling in a positive and negative direction on the plate, eight wave amplitudes must be determined and these are, T_{B5+}, T_{n5+}, T_{L5+}, T_{T5+}, T_{B5-}, T_{n5-}, T_{L5-} and T_{T5-}. These eight waves are in addition to the sixteen waves at junction I and II on plates 1, 2, 3 and 4 discussed in section 5.3.2. Thus twenty-four wave amplitudes must be determined requiring twenty-four equations to solve in a matrix format. The twenty-four equations are,

eqns (5.58) (5.59) (5.61) (5.62) (5.64) (5.65)
(5.67) (5.68) (5.70) (5.72) (5.74) (5.76)
(5.78) (5.79) (5.81) (5.82) (5.84) (5.85)
(5.87) (5.88) (5.90) (5.92) (5.94) (5.96)

5.3.4 *Modelling the plate as an SEA subsystem*

When the size of the frame depth, d, is small then the phase relationship between the waves on the plate must be included. However, if d is very large then the phase will be less important and the plate could be modelled as an SEA plate subsystem, as shown in Fig 5.16.

This model neglects the phase of the waves as they pass from junction I to junction II but would still include the magnitude. The two junctions I and II are then modelled as independent 'T' junctions. This model would be expected to be the same as a finite plate model at high frequencies where d is large compared to the wavelength.

5.3.5 *Determination of the transmission coefficient and coupling loss factor*

Once the amplitudes of the various waves, detailed in section 5.3.2 and 5.3.3, have been calculated the next stage is to determine the transmission coefficient, τ_{ij}, from the source plate, i, to the receiving plates, j. The transmission coefficient between any two plates 1 and 2, τ_{12}, is defined as the ratio of the power transmitted across the joint to plate 2 to the incident power on the joint from plate 1. This may be given by,

$$\tau_{12} = \frac{W_{trans}}{W_{inc.}} \tag{5.97}$$

The power transmitted to plate 2, W_{12}, for a bending, longitudinal or transverse wave may be given by,

$$W_{12_B} = \frac{2|T_{B2}|^2 \rho_{s2} \omega^3 \cos\theta_{B2}}{k_{B2}} \tag{5.98}$$

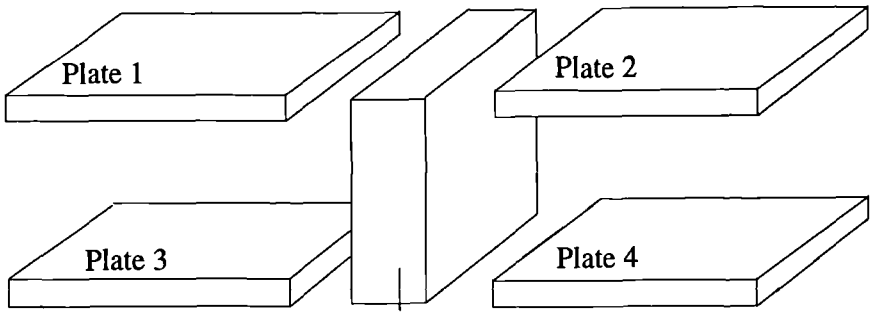

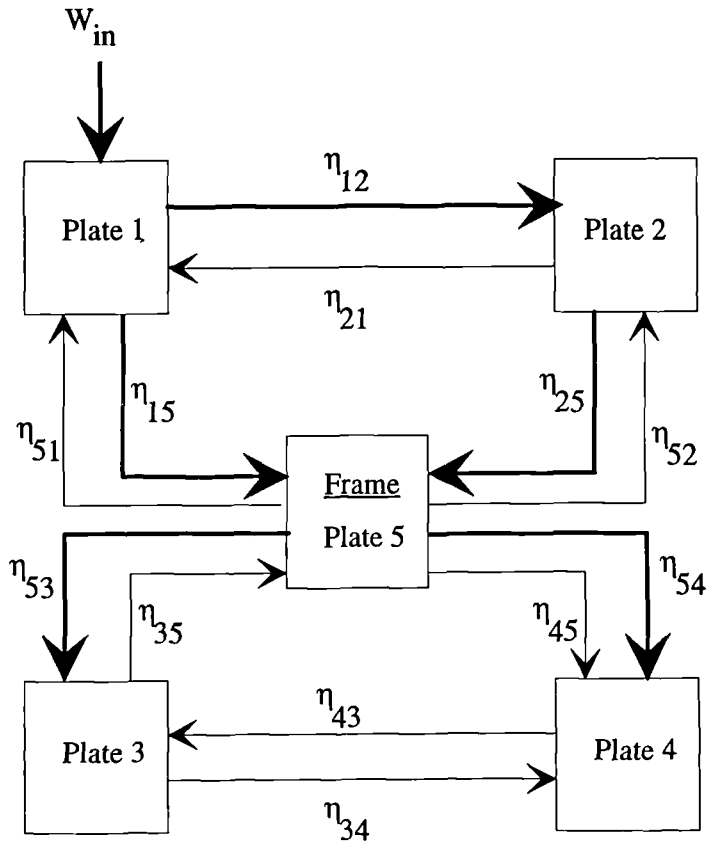

Figure 5.16 Structure configuration and SEA model for parallel plates and frame .

$$W_{12_L} = \frac{|T_{L2}|^2 \rho_{s2} \omega^3 \cos\theta_{L2}}{k_{L2}} \tag{5.99}$$

$$W_{12_T} = \frac{|T_{T2}|^2 \rho_{s2} \omega^3 \cos\theta_{T2}}{k_{T2}} \tag{5.100}$$

From the standard equations [11] for the incident power for a bending, longitudinal or transverse wave at the joint the transmission coefficient, τ_{12}, may be given. Considering an incident wave of unit amplitude, the transmission coefficient can be evaluated for any incident wave being transmitted to a bending wave on plate 2 by

$$\tau(\theta) = \frac{2\rho_{s2}|T_{B2}|^2 \cos\theta_{B2}}{k_{B2}\delta} \tag{5.101}$$

or for any wave being transmitted to a longitudinal wave on plate 2 by

$$\tau(\theta) = \frac{\rho_{s2}|T_{L2}|^2 \cos\theta_{L2}}{k_{L2}\delta} \tag{5.102}$$

and for any incident wave being transmitted to a transverse wave on plate 2 by

$$\tau(\theta) = \frac{\rho_{s2}|T_{T2}|^2 \cos\theta_{T2}}{k_{T2}\delta} \tag{5.103}$$

Where δ is given for an incident bending, longitudinal or transverse wave on plate 1 by,

$$\delta_B = \frac{2\rho_{s1}\cos\theta_{B1}}{k_{B1}} \quad \delta_L = \frac{\rho_{s1}\cos\theta_{L1}}{k_{L1}} \quad \delta_T = \frac{\rho_{s1}\cos\theta_{T1}}{k_{T1}} \tag{5.104a,b,c}$$

In SEA the sound field is assumed to be diffuse making it necessary to determine the angular average transmission coefficient, τ_{av}, in order to predict transmission. This is obtained by solving the equations for specific angles of incidence to obtain, $\tau(\theta)$, and

then numerically averaging these using [44],

$$\tau_{av} = \int_0^{\frac{\pi}{2}} \tau(\theta) \cos\theta \, d(\theta) \tag{5.105}$$

The transmission coefficient may then be used to determine the coupling loss factor [13] as given by,

$$\eta_{12} = \frac{2L_{12}}{\pi k_1 S_1} \tau_{12} \tag{5.106}$$

where S is the surface area of the source plate and L is the common boundary length of the joint. Once the coupling loss factors for the joint are known they can be used as part of an SEA model to predict transmission through the system of interest.

5.4 Comparison of theoretical models

This section compares the various theoretical models discussed in section 5.4. Fig 5.17 shows the standard 'H' structure for parallel plates connected by a frame and Table 5.1 gives the material properties. Studies of the transmission loss between the parallel plates for various types of wave motion are presented including a study of the transmission coefficient as a function of the angle of incident at various frequencies.

In some of the following graph figures there are small fluctuations for the predicted transmission loss and the curves are not always smooth. This is due to the level of computational accuracy. The time required to compute the various line models depends upon the accuracy required. The smooth curves which are presented were computed over a large period of time and to a high level of accuracy involving thousands of incident angles at narrow frequency bands. In some cases this was not always required as the increased computational time did not alter the transmission loss significantly. Hence some figures have small fluctuations in the transmission loss curve due to a smaller period of computation.

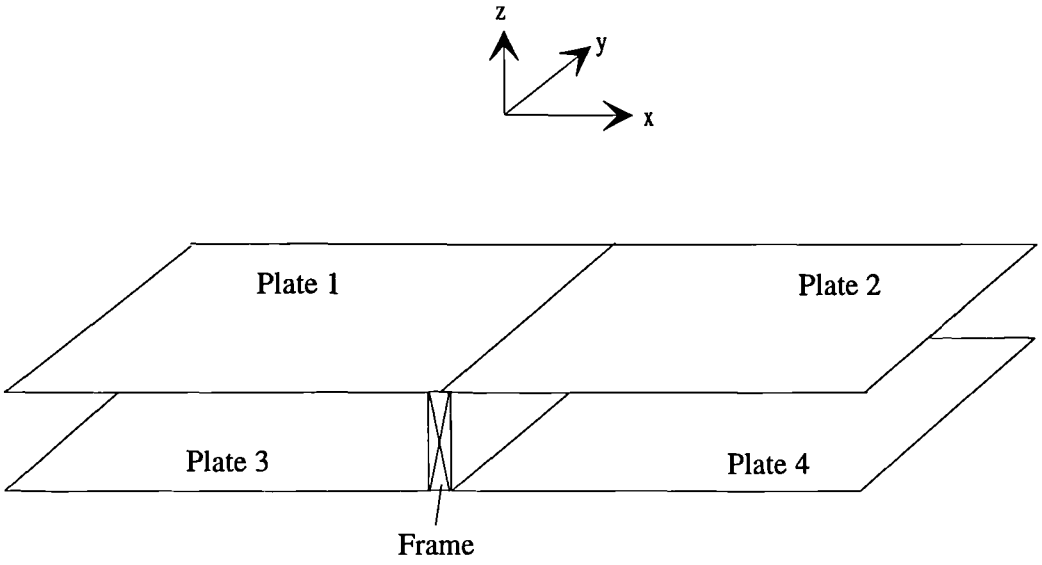

Figure 5.17 Plate configuration for a standard 'H' structure with frame

	Dimensions			ρ (kg/m^3)	E (N/m^2)	μ	η_i (ILF)
	Lx	Ly	Lz				
Plate 1,2, 3 and 4	2.0	2.0	0.013	800	1.966e^9	0.2	0.01
Frame	0.05	2.0	0.25	450	9.113e^9	0.3	0.015

Table 5.1 Material property values for plasterboard plates and timber beam.

Fig 5.18 shows the predicted transmission loss from plate 1 to plates 2, 3 and 4, for transmitted bending, longitudinal and transverse wave motion, due to a source bending wave on plate 1 when modelling the frame as a beam. As may be seen in Fig 5.18 the transmission loss values for plates 2, 3 and 4 are very similar. This is because for an incident bending wave no account is taken for the offset, between the top and bottom plates, and also all transmission to the receiving plates must pass through the beam and are equally affected. It might be expected that the transmission from plate 1 to plate 2 would be stronger than the transmission to the offset plates, but the theory given in eqn(5.22a,b,c) requires that the bending displacement on all four plates is the same. Furthermore in no other equation describing the flexural wave motion is the offset mentioned. However, the theory for inplane displacement on plates 3 and 4, due to an incident longitudinal wave on plate 1 given by eqns(5.28b,c), does require that the offset is taken into account and this will be shown later.

Fig 5.19 shows the predicted transmission loss from plate 1 to plates 2, 3 and 4 for an incident bending wave on plate 1 when the frame is modelled as a plate. At the high frequencies (above 2000Hz) the inplane transmission loss to plates 3 and 4 is of a similar value to the bending to bending transmission loss. Also the flexural transmission loss to plates 2, 3 and 4 is similar up to 8000Hz. The inplane transmission on plates 2, 3 and 4 increases rapidly (about 2000Hz) due to flexural wave motion in the frame and at 8000Hz significant wave transferal occurs at the frame increasing the transmission by up to 8dB. These relate approximately to $\lambda_B/2$ and λ_B flexural conditions. Above 8000Hz the flexural transmission loss is weaker on plates 3 and 4 when compared to plate 2 as the wave motion on the offset plates is dependent upon the inplane wave motion on the frame (plate 5) at these frequencies.

The importance of transferring from one wave type to another is shown in Fig 5.20 which shows the predicted longitudinal transmission loss from plate 1 to plates 2, 3 and 4 for an incident longitudinal wave on plate 1 when modelling the frame as plate. As a result of an incident longitudinal wave on plate 1 this may transfer into a bending wave on plate 5 (the frame) and then transfer into longitudinal wave motion on plate 3 and 4. Therefore when the angle of incidence is capable of transfering a longitudinal wave on plate 1 into a bending wave on plate 5 the transmission loss will increase to

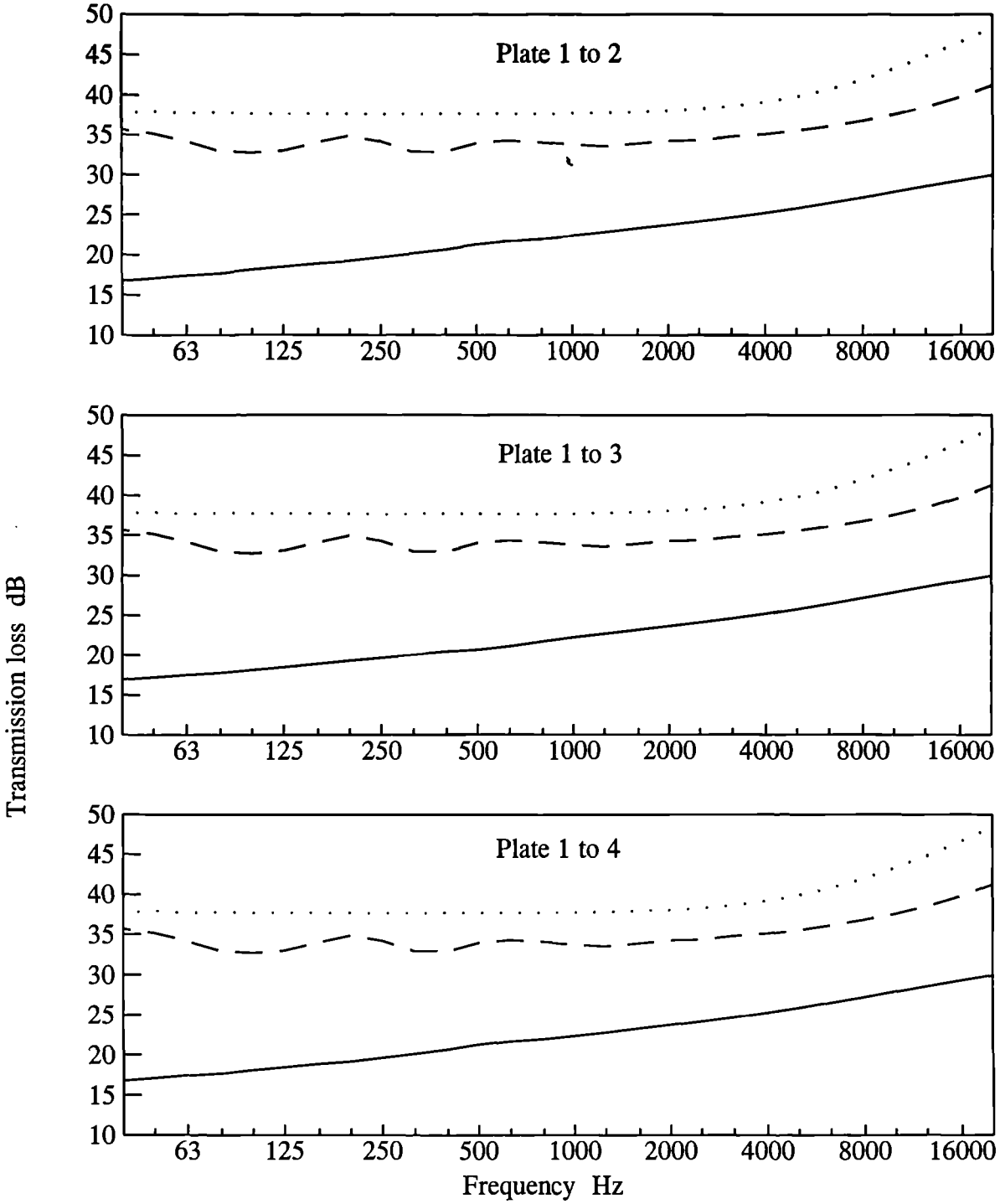

Figure 5.18 Predicted transmission loss from plate 1 to 2, 3 and 4, for transmitted bending, longitudinal and transverse waves, due to a source bending wave on plate 1 when modelling the frame as a beam.
(____) B-B, (....) B-L, (- - -) B-T.

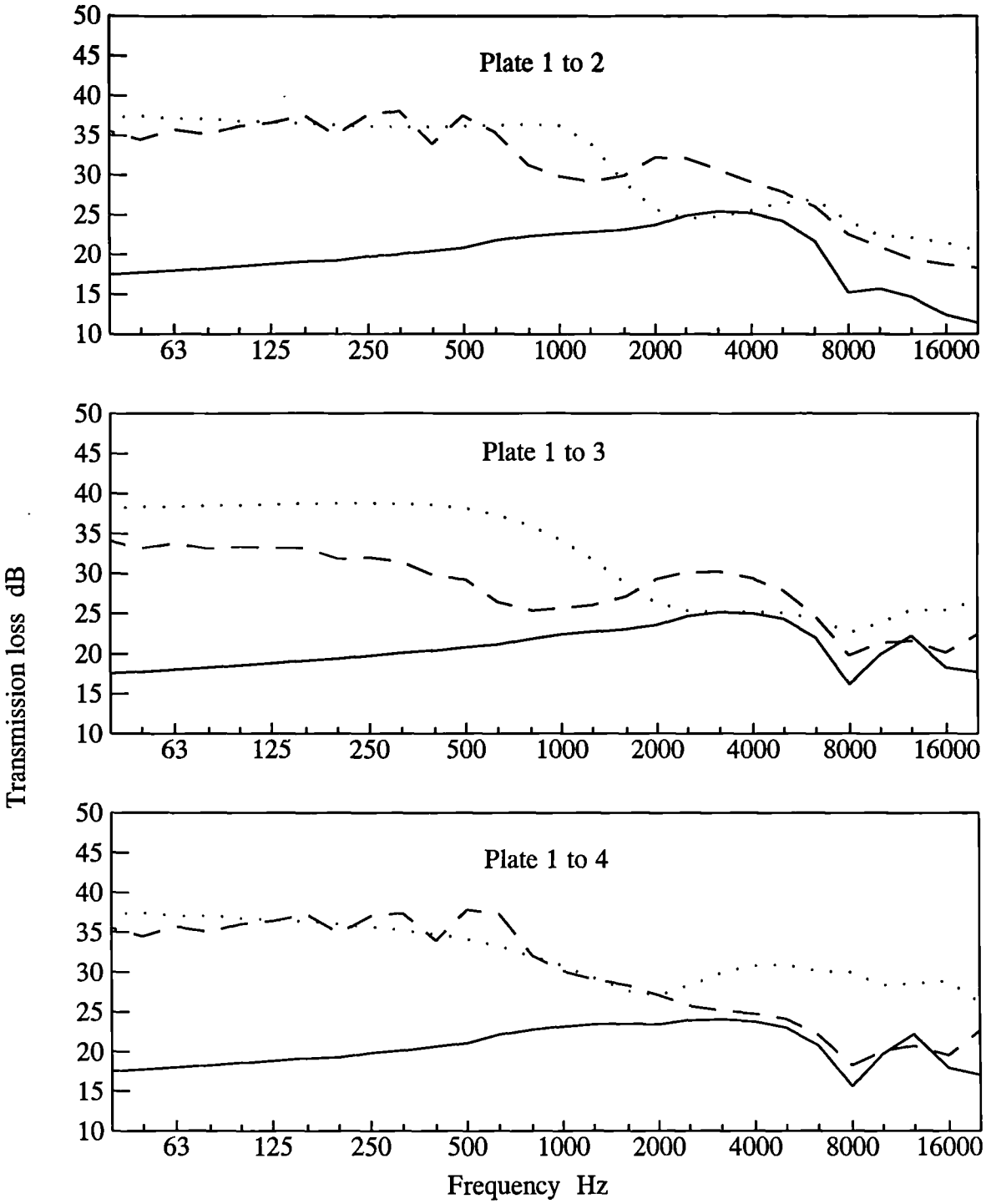

Figure 5.19 Predicted transmission loss from plate 1 to 2,3 and 4, for transmitted bending, longitudinal and transverse waves, due to a source bending wave on plate 1 when modelling the frame as a plate.
(____) B-B, (....) B-L, (- - -) B-T.

plates 3 and 4 and decrease on plate 2 for longitudinal wave motion. Fig 5.20 shows these conditions quite clearly by the increase in transmission resulting in reduced transmission loss for plates 3 and 4 and increasing transmission loss for plate 2 at 2000Hz and 8000Hz. Fig 5.21 shows a similar study to that shown in Fig 5.20 but when modelling the frame as a beam. The lack of wave motion predicted when modelling the frame as a beam is evident by the absence of wave transferal in Fig 5.21 when compared to Fig 5.20. However an important aspect of the predicted results for longitudinal transmission shown in Fig 5.21 is the difference in the values between plates 2 to 3 and 4. As mentioned previously the inplane displacement for the beam model does take account of the offset between plates 2 and 3 and 4 for an incident longitudinal wave on plate 1. Hence the transmission is stronger to plate 2 than to plates 3 and 4 due to the offset.

Fig 5.22 shows the normal and random incidence transmission paths across the frame when modelled as a plate, (only plates 1 to 4 are shown for clarity). Fig 5.23 shows a comparison between random incidence and normal incidence calculated transmission loss for two plates offset by the frame. As expected, the normal incidence transmission is increased (more pronounced) where the wavelength equals or is a multiple of the frame depth. Fig 5.24 and 5.25 show the predicted transmission loss from plate 1 to plates 2, 3 and 4 for an incident transverse wave on plate 1 where the frame is modelled as a plate and a beam. The predicted results for plates 3 and 4 are identical over the majority of the frequency range using the beam theory and are almost identical in the plate model. Due to the offset between the plates, which is accounted for in the theory, this results in weaker transmission to plates 3 and 4.

Fig 5.26 shows the transmission loss as a function of angle of incidence for an 'H' plate structure when modelling the frame as a plate. Transmission to all three plates is increased when $\sin\theta$ equals 0.132 or θ equals 7.5° (relative to the normal). Interestingly the transmission loss for plate 2 in Fig 5.26 shows a strong reflection taking place at the junction between plate 1 and plate 2 due to the sudden increase in transmission loss when $\sin\theta$ equals 0.3. This is where there is high reflection at the joint back to plate 1.

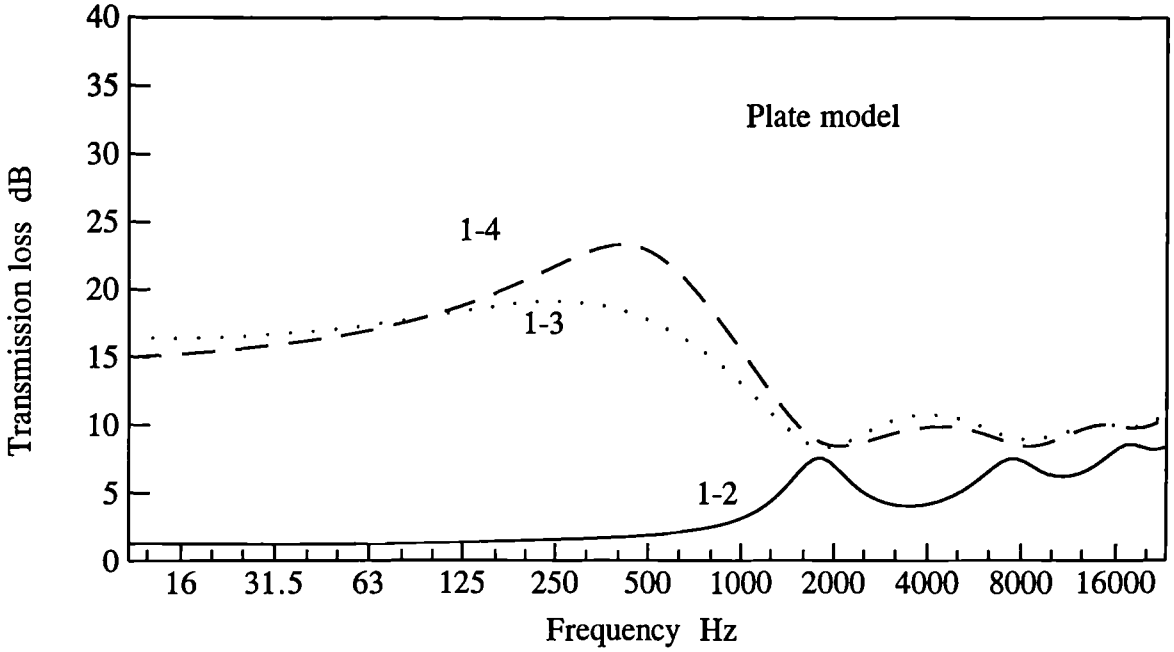

Figure 5.20 Predicted longitudinal transmission loss from plate 1 to 2, 3 and 4 for an incident longitudinal wave on plate 1 when the frame is a plate

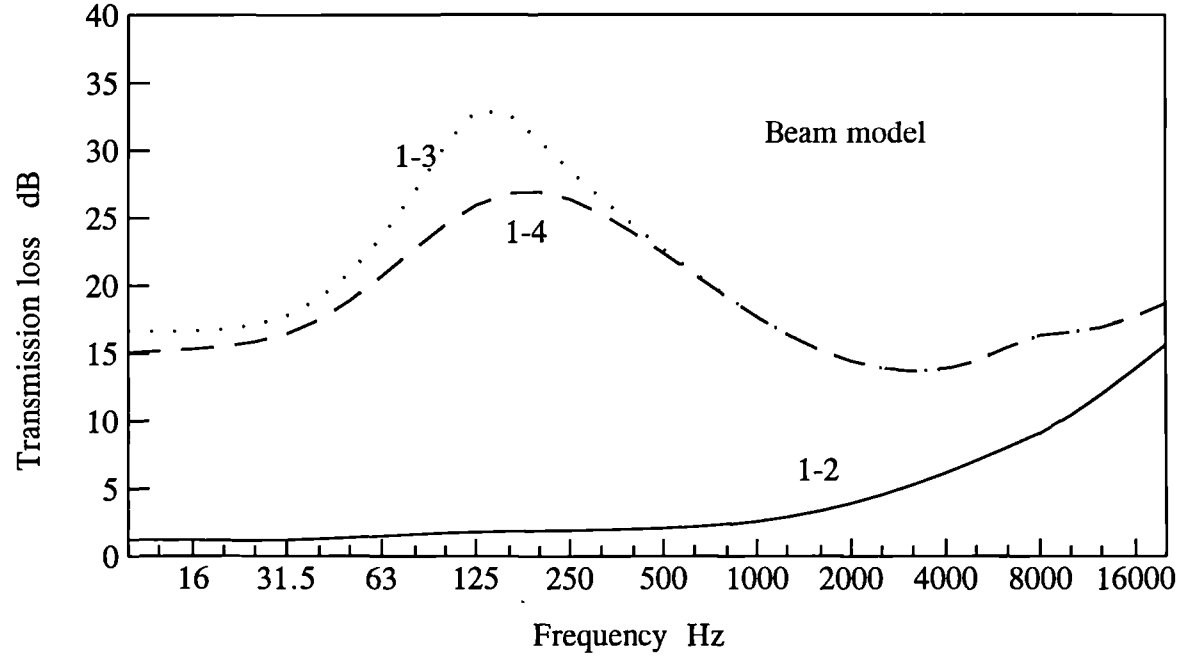

Figure 5.21 Predicted longitudinal transmission loss from plate 1 to 2, 3 and 4 for an incident longitudinal wave on plate 1 when modelling the frame as a beam.

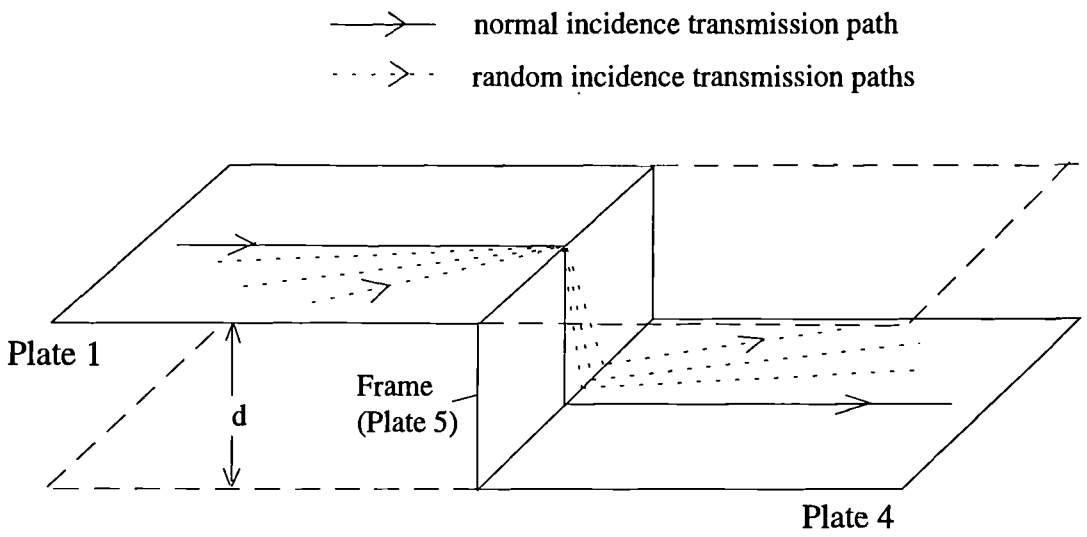

Figure 5.22 Normal and random incidence transmission paths from plate 1 to plate 4 in an 'H' plate structure where the frame is a plate.

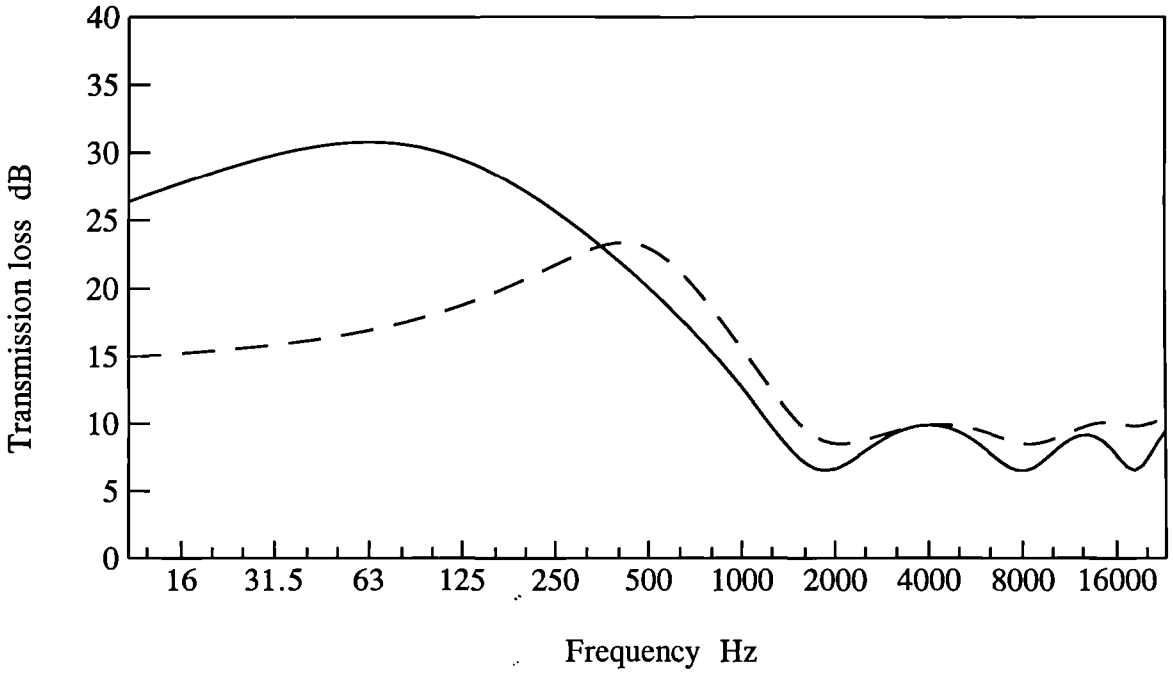

Figure 5.23 Predicted transmission loss from plate 1 to plate 4 for an incident longitudinal wave on plate 1 and longitudinal wave motion on plate 4 comparing normal and random incidence. (____) norm. (- - -) random.

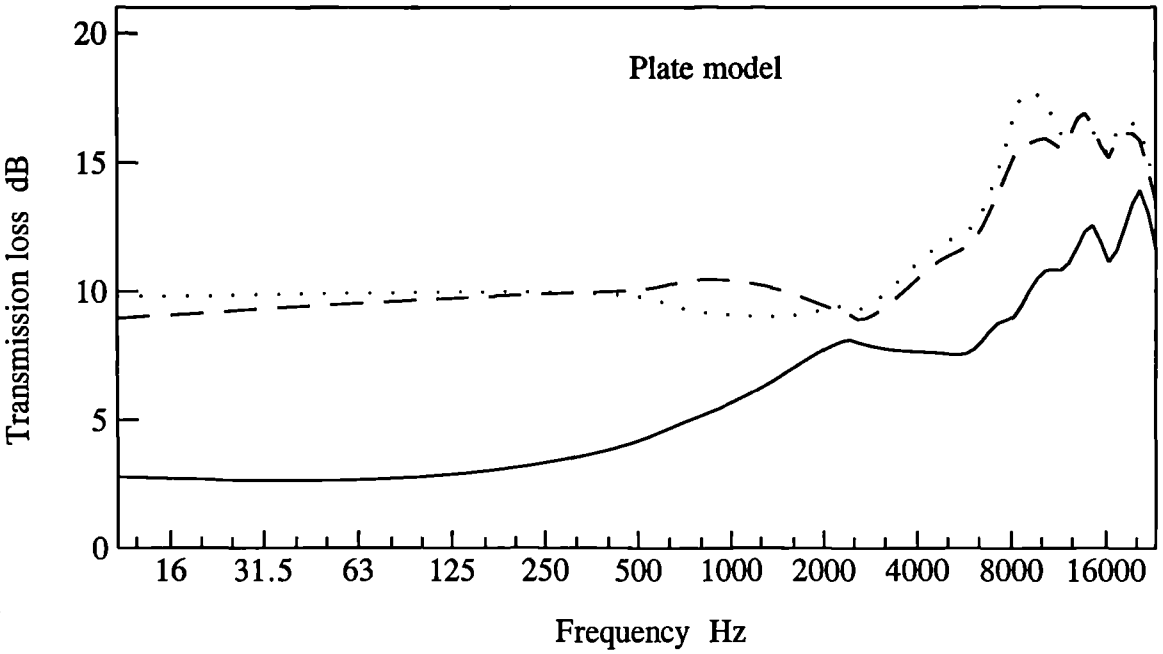

Figure 5.24 Predicted transmission loss for an incident transverse wave on plate 1 and resultant transverse wave motion on plates 2, 3 and 4.where the frame is modelled as a plate. (___) plate 1 to 2, (...) plate 1 to 3, (- - -) plate 1 to 4

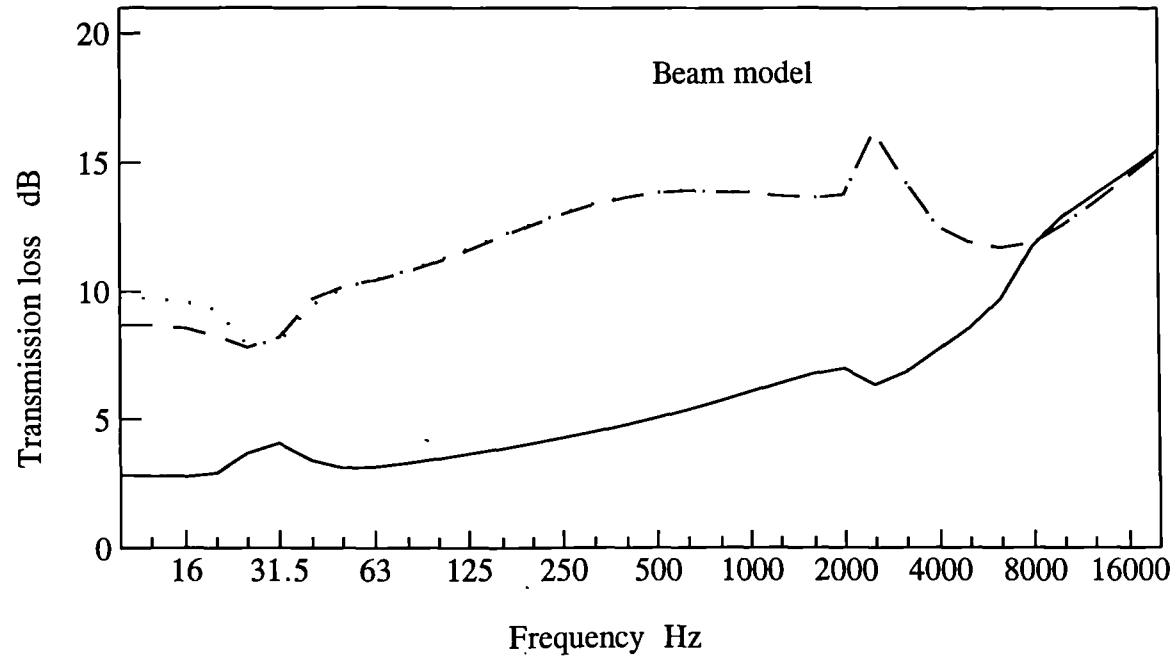

Figure 5.25 Predicted transmission loss for an incident transverse wave on plate 1 and resultant transverse wave motion on plates 2, 3 and 4 where the frame is a beam. (___) plate 1 to 2, (...) plate 1 to 3, (- - -) plate 1 to 4

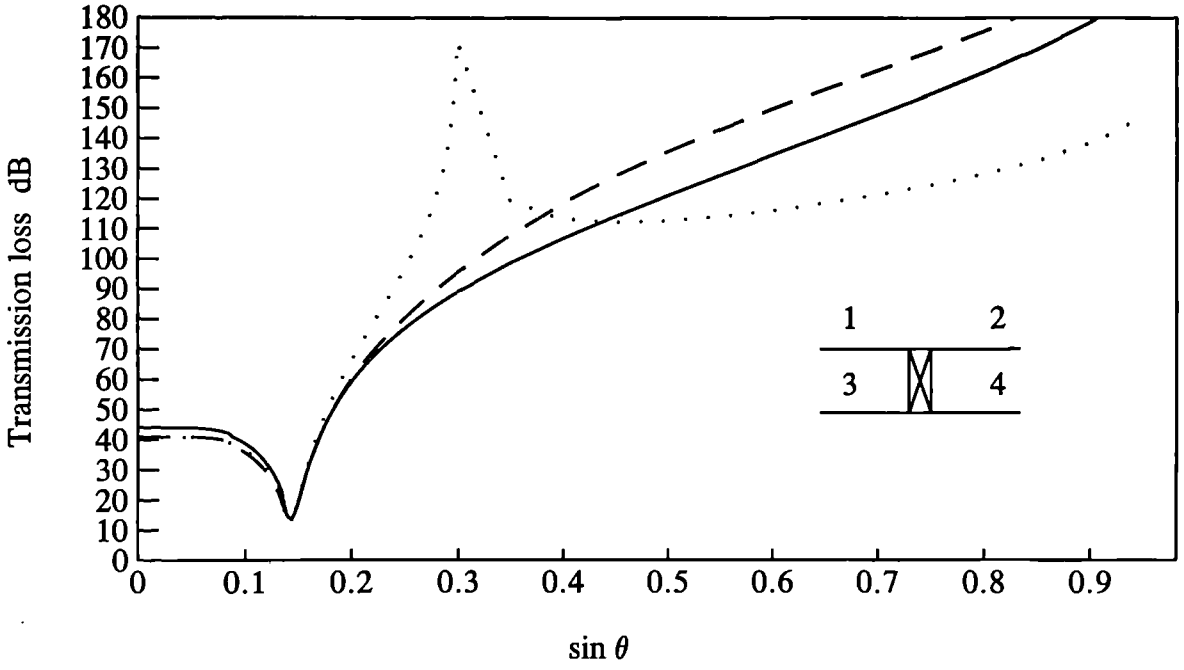

Figure 5.26 Transmission loss as a function of angle of incidence for an 'H' plate structure modelling the frame as a plate at 500Hz.
(....) plate 1 to 2, (- - -) plate 1 to 3, (____) plate 1 to 4.

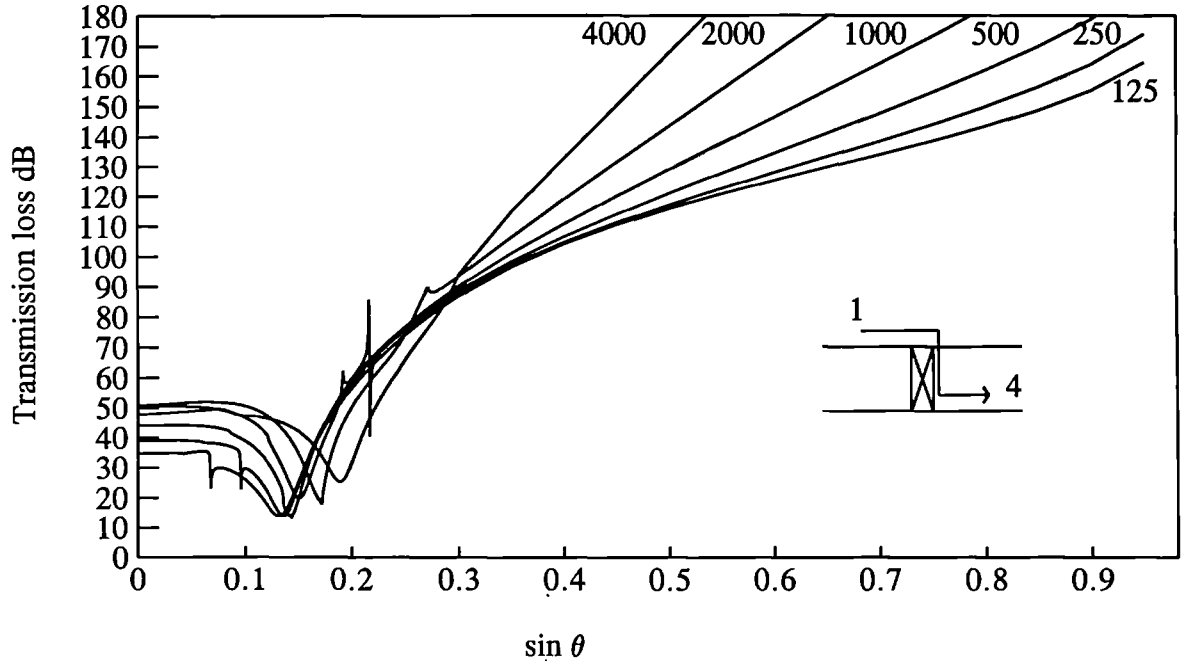

Figure 5.27 Transmission loss as a function of angle of incidence from plate 1 to plate 4 for various frequencies when the frame is modelled as a plate.

Fig 5.27 shows the transmission loss as a function of angle of incidence from plate 1 to plate 4 for an 'H' plate structure calculated for various frequencies when the frame is modelled as a plate. It can be seen that as the frequency increases so the angle where maximum transmission occurs also increases.

Fig 5.28 shows the predicted transmission loss from plate 1 to plate 4 for a standard 'H' structure where the plate thickness of plates 3 and 4 is varied by a factor of 4, 2, 1, 1/2 and 1/4. For an incident bending wave on plate 1 the transmission loss is calculated for the resultant bending, longitudinal and transverse wave motion on plate 4. For transfer to longitudinal and transverse wave motion on plate 4, as the plate thickness increases so the transmission loss increases. However, due to the redistribution of energy for the various types of waves and the bending stiffness increases at a faster rate than the inplane stiffness, the bending to bending has an opposite effect for the frequency range studied. As the plate thickness increases so the transmission loss decreases and increased transmission results.

Fig 5.29 shows the predicted acceleration level difference from plate 1 to plates 2, 3 and 4 for an incident bending wave on plate 1 and resultant bending wave motion on the receiving plates comparing the plate, beam and SEA prediction models. The plate model is similar to the beam model at low frequencies where there are no resonant conditions in the frame due to the frame depth being smaller than the wavelength. At the higher frequencies the SEA model, which models the frame as a plate, is similar to the plate model when there are resonant conditions in the frame. At these higher frequencies the frame depth is large in comparison to the wavelength and thus is able to support full wave motion.

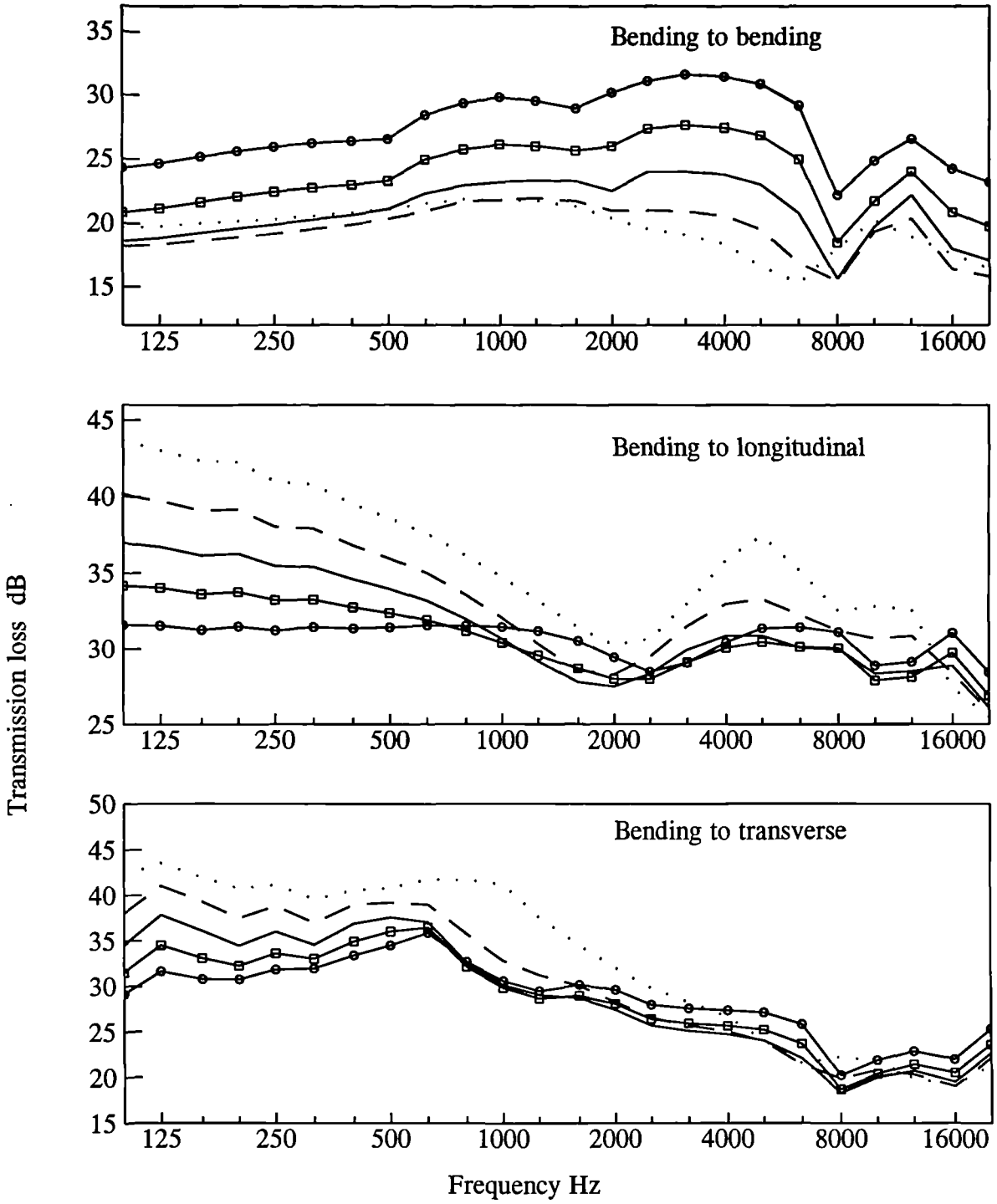

Figure 5.28 Predicted transmission loss from plate 1 to plate 4 for an incident bending wave on plate 1 and resultant bending, longitudinal and transverse waves on plate 4, for varying thickness of plates 3 and 4. Plates 1 and 2, 13mm thick. Plates 3 and 4, (....) 52mm, (- -) 26mm, (___) 13mm, (□) 6.5mm, (o) 3.25mm.

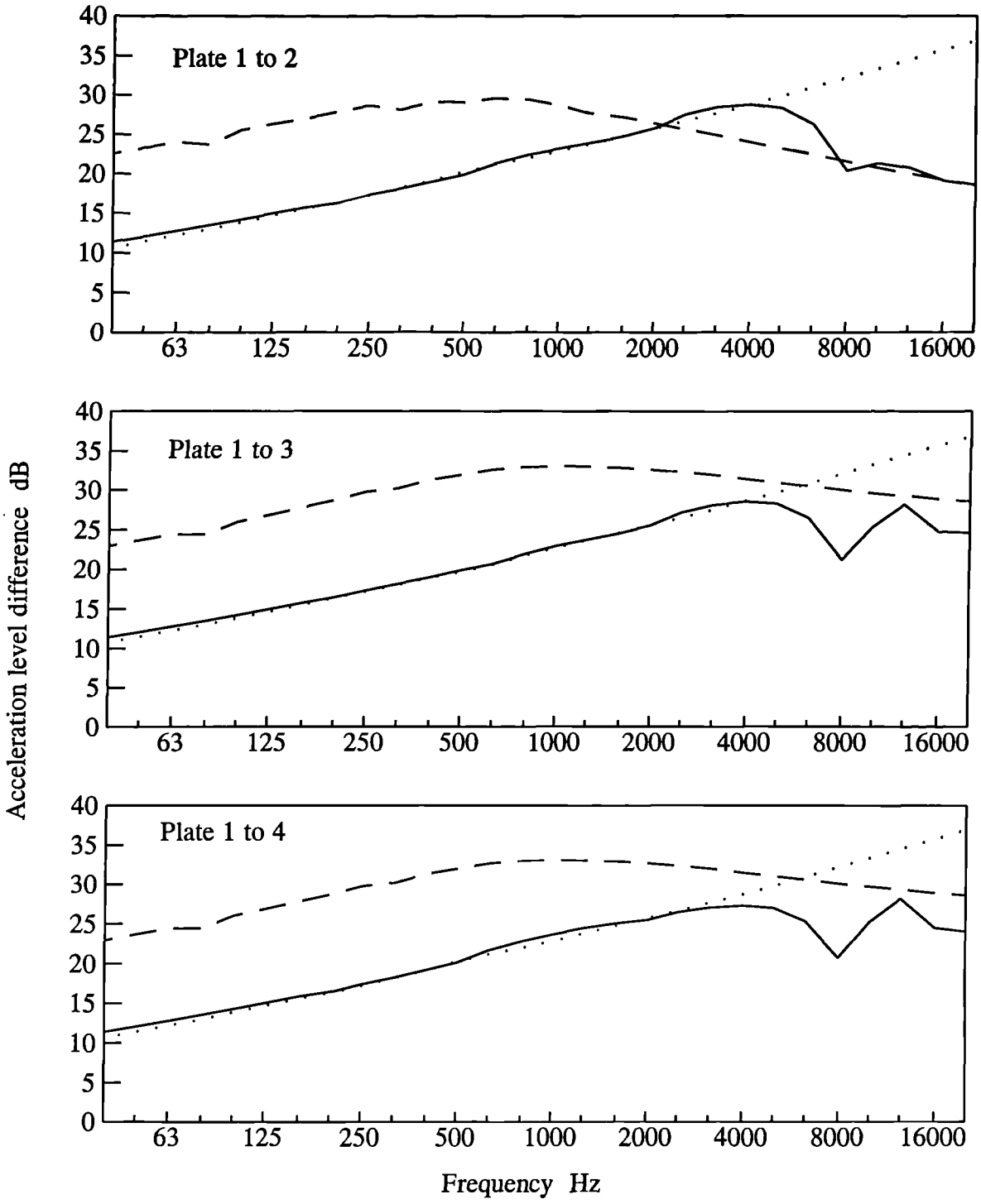

Figure 5.29 Predicted acceleration level difference from plate 1 to plates 2, 3 and 4, comparing plate, beam and SEA models.
(___) plate model, (....) beam model, (- - -) SEA model.

5.5 Parametric survey of the frame using the plate model

Due to the number of material properties of the frame, which if altered may change the transmission loss, the following section is a parametric study of varying such parameters. As will be shown in Chapter 6, which compares the measured and predicted acceleration level differences between plates 1 to 2, 3 and 4, modelling the frame as a plate gives the best comparison with the measured results. Consequently this section describes the possible changes to the transmission loss for parallel plate structures when the frame is modelled as a plate. The following frame parameters are studied:-

* Depth or offset (d),
* Thickness (h),
* Density (ρ),
* Longitudinal wavespeed (C_L),
* and Poisson ratio (μ).

The parametric study presented is for transmission loss (dB) plotted against a frequency range of 100Hz to 10KHz. The structure is that of a full "H" structure as detailed in section 5.5 and the materials used are those as found in a standard plasterboard partition. The transmission loss, given by (10 log $1/\tau$), was calculated for an incident bending wave on plate 1 and the resultant bending wave motion on plate 4. As shown in Fig 5.18 the bending transmission loss to plates 2, 3 and 4 are similar, and thus any changes to the frame parameters will affect all three plates. This study analyses each parameter in turn with the basic plate having the following parameter values;

$$d=0.25m \quad b=0.05m \quad \rho=450kg/m^3 \quad C_L=4500m/s \quad \mu=0.2 \quad ILF=0.015$$

Each of the above parameter values is varied by a multiple of 4, 2, 1, 1/2, and 1/4. All parameter values studied which represent the basic plate or frame are shown in each figure by the following symbol (□).

Fig 5.30 and Fig 5.31 show the effect to transmission loss when varying the values of the frame depth and thickness. From eqn(4.1), which can be used to calculate the

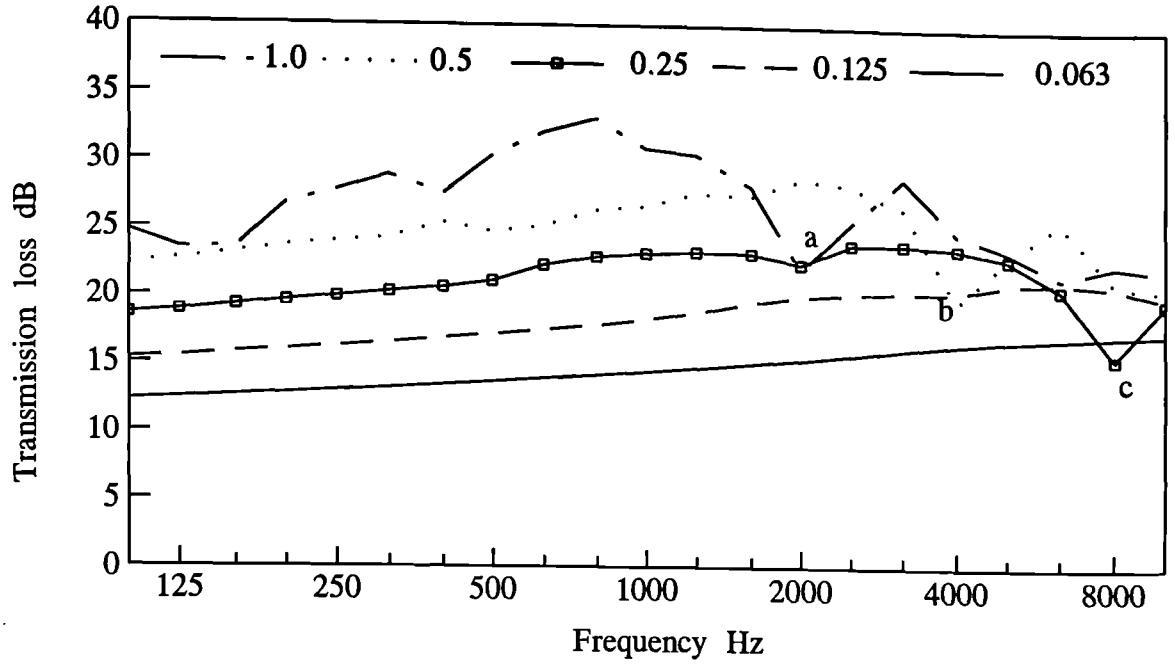

Figure 5.30 Predicted transmission loss from plate 1 to plate 4 with varying frame depth.

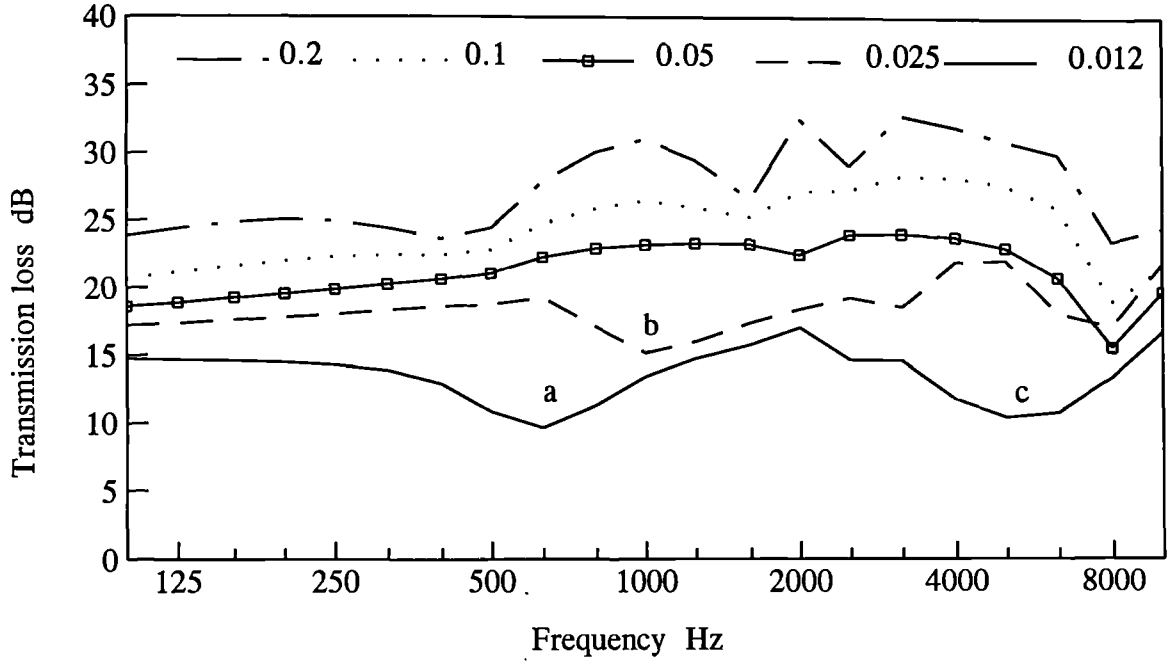

Figure 5.31 Predicted transmission loss from plate 1 to plate 4 with varying plate thickness.

frequencies where the first wavelength may fit into the frame depth, any increase to the plate thickness has the opposite effect to varying the plate depth which is related to the wavelength term in the denominator. Thus in Fig 5.30 as the plate depth increases, by a factor of 2, so the offset between the parallel plates is increased and the transmission loss to plate 4 will be increased by 3dB. However, wave motion will be able to be supported within the frame at a lower frequency and this is shown at points *a, b* and *c* in Fig 5.30.

Varying the frame thickness has the opposite effect as shown in Fig 5.31. As the plate thickness increases, similar to varying the plate depth, the transmission loss increases, however the wave motion is supported in the frame at higher frequencies. Thus increasing both variables, depth and thickness, will increase the transmission loss, but will have the opposite effect for the frequency where the frame may support flexural wave motion.

Fig 5.32 shows the effect to transmission loss when varying the frame density. For every doubling of the frame density the transmission loss increases by 2-3dB in the mid frequency range shown.

Another influential parameter is the longitudinal wavespeed which is shown in Fig 5.33. As will be shown in the next chapter this has an important role when predicting structure borne sound transmission through timber frames in partitions. As the longitudinal wavespeed decreases so the wavelength required to fit within the frame depth occurs at a lower frequency. This is shown in Fig 5.33 at the points labelled *a*, *b*, *c* and *d*. The higher the longitudinal wavespeed the higher the Young's modulus and the higher the bending stiffness. As the frame increases in stiffness so the transmission loss increases.

Fig 5.34 shows the effect to transmission loss by varying the Poisson ratio. The Poisson ratio is defined as the ratio between the relative lateral contraction to the relative longitudinal extension. In order for the volume to remain constant the lower limit of Poisson ratio is 0 and the upper limit is 0.5 [15] and thus only four values of Poisson ratio are shown. As the Poisson ratio approaches 0.5 the material is more soft. Thus typical values for other materials such as steel may be 0.2 and for soft rubber 0.48 [15].

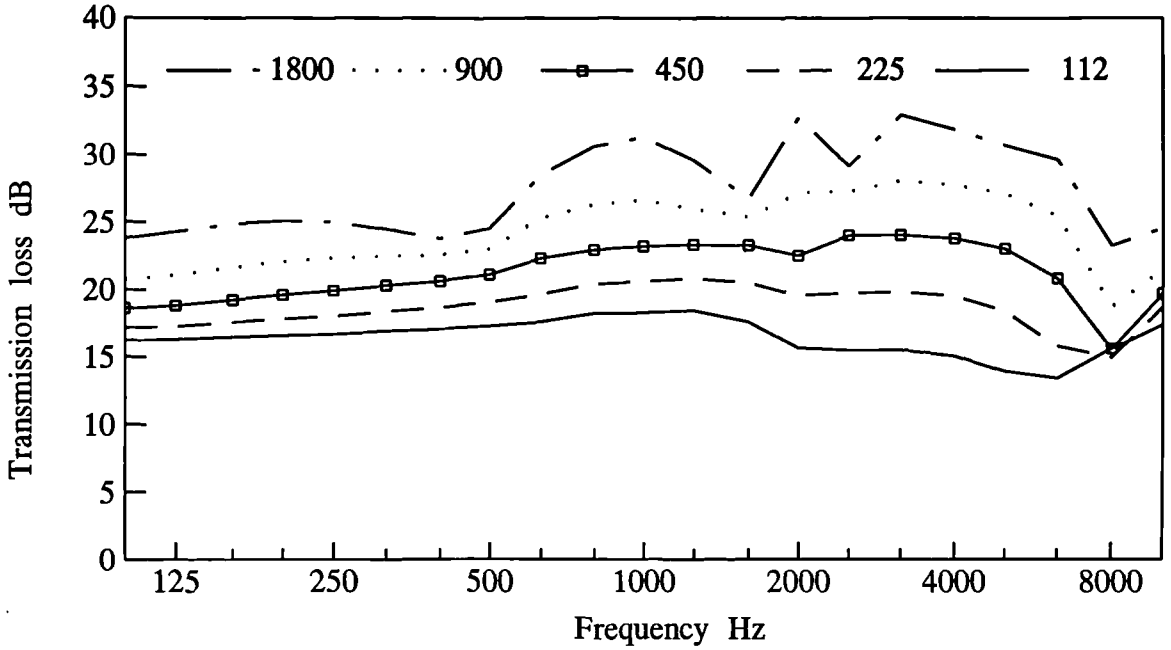

Figure 5.32 Predicted transmission loss from plate 1 to plate 4 with varying frame density.

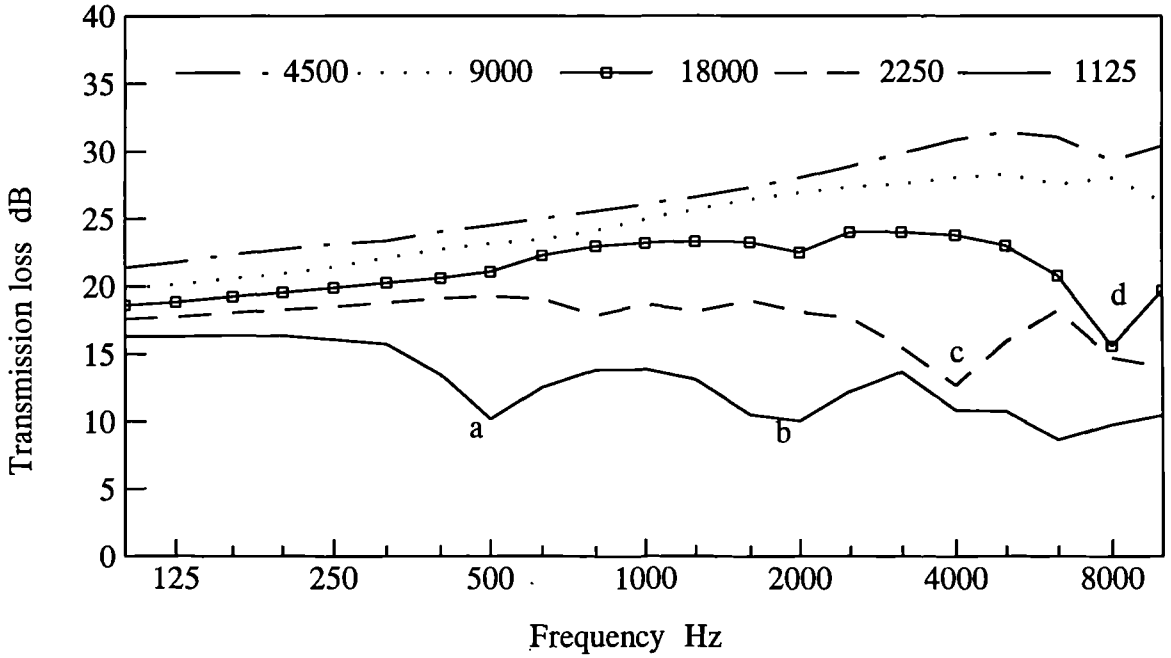

Figure 5.33 Predicted transmission loss from plate 1 to plate 4 with varying frame longitudinal wavespeed.

Fig 5.34 shows that any change to the value of the Poisson ratio for the frame has no real effect on the transmission loss.

5.6 Discussion

The models presented in section 5.3.2 can provide detailed analysis of wave behaviour on the plates. Terms have been included for incident flexural and inplane waves. When the frame is modelled as a finite plate this can include the transmitted and reflected waves between the two junctions. The plate model is similar to the beam model at the low frequencies when the wavelength under study is larger than the frame depth. At the higher ferquencies the plate model is similar to the SEA model, where the junctions are modelled as two 'tee' joints. If the frequency range of interest results in a wavelength which is larger and smaller than the frame depth then the plate model is capable of predicting over the entire frequency range of interest. If the wavelength is constantly larger than the frame depth then the more simplified beam model is sufficient.

The plate model is capable of predicting any changes to the material properties of the frame. It has been shown that if the frame width or depth is varied this can have a considerable effect on the transmission loss. This is important for the design of structures within the area of floors and walls where sizes of the joists or studs are stipulated in the Building Regulations [1,2] primarily for structural reasons. The joists and studs could be designed such that they still met the structural requirements but also they could be sized to reduce the structure borne sound transmission through the walls and floors.

Revising the beam model

In section 5.3.2 the theory was presented for modelling the frame as a beam. Similar to the plate model and SEA model the boundary conditions required that the displacement at the joint was continuous, the slopes or (angular displacement) were equal on all four or five plates and that the sum of the moments and forces in the x, y and z-direction were equal to zero. As has already been discussed there is no account for the offset between the top and bottom plates within the beam model for flexural wave motion. During the course of this work it was found that the slope boundary condition may play a significant role in changing the calculation for flexural wave motion between the

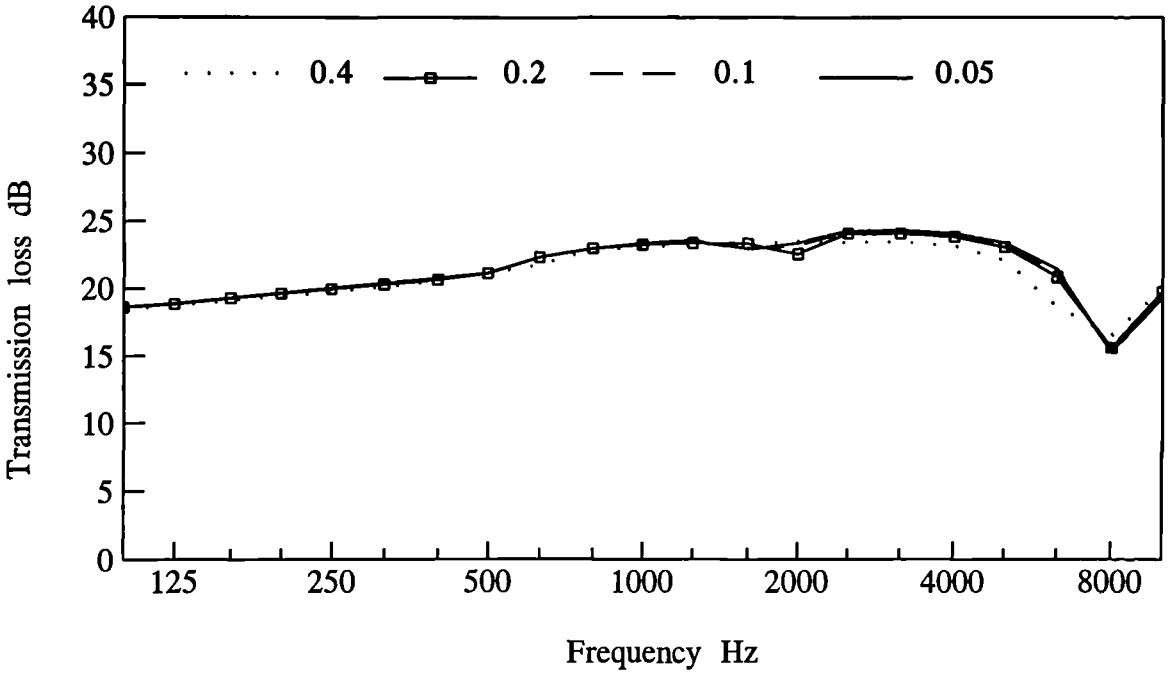

Figure 5.34 Predicted transmission loss from plate 1 to plate 4 with varying frame Poisson ratio.

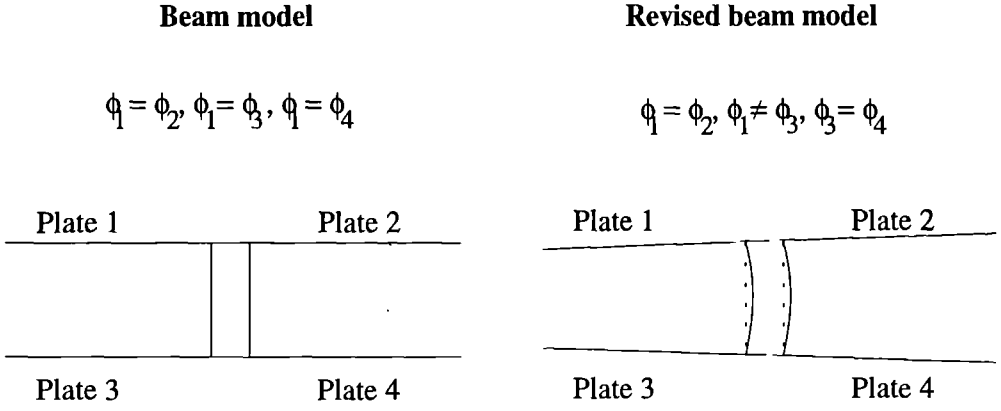

Figure 5.35 Slope boundary conditions for the beam model and revised beam model

parallel plates. Fig 5.35 shows that the slopes between the top and bottom parallel plates may not always be equal and that the beam cross section may bend about the x-axis. Hence the slope boundary conditions are affected and results in changes to the other equations where the slope terms are used. The slope terms appeared in the beam model equations for the moments, displacement in the x-direction and forces in the x-direction. The following outlines the new boundary conditions and changes to the respective equations. Thus the boundary conditions are as follows:-

(i) Continuity of displacement across the joint,
(ii) Slope of plate 1 is not equal to the slope of plates 3 and 4,
(iii) Sum of the bending moment about the y-axis is zero,
(iv) Sum of the forces in the x, y and z-direction are zero.

Changes to the slope

From Fig 5.35 the slope of plate 1 equals the slope of plate 2, but no longer equals that of plates 3 and 4. The slope on plate 3 equals plate 4. Equation (5.36a) remains the same and is given by,

$$\phi_1 = \phi_2 \tag{5.107}$$

The slope on plates 3 and 4 is as a result of the moments on plates 1 and 2 and the beams resistance to bending D_y [44]. Both plates 1 and 2 rotate by an angle as given by eqn(5.7) and plates 3 and 4 rotate with respect to plates 1 and 2 by [44],

$$\phi_1 - \phi_3 = \frac{\partial^2 \eta}{\partial x^2} = -\frac{M_1 - M_2}{D_y} \tag{5.108}$$

Thus the equation for the slope on plate 3 and 4, which replaces eqn(5.36b,c), is given as,

$$\phi_3 = \phi_4 = \phi_1 + \frac{M_1 - M_2}{D_y} \tag{5.109}$$

where D_y is given by,

$$D_y = \frac{Eb^3}{12d} \tag{5.110}$$

Fig 5.36 shows the relationship between the Young's modulus and the various bending stiffnesses of the beam when the frame is timber. Chapter 2 discussed the longitudinal wavespeed properties of timber in the radial, tangential and axial directions.

Changes to the displacement in the x-direction

In eqn(5.28b) the slope of plate 1 was used to determine the displacement in the *x*-direction for plates 3 and 4. As the slope of plate 1 and plate 3 are no longer equal, using eqn(5.108) the inplane displacement for plates 3 and 4 may be written as,

$$\xi_3 = \xi_4 = \xi_1 + \left[\frac{\phi_1 + \phi_3}{2}\right] d = \xi_1 + \left[\phi_1 + \frac{(M_1 - M_2)}{2D_y}\right] d \tag{5.111}$$

Changes to the total resisting moment in the beam

The twisting and torsional moments in the beam also use the slope term which must be altered due to the change in the boundary conditions. The slope of the beam at its centre is required and is given as,

$$\phi^{\diamond} = \frac{\phi_1 + \phi_3}{2} = \phi_1 + \frac{M_1 - M_2}{2D_y} \tag{5.112}$$

Thus eqn(5.41) for the total resisting moment in the beam may be given by,

$$M^{\diamond} = -\omega^2 \Theta \left[\frac{\phi_1 + \phi_3}{2}\right] - G \frac{\partial^2}{\partial y^2} \left[\frac{\phi_1 + \phi_3}{2}\right] \tag{5.113}$$

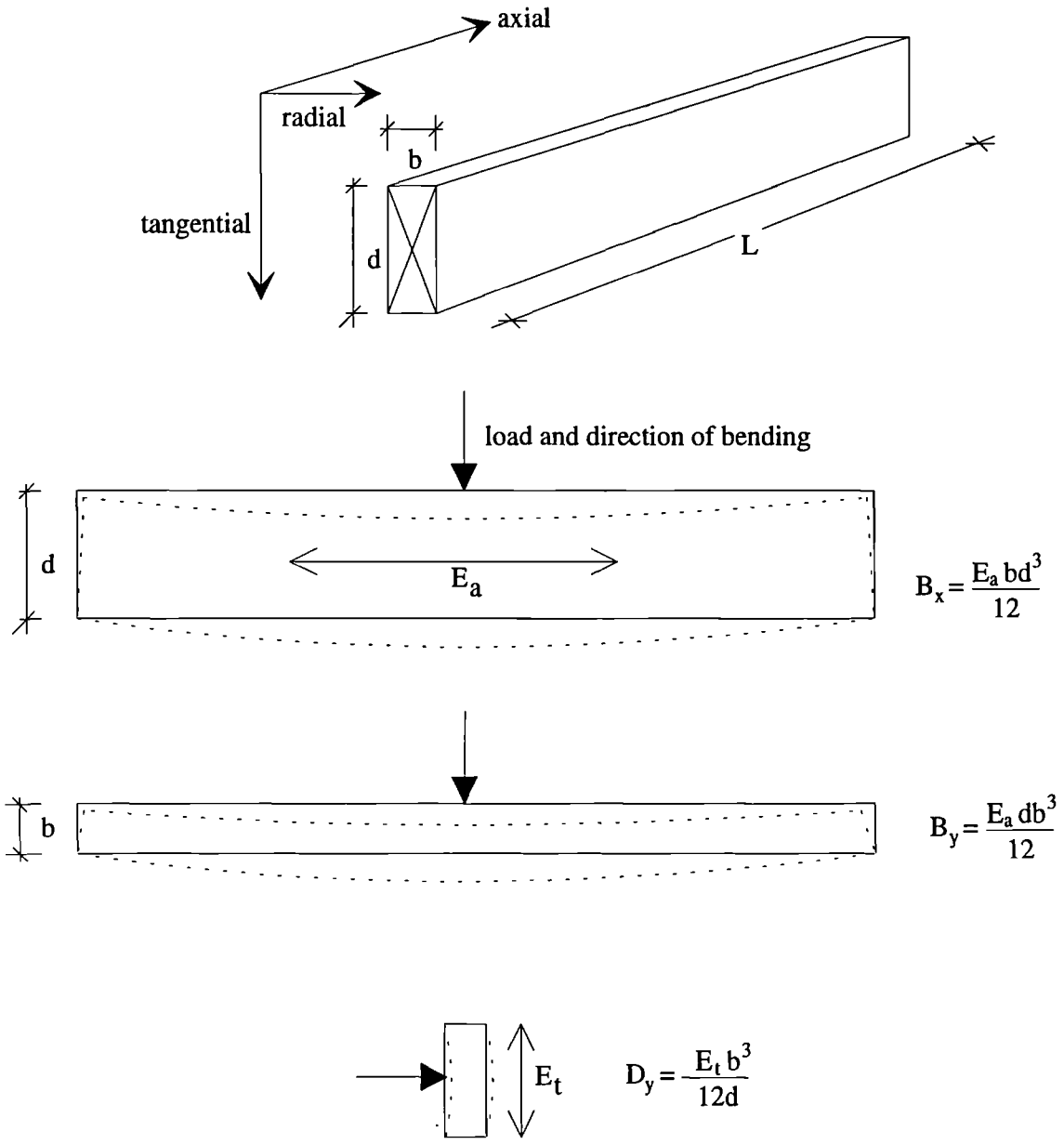

Figure 5.36 The relationship between bending stiffness and Young's modulus

Changes to the forces in the x-direction

As a result of the changes to the displacement in the x-direction the displacement of the beam at its centre is also affected. The total resisting force in the x-direction for the beam was given by eqn(5.49). This is now written as,

$$F_x^{\diamond} = -\omega^2 \rho_l \left[\xi_1 + \left(\frac{\phi_1 + \phi_3}{2} \right) \frac{d}{2} \right] + B_x \frac{\partial^4}{\partial y^4} \left[\xi_1 + \left(\frac{\phi_1 + \phi_3}{2} \right) \frac{d}{2} \right] \qquad (5.114)$$

Figs 5.37 to 5.39 show comparisons between the plate, beam and revised beam models. The revised beam model described above should only alter the flexural wave motion between the top and bottom plates. Fig 5.37 shows the predicted transmission loss for the various models for an incident longitudinal wave on plate 1 and the resultant inplane wave motion on plate 4 for a standard 'H' structure. As expected the inplane wave motion on plate 4 is unaffected by the changes to the slope boundary conditions and the beam and revised beam model are identical.

Fig 5.38 and Fig 5.39 show the predicted transmission loss from plate 1 to plates 2 and 4 for flexural wave motion, comparing the beam, plate and revised beam models. Fig 5.38 shows increased transmission to plate 2 for the revised beam model when compared with the beam model. Fig 5.39 shows that the transmission to the offset plates, plates 3 and 4, are identical. When comparing the transmission to plate 2 and 4 for the revised beam model the change in the slope boundary conditions has accounted for the stronger transmission to the inplane plate, plate 2, and is similar in transmission loss to the plate model.

The above revised theory relies heavily on the frame parameter D_y. In the next chapter, chapter 6, the orthotropic nature of timber and the parameter, D_y may be significant in determining structure borne sound transmission. However, the use of this theory is dependant upon the fact that the slopes should be dissimilar between the top and bottom plates and if this is not the case then this theory should not be used.

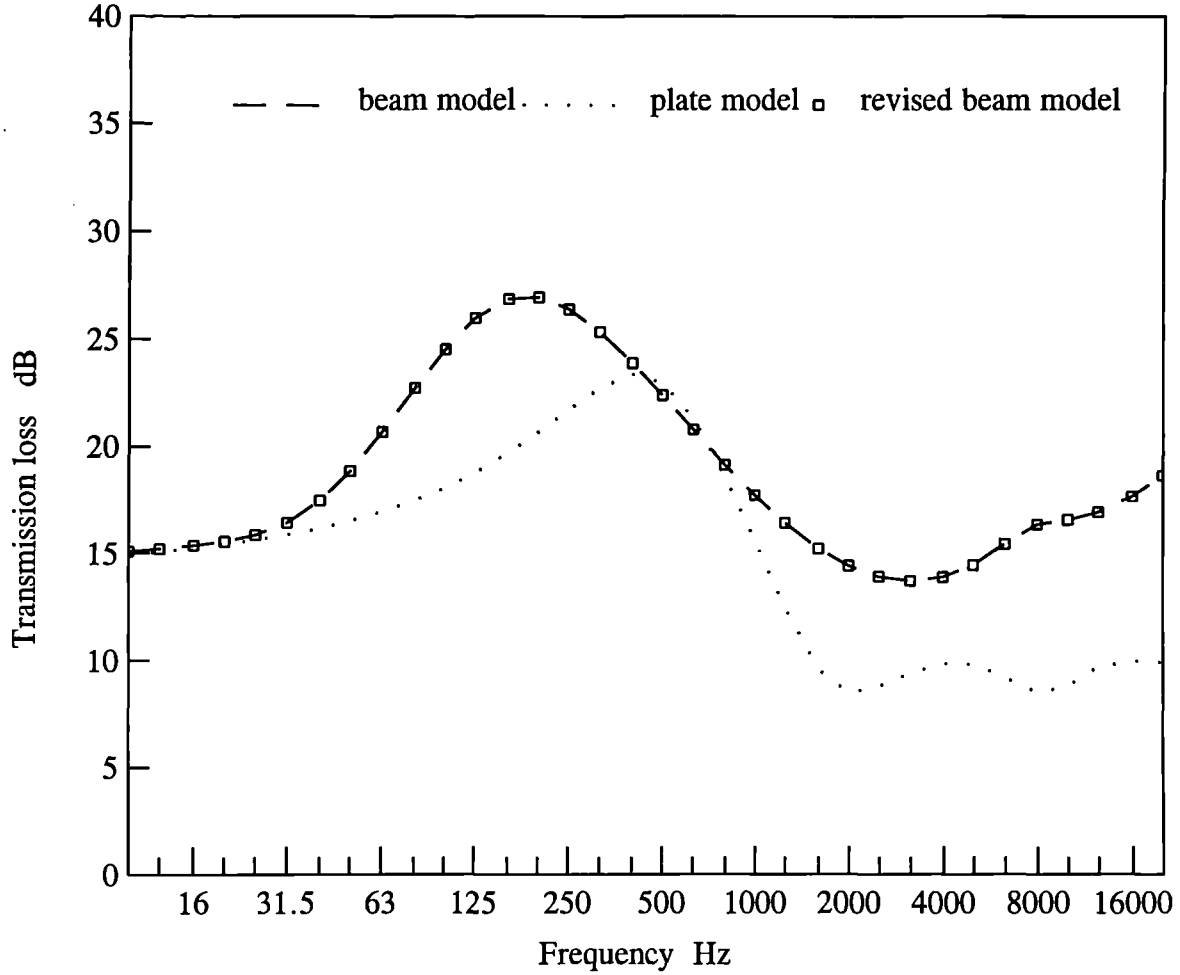

Figure 5.37 Predicted transmission loss from plate 1 to plate 4 comparing beam, plate and revised beam models, for an incident longitudinal wave on plate 1 and resultant inplane wave motion on plate 4.

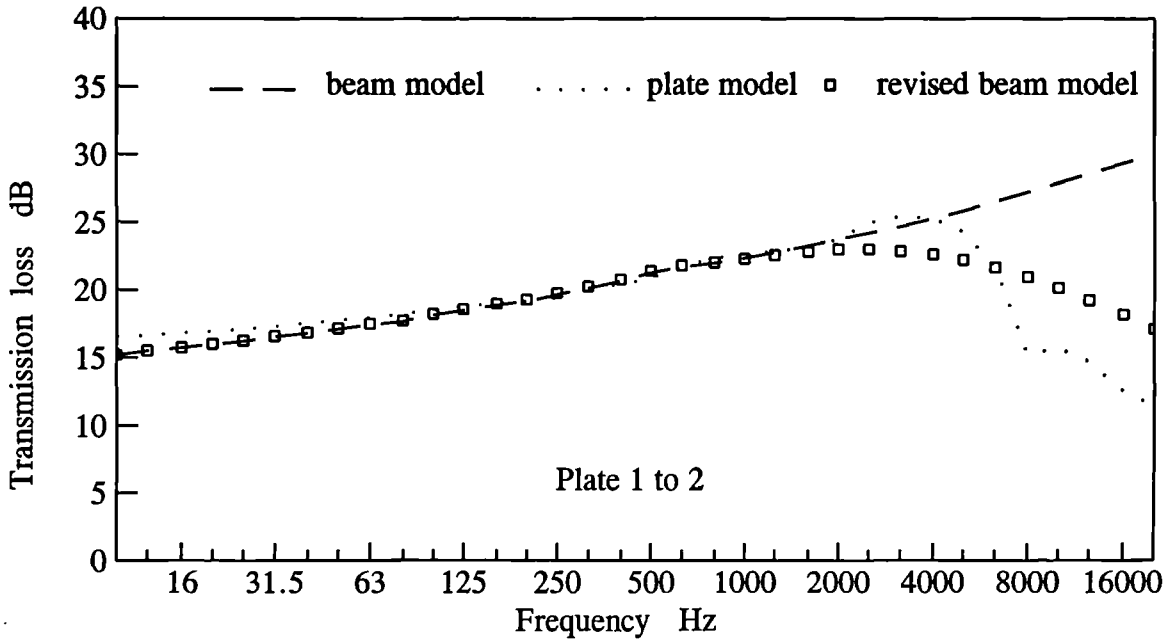

Figure 5.38 Predicted transmission loss from plate 1 to plate 2 comparing beam, plate and revised beam models, for an incident bending wave on plate 1 and resultant flexural wave motion on plate 2.

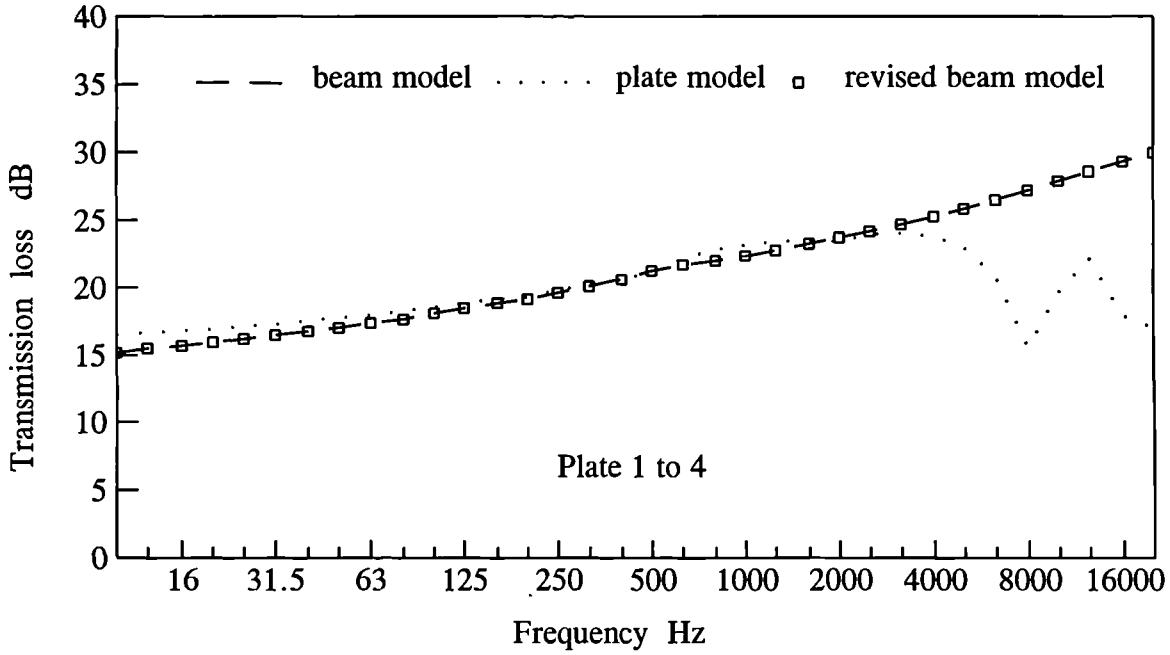

Figure 5.39 Predicted transmission loss from plate 1 to plate 4 comparing beam, plate and revised beam models, for an incident bending wave on plate 1 and resultant flexural wave motion on plate 4.

5.7 Conclusions

This chapter has described the various theories for structure borne sound transmission between parallel plates for a line connection. All theories presented are wave models and detail the bending, longitudinal, transverse and nearfield wave motion. It is also possible to omit any number of plates using these theories. The importance of including inplane wave motion and the transfer from one wave type to another has been shown in the predicted transmission loss between the top and bottom plates.

As the transmission to plates 3 and 4 is similar, for clarity only the transmission to plate 4 has been shown in the figures presented. Interestingly the incident angle at the junction with the frame and plate 1 is within a small range of angles over the frequency range. The beam model and plate model are similar at the low frequencies, and the plate and SEA models are similar at the high frequencies. The case of which model to choose is dependant upon the structure under study and the frequency range of interest. If the frame depth is small in comparison with the wavelength, at low frequencies, then the beam model appears to suffice. However if the frame depth is large in comparison with the wavelength, at higher frequencies, then the SEA or plate model should be used. In the case where the entire frequency range is under study and the frame offset or depth is smaller and larger than the wavelength, as found with internal partitions, then the plate model should be used. It has been shown also that changes to the frame material properties may significantly affect the transmission loss between the top and bottom plates.

Chapter 6
Comparison of Measured and Predicted Results for Parallel Plates with a Line Connection

6.1 Introduction

The previous chapter, chapter 5, described the theory for structure borne sound transmission for parallel plates with a line connection. This chapter will compare the measured and predicted results for such structures.

The standard material used for the frame in internal partitions and beams in floors for domestic construction is wood. Due to the orthotropic nature of wood and its unique and complex structure, careful consideration must be given to the material parameters inserted into any of the theoretical models described in chapter 5. This chapter will describe the effects these have on the structure borne sound transmission between parallel plates.

As shown in the previous chapter, Fig 5.1, some parallel plate structures have plates omitted from the standard 'H' plate structure. This may be due to connections to other walls or jambs with windows or doors. Also as this work is also related to aerospace and flight vehicle structures there may be any number of plates omitted and therefore all possible structures should be examined. This chapter will show the measured and predicted results for the standard 'H' structure and where any combination of plates are omitted from the standard structure. The parametric study covered in chapter 5 also showed that variations to the frames material parameters may affect the resultant transmission loss between parallel plates. The most common parameter to be regularly altered in partitions and timber floors is the frame depth. The sizes varying from 250mm to 50mm. For this reason this chapter will also show the measured and predicted results for varying the frame depth for a combination of structures involving parallel plates.

6.2 Comparison of line connection models

The tangential material properties for the timber frame, discussed in Chapter 2, are used in the revised beam, plate and SEA theoretical models presented in chapter 5. Due to the orthotropic nature of wood the value of the longitudinal wavespeed, $C_{L(t)}$, in the tangential direction may be a factor of two to four times less than in the axial direction, $C_{L(a)}$ [15]. The consequences to the theory described in chapter 5 are significant. The Young's modulus and resultant bending stiffness are dictated by the longitudinal wavespeed. The Young's modulus is effected not by a factor of two to four but by a factor of four to sixteen, as shown by eqns.(3.2 and 3.3). In addition, any changes to the longitudinal wavespeed will also affect the frequency where the modes occur within the frame.

To compare the theoretical models with results from real structures a series of tests were carried out on suspended line connected parallel plate structures. All the structures studied in this chapter were freely suspended in an anechoic chamber to reduce the interference from reflections from surrounding surfaces. All the measured data recorded was for flexural wave motion only. Due to interference from flexural wave motion on the plates causing bending rotation to the accelerometers [87] it is difficult to measure true inplane motion. Table 6.1 shows the material properties of a standard 'H' type parallel plate structure connected by a 200x45mm timber frame, similar to that shown in Fig 6.1. The damping and longitudinal wavespeed of the plasterboard plates were measured as detailed in chapter 3 and the predicted total loss factors of the plates used to determine the predicted acceleration levels shown in the following figures were calculated by summing the coupling loss factors and internal loss factors.

Fig 6.1 shows a typical 'H' structure where plates 1, 2, 3 and 4 are 12.5mm thick plasterboard sheets with dimensions 1.2x1.2m. The inline plates , plates 1 and 2 and plates 3 and 4, are formed from a 2.4x1.2m plasterboard sheets divided by a line of multiple screws at 60mm centres. The structures were excited with a structural source which was an acoustic hammer as detailed in chapter 3.

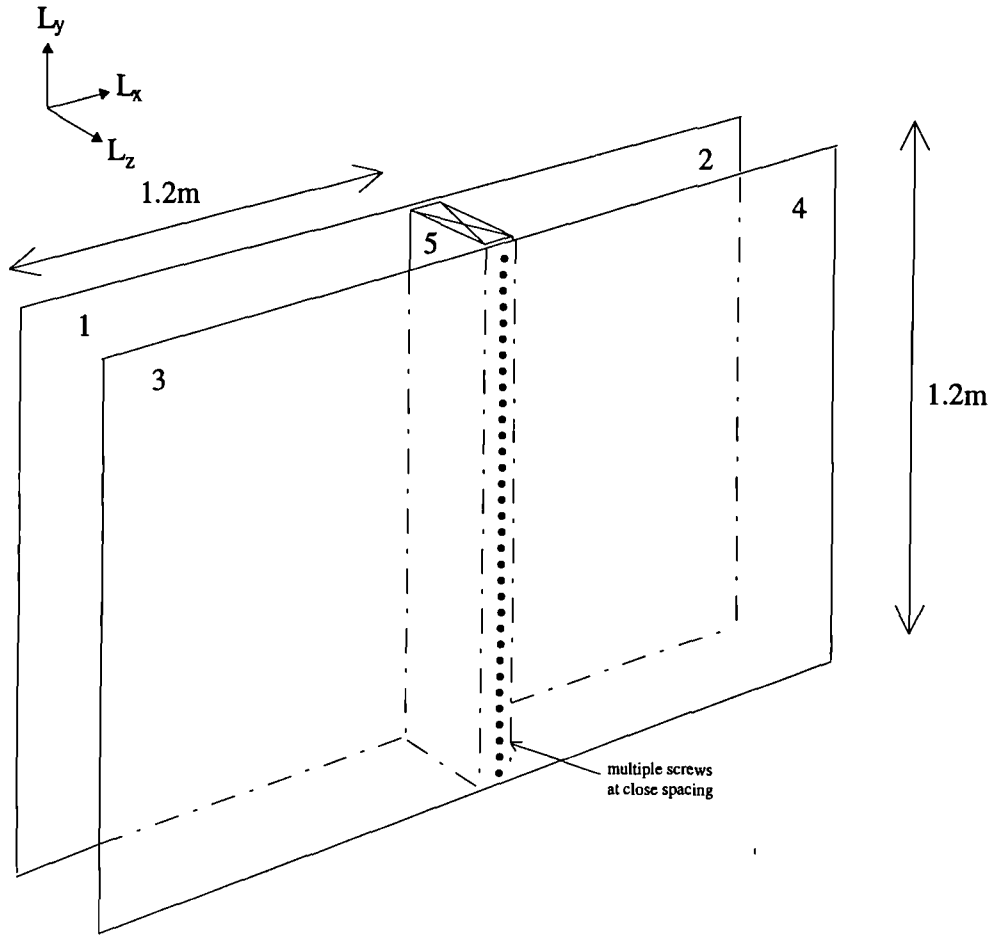

Figure 6.1 Freely suspended 'H' structure for line connection tests.

Subsystem	Dimensions (m)			Material properties				
	Lx	*Ly*	*Lz*	ρ (kg/m^3)	E_a (N/m^2)	E_t (N/m^2)	μ	η_i (ILF)
Plates 1,2,3,4	1.2	1.2	0.0125	806	2.3×10^9	—	0.2	0.01
Frame 5	0.045	1.2	0.2	450	8.752×10^9	1.15×10^9	0.3	0.015

Table 6.1 Material properties of a line connected test structure with a 200x45mm frame.

Fig 6.2 shows the predicted and measured acceleration level difference from plate 1 to plate 3 for the structure given in Table 6.1. Two predicted acceleration level difference results are shown in Fig 6.2. Both predicted results are calculated by using the plate model described in chapter 5. The theory to determine the predicted acceleration level difference is given in chapter 2. The predicted results shown are calculated using the measured axial and tangential longitudinal wavespeed of the timber frame. As can be seen in Fig 6.2 using the tangential longitudinal wavespeed ($C_{L(t)}$=1635m/s) for the plate model theory gives good agreement with the measured results. The predicted acceleration level difference using the axial longitudinal wavespeed ($C_{L(a)}$=4501m/s) has good agreement at the low frequencies. However, the first half wavelength on the test structure frame occurs after 1000Hz and the plate model using $C_{L(t)}$ predicts this well. Using the higher value of axial longitudinal wavespeed, $C_{L(a)}$, results in the predicted flexural modes taking place at higher frequencies, as may be calculated from eqn(4.1). This is shown in Fig 6.2 above 8KHz by a decrease in the predicted plate model acceleration level difference using $C_{L(a)}$.

Fig 6.3 shows a comparison of the various theoretical models described in chapter 5 with measured acceleration level difference from plate 1 to plate 3, for the structure detailed in Table 6.1. The predicted acceleration level difference results are shown for the plate, beam, SEA and revised beam models. The SEA predicted results shown in Fig 6.3 are calculated using the tangential longitudinal wavespeed due to the frame being modelled as a plate. The beam model and revised beam model are slightly different at the higher frequencies as the beam model is calculated with $C_{L(a)}$ and the revised beam model with $C_{L(t)}$. In the theory presented for the beam model in section 5.4.3 the beam's moments and forces are calculated using the axial beam parameters and in particular B_x and B_y. The beam's moments and forces in the revised beam model described in section 5.7 are determined by the slope terms given by eqn(5.112). One parameter of the beam which appears in all of the revised equations, eqns.(5.108 - 5.114), is the parameter D_y. If the same principle is applied for calculating D_y then the timber's tangential longitudinal wavespeed must be used to determine the tangential Young's modulus, which is perpendicular to the direction of bending, as shown in Fig 5.36. Fig 6.3 shows that from the various prediction models presented the plate model using $C_{L(t)}$ has the best comparison with the measured data. The beam and plate models are similar at the low

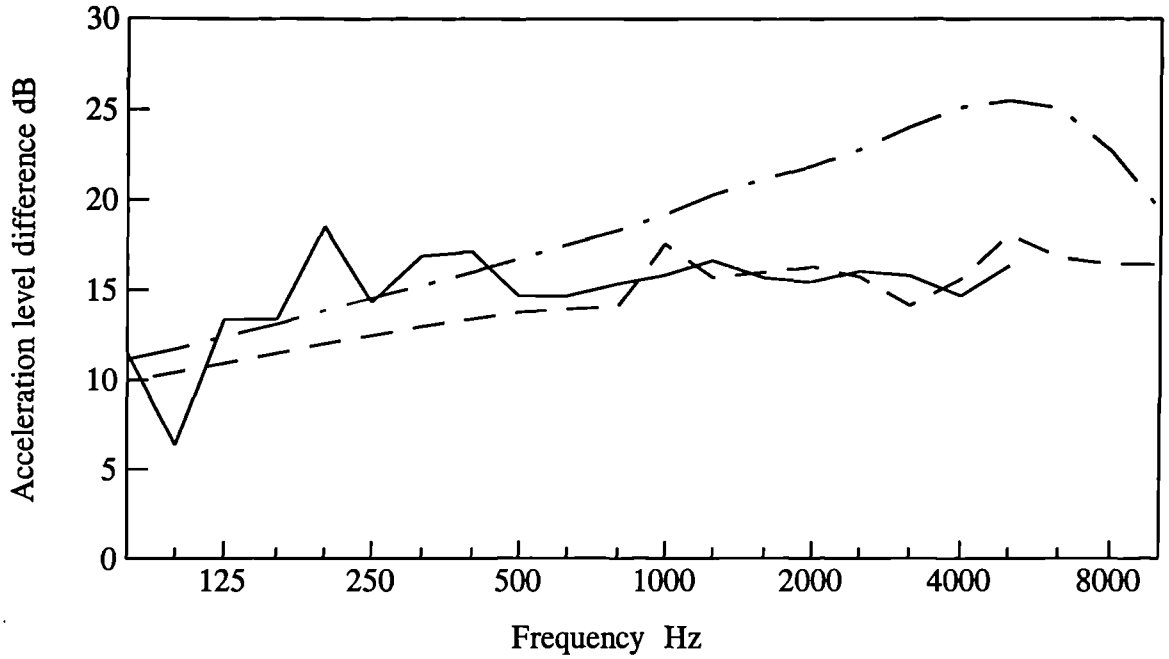

Figure 6.2 Comparison of measured and predicted acceleration level difference from plate 1 to 3 for a standard 'H' structure showing the effect of using the axial and tangential longitudinal wavespeed in the plate model. (____) measured, (_._._.) plate model using $C_{L(a)}$, (- - -) plate model using $C_{L(t)}$.

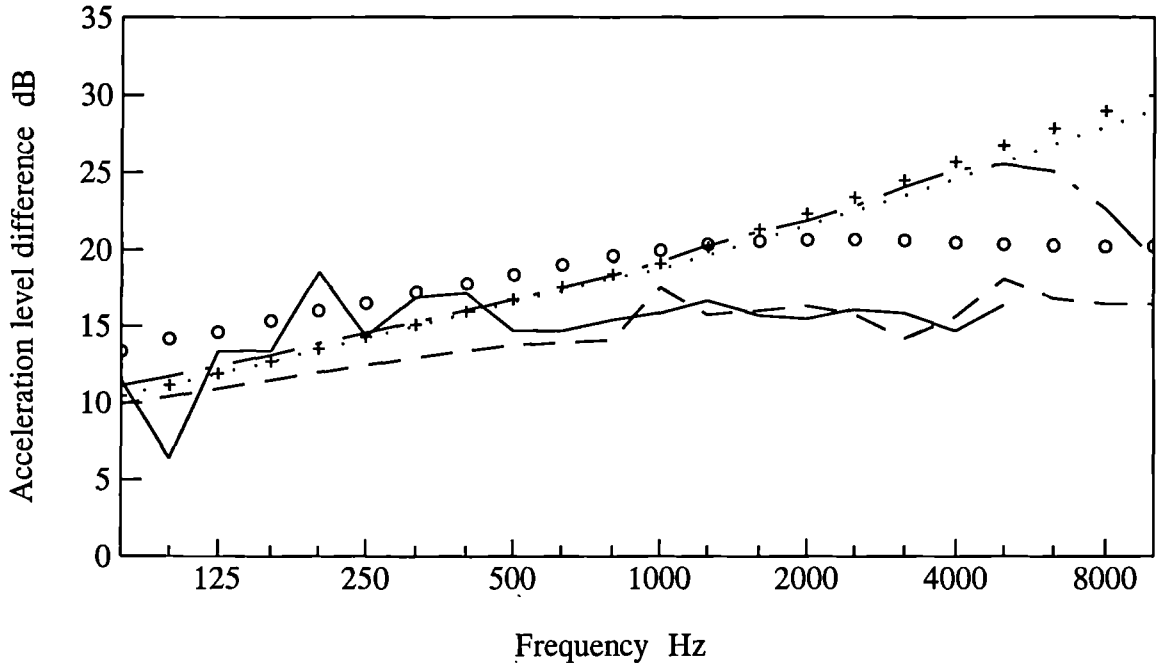

Figure 6.3 Comparison of predicted and measured acceleration level difference from plate 1 to 3 showing the relationship between various theoretical models. (____) measured, (_._._.) plate model using $C_{L(a)}$, (- - -) plate model using $C_{L(t)}$, (O) SEA model using $C_{L(t)}$, (+) beam model using $C_{L(a)}$, (....) beam model using $C_{L(t)}$.

frequencies, where the wavelength is greater than the depth of the frame plate, and compare well with measured data. However as the frequency increases the wavelength becomes shorter and when flexural wavelengths are able to be supported within the frame the plate model predicts these well.

6.3 Varying the depth or the number of plates

Varying the depth

One of the principle parameters that varies from structure to structure is the depth parameter or offset between the parallel plates. This section describes the measured and predicted acceleration level difference for a standard 'H' structure with varying depth of 200, 100 and 50mm. Results for plates 1 to 2, 1 to 3 and 1 to 4 are shown. Figs 6.5-6.7 show the predicted and measured results for the standard 'H' structure, H*, shown in Fig 6.4, where the symbol (*) refers to the various depths tested. Table 6.2 shows the material properties of the plates and the frame for the structure tested. Description of the apparatus used and methods of testing is given in Chapter 3. The plate model is a more accurate form of the SEA model and hence the SEA model is omitted from the graphs for clarity. For this reason only the beam and plate models are compared with measured data.

Fig 6.5 shows the measured and predicted acceleration level difference from plate 1 to the inline plate, plate 2. As the depth parameter increases so both the beam and plate model predict less transmission to plate 2. However, the measured results appear to show that as the depth increases there is very little change to the acceleration level difference and also there is increasingly poor agreement between the measured and predicted data.

Figs 6.10 and 6.11 show the acceleration level difference from plate 1 to the offset plates 3 and 4. As the depth increases by a factor of two so the measured and predicted level difference increases by 3dB. There is generally good agreement between the measured and plate predicted results over the frequency range. The beam and plate predicted results diverge at lower frequencies as the plate depth increases.

Although the beam model works well at low frequencies the plate model works well throughout the frequency range of interest. It appears that even on small depth beams

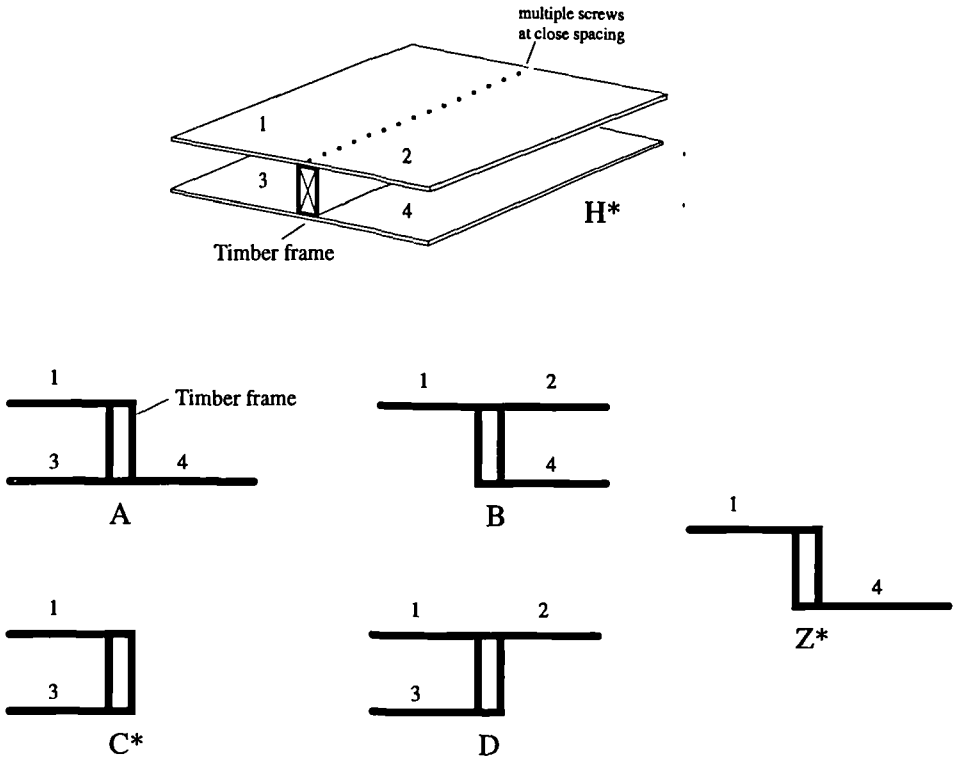

(*) - refers to depth of timber beam 50,100 or 200mm

Figure 6.4 Various structure configurations tested from the standard 'H' structure where plates are omitted.

Subsystem	Dimensions (m)			Material properties				
	Lx	*Ly*	*Lz*	ρ (kg/m^3)	E_a (N/m^2)	E_t (N/m^2)	μ	η_i (ILF)
Plates 1,2,3,4	1.2	1.2	0.0125	806	2.3×10^9	—	0.2	0.01
Frame 5	0.045	1.2	0.2	450	9.1×10^9	5.69×10^8	0.3	0.015
	"	"	0.1	419	8.21×10^9	1.51×10^8	"	"
	"	"	0.05	421	8.21×10^9	1.51×10^8	"	"

Table 6.2 Material properties of line connected test structures with frames of varying depth.

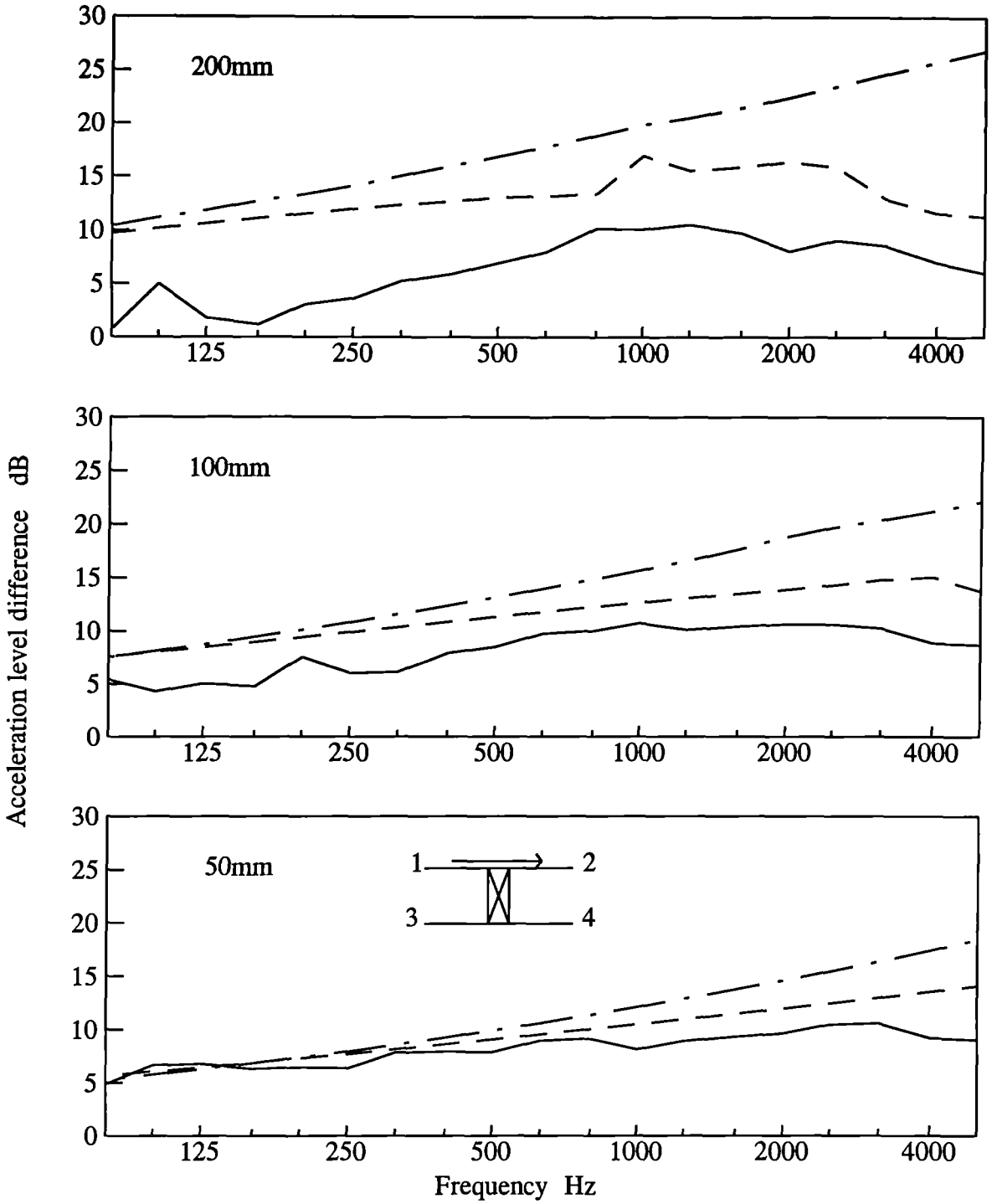

Figure 6.5 Measured and predicted acceleration level difference from plate 1 to plate 2 with varying depth. (____) measured, (_._._.) beam model, (- - -) plate model.

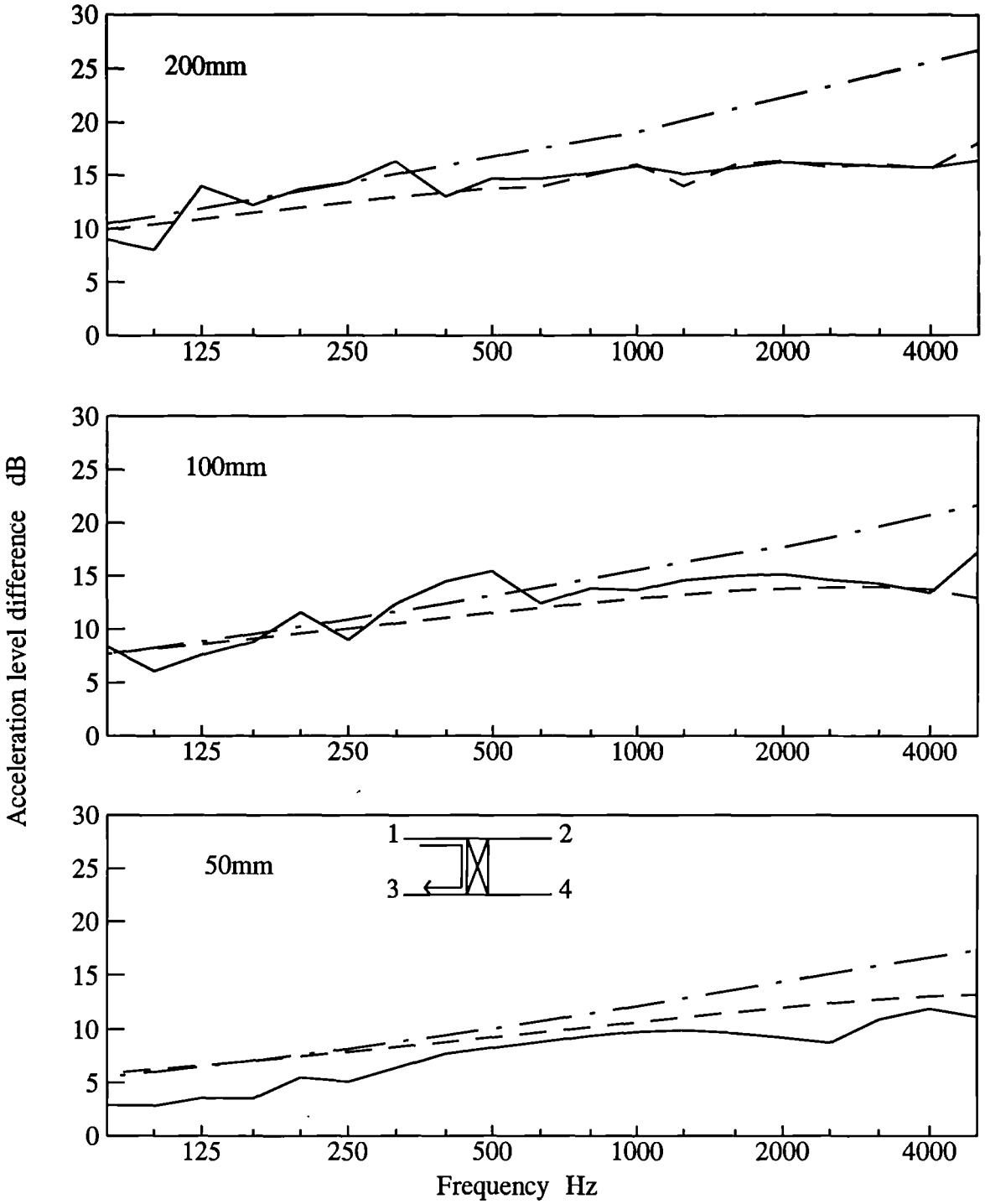

Figure 6.6 Measured and predicted acceleration level difference from plate 1 to plate 3 with varying depth. (____) measured, (_._._.) beam model, (- - -) plate model.

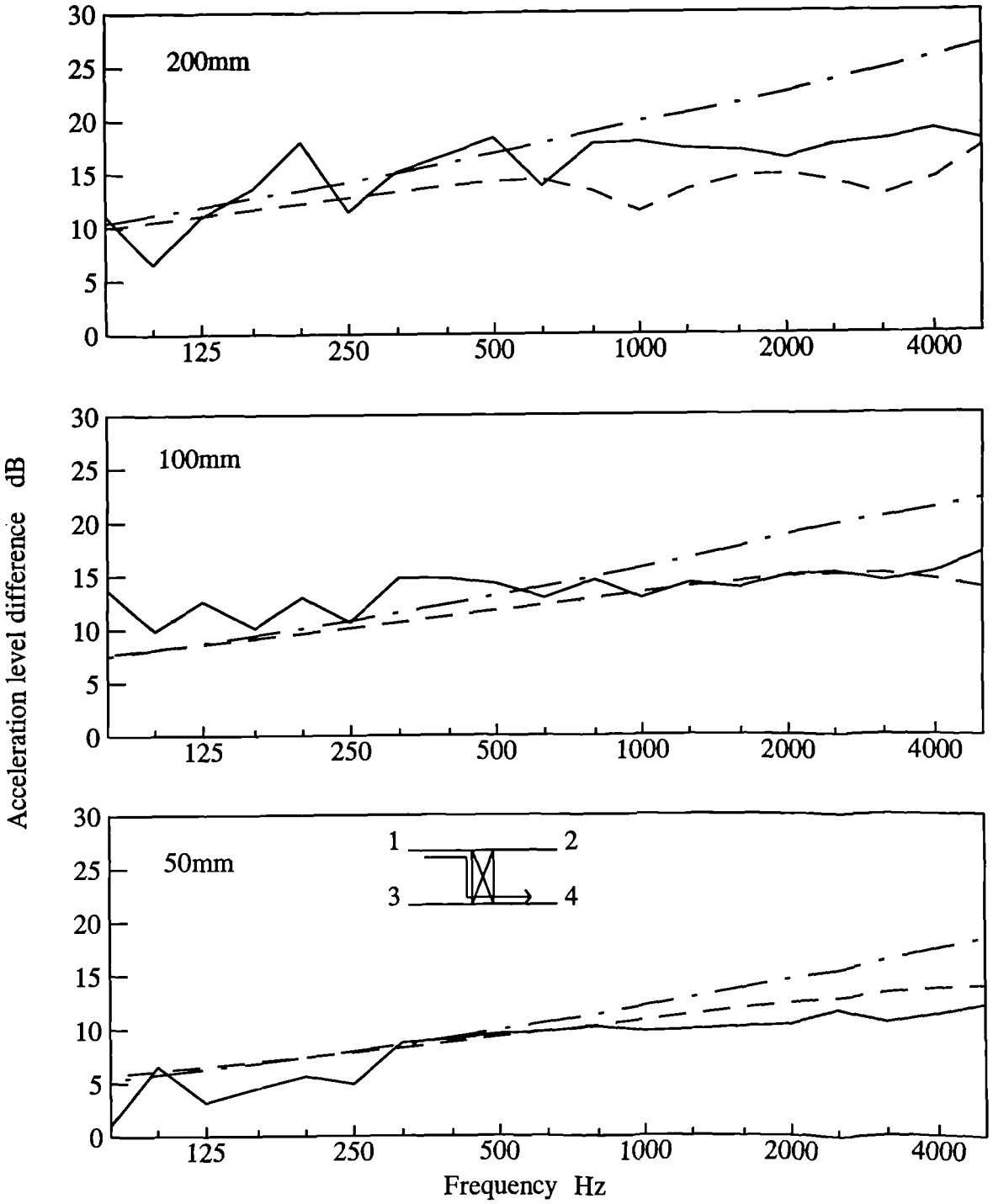

Figure 6.7 Measured and predicted acceleration level difference from plate 1 to plate 4 with varying depth. (____) measured, (_._._.) beam model, (- - -) plate model.

such as 50mm the beam model is still not as accurate in the prediction of the acceleration level difference as the plate model.

Omitting Various Plates from the Standard 'H' Section

This section shows the measured and predicted acceleration level difference for the various combinations of structure possible from the standard 'H' section. These structures are shown in Fig 6.4 and the material properties are shown in Table 6.2. For simplicity the structures have been labelled A (plates 1,3 and 4), B (plates 1,2 and 4), C* (plates 1 and 3), D (plates 1,2 and 3) and Z* plates 1 and 4.

In addition the effects of varying the depth for all the above named structures was undertaken. For simplicity not all the structures tested with varying depth are shown in this chapter and only structures C* and Z* are presented with varying depth.

Fig 6.8 shows the measured and predicted acceleration level difference from plate 1 to plates 3 and 4 when plate 2 is omitted. Generally the agreement between the measured and plate predicted results are good. However, Fig 6.9 and 6.10 show test structures B and D which include plate 2 and omit plate 3 or 4. As found with the H* structure shown in Fig 6.5, which also included results for plate 2, the predicted theory consistently under estimates the strength of transmission to plate 2, particularly with increasing frame depth. The increased measured transmission to plate 2 results in a difference between the measured and predicted plate model acceleration level difference of 3-5dB over the frequency range of interest.

Fig 6.11 and Fig 6.12 show the measured and predicted acceleration level difference for the structures C* and Z*. Fig 6.11 shows excellent agreement between the measured and predicted plate model results for plates 1 to 3. The agreement is not as good for plates 1 to 4 shown in Fig 6.12.

The measured and predicted results for these test structures show reasonable agreement over the frequency range. The plate model is the most detailed and thus the most accurate. For some of the results the agreement is excellent. The plate model is able to take account of any number of plates being omitted.

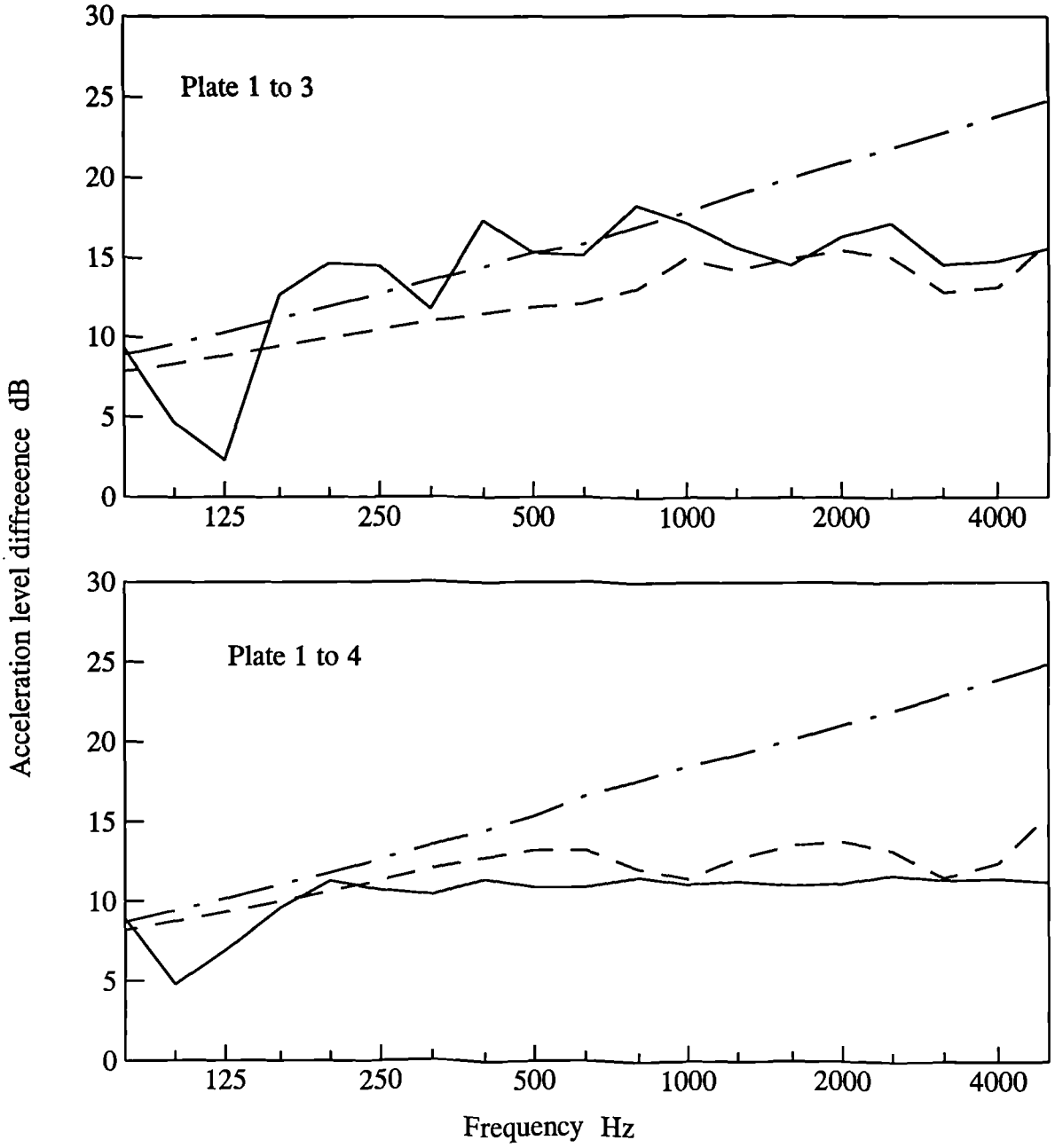

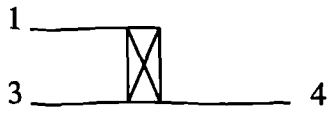

Figure 6.8 Measured and predicted acceleration level difference from plate 1 to plates 3 and 4 with a 200x45mm frame and omitting plate 2. (___), measured, (_._._) beam model, (- - -) plate model.

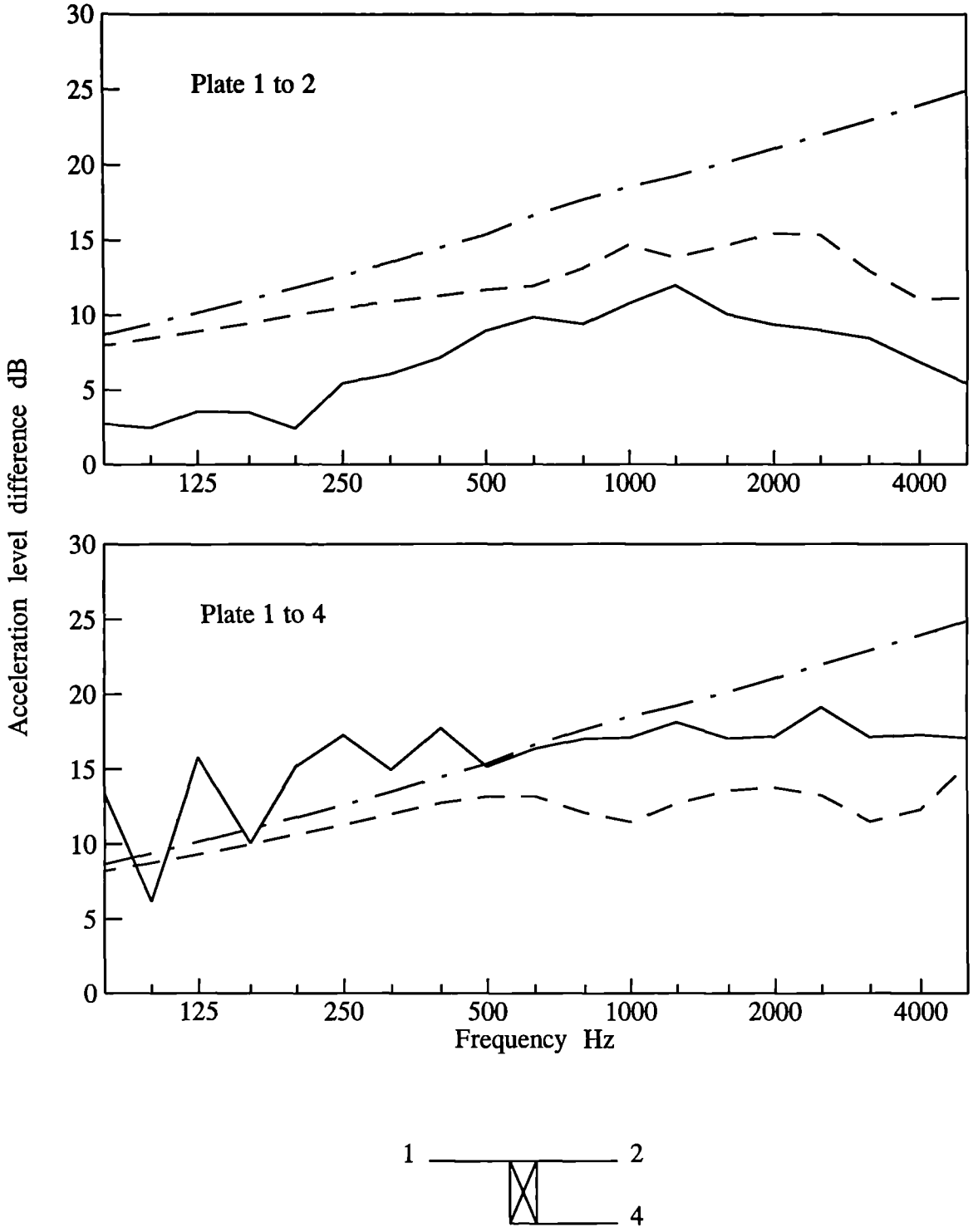

Figure 6.9 Measured and predicted acceleration level difference from plate 1 to plates 2 and 4 with a 200x45mm frame and omitting plate 3. (___), measured, (_._._) beam model, (- - -) plate model.

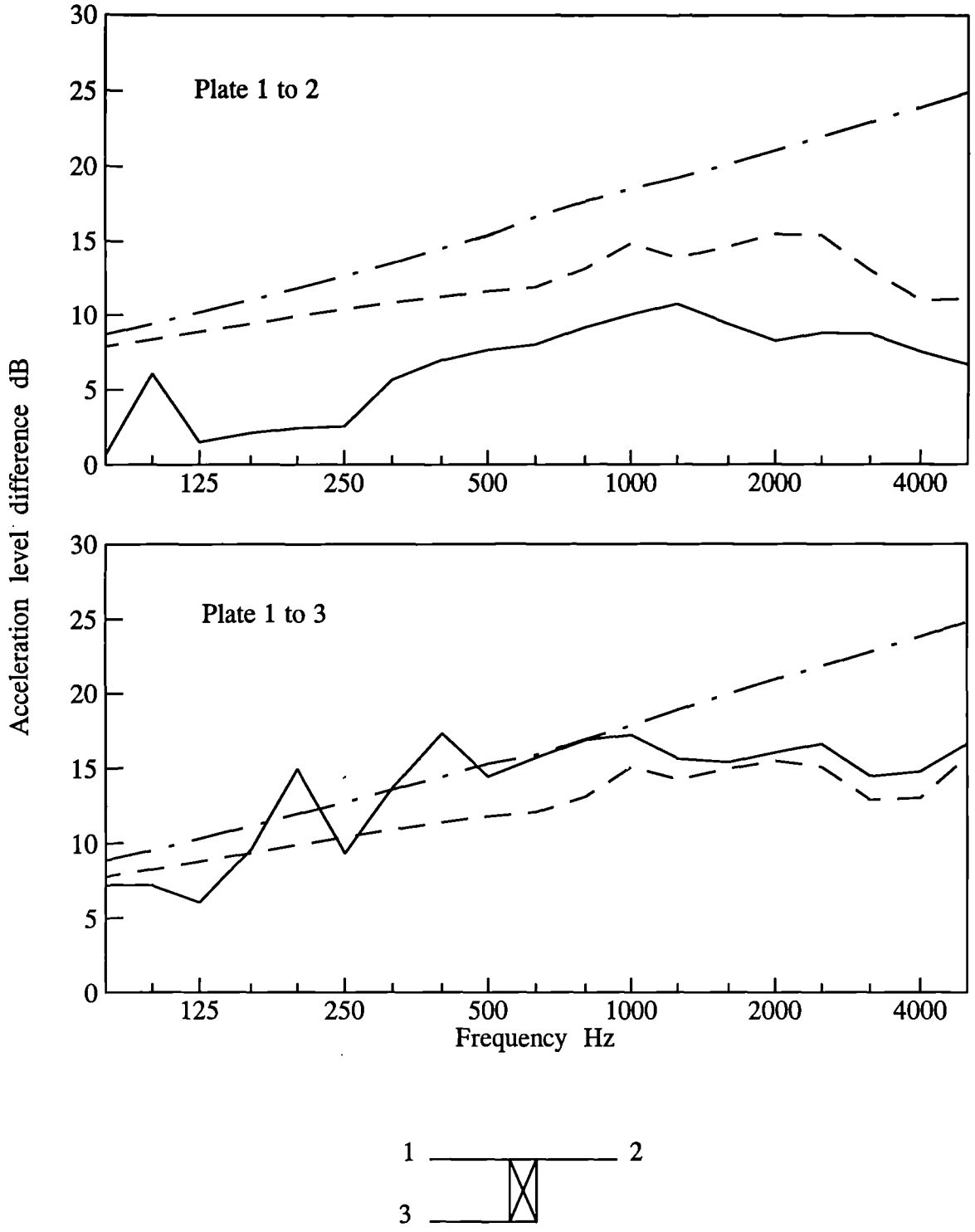

Figure 6.10 Measured and predicted acceleration level difference from plate 1 to plates 2 and 3 with a 200x45mm frame and omitting plate 4. (___), measured, (_._._) beam model, (- - -) plate model.

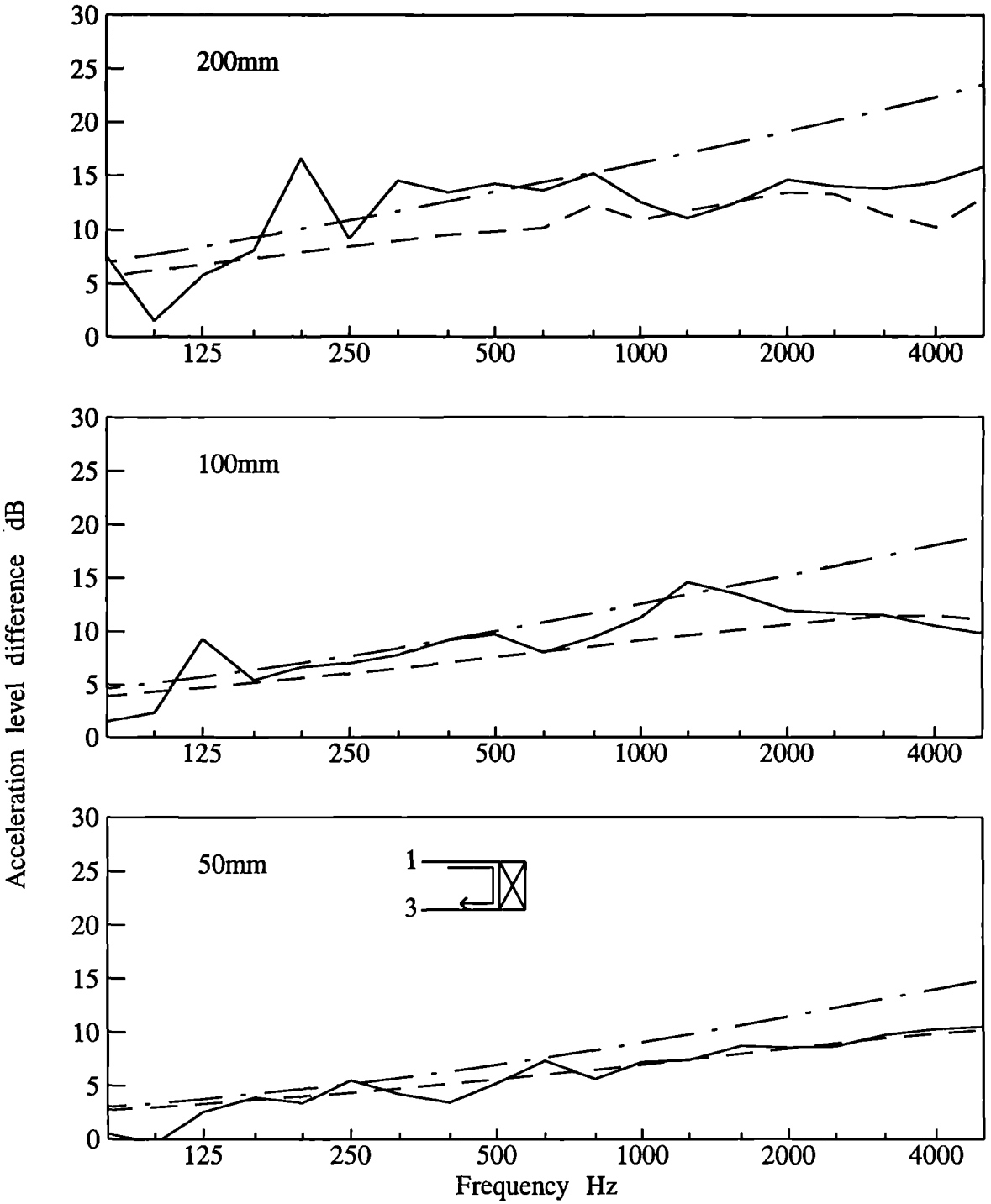

Figure 6.11 Measured and predicted acceleration level difference from plate 1 to plate 3 with varying depth. (____) measured, (_._._.) beam model, (- - -) plate model.

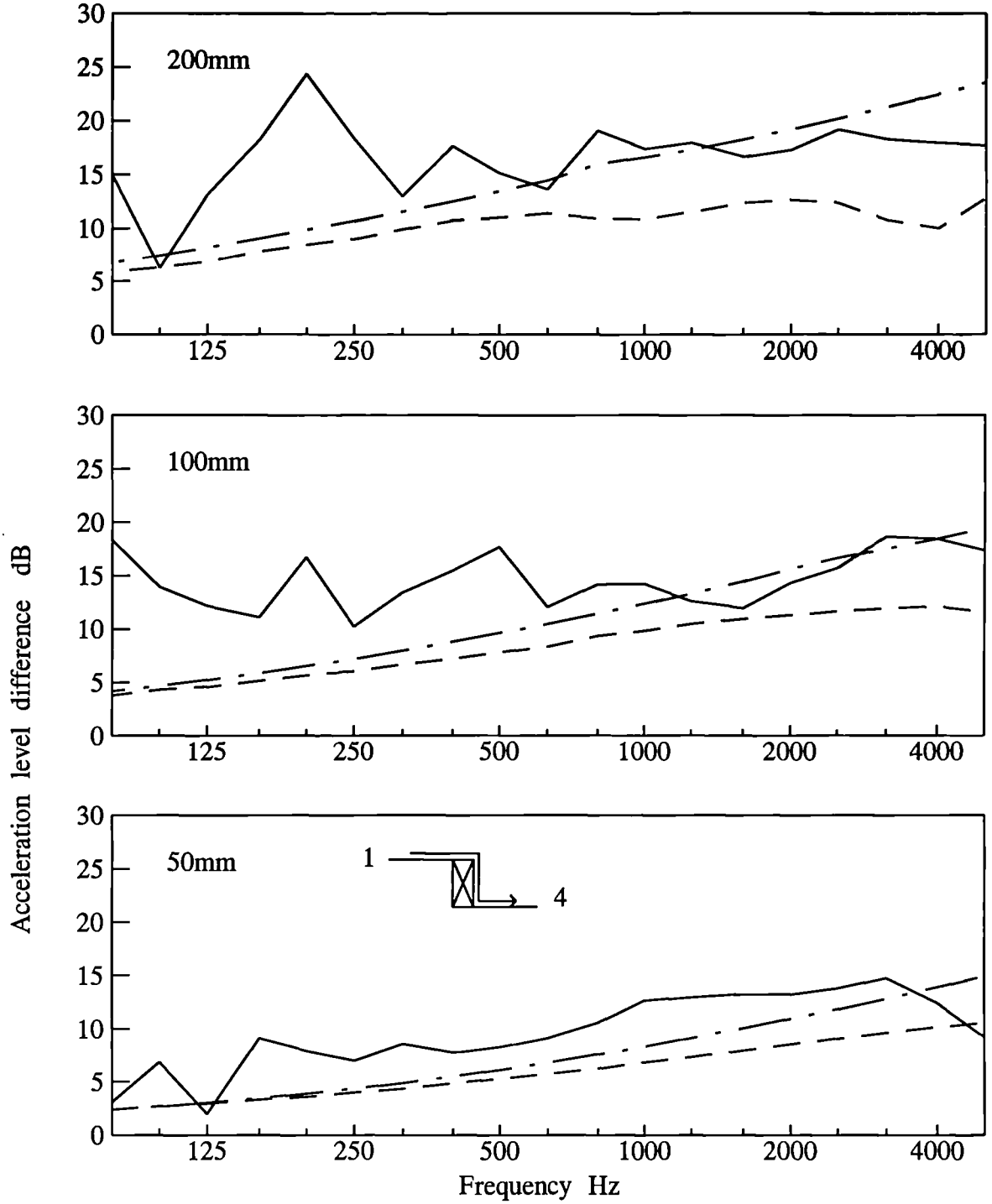

Figure 6.12 Measured and predicted acceleration level difference from plate 1 to plate 4 with varying frame depth. (____) measured, (_._._.) beam model, (- - -) plate model.

Also as the depth parameter is increased so the level difference from plate 1 to the offset plates 3 and 4 increases. This is well predicted by the plate model. The plasterboard plates that were used for the test structures had very few modes at the low frequencies. As SEA requires several modes per frequency band to obtain a mean average the agreement at the lower frequencies between the measured and predicted results is not as good. In hindsight, it may have been better to use larger plates or another material. However, the results are significant to assume that the models are working well. The beam model works well at the low frequencies up to the frequency where the first half wavelength fits into the depth of the frame. The plate model works well over all the frequencies and is able to predict when the first half wavelength fits into the frame.

6.4 Replacing the timber stud with a metal stud

In the construction of modern internal partitions for offices the primary material now used for the frame is a metal channel. Although this thesis concentrates more specifically on the application of the theoretical models for internal partitions in houses it was thought appropriate to carry out structure borne sound measurements on a metal channel partition. This would hopefully support the credibility of these models and the wide range of applications to which the theory may be applied.

An 'H' type structure was built, as shown in Fig 6.13, using plasterboard sheets for the plates with material properties as given in Table 6.3. The metal channel was 1.2m long with a depth, or offset between the plates, of 70mm and a thickness of 1mm. Most metal channels used for internal office partitions are open channels. This means that they are not closed on all sides. The open channel used for the frame which was a "C" shape aluminium metal channel with a density of 3571kg/m^3 and a longitudinal wavespeed of 5070m/s.

The small metal flanges of the channel shown in Fig 6.13, which are perpendicular to the plates, are not included in the model for simplicity. Fig 6.14 shows the measured and predicted acceleration level difference for transmission from plate 1 to plates 2, 3 and 4. Generally there is good agreement between the measured and predicted results. Above 2500Hz the 60mm spacing of the screws, connecting the plates to the frame, makes it

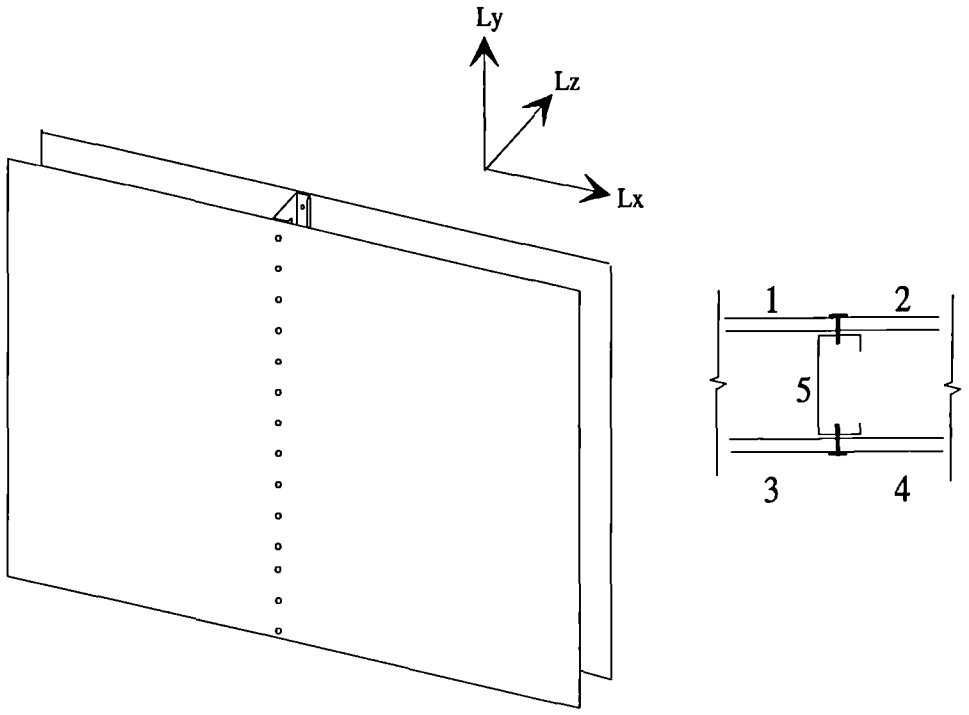

Figure 6.13 Plate configuration with metal channel.

Subsystem	Dimensions (m)			Material properties			
	Lx	*Ly*	*Lz*	ρ (kg/m^3)	E (N/m^2)	μ	η_i (ILF)
Plates 1,2,3,4	1.2	1.2	0.0125	806	2.3×10^9	0.2	0.01
Frame 5	0.001	1.2	0.07	3571	9.179×10^{10}	0.2	0.015

Table 6.3 Material properties of a line connected test structure with a metal channel.

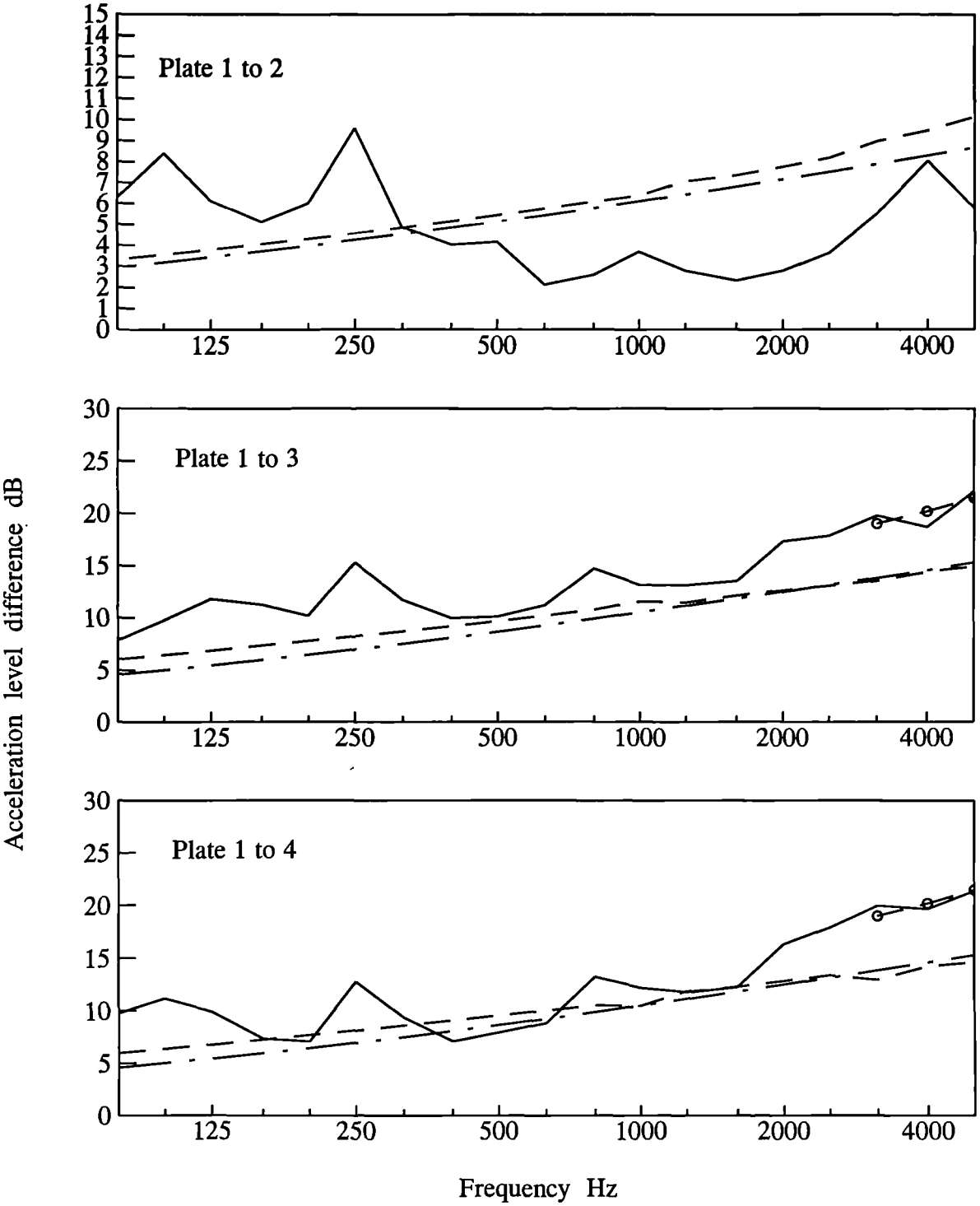

Figure 6.14 Measured and predicted acceleration level difference from plate 1 to plates 2, 3 and 4 for an 'H' type structure with a metal frame. (____) measured, (_._._._) revised beam model, (- - -) plate model. (-O-) point model.

possible for the plate flexural wavelengths to fit between the screws and may be modelled as point connected plates, as described in chapter 4. The point connection model results are also shown in Fig 6.14 for transmission to plates 3 and 4 and there is generally good agreement.

As previously discussed, the revised beam model was not calculated for the timber frame structures because no evidence could be found that the slopes were different or that the timber frame was bending about the x-axis. The value of the bending stiffness D_y for the timber frames was for a 100mm offset typically 49,810 N/m^2. However, in the case of the metal channel being only 1mm thick and has a much lower value of D_y, typically 190 N/m^2. The metal channel was far more flexible than the timber frame and for this reason the revised beam model was calculated along with the plate model to compare with the measured data.

These results show that the plate model again is able to predict the transmission quite accurately across the frame. It is pleasing to note how well the point connection model predicts the transmission to plates 3 and 4. Once again the prediction for transmission to plate 2 is underestimating the strength of coupling.

6.5 Discussion

As shown from the measured and predicted results from Fig 6.5 to Fig 6.14 the strength in transmission from plate 1 to the inline plate, plate 2, is consistently under predicted. The measured acceleration level difference is much lower than the predicted acceleration level difference over the frequency range. On analysis of the results, for plates 1 to 2, from the test structures H, B and D and discovering the large discrepancy between the predicted and measured results it was thought that there may be two reasons for this error.

Firstly, that the behaviour of the plates directly at the junction was possibly dissimilar to that given by the boundary conditions. The boundary conditions for both the plate and beam model assume that the flexural displacement at the joint on plates 2, 3 and 4 will be similar until the frame can support flexural wave motion.

Secondly, that the fault may lie in the structure itself. Plates 1 and 2 are formed by the division of a large plate, 2.4x1.2m, into two smaller plates, 1.2x1.2m, by the line of screws connecting the frame to the plates. As there is a continuous plate, there may be prevention of moments or forces being transmitted which would act at the plate edge.

These two assumptions were examined further and measurements were carried out on the test structures. The first assumption, that perhaps the behaviour at the junction of the plates did not conform with the boundary conditions, was investigated by taking measurements of the acceleration level of the four plates directly at the junction with the frame. The structure tested is similar to that shown in Fig 6.1. The plasterboard plates are 1.2x1.2x0.0125m with a density of 806kg/m^3 and a longitudinal wavespeed of 1702m/s. The timber frame is 1.2x0.045x0.2m with a density of 451 kg/m^3 and a $C_{L(a)}$ of 4448m/s and a $C_{L(t)}$ of 1675m/s.

Fig 6.15 shows the measured acceleration level difference for the plates 1 to 2, 1 to 3 and 1 to 4 when placing the accelerometers at the junction of the frame and plates. As can be seen the acceleration level difference from plates 1 to 2, 3 and 4 is similar up to 1600Hz. At 2000Hz modes may be supported in the frame and the value for plates 3 and 4 diverge from plate 2. As this shows the level difference for the plates with respect to plate 1 it can be seen that the acceleration on plate 1 is not equal to that on the other plates. If all four plates were equal then there would be no level difference. This may be due to the accelerometers not being placed at the beams centre and shear forces may be acting on either side of frame's width. These results however are not conclusive.

The second assumption that the continuous plate may cause increased transmission from plate 1 to plate 2 was also investigated. Tests were carried out on two test structures involving two plates, plates 1 and 2, connected by a timber frame but plates 3 and 4 were omitted. Both structures are shown in Fig 6.16. The first structure incorporated a 12.5mm plasterboard sheet of dimensions 2.4x1.2m connected to a timber frame by two lines of screws at 60mm centres. This divided the 2.4x1.2m plate into two 1.2x1.2m plates. For the second test structure the plasterboard plate and timber beam were decoupled and the 2.4x1.2m plasterboard plate was cut in half to form two separate plates, 1.2x1.2m each. These two plates were then individually recoupled to the timber

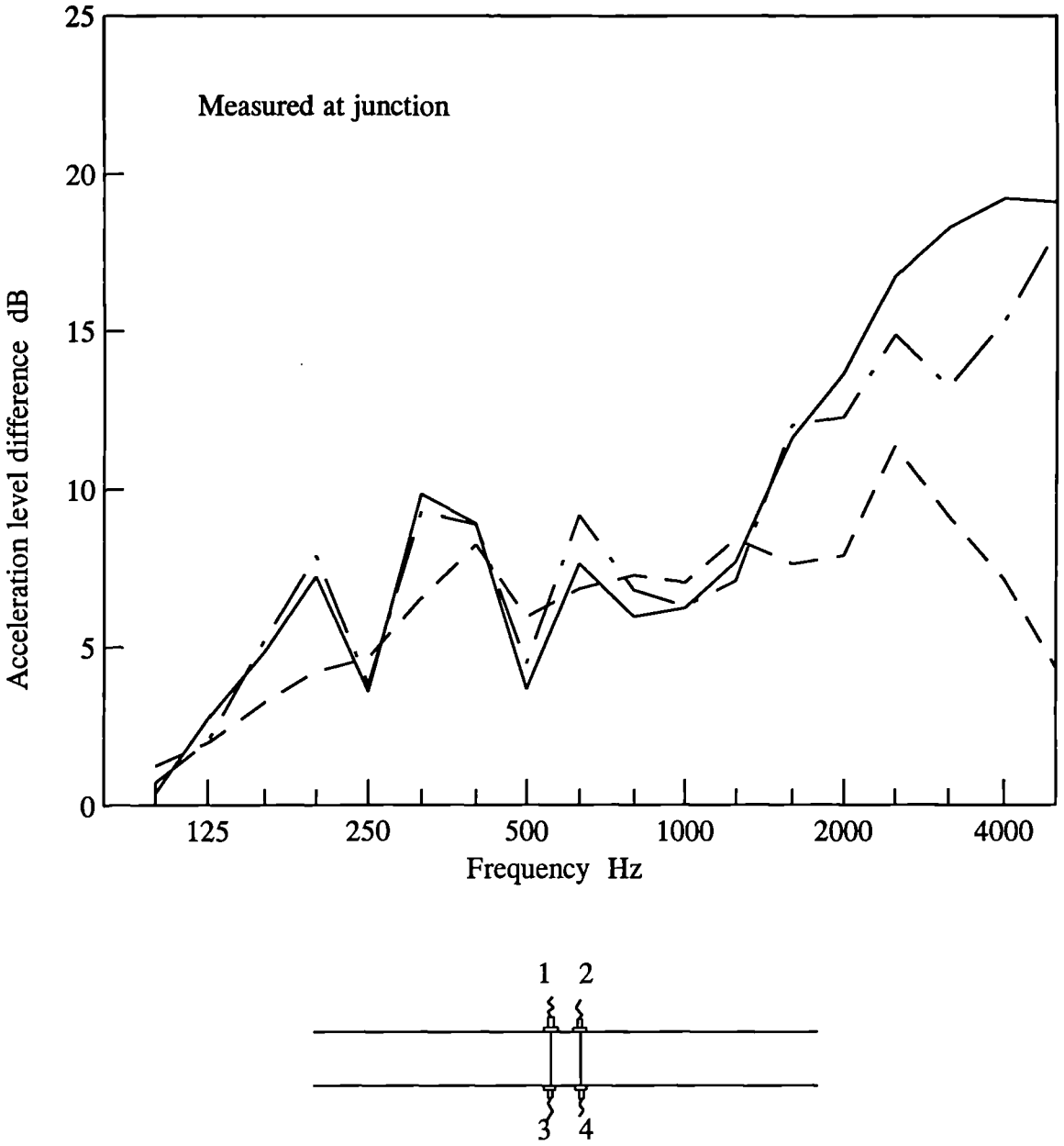

Figure 6.15 Measured acceleration level difference from plate 1 to plates 2, 3 and 4 when the accelerometers are placed at the junction.
(- - -) Plate 1 to 2, (_._._) Plate 1 to 3, (____) Plate 1 to 4.

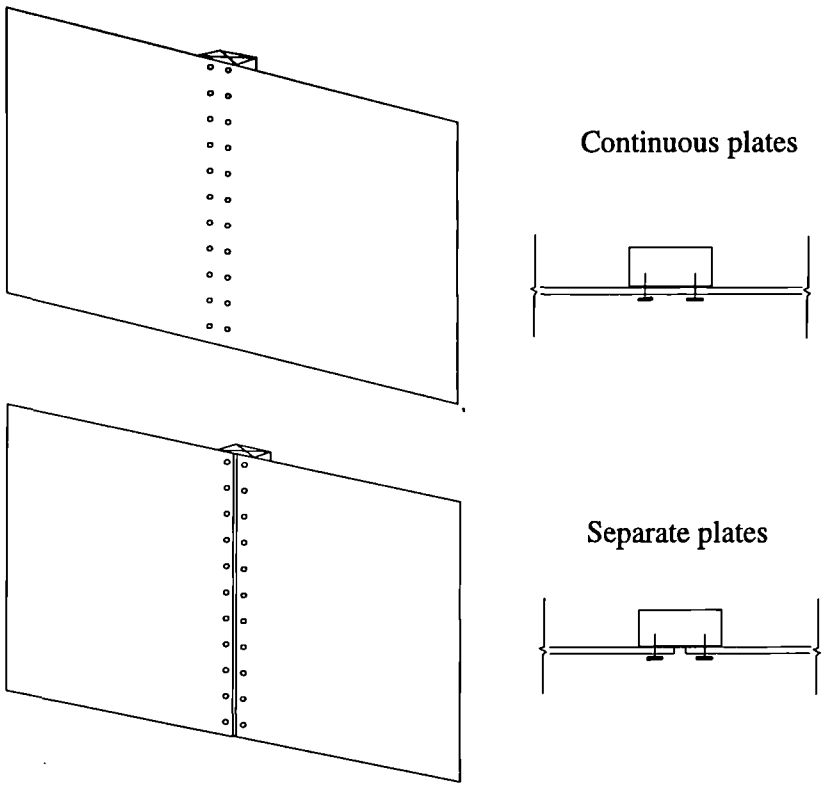

Figure 6.16 Schematic of continuous plate and separate plate structures tested

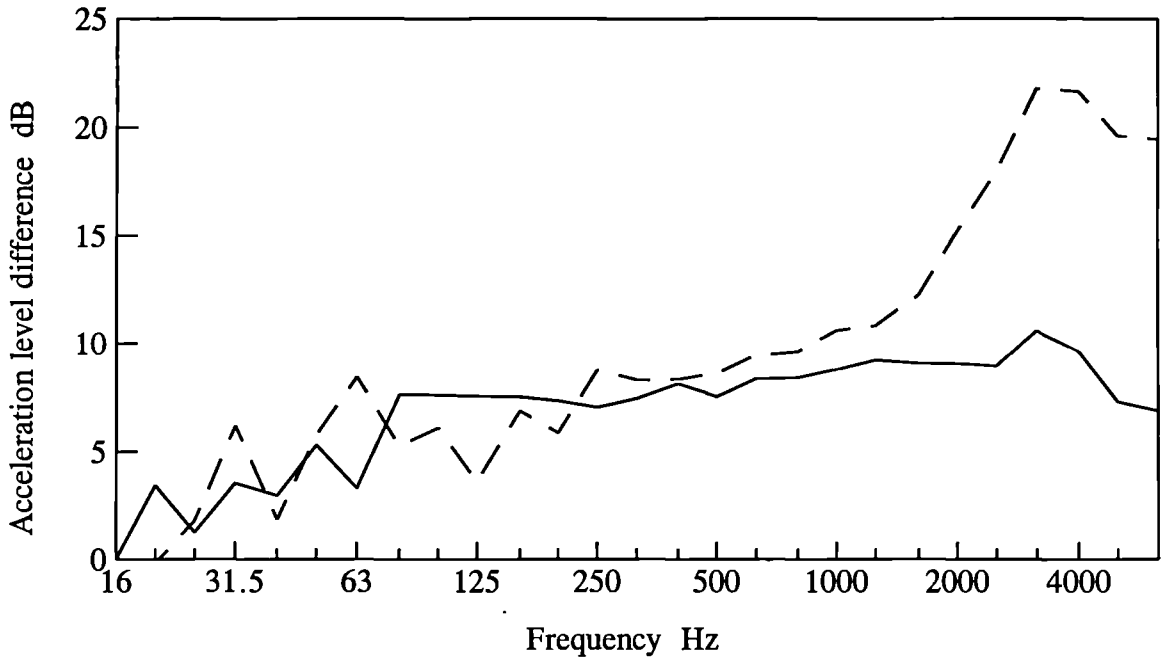

Figure 6.17 Measured acceleration level difference from plate 1 to plate 2 for continuous and separate plates. (___) continuous, (- - -) separate

frame by a line of screws each, at centres of 60mm. The reason for using a much thicker frame, shown in Fig 6.16, is to prevent the plasterboard sheets from breaking off from the frame if the contact area between plate and frame had been smaller. By decoupling plates 1 and 2 from each other, splitting the continuous plate, then the plates would both have real edges for the respective moments and forces.

Fig 6.17 shows the measured acceleration level difference from plates 1 to 2 for both the continuous and separate plate structures. There is only a significant difference in the measured results between the two structures at the higher frequencies above 2000Hz. This large difference at these frequencies is due to the spacing of the screw connections. For a spacing of 60mm the first half wavelength that fits between the screws will occur at approximately 2500Hz. At this frequency the structure is assumed to be no longer connected by a line connection but at specific points where the screws contact with the frame. Thus the structure at and above this frequency may be assumed to be point connected and effectively by being point connected there is an increase in acceleration level difference of up to 11dB.

The fact that there is practically no difference in the measured results between the two structures below 2000Hz suggests that the structure borne transmission is unrestricted by the continuous plate and is therefore being modelled correctly. However, this still does not solve the anomaly of why there is such strong coupling to plate 2 in the structures discussed in sections 6.3 and 6.4.

From Fig 6.17 the acceleration level difference between the continuous and separate plates is approximately 11dB at the frequencies where the structures are point connected, as shown in Fig 6.18. This means that the continuous plate has increased transmission between plate 1 to plate 2 of 11dB between the points of contact when compared to the separate plates. During the process of the tests carried out for section 3 a test was carried out to measure the acceleration level at the screws and between the screws. Although of a similar size and construction this was a different test structure to the continuous plate. Fig 6.19 shows the position of the accelerometers on the structure, on the screws(A) and between the screws(B), and it also shows the acceleration level difference between positions (A) and (B). The screws were at 60mm centres and similar to the above

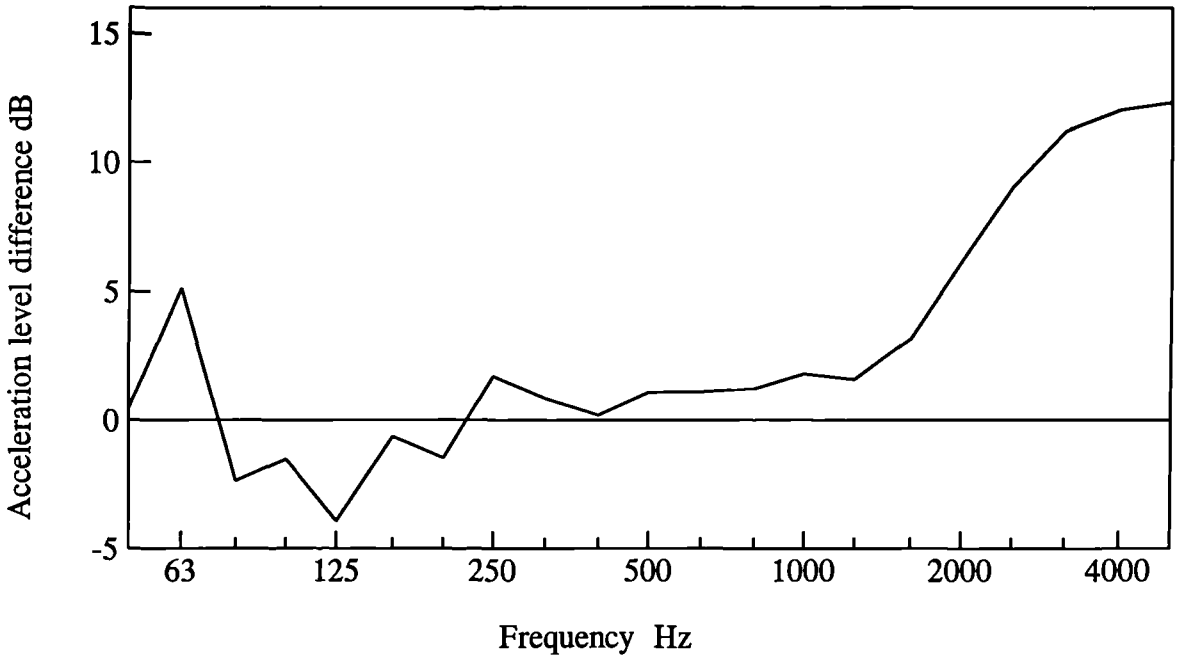

Figure 6.18 Measured acceleration level difference between the continuous test structure and separate test structure.

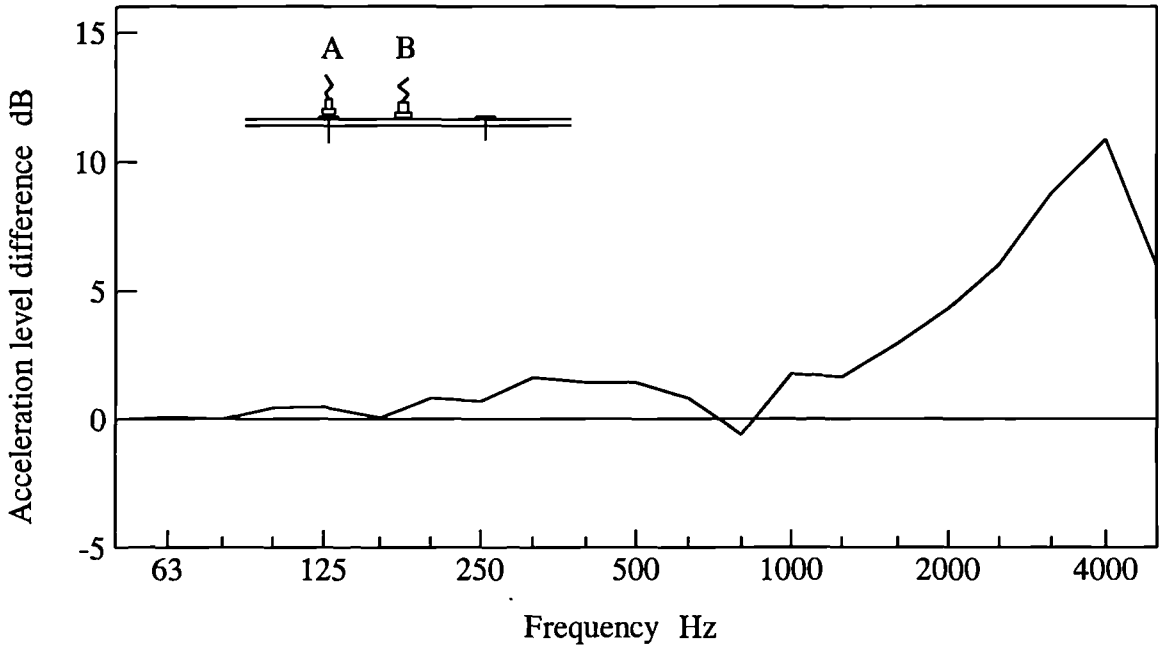

Figure 6.19 Measured acceleration level difference when measuring at the screws and measuring between the screws.

structure that decoupled the plates there is a significant acceleration level difference at 2000Hz and above. The measured difference in acceleration level between positions (A) and (B), as shown in Fig 6.19, should be the same as the measured difference in acceleration level shown in Fig 6.18. The transmitted energy lost when the plates are decoupled should be the same as that only going through the screw connections. As can be seen this is the case and this reaffirms the credibility and repeatability of the tests carried out.

6.6 Conclusions

This chapter has shown that the plate model is capable of predicting the acceleration level difference reasonably well between parallel plates. However, in the case of transmission from plate 1 to plate 2 all the models under predict the transmission and this is an area which requires further work.

The beam model and revised beam models work well at low frequencies before a wavelength is able fit within the frame depth. The metal channels tested proved that when there is a very flexible frame with a low value of D_y then the revised beam model works well. However, in the case of predicting the structure borne sound transmission between parallel plates over the entire frequency range, if the offset is small or large between the plates then the plate model theory copes well when compared with measured data. The plate model was adequate in predicting the change to transmission as result of increasing depth and omitting plates.

Chapter 7

Sound Transmission into Cavities

7.1 Introduction

This chapter describes the different types of cavity construction found in double walls and timber floors and reviews previous author's work in this area. Measured and predicted results are shown for transmission into double wall cavities. As part of this study tests were carried out on sound transmission into an isolated cavity test structure with one flexible plate in addition to tests on double wall cavities with two flexible plates.

This thesis is primarily concerned with the structural coupling that occurs in double walls. However for completeness, the radiation into cavities and adjacent rooms from double walls was also studied. Hence, this chapter aims to investigate the accuracy of existing SEA theories for predicting sound transmission into cavities.

7.2 Cavities in double wall construction

Fig 7.1 shows a variety of cavity constructions for basic lightweight partitions and timber floors with and without absorption. The cavity depth can vary from 25mm to 250mm depending upon the construction design. The cavity is bounded on all sides and closed. The plasterboard plates and timber studs of the frame in lightweight partitions result in structural elements forming perpendicular junctions at the cavity's perimeter. In timber floors the cavity is formed between the flooring, ceiling and timber joists. In domestic construction the partition frame is composed of timber and in office lightweight partitions metal channels are used.

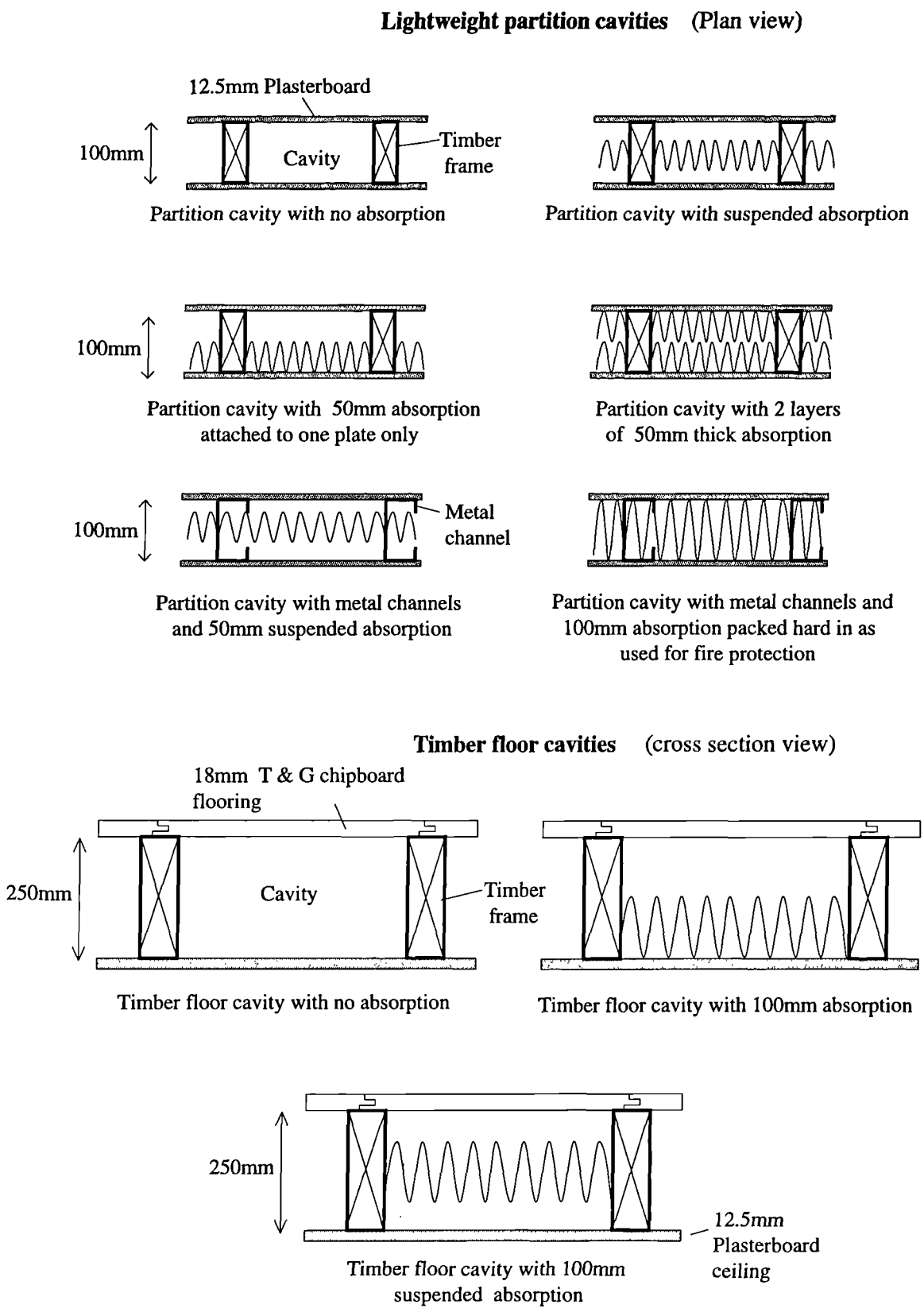

Figure 7.1 Types of cavity design found in basic lightweight partitions and timber floors with and without absorption.

Absorption can be present in cavities for three reasons. Firstly as an acoustic absorber to increase the damping of the cavity and assist in reducing the transmission through the cavity. Secondly, as insulation to reduce heat loss within the construction and thirdly as fire protection. Materials such as "Rockwool" insulation can increase the fire resistance of structural components and reduce the passage of smoke and fire through voids such as cavities. Some insulation products for thermal and fire use can also be used for acoustic absorption due to their high damping and absorption characteristics.

The structure of partitions and timber floors in today's construction industry are becoming more complex in design. However, for the purpose of this study, to develop SEA models for predicting sound transmission into and through such structures, the cavity and double wall structures studied are basic in design. This reduces the number of variables and assists in understanding the acoustic behaviour of the structures to then develop theoretical prediction models.

7.3 Review of past work on cavities

The section briefly mentions the authors who have studied sound transmission into cavities. The cavities studied had one dimension much smaller than the acoustical wavelengths possible under the frequency range of interest, thus creating a two dimensional acoustic void. Most of the authors have studied this transmission for a cavity where there is an airborne source in a room and finite flexible plate divides the room from the cavity, as shown in Fig 7.2. There are two important sound transmission paths into a cavity which are incorporated in an SEA model, the non-resonant path *room to cavity* and the resonant path *plate to cavity*. Some authors have chosen to study one path and others both paths.

Dowell and Voss [88] and Pretlove [89] provide similar 'exact' solutions using wave motion to describe the transmission from the plate to the cavity. Bhattacharya [51] studied double walls as described in Chapter 2. As part of this work he studied transmission into a cavity backed panel (plate) using a wave analysis. Guy [90] also studied this problem and like Bhattacharya produced a complex wave analysis solution which is not easily applicable to SEA techniques. Both solutions by these authors are for

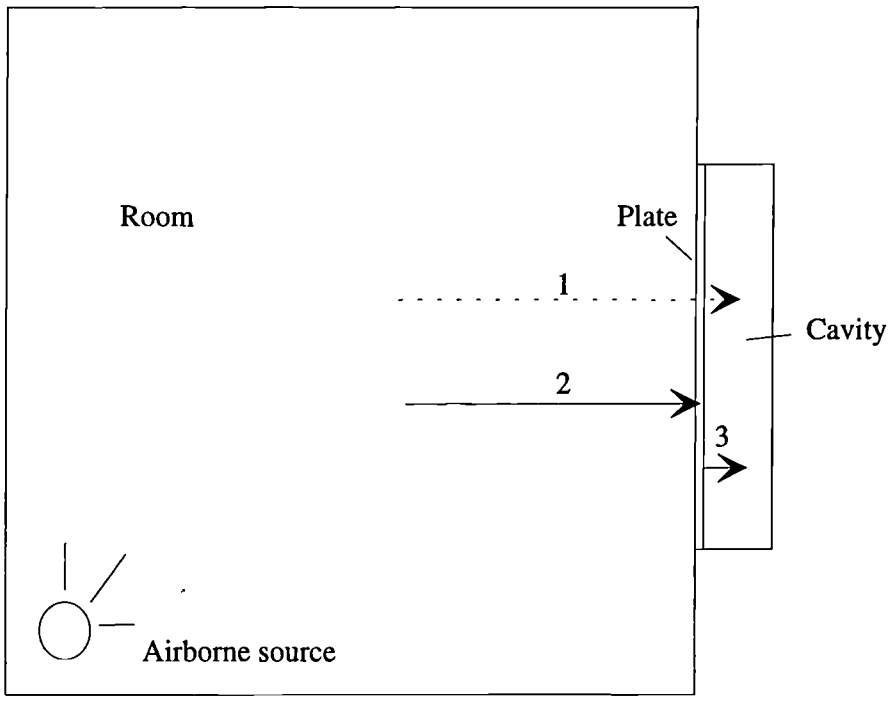

1 Non-resonant sound transmission path - ***Room to cavity***

2 Resonant sound transmission path - ***Room to plate***

3 Resonant sound transmission path - ***Plate to cavity***

Figure 7.2 Typical setup and SEA transmision paths for transmission from a room to a cavity through a finite plate.

general sound transmission into cavities. They do not differentiate between resonant and non-resonant transmission paths which would be useful for an SEA model. Cummings [91] has carried out substantial work on ducts, which are cavities with infinite length, four flexible plates and have attenuation with distance. The solutions provided are to calculate the "break-in" and "break-out" of the duct and these theories like those described above cannot be readily applied to SEA techniques.

Price and Crocker [49] provided an SEA solution to determine the transmission into a cavity in a double wall. The solutions were criticised, as described in Chapter 2, for not taking into account the cavity depth. However, some authors such as Elmallawany [52], have shown this not to be an important parameter provided the damping of the cavity is known.

The work of Price and Crocker has been cited by many authors to describe sound transmission through double walls using SEA. Interestingly none of the authors mentioned in Chapter 2 for their work on double walls have presented measurements of the transmission loss into the cavity and only Guy [90], described above, showed measured and predicted results together. The absence of these results in the double wall research may have been due to the transmission path through the cavity being weak or the presence of line structural coupling, connecting the plates of the double walls by a structural frame. The line connection between the plates can be strong and as such it may obscure the transmission path through the cavity. Several authors who have studied double walls have found that in their test structures the cavity path was very weak for most of the frequency range, such as Lin and Garrelick [32], Wilson [8] and Sullivan [54].

However, not all walls are line connected, some may be point connected and thus the structural path is not as strong. If the structural path is weaker the cavity may have a more important role. This chapter presents measured and predicted results for transmission into an isolated cavity test structure and also for cavities in double walls. Both types of structure were tested with varying depths. The SEA model provided by Price and Crocker was used to calculate the predicted airborne level difference.

7.4 Test structures

The two types of cavity test structure used in this study are shown in Fig 7.3 and 7.4. Fig 7.3 shows the point connected double wall structures, consisting of plasterboard sheets supported on a timber frame forming cavities between the plates and the frame. The 150mm double wall was composed of chipboard and plasterboard plates and was built to assist in understanding the sound transmission into timber floor or double wall cavities. The isolated cavity test structure shown in Fig 7.4 was composed of a sheet of 12.5mm plasterboard placed over a cavity formed from brick and concrete. This special test cavity would allow the study of sound transmission into a cavity independent of the rest of the wall. The cavities for both test structures were fully sealed.

The 12.5mm thick plasterboard plates in the double wall structures were 1.2x2.4m in dimension and each sheet covered three cavities with point connection to the frame at 300mm centres. The total area of each side of the double wall was $12m^2$. The 12.5mm thick plasterboard plates in the single cavity test structure was 1.9x0.96m in dimension and sealed at the edges by mortar.

The depth of the cavities were varied from 25mm-150mm to analyse sound transmission into cavities as would be found in real walls or floors. Absorption was sometimes placed in the cavities and consisted of "Rockwool" fibreglass insulation. Further discussion of the test structures and the experiment techniques to measure the airborne level difference can be found in Chapter 3.

7.5 Theory and SEA models

Fig 7.5 shows the SEA models for both test structures. The equations for coupling loss factors (CLF's) for resonant transmission between room, plate and cavity and non resonant transmission between room and cavity are discussed in Chapter 2. The non resonant transmission coefficient was computed from theory given by Leppington *et al* [43] and the radiation efficiency required for resonant transmission was calculated using Leppington *et al* [41], as described in Chapter 2.

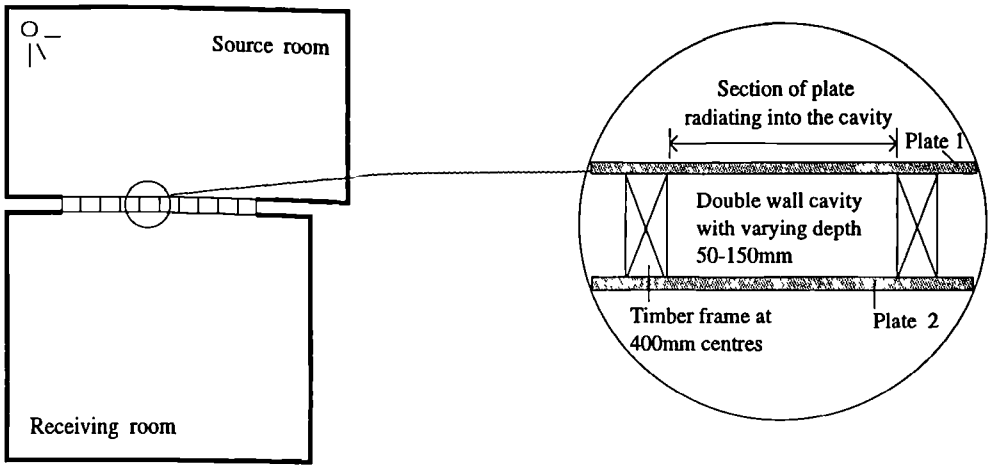

150mm Double wall cavity								
Subsystem	L(m)	b(m)	h(m)	C_L(m/s)	ILF	ρ (kg/m^3)	μ	E_a(N/m^2)
Source room	10	4	3					
Receiving room	7	6	5					
Plate 1 Chipboard	4	3	0.018	1506	0.015	680	0.2	
Plate 2 Plasterboard	4	3	0.0125	1736	0.01	801	0.2	
Cavity (10 No.)	0.35	3	0.15					
Frame	0.05	3	0.15	3846	0.015	469	0.2	6.94×10^9
100mm Double wall cavity								
Subsystem	L(m)	b(m)	h(m)	C_L(m/s)	ILF	ρ (kg/m^3)	μ	E_a(N/m^2)
Source room	6.7	4	3					
Receiving room	7	6	5					
Plate 1 Plasterboard	4	3	0.0125	1974	0.01	723	0.2	
Plate 2 Plasterboard	4	3	0.0125	1701	0.01	809	0.2	
Cavity (10 No.)	0.35	3	0.10					
Frame	0.05	3	0.10	4165	0.015	475	0.2	8.24×10^9
50mm Double wall cavity								
Subsystem	L(m)	b(m)	h(m)	C_L(m/s)	ILF	ρ (kg/m^3)	μ	E_a(N/m^2)
Source room	6.7	4	3					
Receiving room	7	6	5					
Plate 1 Plasterboard	4	3	0.0125	1701	0.01	710	0.2	
Plate 2 Plasterboard	4	3	0.0125	1973	0.01	806	0.2	
Cavity (10 No.)	0.35	3	0.05					
Frame	0.05	3	0.05	4484	0.015	380	0.2	7.64×10^9

Figure 7.3 Double wall test structures and subsystem properties for transmission into cavities.

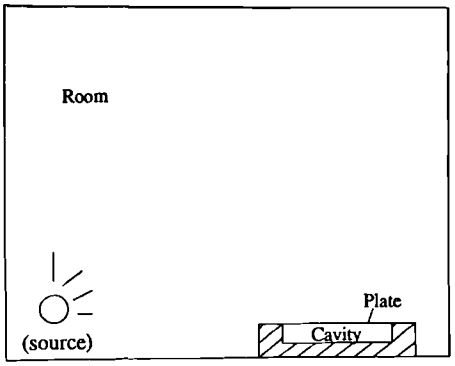

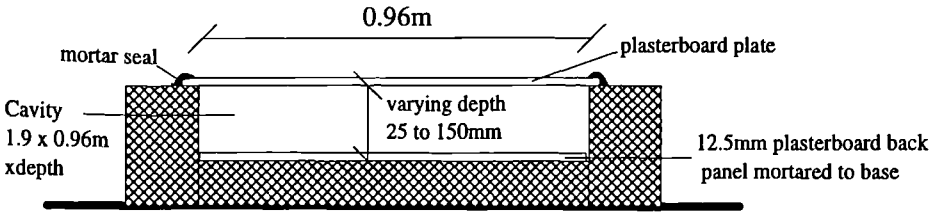

150mm cavity test structure							
Subsystem	L(m)	b(m)	h(m)	C_L(m/s)	ILF	ρ (kg/m^3)	μ
Room	7.2	10	4				
Plate	1.9	0.96	0.0125	1806	0.01	755	0.2
Cavity	1.9	0.96	0.15				
100mm cavity test structure							
Subsystem	L(m)	b(m)	h(m)	C_L(m/s)	ILF	ρ (kg/m^3)	μ
Room	7	6	5				
Plate	2.2	0.96	0.0125	1744	0.01	880	0.2
Cavity	2.2	0.96	0.10				
50mm cavity test structure							
Subsystem	L(m)	b(m)	h(m)	C_L(m/s)	ILF	ρ (kg/m^3)	μ
Room	7	6	5				
Plate	1.9	0.96	0.0125	1806	0.01	755	0.2
Cavity	1.9	0.96	0.05				
25mm cavity test structure							
Subsystem	L(m)	b(m)	h(m)	C_L(m/s)	ILF	ρ (kg/m^3)	μ
Room	7	6	5				
Plate	2.2	0.96	0.0125	2007	0.01	680	0.2
Cavity	2.2	0.96	0.025				

Figure 7.4 Isolated cavity test structure and subsystem properties

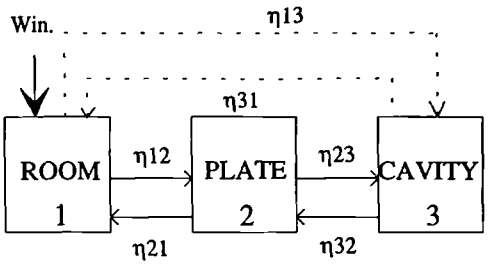

(a) Three subsystem model for transmission into cavity test structure

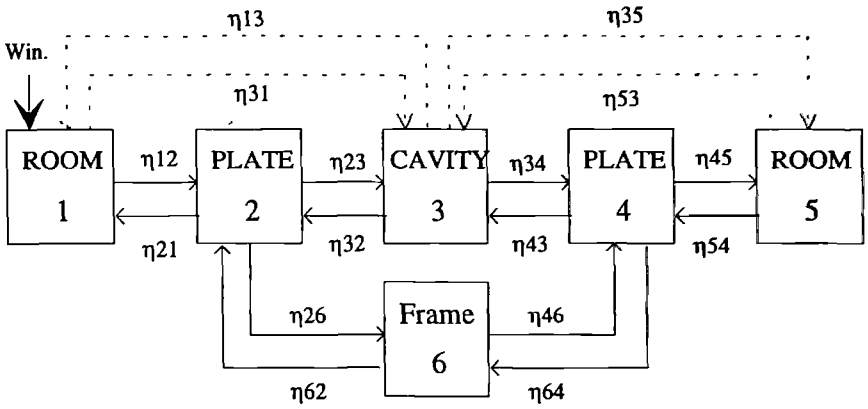

(b) Multi subsystem model for double wall structure with cavities

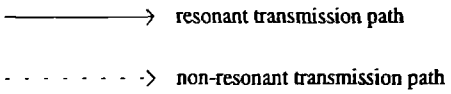

Figure 7.5 SEA models for test cavity structure and cavities in double walls

The multiplier factor discussed in Chapter 2 is also used here. The plasterboard plates for the isolated cavity test structure were sealed along the length of their edges by mortar and were assumed to be clamped resulting in a multiplier of two. The plates were also radiating into a quarter space due to the right angle baffles and this also resulted in a multiplier of two. Thus the total multiplier for the radiation from the plates to the cavity was a multiplier of four.

In the case of double walls, the plates covered more than the cavity under test and were point connected and assumed to be simply supported. However the plates were radiating into a quarter space and a multiplier of 2 was given. In addition, as the plates were only continuous and connected by points on two edges it was assumed that account should be given to the remaining plate edges and thus a total multiplier of 3 was given.

The internal loss factor (ILF) of the plasterboard plates was measured as described in Chapter 3 and an approximate value of 0.01 was used. The total loss factor of the plasterboard plate was calculated form summing the CLF's and ILF. When absorption was present in the cavities and in contact with the plates the TLF of the plates were measured as described in Chapter 3. The total loss factor of the room was calculated from the measured reverberation time using eqn(2.40).

7.6 Measuring the total loss factor of the cavities

In order to calculate the energy level difference between the source room and cavities the cavity total loss factor was required. This was calculated from eqn(2.40) where the reverberation time, T_{60}, was measured. The method used to measure the cavity T_{60}, was the standard decay method, using MLSSA as described in Chapter 3. Fig 7.6 shows the reverberation time for a 100mm deep double wall cavity with and without absorption. For the case with absorption, the cavity was partly filled with two layers of 25mm thick "Rockwool" fibreglass quilt. The quilt was suspended in such a way that it did not touch the plasterboard sheets that formed the sides of the cavity. It can be seen that the reverberation time is much shorter with absorption present and is close to the limit of the third octave band filter, which is also shown.

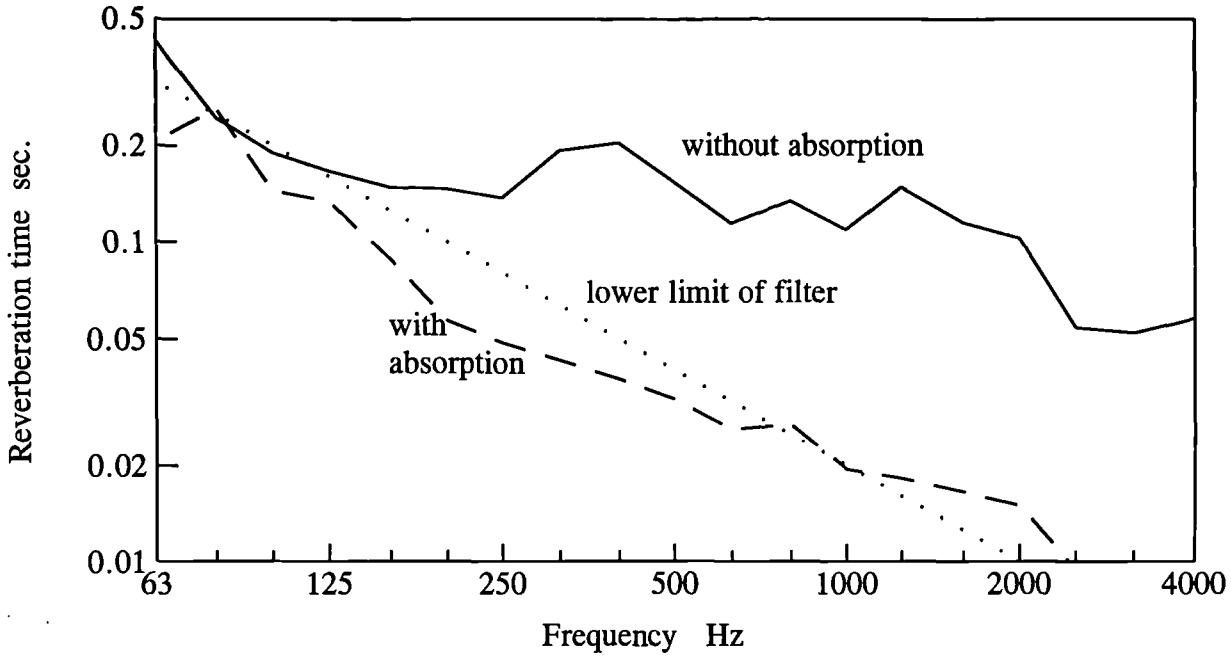

Figure 7.6 Reverberation time for a 100mm double wall cavity showing a comparison for without absorption, with 50mm suspended absorption and the lower filter limit.

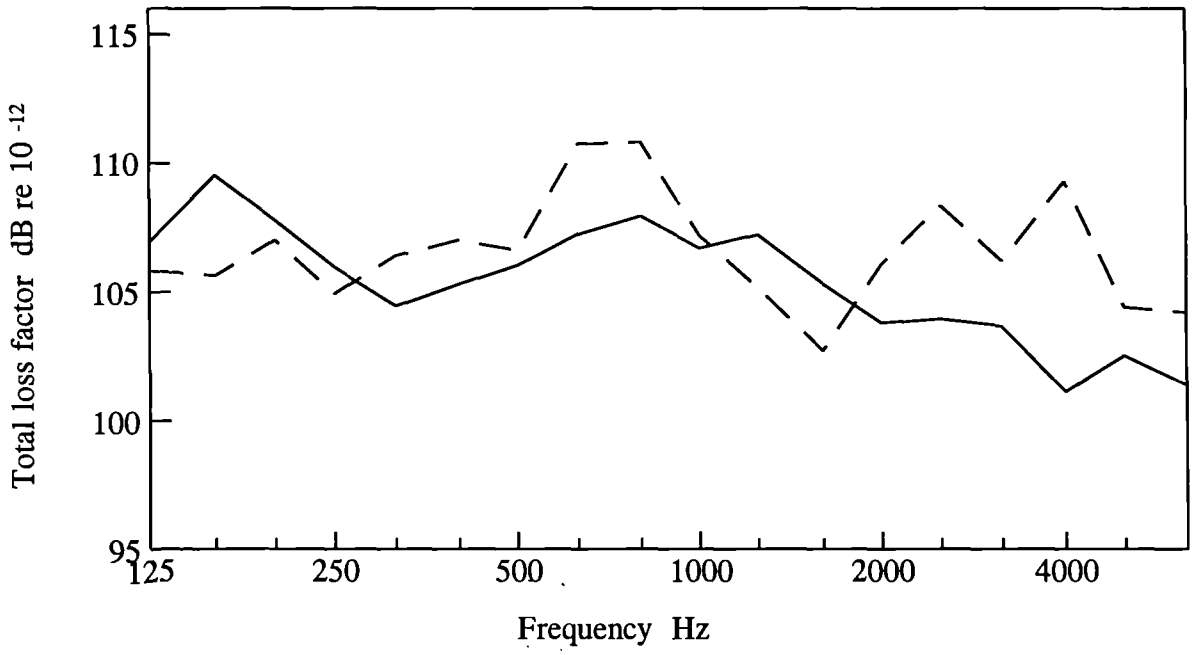

Figure 7.7 Total loss factor for a 25mm test cavity with no absorption showing a comparison between the standard decay method and the power injection method. (- - -) pow. inj. method, (____) decay method.

In hindsight, the standard decay method was not the best option available to measure the damping of the cavity. Another option which may have been used was the power injection method. Fig 7.7 shows a comparison between the standard MLSSA decay method and the power injection method.

The power injection method measures the reverberation time by an indirect process involving two separate measurements. The first measurement involves leaving the cavity open and not fixing the flexible plate, as shown in Fig 7.8a. The speaker, which is built into the cavity, produces a source pink noise spectrum driven by a noise generator, in this case a Nortronics. The sound pressure level in the room is measured, Lp_1, and if the reverberation time for the room has been measured, T_1 and the volume of the room is known, V_1, then using the following equation the sound power level, Lw_1, in the room may be calculated,

$$Lw_1 = Lp_1 + 10\log\frac{V_1}{T_1} - 14 \qquad (7.1)$$

This test process is repeated but the cavity is closed with the finite plate, as shown in Fig 7.8b, and the sound pressure level in the cavity, Lp_3, is measured. From the previous test the power output, Lw_1, is known and if the volume of the room is known, V_3, then the reverberation time of the cavity, T_3, may be solved from the following equation,

$$Lw_1 = Lp_3 + 10\log\frac{V_3}{T_3} - 14 \qquad (7.2)$$

The agreement shown in Fig 7.7 is good over the frequency range. At the outset of this particular work from the two methods the standard decay method was adopted for measuring the reverberation time of cavities. As the cavity volume decreased so did the reverberation time and when absorption was present the decay time was even shorter. By using the decay method to measure the reverberation time this was restricted by the limit of the 1/3 octave band filter (the limit being caused by filter ringing). Unfortunately, this was not discovered until late on in the tests. The measured decay time for cavities without absorption appears to have been unaffected. However, when absorption was present the decay time was affected by the filtering process. Whilst in

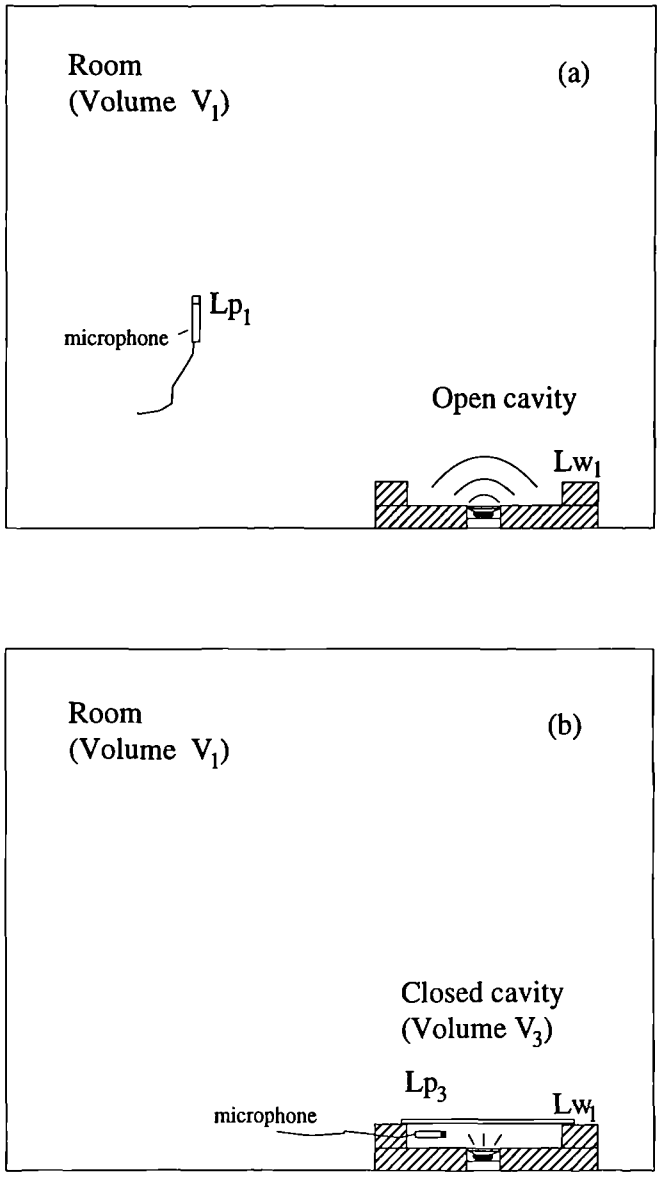

Figure 7.8 Schematic of power injection method

hindsight the power injection method may have been a better option there is no guarantee that this would be the correct method due to the acoustic power being altered by the very close obstruction caused by the plasterboard plate.

7.7 Transmission into an isolated cavity

This section describes the measured and predicted airborne level difference for transmission into an isolated special test cavity, as described earlier. This made it possible to study transmission into the cavity independent of the rest of the wall. The following section describes similar experiments but for transmission into a double wall cavity. Testing was restricted to measuring airborne level difference into the cavity as there were problems generating a uniform sound field in the cavity (to measure transmission from the cavity to the room) and uniform excitation of the panel (to measure radiation). Any source in the cavity, in this case a small built-in speaker, must be acoustically close to the plate resulting in non uniform excitation of the plasterboard.

Four cavities were tested, 25, 50, 100 and 150mm deep and transmission was through a 12.5mm sheet of plasterboard (critical frequency 2980Hz) for each case except the 25mm cavity where the thickness was 9mm resulting in a higher critical frequency (4274Hz).

Fig 7.9 shows the measured and predicted airborne level difference for transmission into the test cavity structure for various depths without absorption. The agreement is good over the frequency range. The reduction in level difference at 2500-3150Hz is due to the critical frequency of the plasterboard. The predicted results used the Price and Crocker [49] SEA model and equations for the CLF's. The reverberation time was measured for each cavity to determine the TLF. The sound pressure level was measured both in the room and the cavity at a sufficient number of positions to give a 95% confidence interval of the level difference of less than ± 2dB up to 125Hz and less than ± 1dB at higher frequencies.

One of the attractions of using SEA is its ability to analyse individual transmission mechanisms and paths. An analysis of the relative contributions of resonant and non

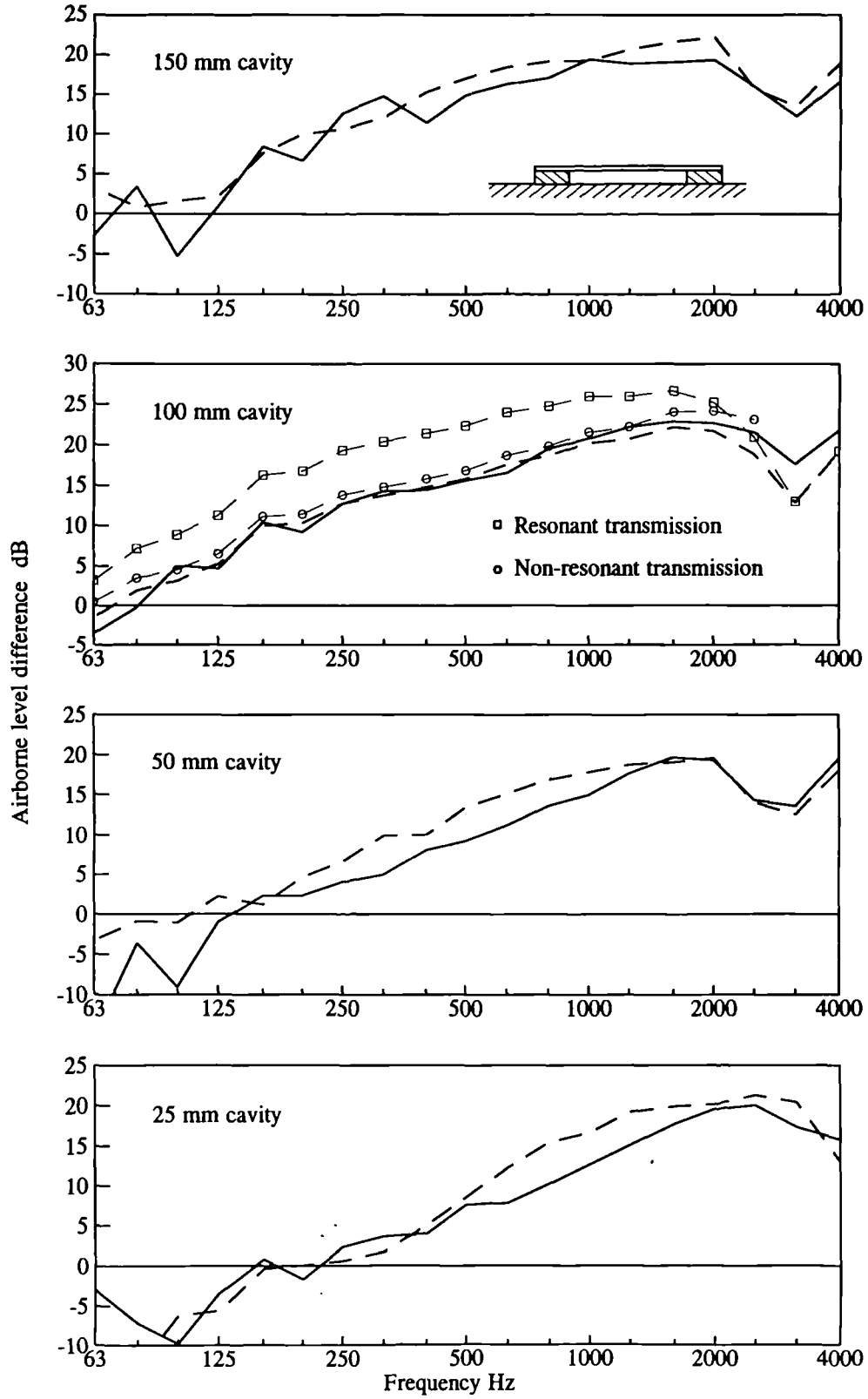

Figure 7.9 Measured and predicted airborne level difference for transmission from a room into the cavity test structure with varying depths.

resonant transmission is shown for the 100mm cavity in Fig 7.9. As would be expected the transmission is dominated by non-resonant transmission below the critical frequency and the resonant path is over 5dB less important than the non-resonant path. A feature of the results is that the level difference is negative at low frequencies (it is louder inside than outside). This is due to the two dimensional nature of the cavity and is less significant as the depth increases.

7.8 Transmission into a double wall cavity

Similar tests were carried out to give transmission from a room into the cavity of a double wall. Tests were only carried out for transmission into the cavity in double wall structures where there was no added absorption, since the reverberation time could not be measured accurately with absorption present. Measurements were made to the same level of accuracy as the separate test cavity and the total loss factor for the cavity was calculated from the reverberation time using the decay method. The cavities were all 3 x 0.35m, (stud spacing of 0.4m centres), and were 50, 100 and 150mm deep so as to give some comparisons with Fig 7.9. The coupling from the room to the plate involves the total area of the plate, but the coupling between the plate and cavity must only involve the area of the plate directly radiating into the cavity. The total area of the wall was $12m^2$ and the plate area radiating into the cavity was $1.05m^2$.

The measured and predicted airborne level differences are shown in Fig 7.10. There is reasonable agreement between the measured and predicted results for the 150mm double wall cavity, but as the cavity depth decreases so the difference increases. The agreement is not as good as when compared with the results shown in Fig 7.9. The predicted airborne level difference for the 50mm cavity has no data from 80-160Hz and this was due to the predicted TLF fractionally exceeding the measured TLF and the software used ignores this data.

In the double wall the ratio of cavity perimeter length to area (6.7:1.05) is greater than for the test cavity structure (5.72:1.82) so that the resonant transmission is relatively more important in the double wall. This is shown in Fig 7.10 for the 100mm double wall cavity. When compared with the transmission paths into the 100mm cavity in Fig

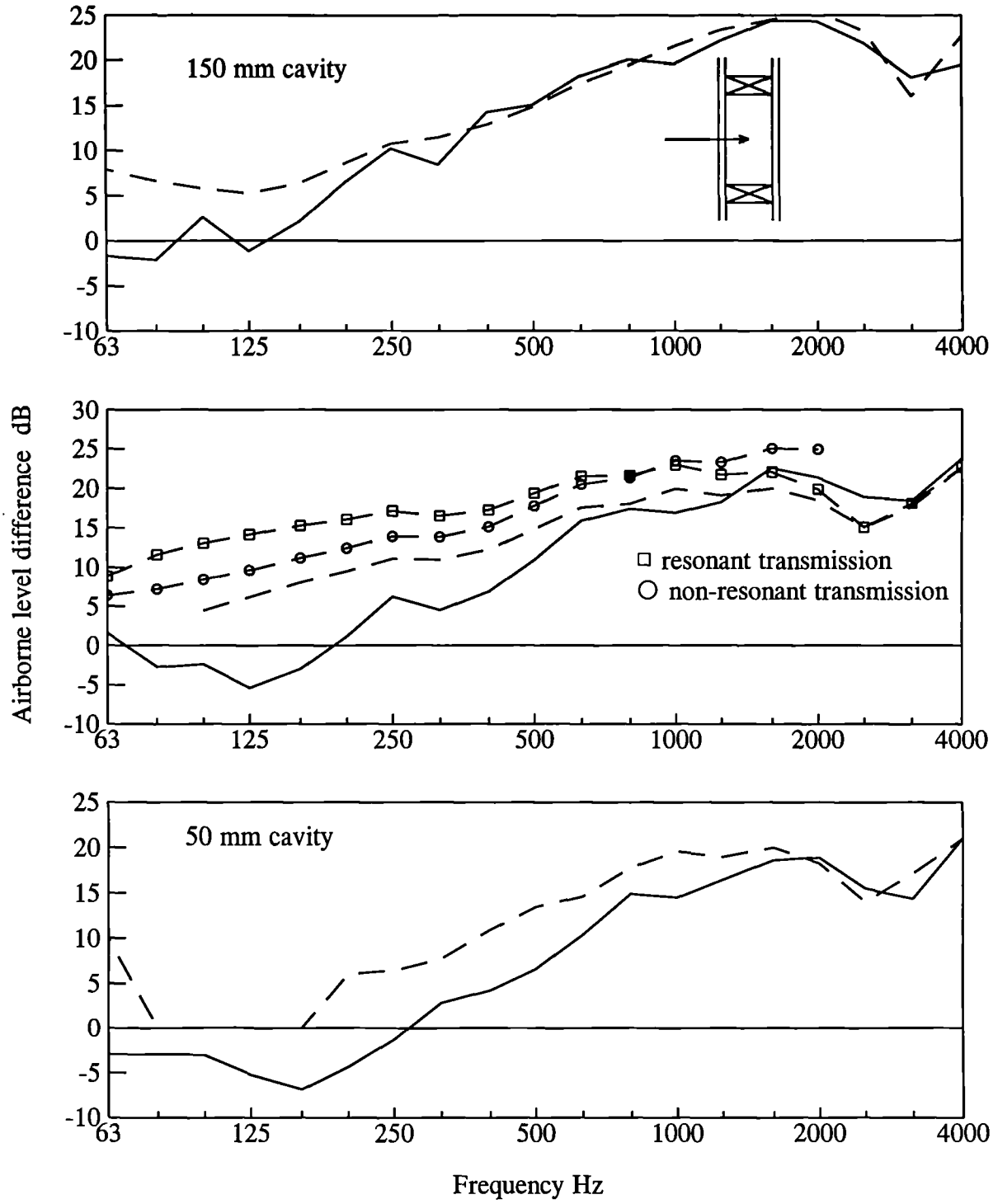

Figure 7.10 Measured and predicted airborne level difference for transmission from a room into double wall cavities with varying depth.
(- - -) predicted, (____) measured.

7.9 the resonant path is stronger.

The other difference between the results of Fig 7.9 and 7.10 is the property of the back plate. A final test of transmission into a cavity was carried out using a 75mm deep cavity that was part of a double wall. This was specially constructed so that the back panel could be removed whilst leaving the panel through which sound transmitted unchanged. Two cases were measured and the results are also shown in Fig 7.11. The first case is where the back panel was a flexible sheet of plasterboard and in the second case the back panel was rigid 102mm thick brick wall. The predicted results are different due to the different damping of the cavity. It can be seen that there is better agreement between the measured and predicted results when the back plate is rigid particularly in the frequency region 200-1000Hz.

7.9 Discussion

The agreement between the predicted and measured results for transmission into the isolated test cavity structure is good. When absorption is placed in the cavity the reverberation time would be best measured by the power injection method. The filter limit of the equipment restricted the range of test structures possible when absorption was present.

The agreement for similar transmission into a double wall cavity is not as good. This may be due to the presence of the flexible back plate. The tests on the wall where the back plate was replaceable suggest that the flexible plate was influencing the sound transmission into the cavity but it is not clear what mechanism of transmission is causing this effect. The change in cavity damping due to the different back plates was as much as 5dB shown by the difference in the predicted results.

As shown in Fig 7.1 there are several designs of double wall and timber floor cavities which incorporate absorption. The inability to accurately measure the damping of the cavity with absorption present suggests that more work should be carried out in this area so that all types of construction may be modelled.

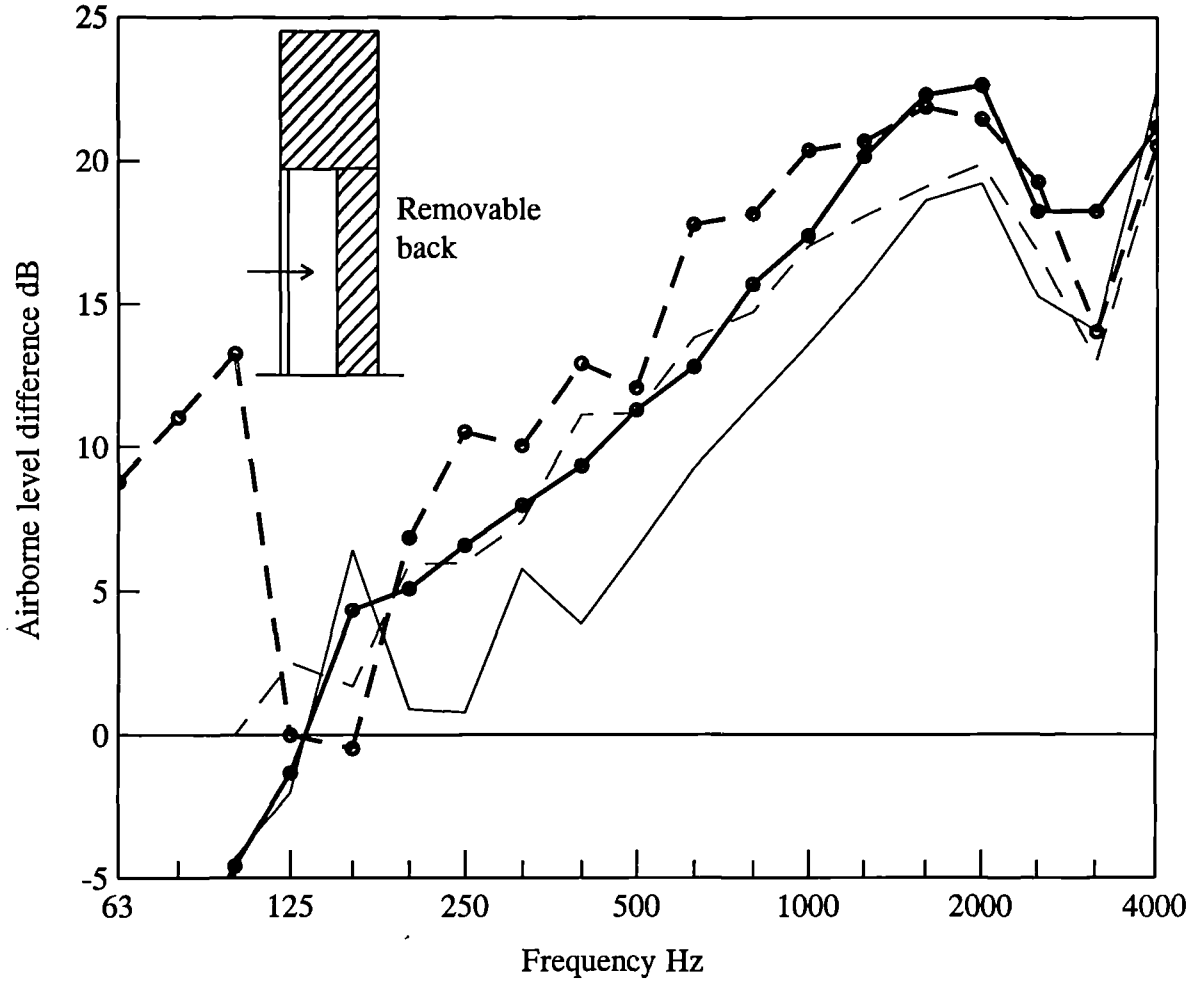

Figure 7.11 Airborne level difference for transmission into a cavity with flexible or rigid backing.

7.10 Conclusions

This chapter has shown that the method presented by Price and Crocker is adequate for predicting sound transmission into a cavity. For double wall cavities the theoretical model requires further work. As the cavity depth decreases the difference in the measured and predicted airborne level difference increases. The presence of the flexible plate may be affecting the transmission into double walls.

The SEA model is able to analyse the effect of different transmission mechanisms. The transmission into a cavity is dominated by the non-resonant transmission. For double wall cavities the increased ratio of the perimeter length to surface area of the panels radiating into the cavity increases the resonant transmission path. At low frequencies up to 125Hz the transmission is a negative value. However, as will be shown in the following chapter the double walls behave as single subsystems at these frequencies and the transmission into the cavities is not important at these frequencies.

This work has dealt with real double walls incorporating finite plates and cavities, coupling from rooms to cavities and radiation from plates to cavities. Past authors who have suggested that this area can be predicted have proposed complex theories which are not adequate for real walls. SEA can be used as a design tool when predicting sound transmission into cavities but further work is required to investigate the transmission and behaviour of narrow cavities in real double walls.

Chapter 8

Sound Transmission Through Real Walls

8.1 Introduction

This chapter compares measured and predicted data from SEA theoretical models for a variety of real walls and for a full scale timber floor. The results for real walls include single plate walls, ribbed walls and double walls with point and line connection. In addition to the overall airborne level difference results from the source room to the receiving room, data is also presented for the acceleration level of the various structural elements of the walls as a result of an airborne source and also for structure borne sound sources.

8.2 SEA theoretical models

This chapter also describes the SEA models for the various structures bringing together the theory presented in the previous chapters for airborne and structural coupling. The basic equations for coupling between plate and rooms were described in Chapter 2. The radiation efficiency which was used to determine the SEA resonant transmission, for plate to room and plate to cavity, was calculated using Leppington *et al* [41]. The non-resonant transmission coefficient used in the SEA models, for transmission paths such as room to room and room to cavity, was calculated using Leppington *et al* [43] as described in Chapter 2. All the test walls were mounted on a timber support frame and were assumed to be clamped to the frame and the radiation efficiency was increased by a factor of 2 as discussed in Chapter 2.

The total loss factors (TLF's) of the walls, rooms and cavities were measured for all test structures. Due to the good agreement between the measured and predicted TLF for the double walls discussed in Chapter 3 and for simplicity the predicted TLF for the plates was used in the SEA models. However, where there was absorption present in the double walls the measured TLF was used as the predicted theory could not account for the increase in damping due to absorption touching the plates. The internal loss factor (ILF) of the plasterboard and chipboard plate materials, used in the following constructions, was measured as discussed in Chapter 3 and values of 0.01 and 0.018 were given respectively.

The theories included in these models involve point coupling which was discussed in Chapter 4, line coupling discussed in Chapter 5 and transmission into the double wall cavities which was discussed in Chapter 7. Some of the figures in this chapter have units which are normalised. For example if the acceleration level of a plate or structural element is normalised for an airborne source, this would be calculated by subtracting the source sound pressure level, (acceleration level - sound pressure level (source)). Sometimes the acceleration level is normalised for a structural source. This is calculated by subtracting the acceleration level of the source plate from the plate under test. This assists in analysing the particular plate under test independent of the source level.

8.3 Single plate and ribbed plate walls

SEA model and test structures for single walls

Fig 8.1 shows a single leaf wall made of 18mm thick chipboard plates connected by tongue and groove (T&G) joints bonded and sealed with adhesive. These large plate structures may be found in timber floors. The chipboard wall was constructed between two test chambers so that it could be studied in isolation from the other components found in a timber floor, such as joists and cavities. The total chipboard wall area was $12m^2$ and had an external perimeter length of 14m. Fig 8.1 also shows the material properties for this single wall construction. The SEA model for the chipboard wall dividing two rooms is shown in Fig 8.2 and is similar to the Crocker and Price SEA model [48] but also includes the weaker reciprocal transmission paths for completeness.

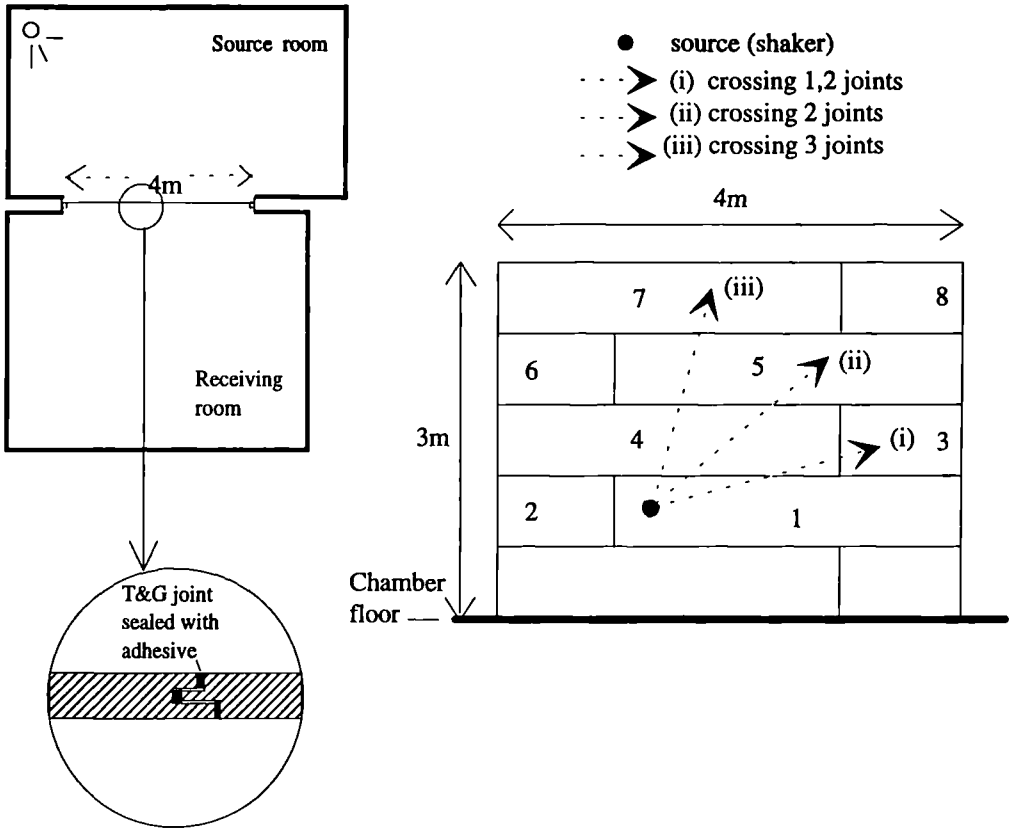

18mm T&G chipboard single wall							
Subsystem	L(m)	b(m)	h(m)	C_L(m/s)	ILF	ρ (kg/m^3)	μ
Source room	10	4	3				
Chipboard wall	4	3	0.018	1821	0.015	660	0.2
Recieving room	7	6	5				

Figure 8.1 Plan, elevation and table of material properties for chipboard single plate wall.

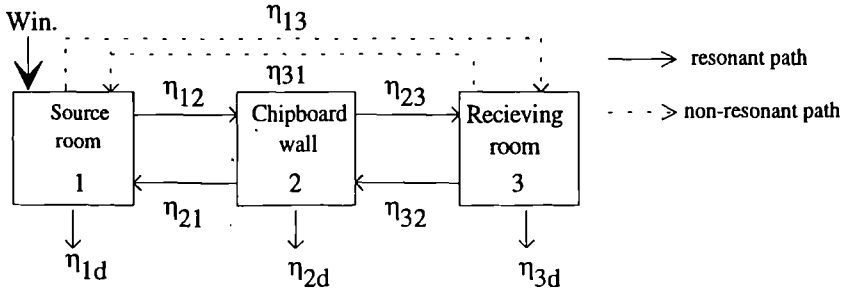

Figure 8.2 SEA model for two rooms separated by a chipboard wall.

Using a B&K shaker type 4810 as a structural source exciting the wall, tests were carried out to look at the effect, if any, of the T&G joints on the structure borne sound transmission across the chipboard wall. Also if the joints were dividing the $12m^2$ chipboard wall into smaller plates it was of interest to see if this might affect the radiation of the plate and its perimeter length.

Measurements were made near the source and also at three positions equidistant from the source. However, the three receiving positions were separated from the source plate by 1, 2 and 3 T&G joints. By measuring at equal distances the effect of attenuation with distance could be ignored and hopefully only the effect of the joints could be analysed. Fig 8.3 shows the normalised acceleration level difference between the source and receiving positions, where the source level was measured sufficiently far away from the shaker to avoid nearfield and non-linear effects. The acceleration level difference of the three positions are very similar with a difference of +/- 1.5dB for most of the frequency range. This suggests that the T&G joints may be attenuating the acceleration level across the plate but not significantly.

Fig 8.4 shows the measured and predicted acceleration level for the chipboard wall normalised for an airborne source and there is good agreement. The prediction model was calculated using the perimeter length of the total wall, 14m, and modelling the multiple panels as one large plate of $12m^2$.

Fig 8.5 shows the measured and predicted airborne level difference between the source and receiving rooms through the chipboard wall. The agreement between the measured and predicted results is good and the dip at approximately 2000Hz is due to the critical frequency of the chipboard.

Fig 8.6 shows the individual SEA transmission paths, the non-resonant path (*room-room*), and the resonant path (*room-chipboard-room*). As can be seen the non-resonant path is the dominant path up to the critical frequency, after which only the resonant path is present. The SEA prediction model works well over the frequency range and the wall is behaving as one large plate subsystem.

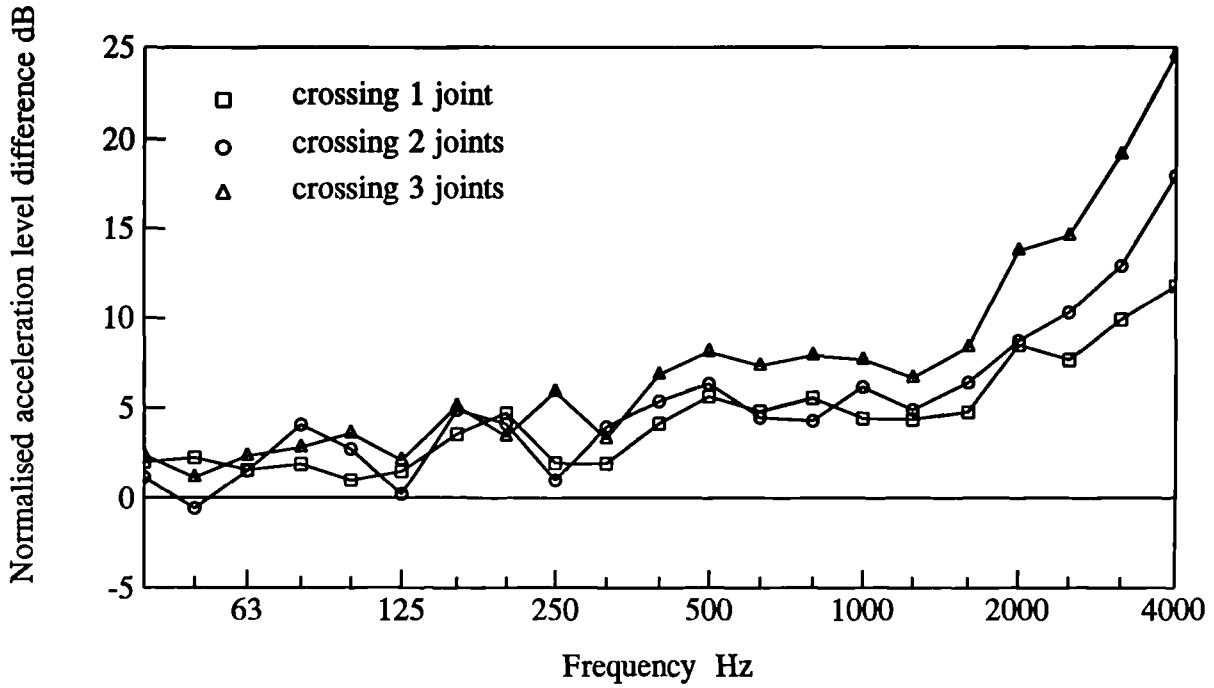

Figure 8.3 Measured acceleration level difference between chipboard panels where the various receiving panels are equidistant from the source panel but are separated by increasing number of T&G joints.

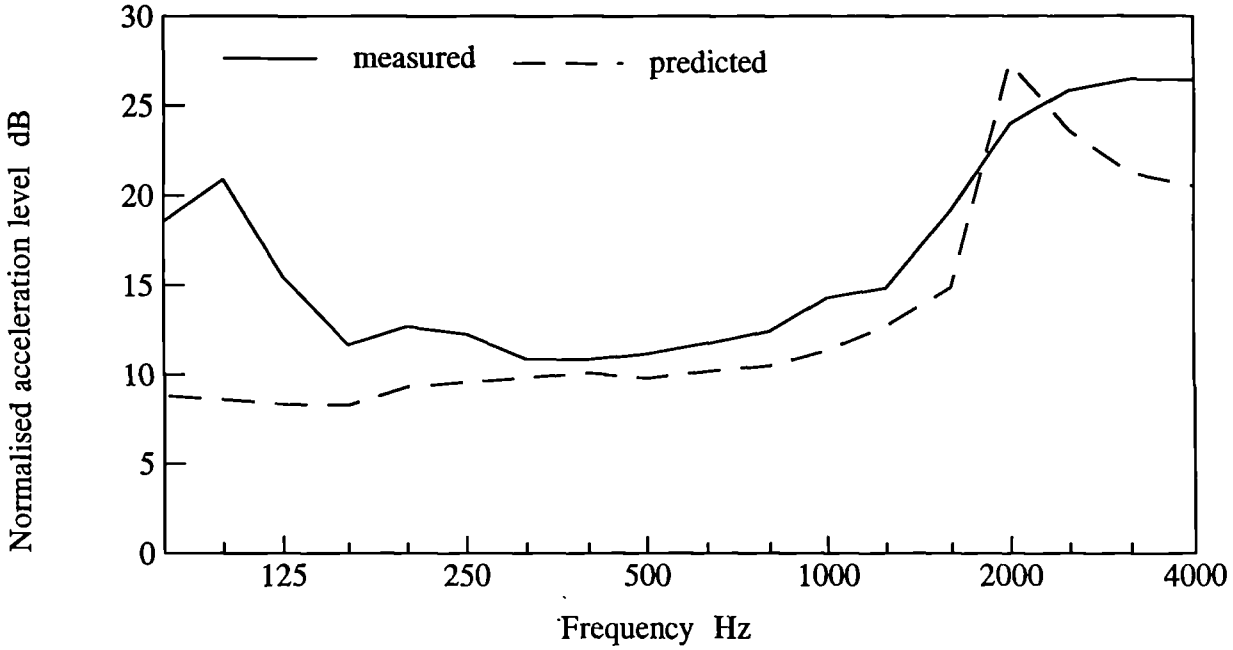

Figure 8.4 Measured and predicted acceleration level for a chipboard plate.

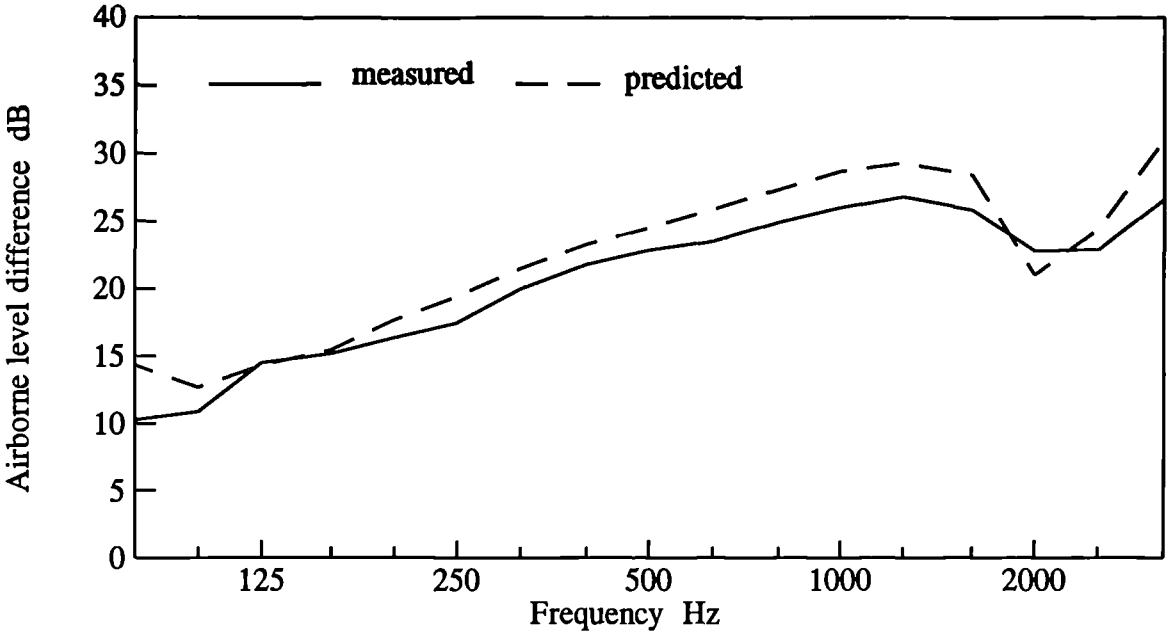

Figure 8.5 Measured and predicted airborne level difference for transmission through a chipboard wall.

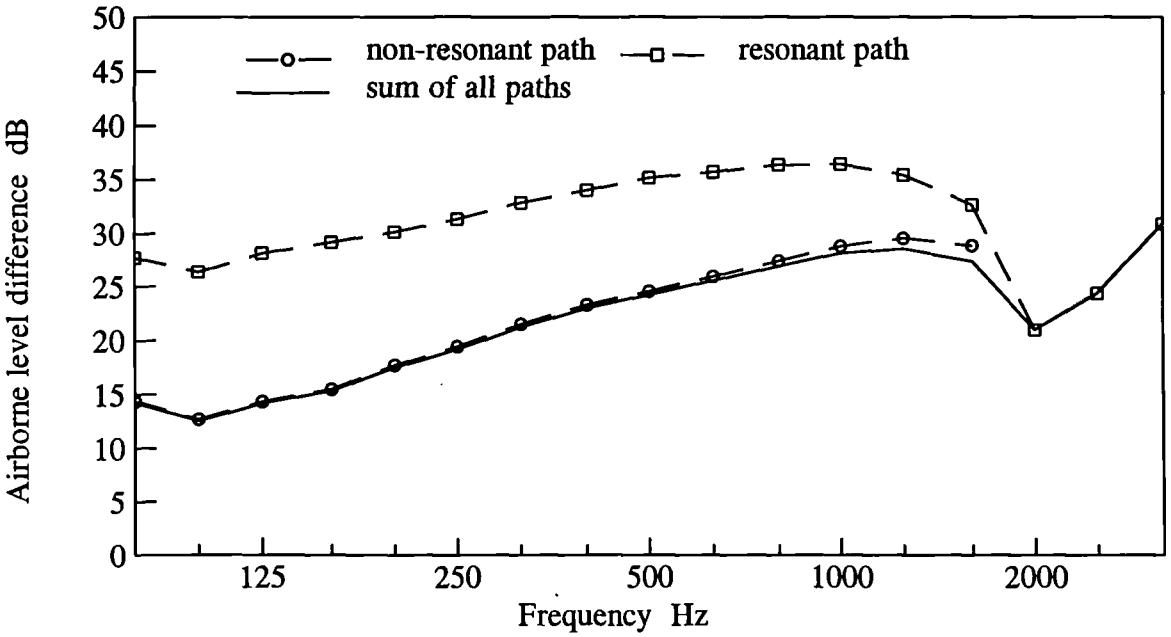

Figure 8.6 Predicted airborne level difference showing an SEA path analysis for transmission through a chipboard single plate wall.

SEA model and ribbed wall test structures

Fig 8.7 shows the plan and elevation of a ribbed plasterboard wall. The total wall area was $12m^2$ and was made of 12.5mm thick plasterboard connected by nails at 600mm centres to nine 50x50mm softwood ribs equally spaced at 400mm intervals. The wall was composed of three plasterboard sheets of 1.2x2.4m dimension and the remaining areas were cut from other sheets to fit the void. This caused some plasterboard sheets to be connected continuously across a rib and for others to be butt-jointed at the same rib, as shown in Fig 8.7. The spacing of the nails connecting the plasterboard to the ribs resulted in a change from line to point connection at 28Hz. This effect was discussed in Chapter 4. Consequently the wall was assumed to be point connected to the ribs for the entire frequency range of interest, 63-4000Hz.

The SEA model for the ribbed wall is shown in Fig 8.8 and the theory used to describe the point connection between two subsystems, plate and beam, was discussed in Chapter 4. The plasterboard ribbed wall was mounted on a 50x50mm softwood frame attached to the receiving room chamber wall at the common opening and was assumed to be clamped and a radiation multiplier of two was used. Fig 8.8 shows the layout of the plasterboard panels and their connection to the ribs. The plasterboard plate was assumed to be one subsystem of $12m^2$ area with a perimeter length of the source side (plain side - no ribs) of 27m to account for the plasterboard sheets edges and the ribbed side was assumed to have a perimeter length of 68m to take account of the ribs, (9x3x2), as there are two sides to the ribs. The radiation efficiency was increased by a factor of two due to the right angled baffles on the ribbed side of the wall, (i.e. the presence of the ribs). The plate edges were point connected to the ribs and assumed to be simply supported. These effects were discussed in Chapter 2, Fig 2.9.

All structural level difference measurements presented in this section for the ribbed walls and for the following section on double walls used an acoustic hammer as the structural source.

Due to some of the plasterboard plates meeting at the same rib, as shown in Fig 8.7, tests were carried out to determine the transmission of sound across the ribs between the adjacent plates. Fig 8.9 shows the measured acceleration level difference between two

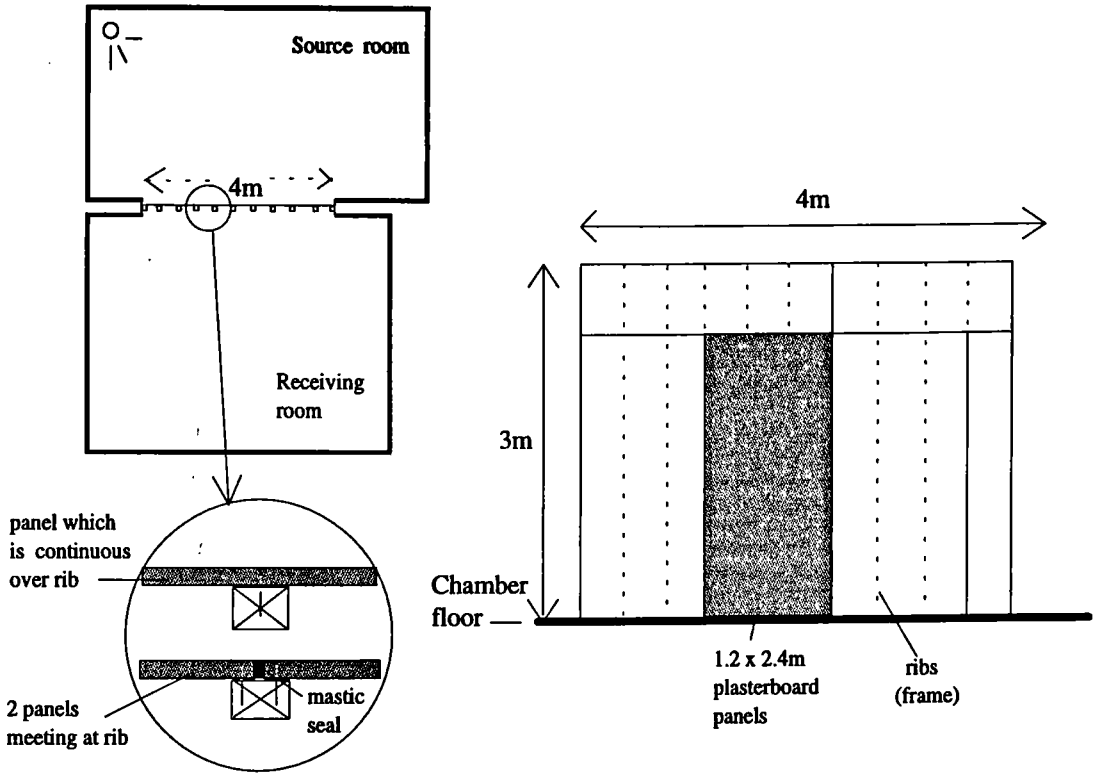

50x50mm ribbed plasterboard wall							
Subsystem	L(m)	b(m)	h(m)	C_L(m/s)	ILF	ρ (kg/m^3)	μ
Source room	10	4	3				
Plasterboard wall	4	3	0.0125	1702	0.015	660	0.2
ribs / frame	0.05	3	0.05	4483	0.015	382	0.2
Recieving room	7	6	5				

Figure 8.7 Plan, elevation and table of material properties for ribbed plasterboard wall.

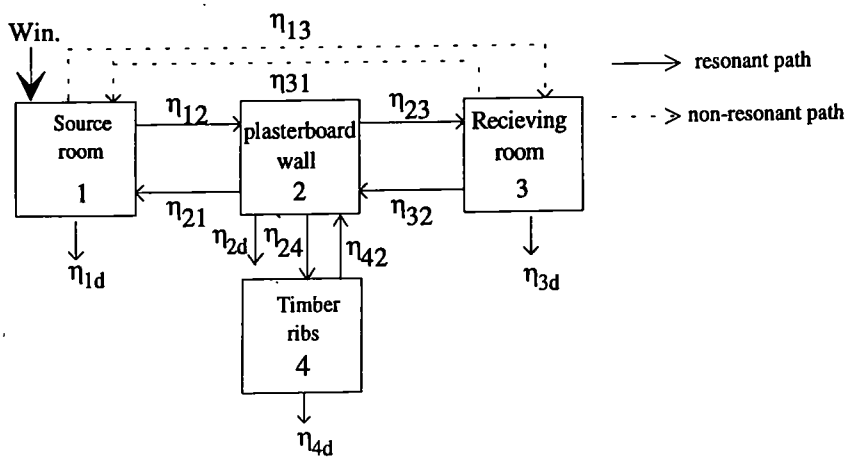

Figure 8.8 SEA model for two rooms separated by a ribbed plasterboard wall.

plates joined to the same rib. Prediction models for both point and line connection for this joint were carried out and are also shown in Fig 8.9. Using eqn(4.1) the transition frequency from line to point connection would occur at 106Hz. As can be seen there is more transmission than expected for a point connection and the measured results are closer to the line predicted results. The increased transmission may be due to the fact that the plates were butt-jointed and also connected by a thin mastic seal and therefore the coupling was not only through the nails and the rib. This supported the assumption that the plasterboard plates could be treated as one subsystem.

Fig 8.10 shows the measured and predicted acceleration level difference between the plasterboard plate and a rib. The prediction model assumed that the plate was $12m^2$ in area and was point connected to the rib. The agreement between the measured and predicted data is very good and supports the assumption that the plate was acting as one subsystem connected by points to multiple ribs.

Fig 8.11 shows the measured and predicted acceleration level of the plasterboard plate, normalised for an airborne source, and there is good agreement. The increase in acceleration level at 3150Hz is due to the critical frequency of the plate.

The measured and predicted airborne level difference through the ribbed plasterboard wall is shown in Fig 8.12. The agreement is very good and the assumptions that were made regarding the plate edges and perimeter length appear to be justified.

However, in order to test that the assumptions were justified further tests were carried out to examine in more detail the effect of the ribs. A smaller ribbed wall was built which would reduce the effect of multiple plasterboard panels connected to multiple ribs. Fig 8.13 shows a small 12.5mm thick plasterboard wall which was connected to 45x75mm timber frame and mounted in a 1.7x1.7m opening between two room test chambers. From this construction three different types of wall could be tested of which the first wall had only a perimeter frame, the second wall had a single rib connected to its centre by nails at 600mm centres and the third wall had three ribs connected to the plasterboard plate. The walls were excited by an airborne source and the SEA prediction model was similar to that shown in Fig 8.8.

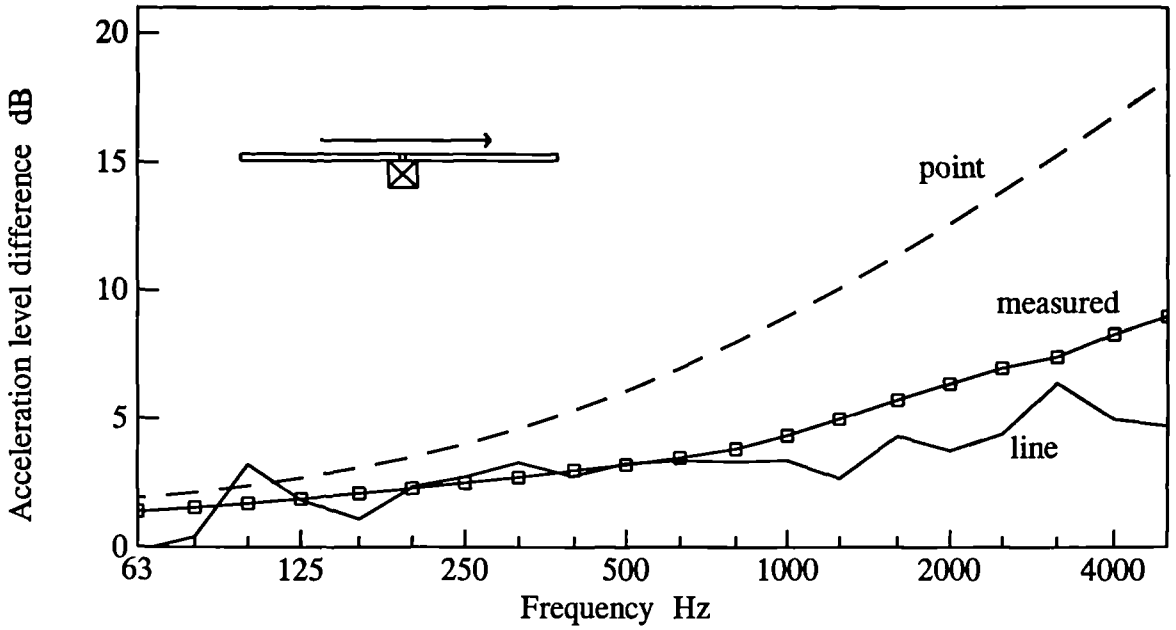

Figure 8.9 Measured and predicted acceleration level difference between two plates where they meet at a rib showing point and line models.

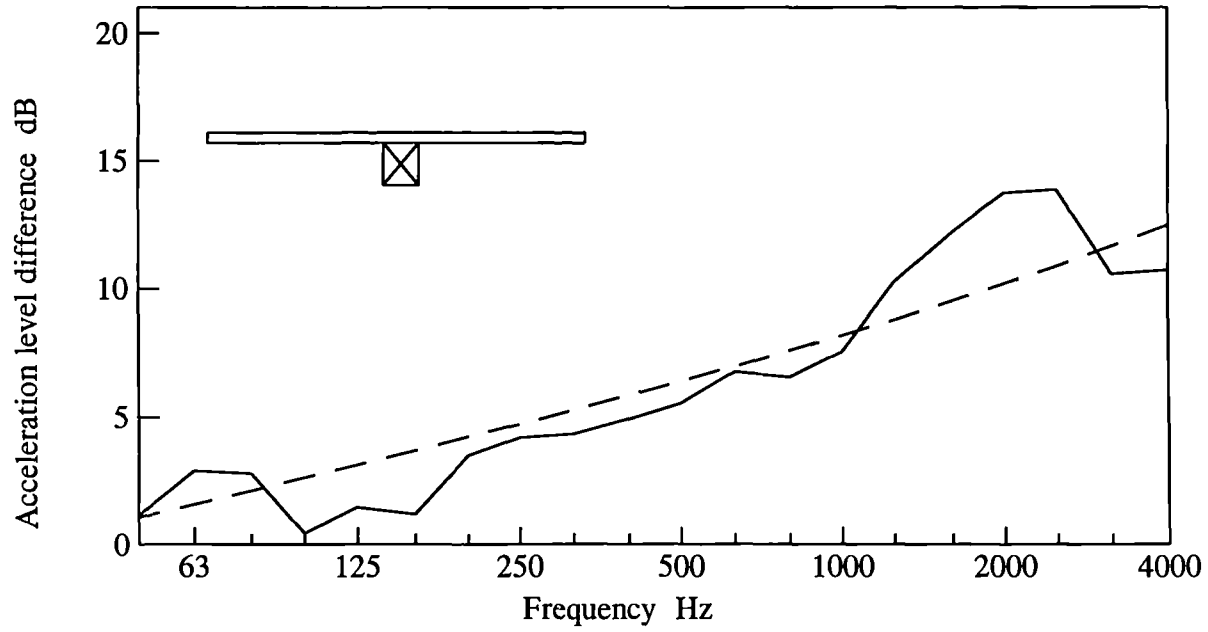

Figure 8.10 Measured and predicted acceleration level difference between plate and rib. (____) measured, (- - -) predicted.

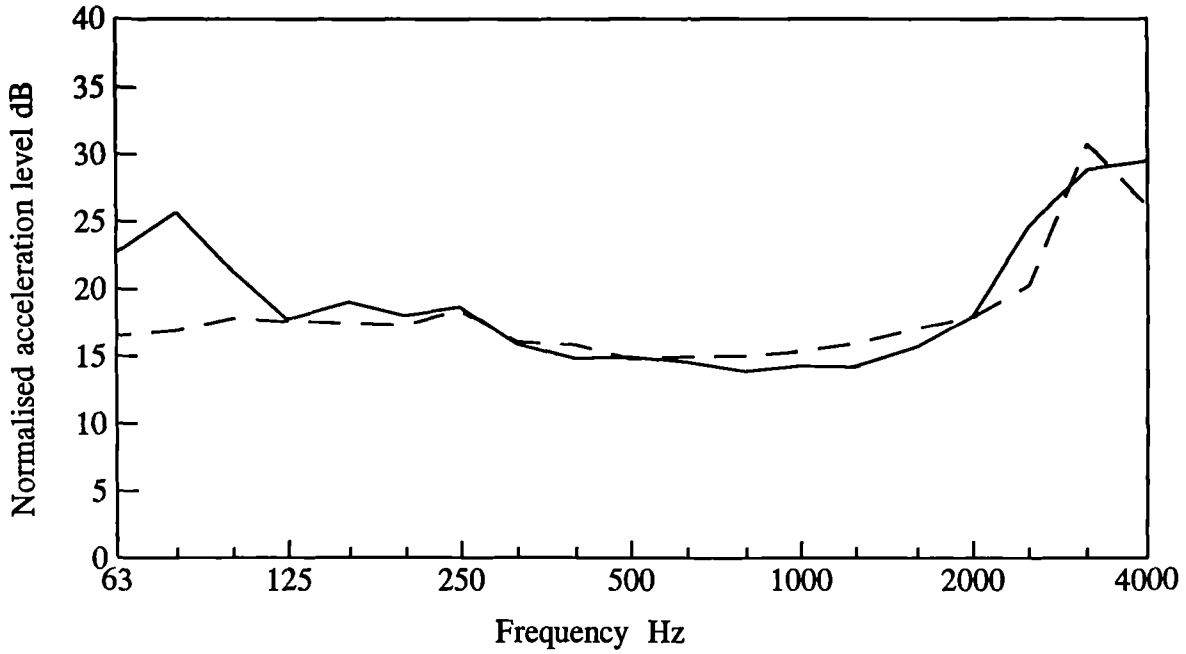

Figure 8.11 Measured and predicted acceleration level for a ribbed plasterboard wall. (____) measured, (- - -) predicted.

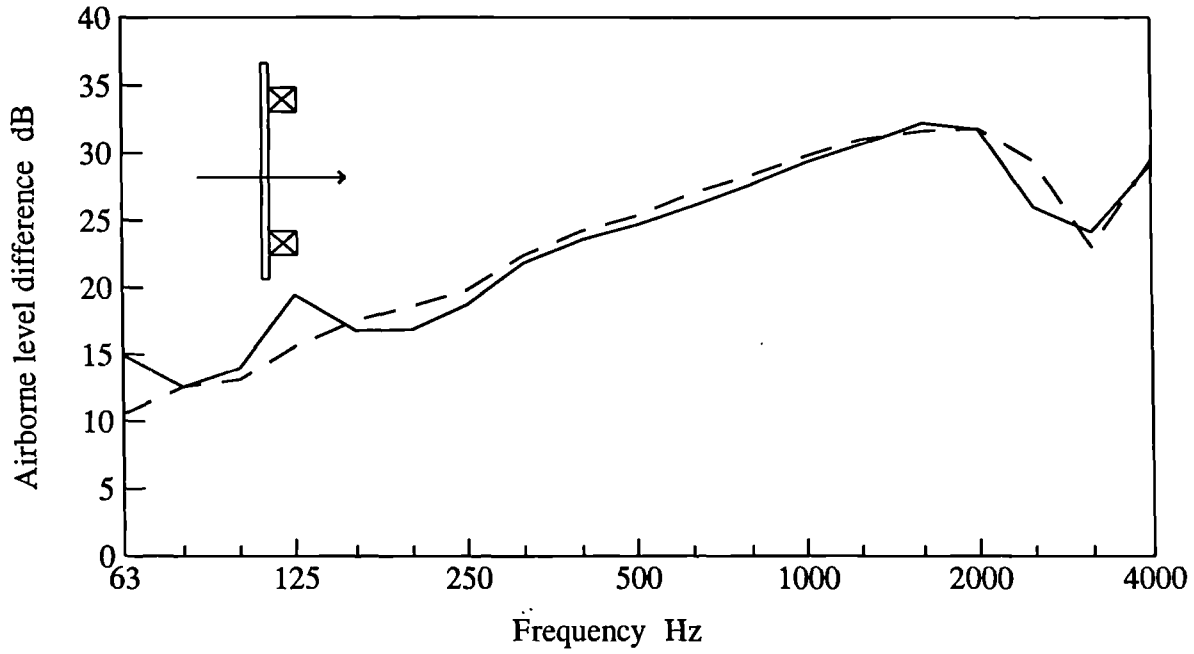

Figure 8.12 Measured and predicted airborne level difference through a ribbed plasterboard wall. (____) measured, (- - -) predicted.

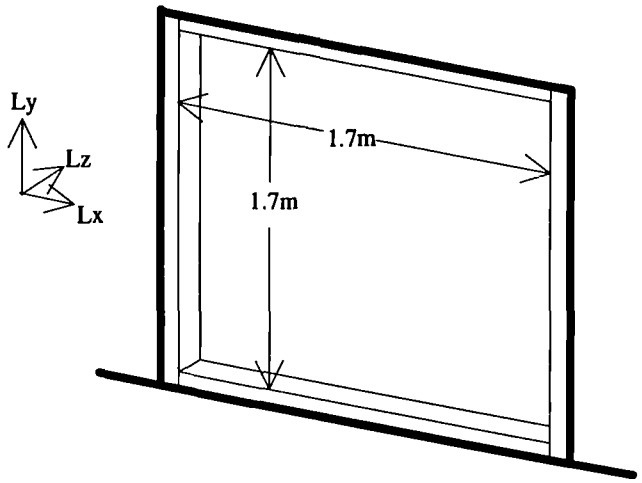

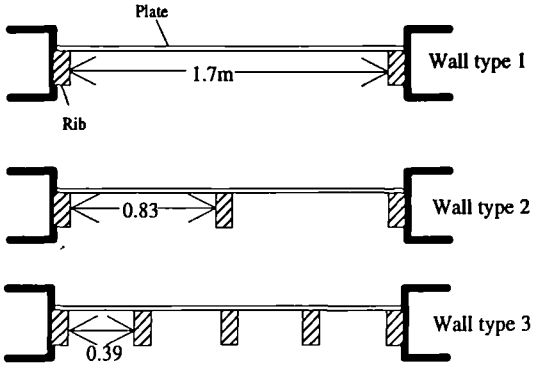

Subsystem	Dimensions			ρ (kg/m^3)	E (N/m^2)			μ	η_i (ILF)
	Lx	Ly	Lz						
Plates	1.8	1.8	0.0013	800	2.4e^9			0.2	0.01
Ribs	0.045	1.8	0.075	392	Ea	Et	Er	0.3	0.015
					6.3e^9	5.6e^8	1.4e^8		

Figure 8.13 Dimensions and material properties for small plasterboard ribbed walls.

Fig 8.14 shows the measured acceleration levels of the three types of wall. It is noticeable that at the higher frequencies as more ribs are attached the acceleration level decreases slightly. This may be due to the presence of the ribs increasing the damping of the plate. Fig 8.15 shows similar good agreement between measured and predicted acceleration level of the wall as was found on the large $12m^2$ ribbed wall.

Fig 8.16 shows the measured airborne level difference for the three types of wall. As more ribs are attached the perimeter length on the receiving room side of the wall is increased, resulting in increased transmission between 500Hz and the critical frequency of the plasterboard due to increased radiation from the edge modes. Fig 8.17 shows the measured and predicted airborne level difference through a ribbed wall, wall type 3, and good agreement is found.

In order to measure the effect of the ribs on the radiation of a panel a test was carried out where the wall was excited by an airborne sound from each side independently and the acceleration level of the wall was measured as shown in Fig 8.18. On the plain side the perimeter was 6.8m and the radiation was given a factor of four to account for clamping to the frame and connection to right angled baffles. On the ribbed side the perimeter length was increased by 10.2m (3 ribs each 1.7m long) increased by two as there are two sides to the rib. The attachment of the ribs results in right angled baffles on the ribbed side and the radiation efficiency is multiplied by a factor of 2. This gives a predicted difference of 2.4dB in the radiation efficiency and hence plate response. At low frequencies where the acoustic wavelength is large compared to the dimensions of the ribs the response of the plate is the same for both cases as the acoustic wave does not "see" the rib. However, at high frequencies (from 500Hz) there is a difference in the plate response which is approximately the same as that estimated from the difference in perimeter length.

8.4 Double walls with point and line connection

Fig 8.19 shows the point connected double walls that were constructed to compare experimental data with the SEA predicted data. As was discussed in Chapter 3 the double walls were constructed on the receiving room side of the common opening. Five

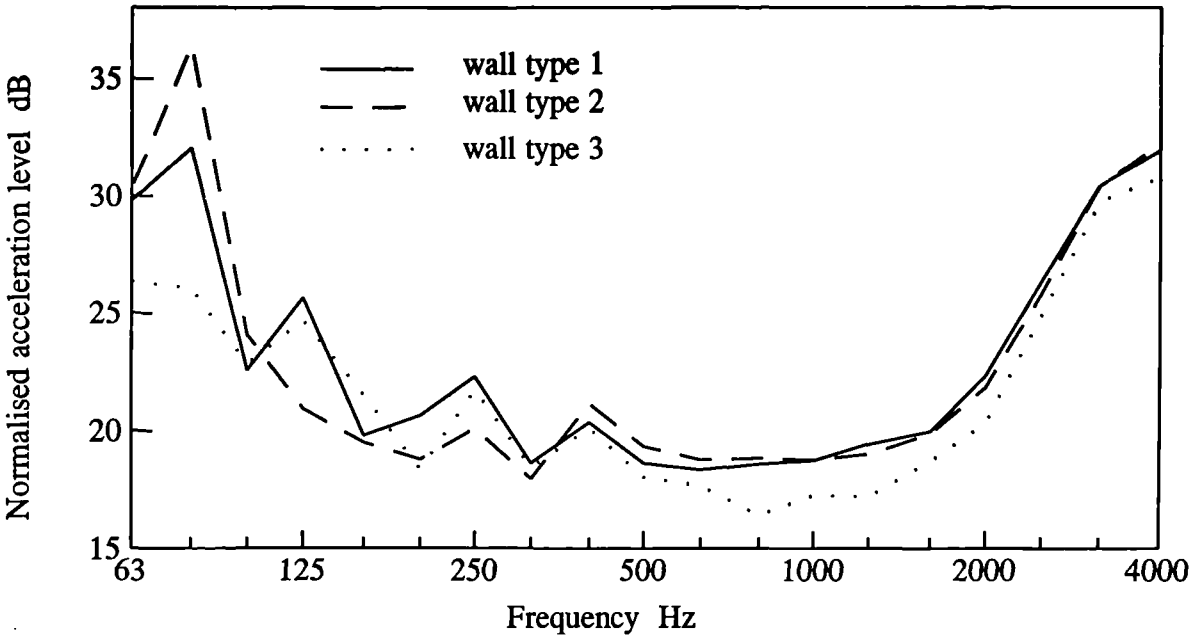

Figure 8.14 Comparison of measured acceleration levels for ribbed walls with increasing number of ribs.

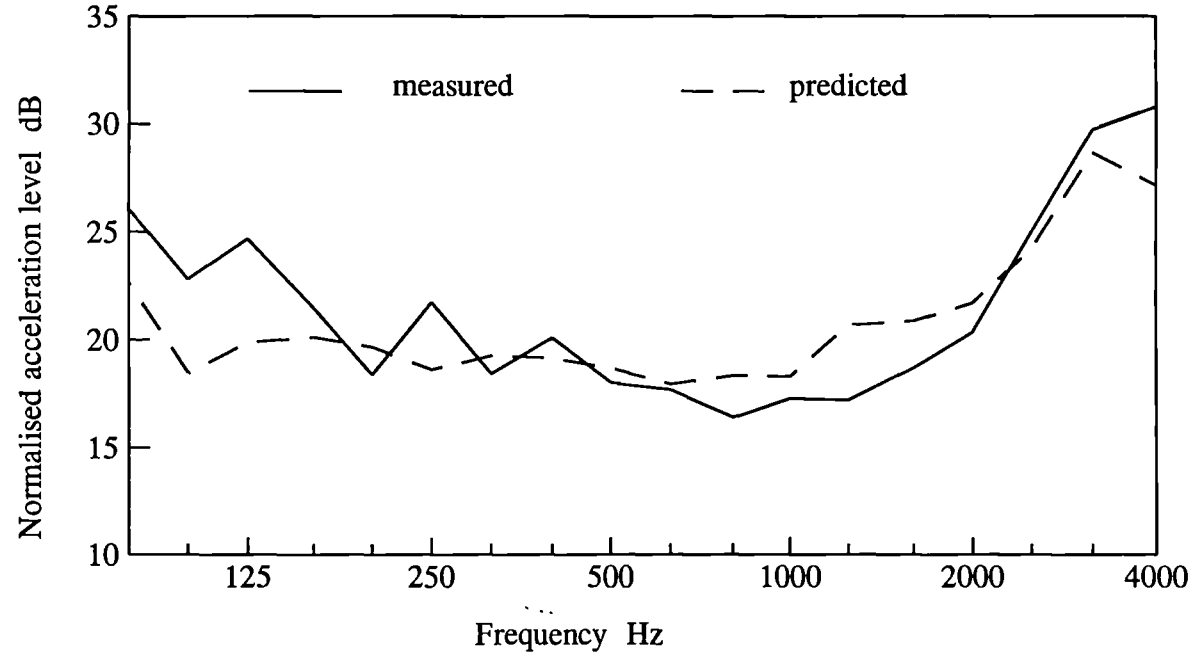

Figure 8.15 Measured and predicted acceleration level for a ribbed plasterboard wall, wall type 3.

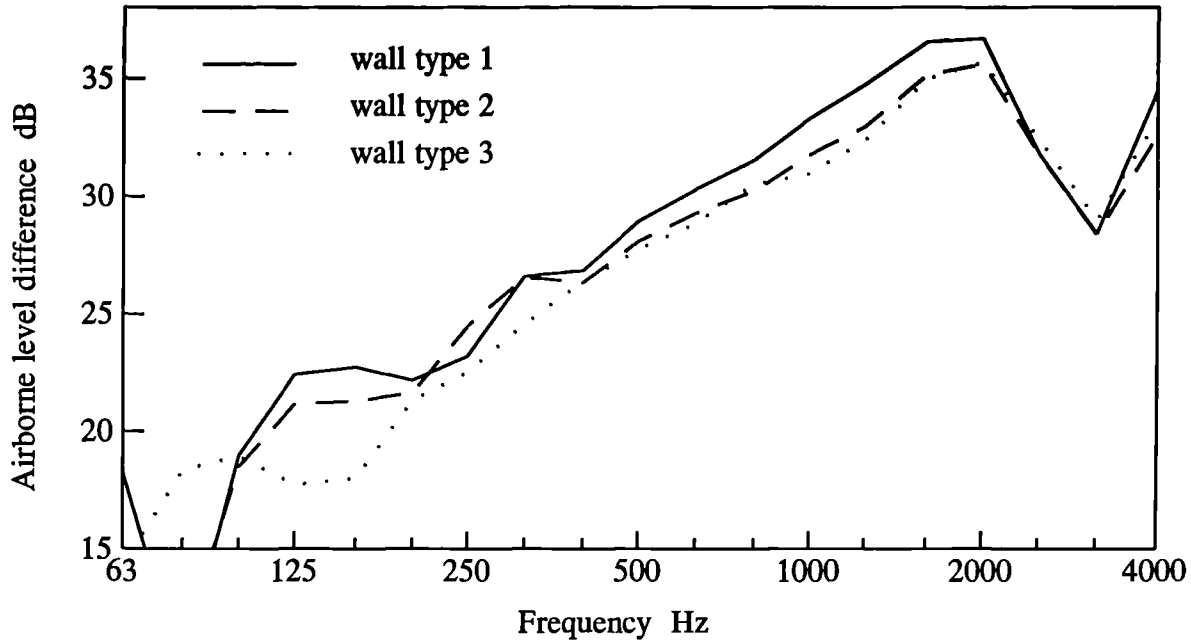

Figure 8.16 Comparison of measured airborne level difference through ribbed walls with increasing number of ribs.

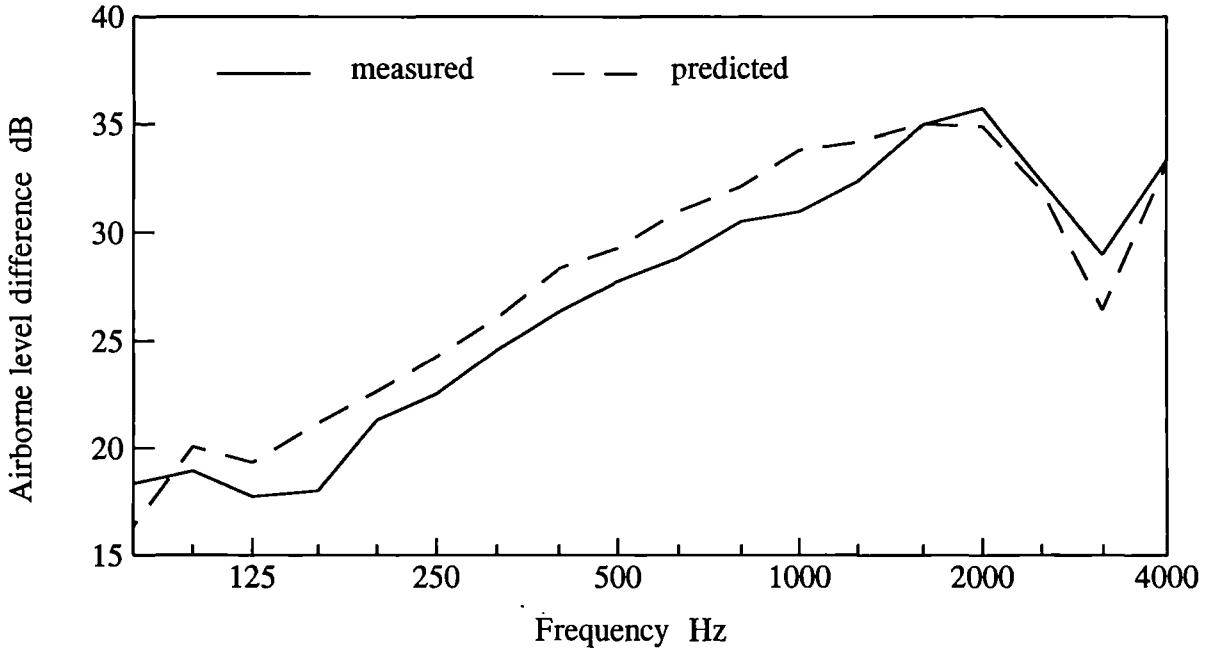

Figure 8.17 Comparison of measured and predicted airborne level difference for a ribbed plasterboard wall, wall type 3.

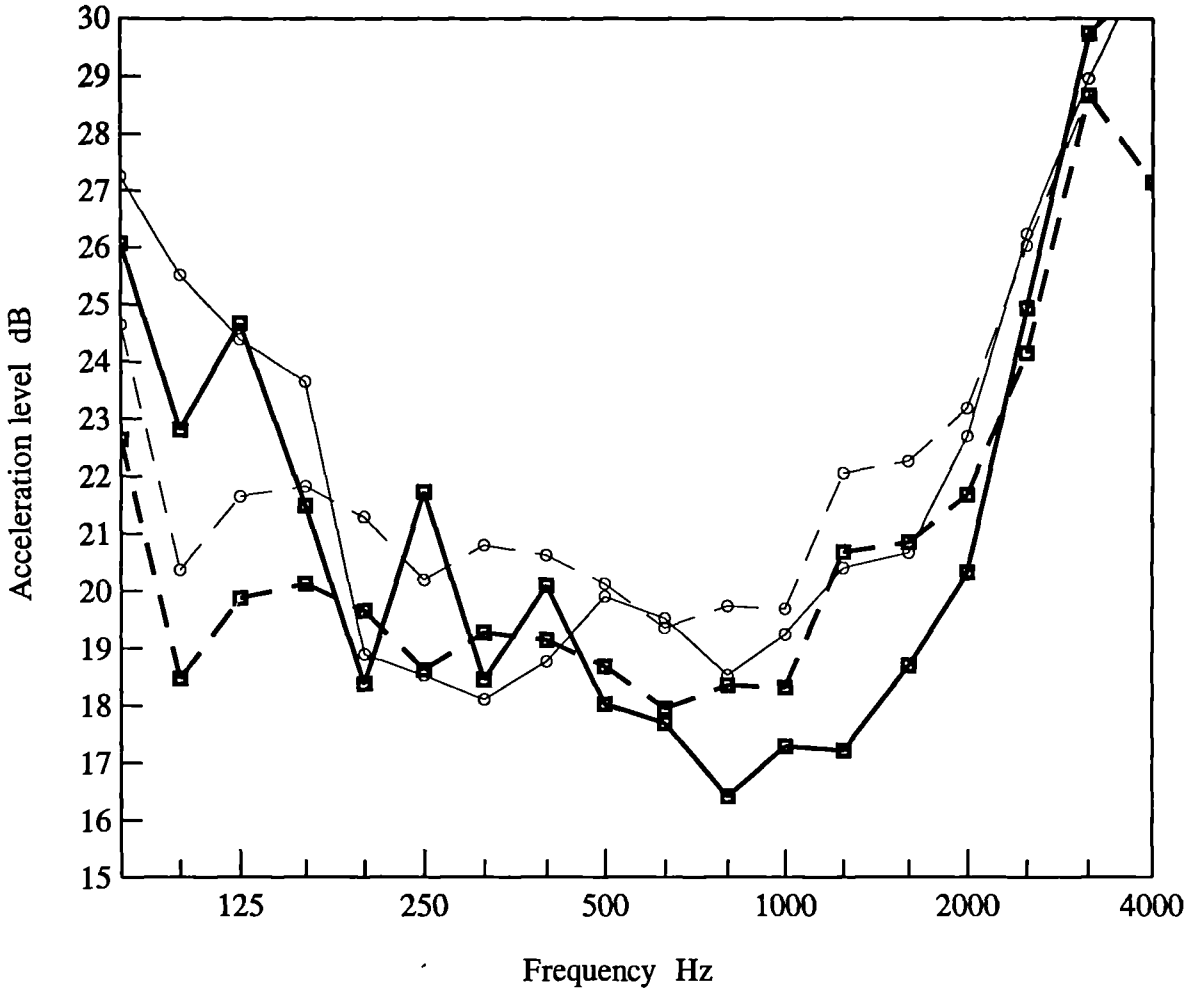

Figure 8.18 Measured and predicted acceleration level for a ribbed wall comparing the two sides of the wall, ribbed and plain.

separate lightweight partition walls were constructed and consisted of a 150mm double wall composed of 18mm thick chipboard and 12.5mm plasterboard, 100mm double wall made of plasterboard with and without absorption and a 50mm double wall again composed of plasterboard with and without absorption. For the walls with absorption the 50mm double wall had 2 layers of 25mm "Rockwool" fibreglass packed hard-in touching both sides of the wall. The 100mm double wall also had two layers of the same absorption material but suspended and not touching either side of the wall. The material properties of these walls may be found in Chapter 7, Fig 7.3.

Low frequency SEA model for double walls

To model these double walls several different SEA models may be required depending on the details of construction and the frequency range of interest. At low frequencies all partitions behave as single leaf walls. Fig 8.20 shows the SEA model for low frequencies for a double wall. The wall is orthotropic in that the bending stiffness is different in the two directions. The wall is stiffer when bent across the timber frame or studs than it is when bent along the studs.

To model the double wall at low frequencies when it is a single wall subsystem it is necessary to know its thickness, its mass and its stiffness. The thickness is the distance between the outer edges of the linings, Q, shown in Fig 8.21 and the mass is the sum of the two plates and studs. The stiffness can be obtained using the theory for beams made from two materials [92]. Using the notation shown in Fig 8.21, the combined stiffness of a single stud and plates fixed to it can be given by,

$$B = \frac{E_f H^3 W}{12} + 2E_p \left[\frac{h^3 w}{12} + whd^2 \right] \tag{8.1}$$

where E_f is the Young's modulus of the frame (stud) and E_p is the Young's modulus of the plates, given by eqn(3.2 and 3.3). The bending stiffness for 1m of the wall can be obtained by multiplying this by the number of joints per metre. Due to the frame spanning in one direction the wall is orthotropic and the other bending stiffness about the axis running parallel to the joists is calculated from the double wall plates and there separation distance, as given by [92],

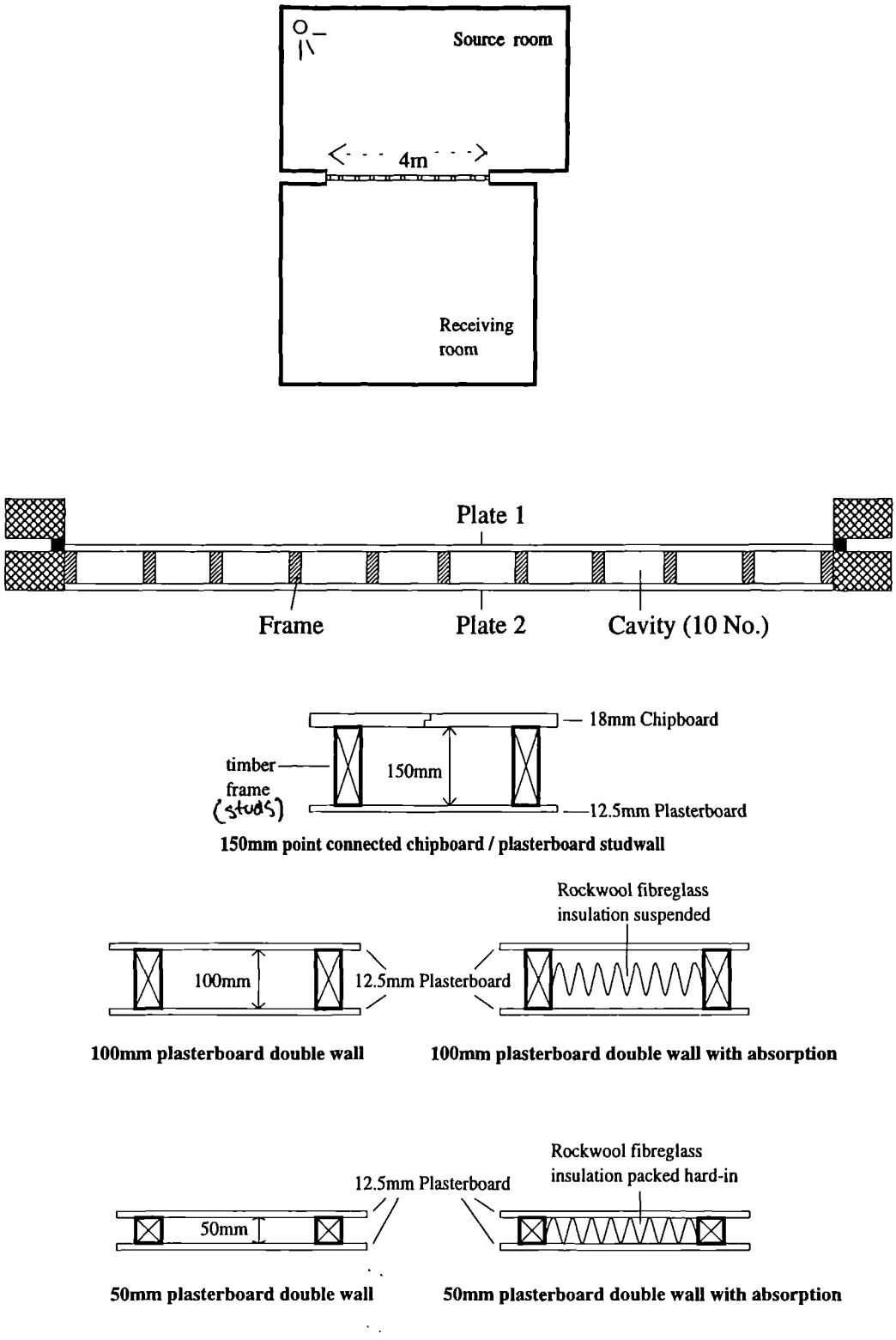

Figure 8.19 Construction of point connected double wall test structures.

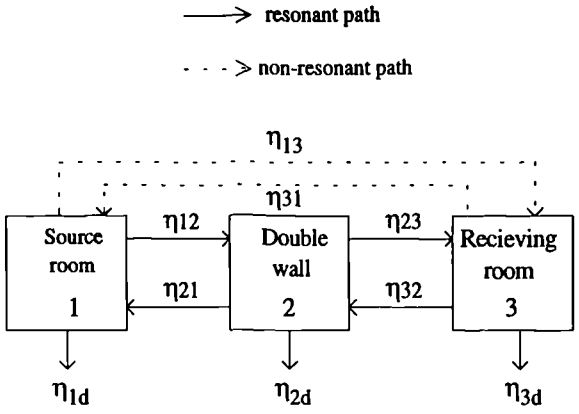

Figure 8.20 Low frequency SEA model for two rooms separated by a double wall.

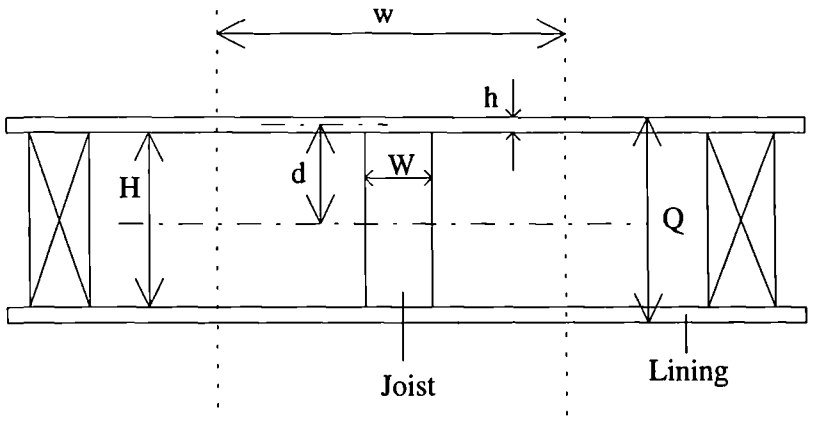

Figure 8.21 Section through a lightweight partition showing the dimensions of the components.

$$B - E_p\left[\frac{Q^3-H^3}{12}\right] \tag{8.2}$$

For a 150x50mm timber frame with 12.5mm plasterboard the bending stiffness using eqn(8.1) and (8.2) is 658,530Nm and 517,500Nm respectively. Thus including the joists in calculating the bending stiffness results in a small increase, but does not significantly effect the sound transmission. The bending stiffness for the wall, in the SEA low frequency models, was calculated using eqn(8.1).

The basic SEA theory for the resonant coupling between this large plate and the source and receiving rooms and the non-resonant coupling between the rooms may be found in Chapter 2.

At higher frequencies the two plates of the double wall do not move with the same velocity and phase and so must be modelled as two separate subsystems coupled by a cavity (which is also a subsystem). If there is no structural coupling then the SEA model is basically two single leaf models placed side by side. This is the SEA model that was used by Price and Crocker [49] and was discussed in Chapter 2.

The transition between a single leaf, low frequency model, and a high frequency model is usually well defined and a good transition frequency is the mass-spring-mass resonance, f_0, of the two leaves of the wall and the air inside given by [44],

$$f_0 = \frac{1}{2\pi}\left[\frac{K}{\rho_{s1}} + \frac{K}{\rho_{s2}}\right]^{1/2} \tag{8.3}$$

where ρ_s is the surface density of each leaf, K is the stiffness/m^2 of the air (1.4 x 10^5/d) [44] , and d is the cavity depth.

At the low frequencies the two plates of a double wall have the same velocity or acceleration level and thus have zero velocity or acceleration level difference. The two plates are connected by a soft spring (air) and as the first plate deflects this causes the air to compress and move the second plate [93], hence the term mass-spring-mass

(MSM). After this frequency the coupling by the air is weak and the two plates move independently. Further discussion on the mass-spring-mass frequency for double walls may be found in Goesele [94], Beranek and Ver [93] and Craik [13].

Phase measurements were carried out on the 100mm and 50mm double walls with absorption using two accelerometers placed directly opposite each other which can be used to determine experimentally the mass-spring-mass frequency. The phase was measured rather than the amplitude as there is a lack of definition of the MSM when measuring the amplitude. Fig 8.22 shows the position of the accelerometers. Three different parts of the double wall were measured. Firstly on the plasterboard plates over the cavities, (A), secondly on the point connections, nails, coupling the plasterboard plates to the frame, (B) and thirdly between the nails on the plasterboard plates directly over the frame, (C). If as assumed the walls are point connected at the frequency area of interest then positions (A) and (C) would be similar in their phase response and the nails would appear to be unaffected.

Fig 8.23 shows the phase relationship between the two plates of the 100mm double wall with absorption for the various positions. Using eqn(8.3) the predicted mass-spring-mass is 82Hz. As can be seen both positions (A) and (C) show f_0 to be about 80Hz where the phase difference is random. Positions (B) shows practically no change in phase. This would be expected due to the strong coupling of the nails being attached to the frame.

The 50mm and 100mm double walls with absorption are now compared, as shown in Fig 8.24. The predicted f_0 for the 50mm wall using eqn(8.3) is 119Hz and when this is compared with the measured results for the mass-spring-mass frequency there is found to be good agreement. The measured and predicted sound reduction index for double walls at low frequencies is shown later in this section with the predicted high frequency results.

High frequency SEA model for point connected double walls

As discussed previously at high frequencies the plates have a random phase and behave as separate plates. The single subsystem wall which was used at low frequencies is now broken down into further subsystems, the two plates, the cavities and the frame or studs

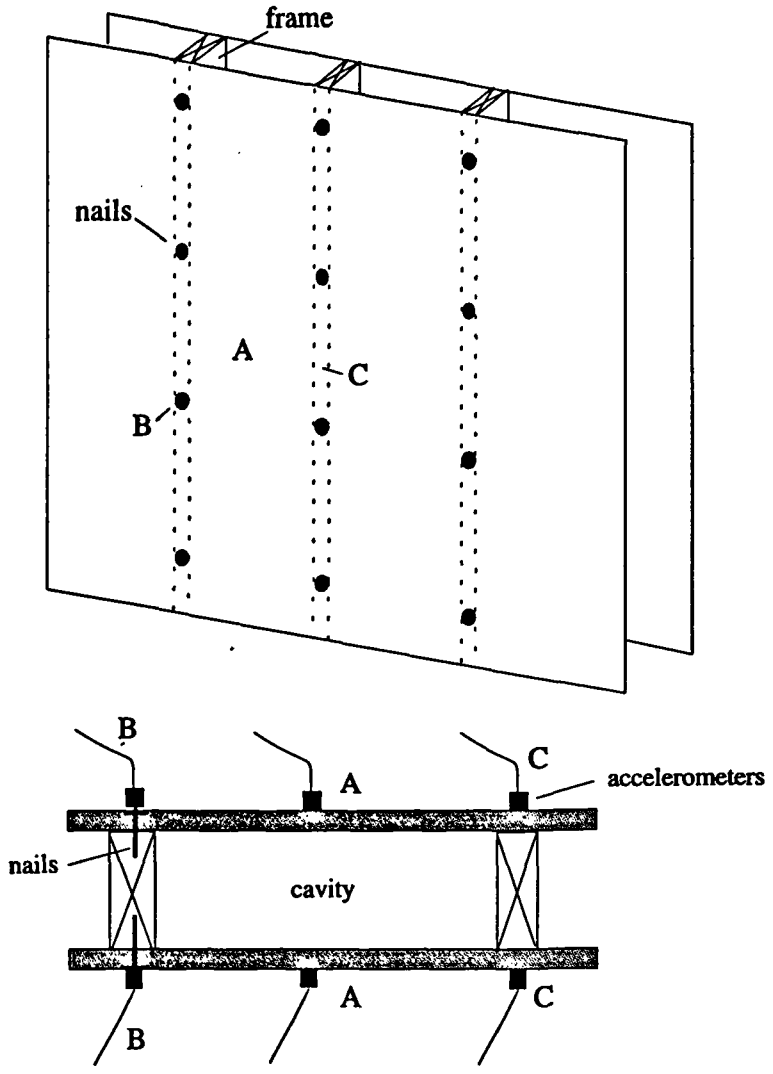

Position A - accelerometers placed on front and back plates over cavity

Position B - accelerometers placed directly on nails connecting plates to frame

Position C - accelerometers placed on plates over frame between nails

Figure 8.22 Section through full scale double wall showing positions of accelerometers for phase measurements, A, B and C.

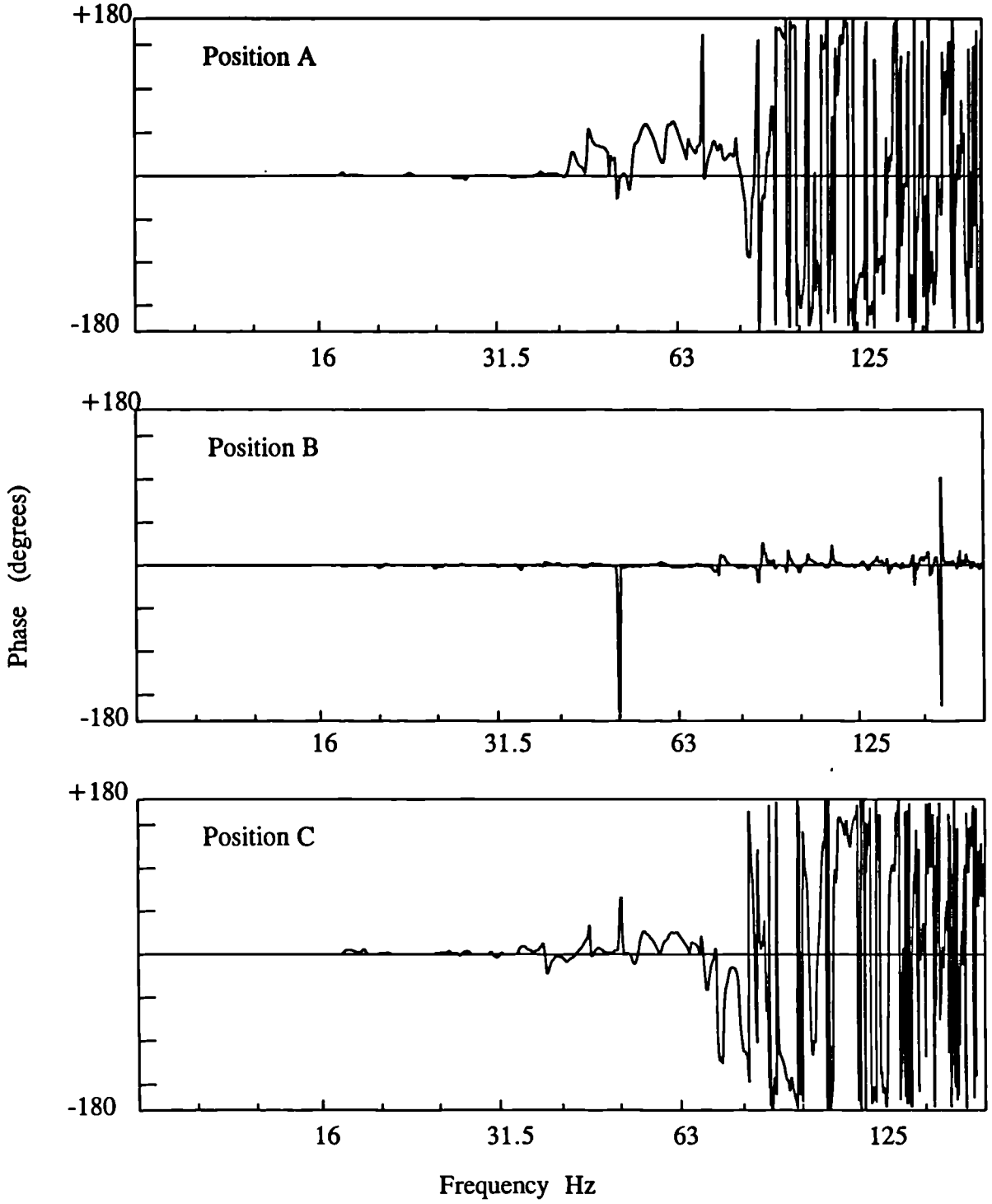

Figure 8.23 Phase relationship between the front and back plate of a double wall at various positions on the plates.

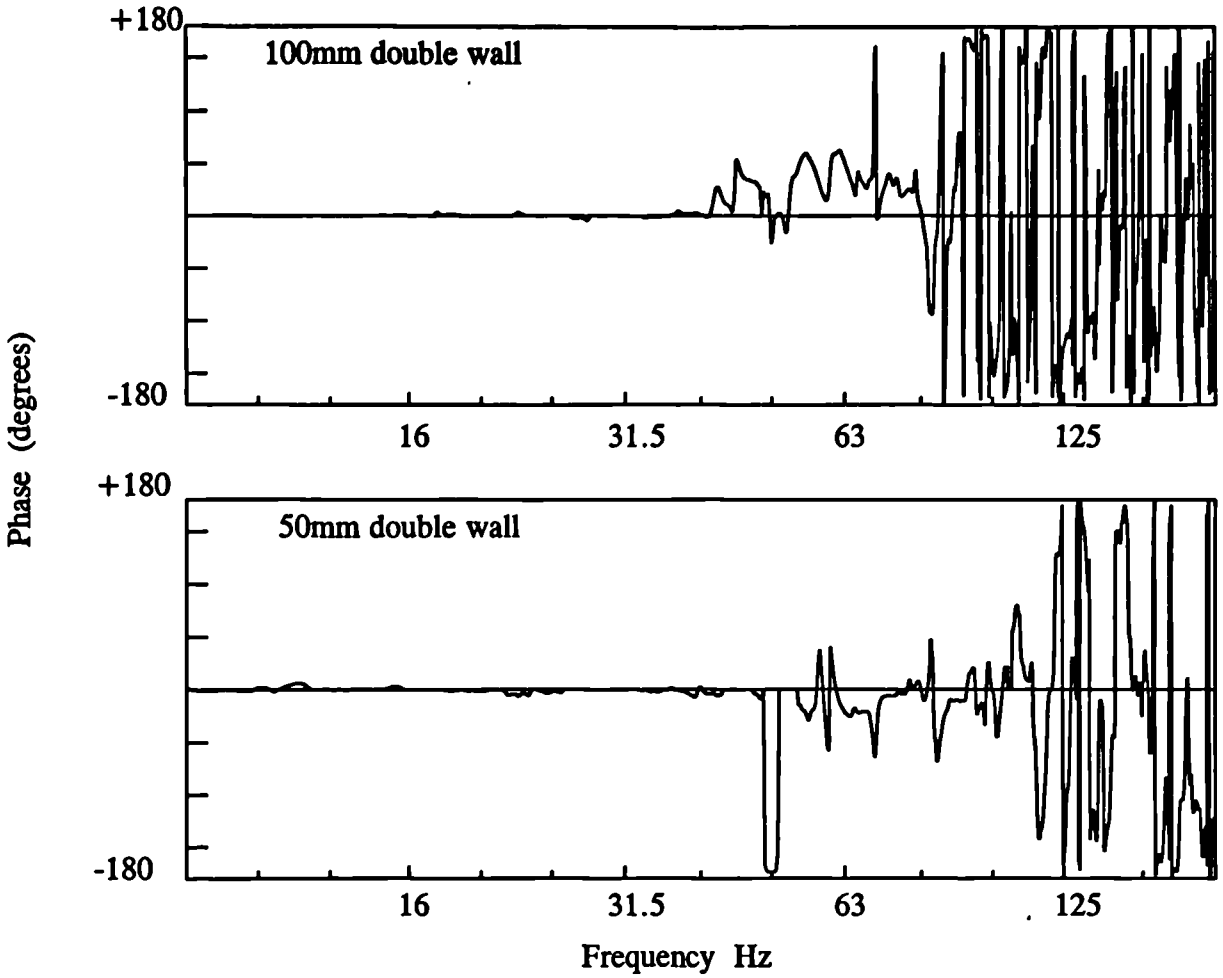

Figure 8.24 Comparison between a 50mm and a 100mm double wall showing the phase relationship between front and back plates.

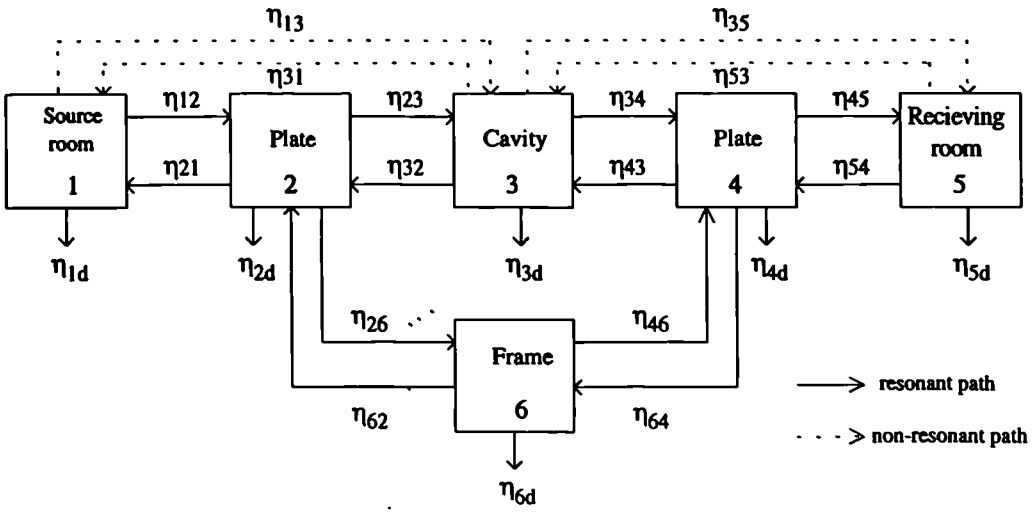

Figure 8.25 High frequency SEA model for two rooms separated by a point connected double wall.

as shown in Fig 8.25. If the plasterboard is attached at points, where the spacing of the points is such that it is larger than the $\lambda_B/2$, then the wall may be modelled as point connected. This was discussed in Chapter 4 where the point mobility method was used to determine the coupling between the plates and the frame.

Coupling between the rooms and the cavities and the plates and the cavities also occurs as shown in Fig 8.25. The radiation efficiency was multiplied by a factor of 2 for coupling from the plate to the cavity due to the right angle baffles. The edge of the plates coupled to the perimeter frame were assumed to be clamped and the radiation efficiency was increased by a factor of 4,(2 for clamping and 2 for right angle baffles). Fig 2.9 in Chapter 2 discussed the radiation multiplier in more detail. The transmission from the room into the double wall cavities was discussed in Chapter 7.

As the two plates of the double wall are separate subsystems then the front plate closest to the source room will have a higher acceleration level than the back plate. The acceleration level of the back plate will depend upon the coupling through the frame and the cavity. Fig 8.26 shows the measured and predicted acceleration levels of the front and back plates of the various point connected double walls normalised for an airborne sound source. Good agreement is found between the measured and predicted results and as expected the acceleration level on the front plate is higher than the back plate due to being nearer the source.

Fig 8.27 shows the measured and predicted acceleration level difference between the two plates and in addition the contributions of the SEA transmission paths, *plate-stud-plate* and *plate-cavity-plate*, are also shown. The dominant transmission path is through the stud. Only at the critical frequency is the cavity path more dominant.

Fig 8.28 shows the measured results for the acceleration level of the front plate for the 50mm double wall with absorption and a nail spacing of approximately 150mm. The accelerometer was placed on the front plate of the double wall at three positions (A), (B) and (C), similar to those described in Fig 8.22. As discussed in Chapter 4, part of the behaviour of the plate is dependant upon the nail spacing. At low frequencies the nail spacing is shorter than the wavelength capable of fitting between the point connections

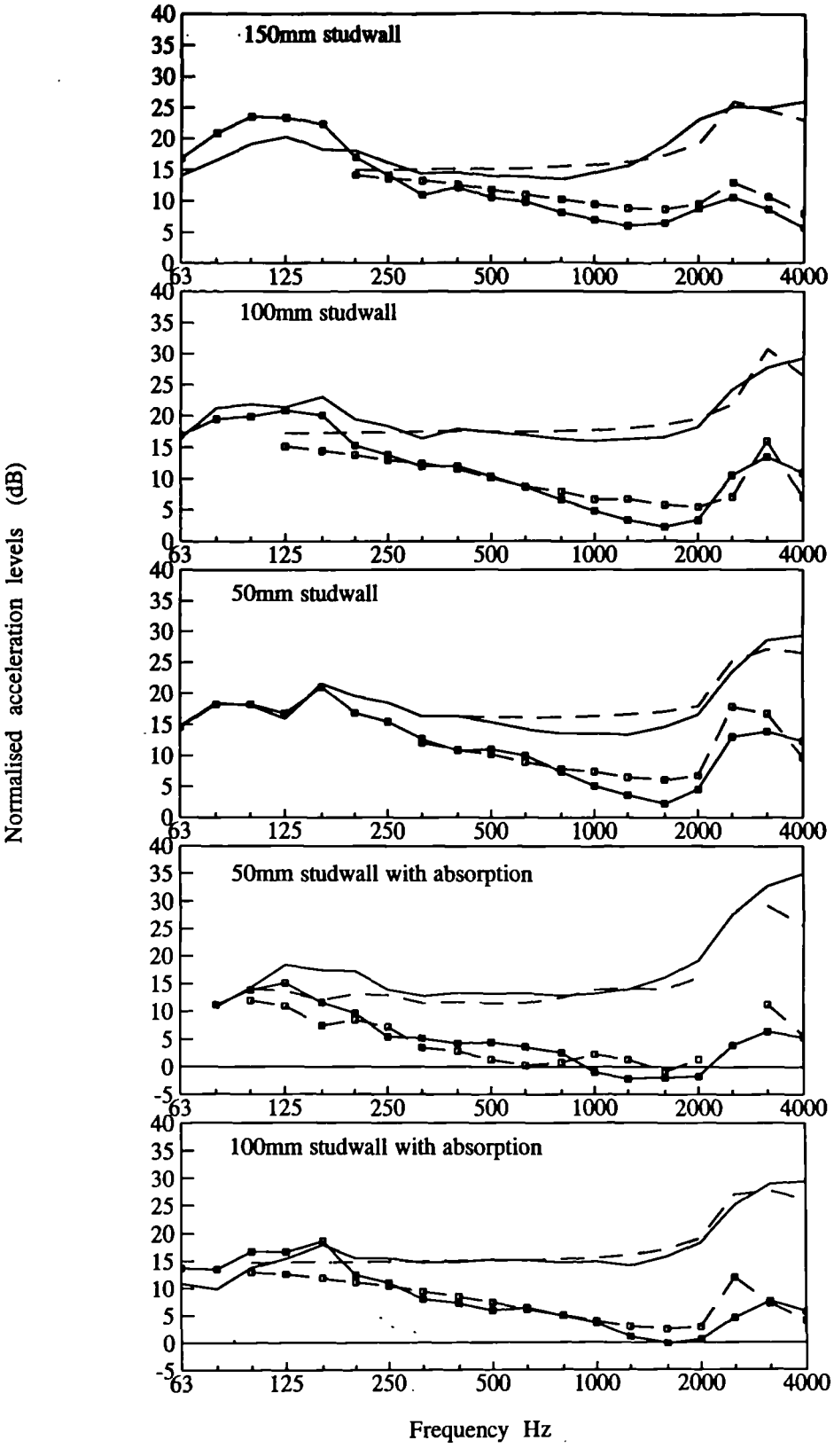

Figure 8.26 Measured and predicted acceleration levels of the front and back plates for a variety of double wall structures.

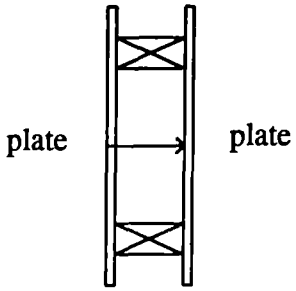

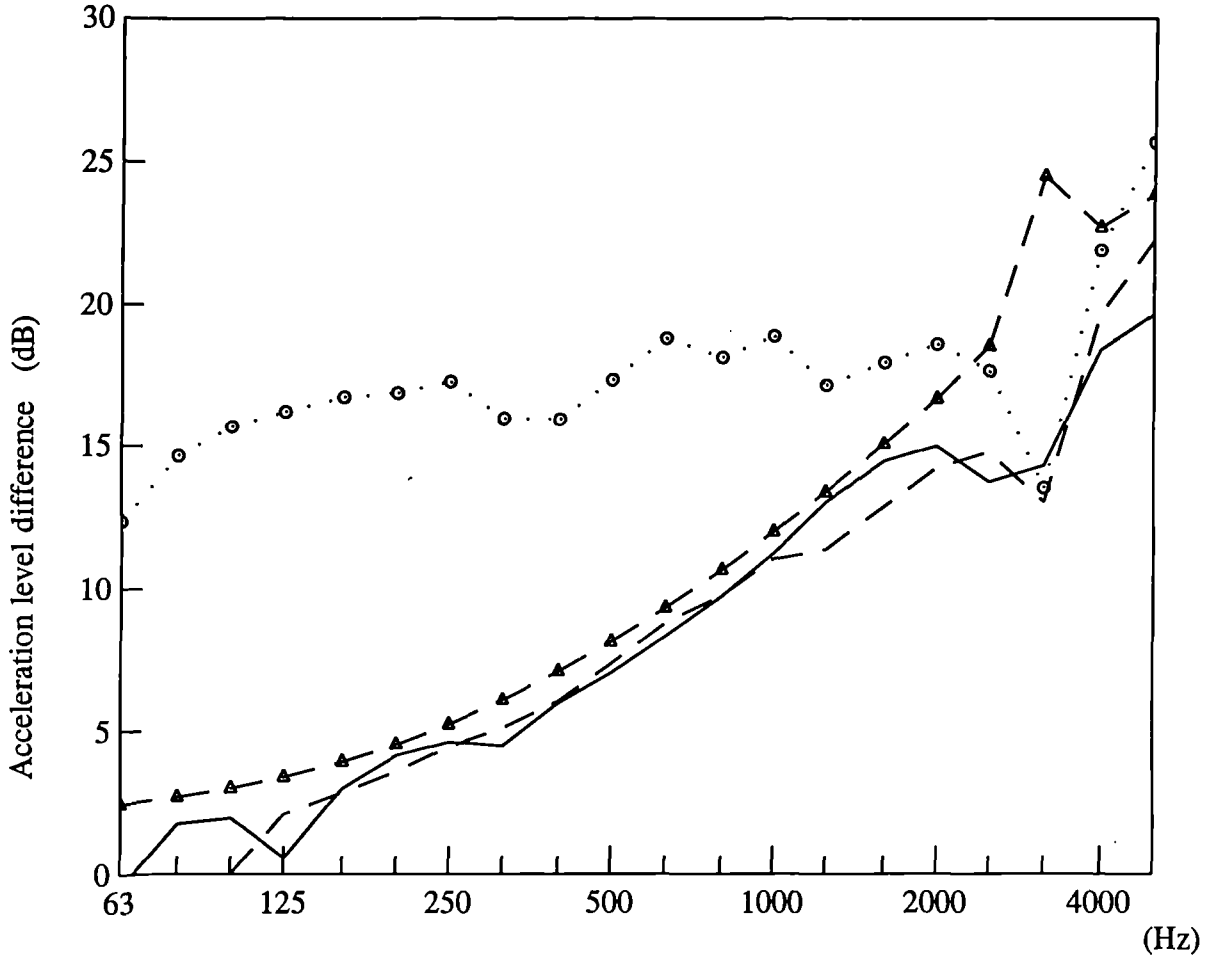

——— Measured plate to plate acceleration level difference

— — Sum of predicted paths plate to plate acceleration level difference

—△— Structural path (plate - stud - plate)

· ·○· · Cavity path (plate - cavity - plate)

Figure 8.27 Measured and predicted acceleration level difference showing the relative contributions of transmission paths from plate to plate for a double wall with an airborne source.

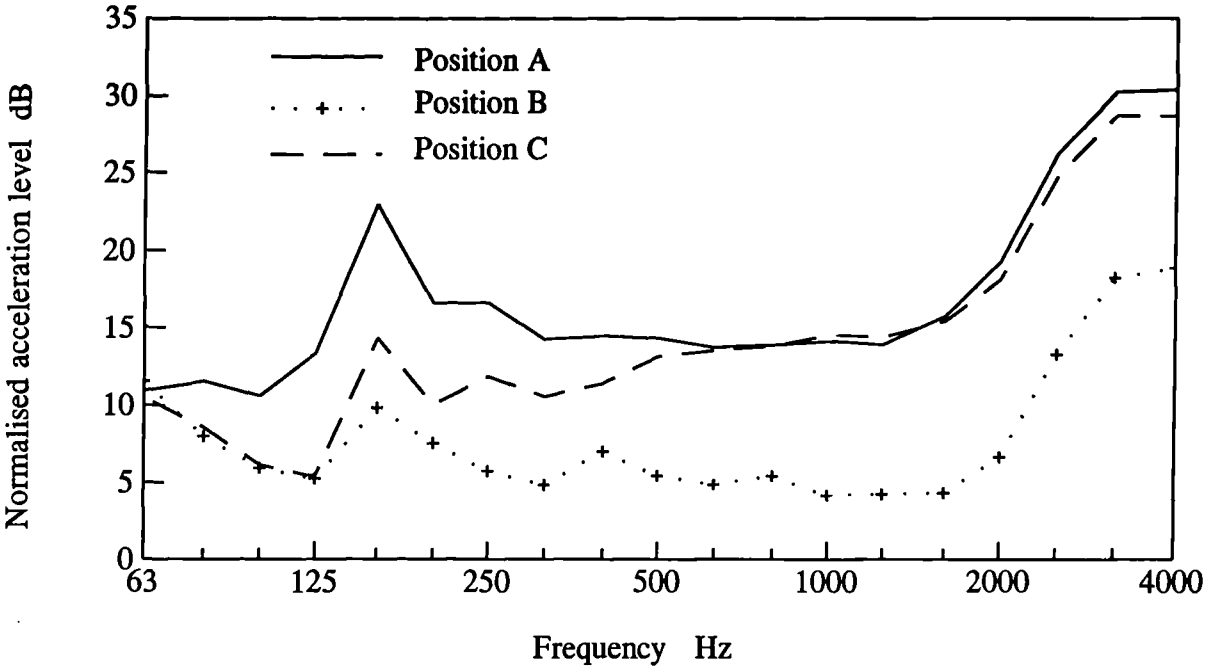

Figure 8.28 Measured acceleration levels on a double wall front plate where the accelerometers are placed on the plate (A), on the nails (B) and between the nails on the plate over the frame (C).

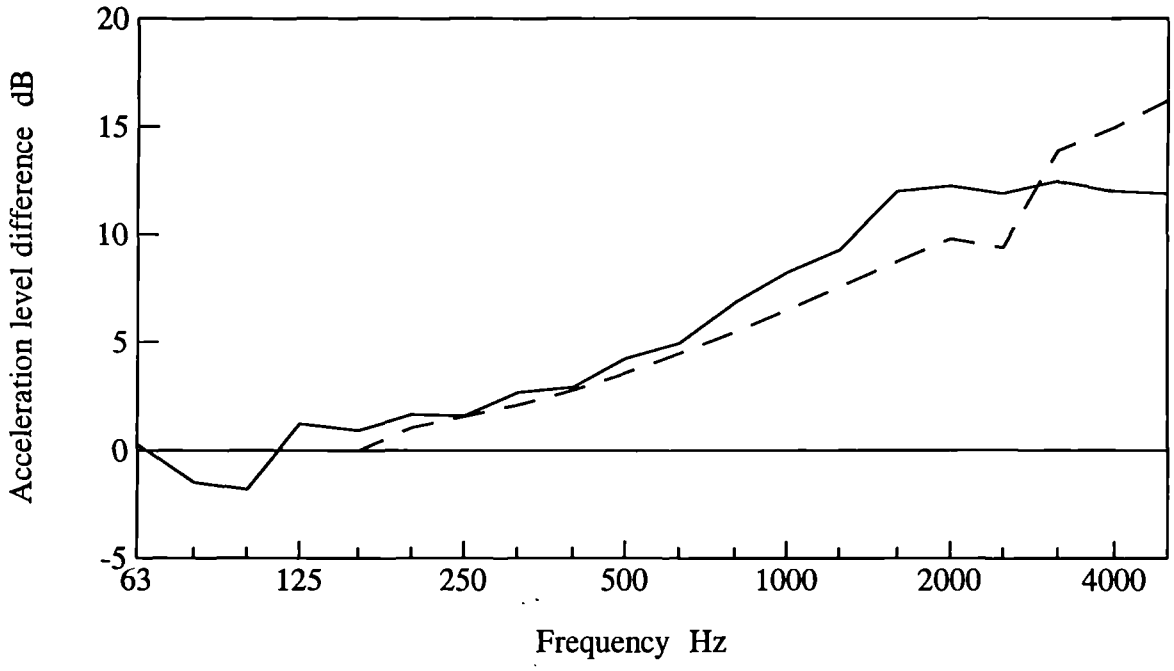

Figure 8.29 Measured and predicted acceleration level difference between the two plates of a 150mm double wall with a structural source.

and is assumed to be effectively a line connection. It is assumed that the nails, positions (B), and the area of plate between the nails over the frame, (C) would be similar and this is the case when measured, shown in Fig 8.28. As the frequency increases so the behaviour of the double wall plates change to a point connection. It can be seen that the plate behaviour at position (B) equals that of the plates, (A), at 500Hz. Using eqn(4.1) in Chapter 4 the predicted frequency where the double wall plates behave as a point connection is approx. 500Hz. It is noticeable that there is not a sudden change from line to point connection as the frequency increases.

Fig 8.29 shows the measured and predicted acceleration level difference between the two plates of a 150mm double wall due to a structural source. The excellent agreement shown in this figure is similar to the level difference between the two plates for an airborne source shown in Fig 8.27.

Fig 8.30 shows the measured and predicted sound reduction index (SRI) for the 50, 100 and 150mm double walls without absorption. The predicted low frequency results are also shown. At the low frequencies where the double walls behave as one large plate there is reasonable agreement between the measured data and the single subsystem theory and there is a clear increase in SRI at the transition from single to double wall behaviour. At higher frequencies the wall is modelled as a series of interconnected subsystems. Fig 8.30 shows that there is good agreement between the measured and predicted results at high frequencies but there is an increasing error as the frequency decreases and as the cavity depth decreases. The error in the overall transmission is approximately double the error of transmission into the cavity, as was shown in Chapter 7, Fig 7.10. This would be expected where the cavity is an important transmission path.

Fig 8.31 shows the predicted energy level difference for the contributions of the various SEA transmission paths for a 50mm double wall with no absorption. The most dominant transmission path over most of the frequency range is through the frame. As has been shown in the previous figures the structural path is well predicted. However, the second most important path is the non-resonant path through the cavity. The importance of the non-resonant transmission associated with the cavity is also shown by the 8dB difference at the lower frequencies between the purely resonant path, *room-plate-cavity-plate-room*

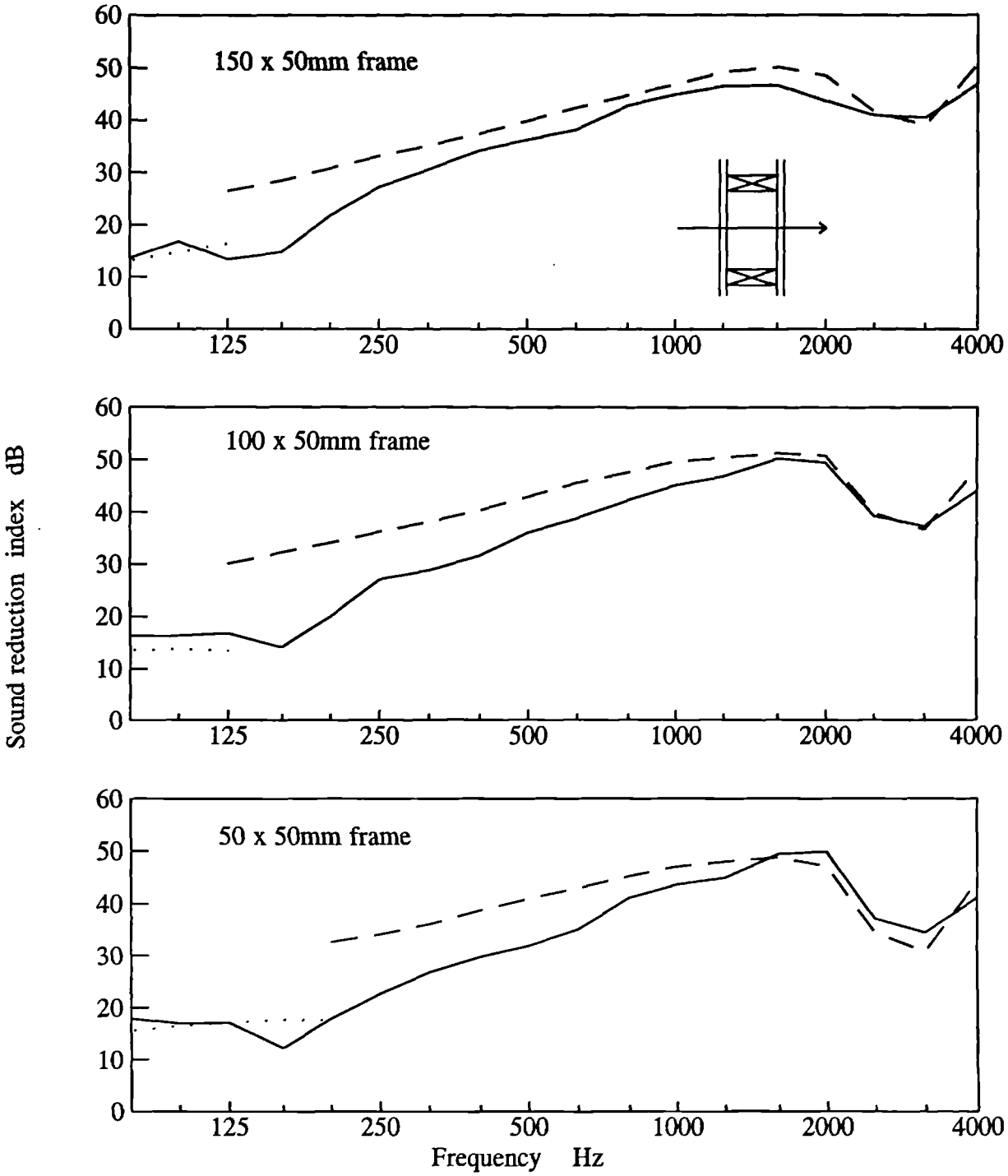

Figure 8.30 Measured and predicted sound reduction index for 150, 100 and 50mm point connected double walls without absorption. (____) measured, (- - -) predicted high freq. model, (....) predicted low freq. model.

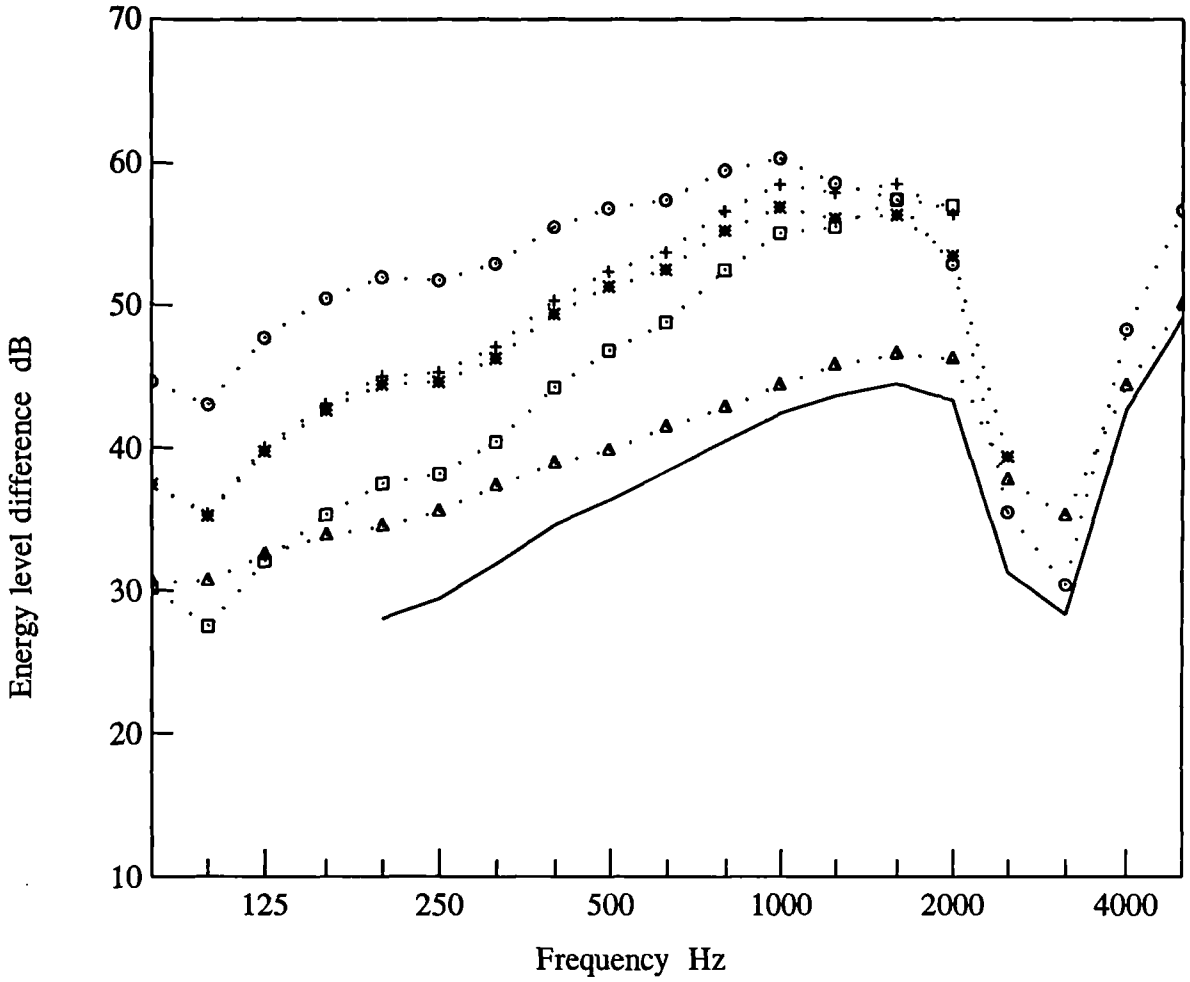

——— sum of all predicted paths
. . □ . . . . . room-cavity-room
. . o . . . . . room-plate-cavity-plate-room
. . Δ . . . . . room-plate-frame-plate-room
. . ✱ . . . . . room-plate-cavity-room
. . + ... room-cavity-plate-room

Figure 8.31 Predicted energy level difference for a 50mm double wall with no absorption showing the contributions from the various SEA paths.

(○), and the resonant and non-resonant path, *room-plate-cavity-room* (*).

The doubling of the error associated with the cavity can be seen when comparing Fig 8.30 and 7.10. The error in the theory for transmission into the cavity is also similar to the error for transmission out of the cavity, thus giving a doubling effect. The error shown in Fig 8.30 is reduced as the cavity depth increases and so the agreement between the measured and predicted results is best for the 150mm double wall, as was found for the same double wall cavity in Fig 7.10. This is consistent with the results of Craik, Nightingale and Steel [95] who obtained good agreement between measurement and the theory for transmission through a double wall with a 300mm thick cavity with no structural coupling.

If the error in transmission is due to transmission through the cavity then it would be expected that adding absorption would decrease the contribution of the cavity paths and therefore increase the importance of structural coupling which, as was shown in Fig 8.27, can be well predicted. The results for transmission through a 100mm double wall with added absorption can be seen in Fig 8.32. The absorption was suspended is such a way that it did not touch the plasterboard plates. This decreased the importance of the cavity paths and, as can be seen, there is much better agreement with the theory. Although there is some uncertainty about the cavity damping after the addition of the cavity absorption, the damping is sufficient to make the cavity path less important and reduce the error between the measured and predicted results.

The change to the sound reduction index as the number of nails is increased can be seen in Fig 8.33 and Fig 8.34. In Fig 8.33 the double wall consisted of a 50mm cavity with added absorption. The number of nails on both sides of the wall was set at 600mm centres (5 over a 3m length). The number of nails was then doubled (11 nails in a 3m length at approximately 300mm centres) and then doubled again (21 nails in a 3m length at approximately 150mm centres). When the nails are at 600mm centres the predicted dominant transmission path is still through the frame but the non-resonant cavity path at low frequencies is almost as equally important. Doubling the number of nails increases the structural coupling but the transmission through the cavity is still important. Doubling the number of nails again means that from 160-400Hz the connection behaves

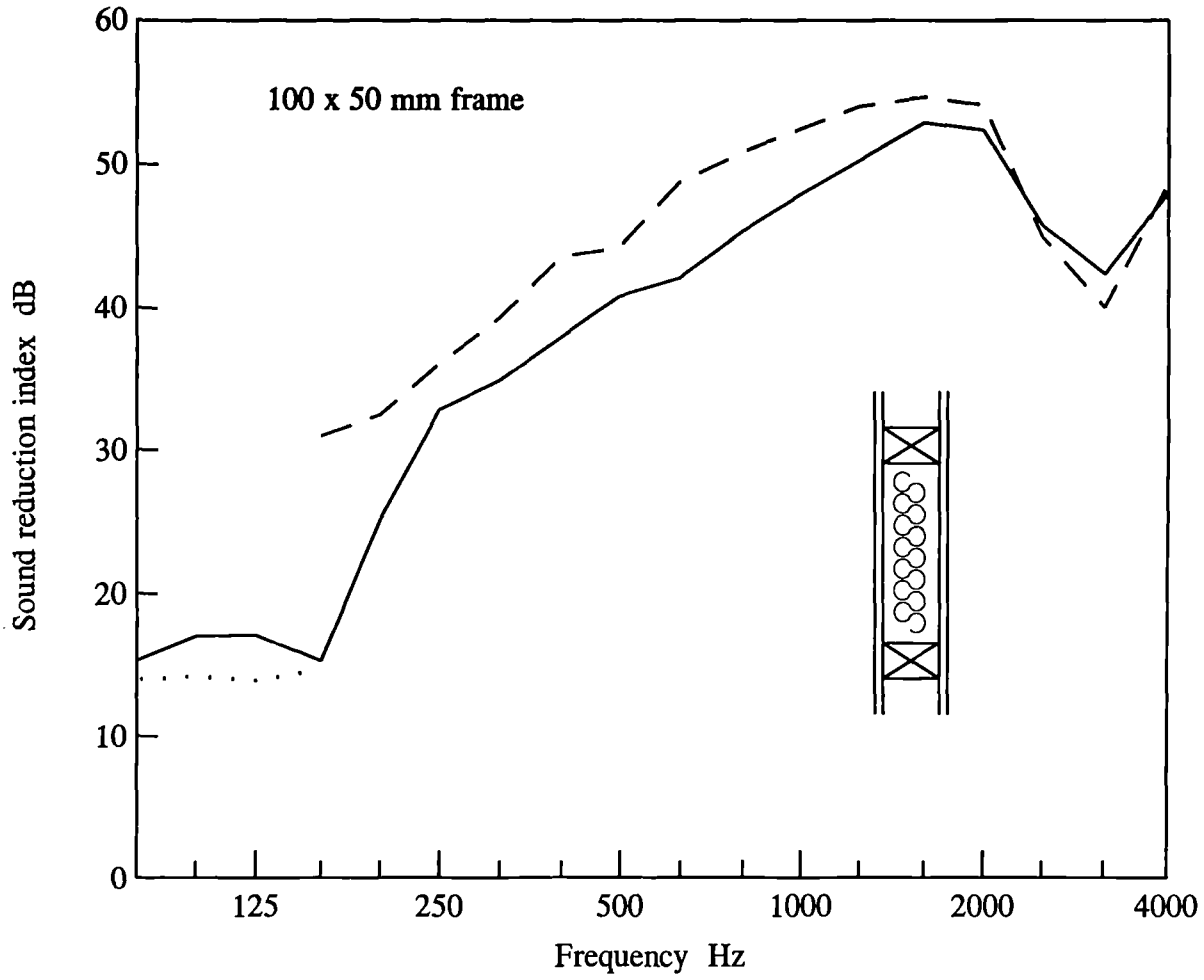

. . . . . predicted low frequency SEA model
— — — — predicted high frequency SEA model
_____ measured

Figure 8.32 Measured and predicted sound reduction index for a 100mm double wall with 50mm suspended absorption and is point connected.

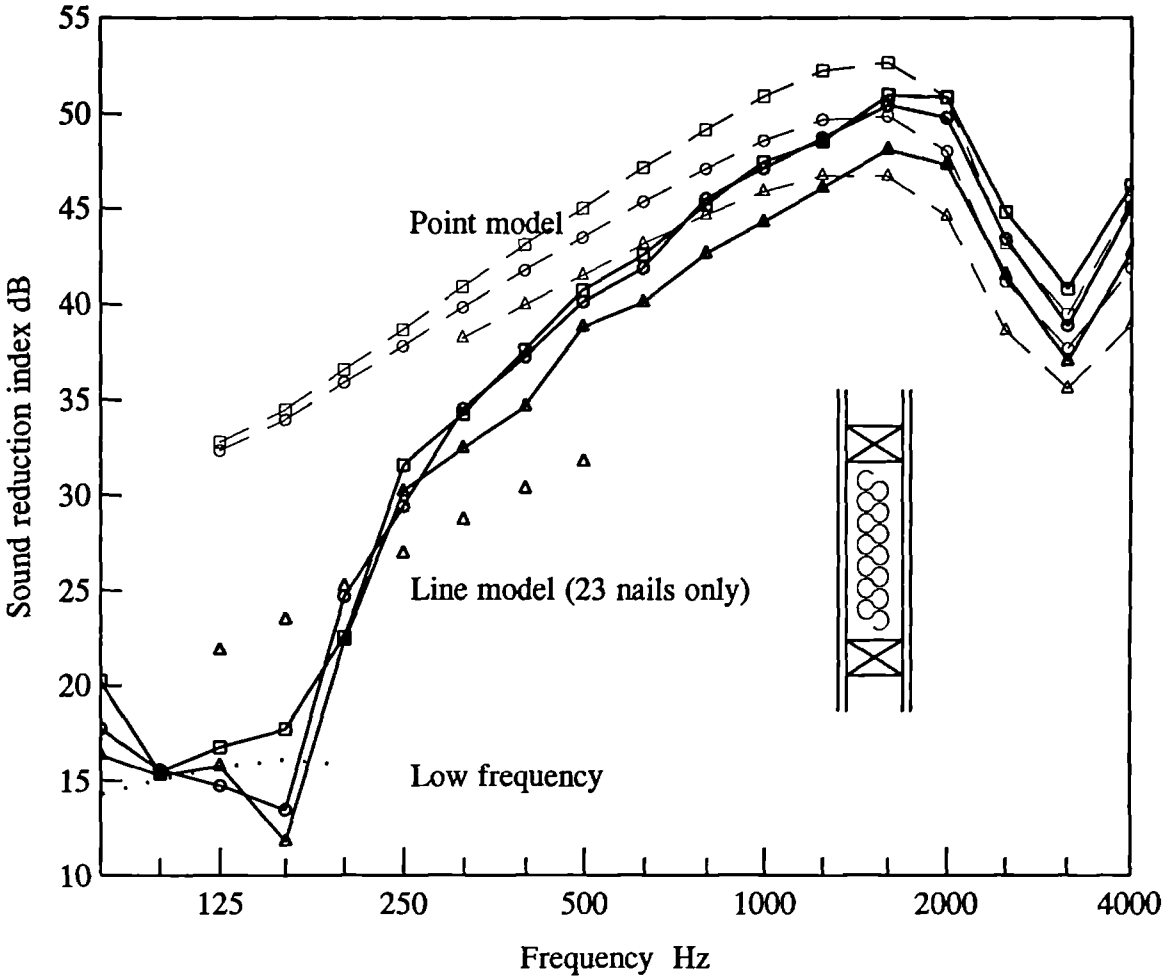

—o— — — predicted (11) nails
—o——— measured (11) nails
—□— — — predicted (6) nails
—□——— measured (6) nails
. . . . . low frequency SEA model
—△— — — predicted (21) nails
—△——— measured (21) nails
△ line model (valid up to 400Hz)

Figure 8.33 Measured and predicted sound reduction index for a 50mm point connected double wall with 50mm absorption showing an increase in the number of point connections.

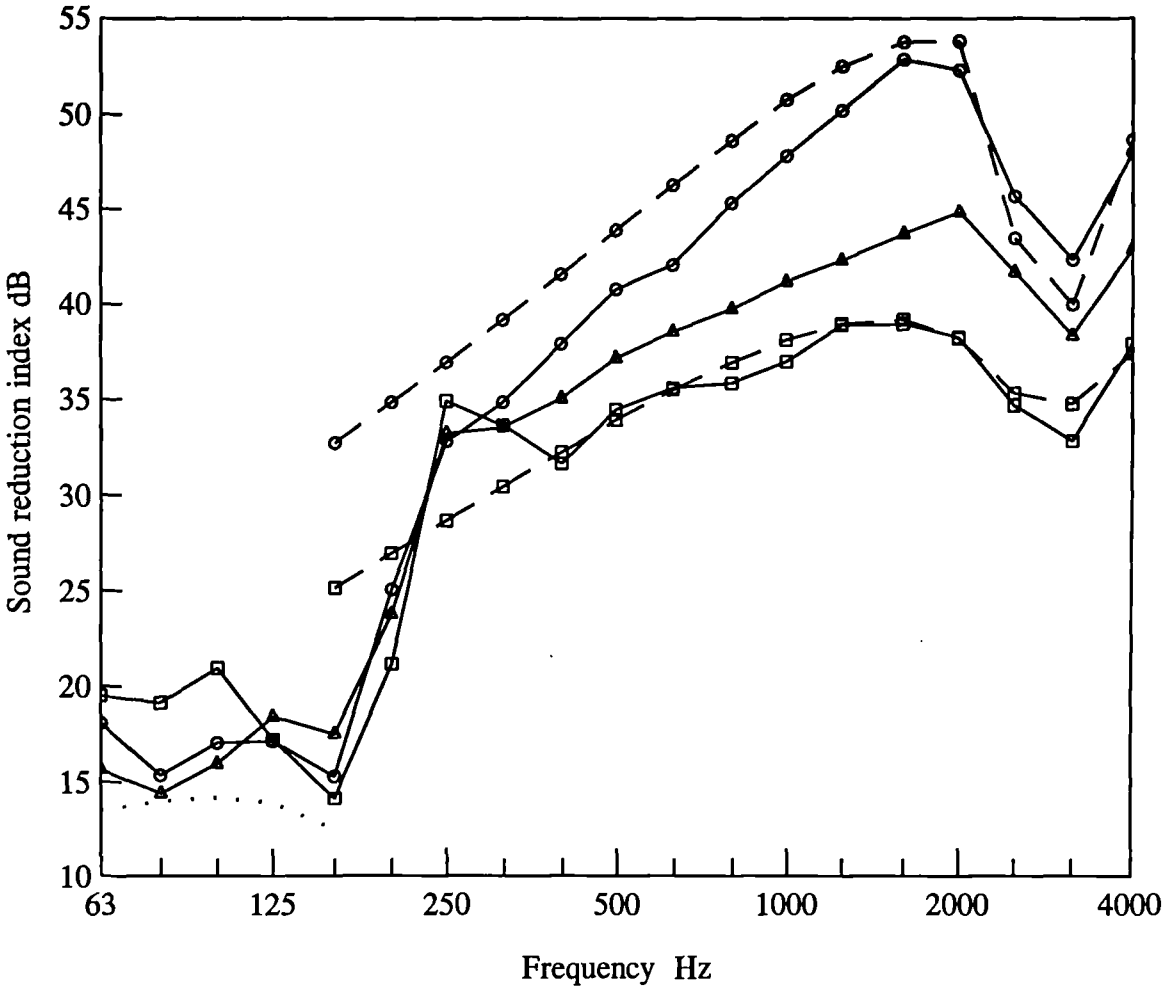

—□— — - predicted using SEA line model
—□——— measured (line connection both sides)
—o— — - predicted using SEA point model
—o——— measured (point connection both sides)
—△——— measured (point/line)
. . . . . predicted using SEA low frequency model.

Figure 8.34 Measured and predicted sound reduction index for a 100mm double wall, where the connection on either side of the wall is point, line and point and line.

like a line connection and above 400Hz like a series of independent points, as was also shown in Fig 8.28. This increased coupling results in a decrease in the SRI of the wall. It is expected that the effect of adding the additional nails would be more apparent after the first increase if the absorption had not been touching the plates and the frame and hence increased the damping of the plates.

This last statement is supported by the results shown in Fig 8.34. The wall shown is the 100mm double wall with 50mm suspended absorption. Many nails were added first to one side and then the other. The systematic decrease in the SRI can be seen each time additional nails are added to the wall. Absorption is present in the cavity similar to Fig 8.33 but is suspended and not touching the plates, which results in a more pronounced increase in transmission due to an increase in the structural coupling, without absorption touching both plates and frame.

High frequency SEA model for line connected double walls

If the plasterboard sheets are bonded to the frame or the nail spacing is small such that the wavelength of the plate is unable to fit between them, as discussed in Chapter 4, then the coupling may be modelled as a line connection. When this is the case the coupling between the plates can be characterised by the structural transmission coefficient, discussed in Chapter 5. Fig 8.35 shows the SEA model and transmission paths for a line connected double wall. The two plates of the wall are effectively divided into subpanels dictated by the line connection of the plates to the frame. The perimeter length of the overall plates is therefore increased and the subpanels are assumed to be clamped, as discussed in Chapter 2.

Fig 8.36 shows the measured acceleration level of a front subpanel of a 100mm line connected double wall normalised for an airborne source. In addition, measured results are also shown in Fig 8.36 when the accelerometer is positioned on the nails and between the nails, as detailed in Fig 8.37. The nail spacing is 100mm which results in the first half bending wavelength fitting between the nails at 1000Hz. The first full wavelength fits between the nails at approximately 4000Hz. Thus as expected the measured acceleration level of the nails and between the nails is the same up to these frequencies and the coupling between the plates and frame may be assumed to be a line

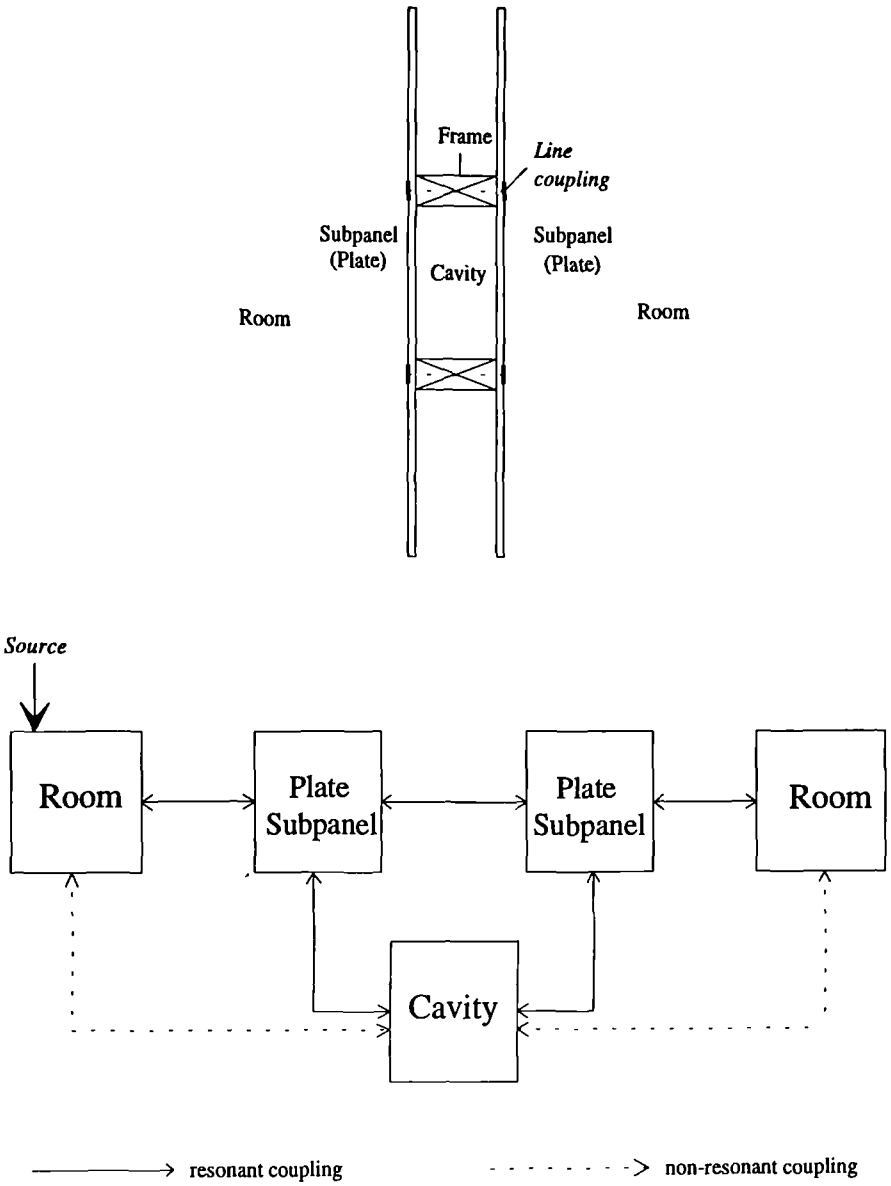

Figure 8.35 High frequency SEA model for a line connected double wall.

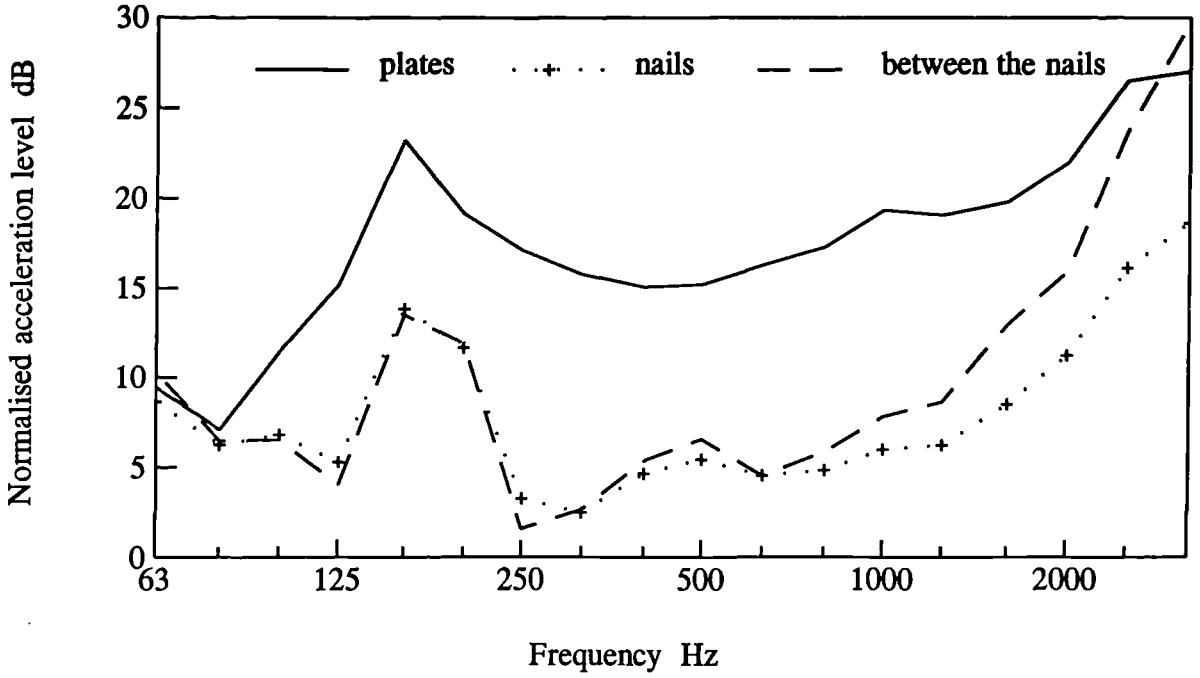

Figure 8.36 Measured acceleration level of a front subpanel of a 100mm line connected double wall with 50mm absorption showing the effect of placing the accelerometer on the nails, plate and between the nails.

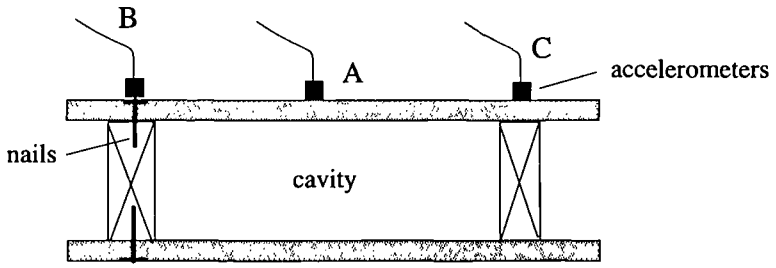

Position A - accelerometers placed on front plates over cavity

Position B - accelerometers placed directly on nails connecting plates to frame

Position C - accelerometers placed on plates over frame between nails

Figure 8.37 Section through full scale double wall showing positions of accelerometer.

connection.

Fig 8.38 shows the measured and predicted acceleration level difference between the front and back plates of a line connected double wall normalised for an airborne source. The predicted sound transmission for the line connection, coupling the plates and the frame, was calculated using the theory in Chapter 5 where the frame is modelled as a plate. The agreement is good over the frequency range. The measured results are negative at the low frequencies and this occurs at the mass-spring-mass frequency, f_0. However, Fig 8.39 shows the measured and predicted acceleration level difference between two subpanels on the 100mm line connected double wall due to a structural source, an acoustic hammer. The agreement is reasonable at the higher frequencies but at the low frequencies the agreement is poor. This may be due to the aspect ratio of the subpanels. The measured and predicted results for transmission between the inline plates in Chapter 6 did not have good agreement and due to the aspect ratio of these smaller panels it is not possible to accurately predict the distribution of energy on the source side, thus the level difference cannot be predicted. However, for an airborne source there is no such difficulty and it is possible to predict the level difference.

Fig 8.40 shows the SRI for a 100mm double wall with 50mm suspended absorption in the cavity. Both the low and high frequencies predicted results are shown. The agreement is very good over the entire frequency range. At the mass-spring-mass resonance there is a significant transition in the measured SRI as the single subsystem wall separates into numerous subsystems.

8.5 Complete timber floor

As discussed in the previous chapters one of the applications of parallel plate structures is in timber floors. Included in the experimental work for this study tests were carried out on a 150mm timber floor which was built-in at one end of the joists to a 100mm concrete block wall. Chapter 3 described the test facility for the timber floor structure. Building in one end of the joists to the wall allowed the possibility of studying flanking transmission past the end of a joist as shown in Fig 8.41.

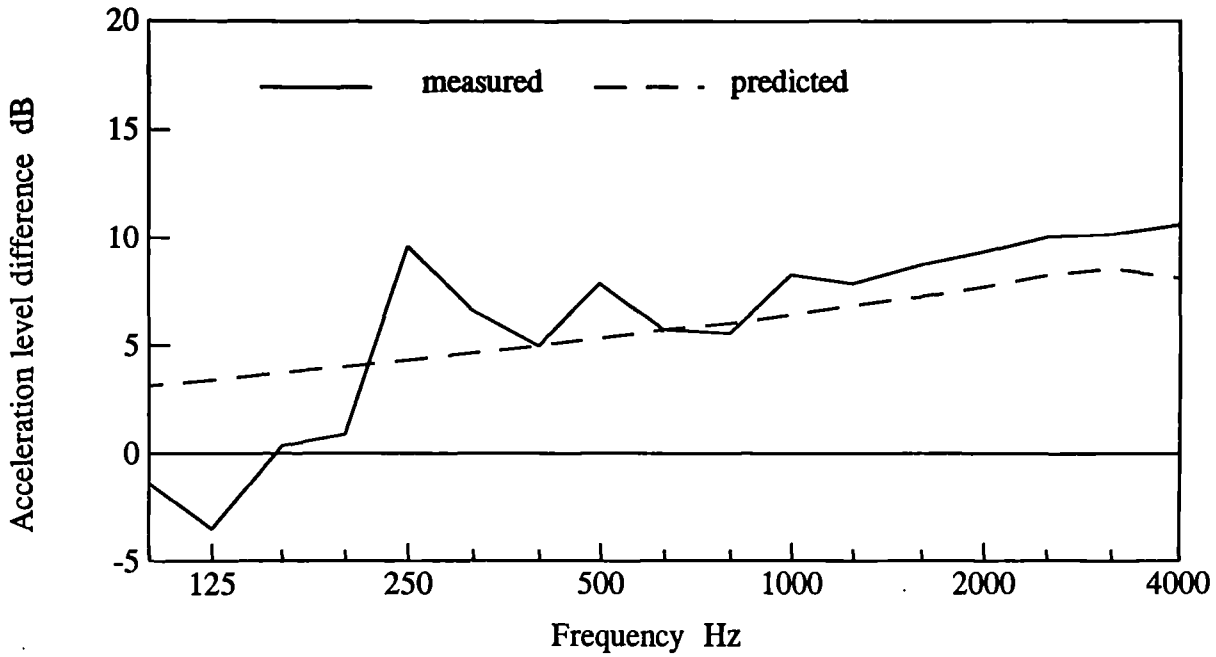

Figure 8.38 Measured and predicted acceleration level difference between the plates of a 100mm line connected double wall due to an airborne source.

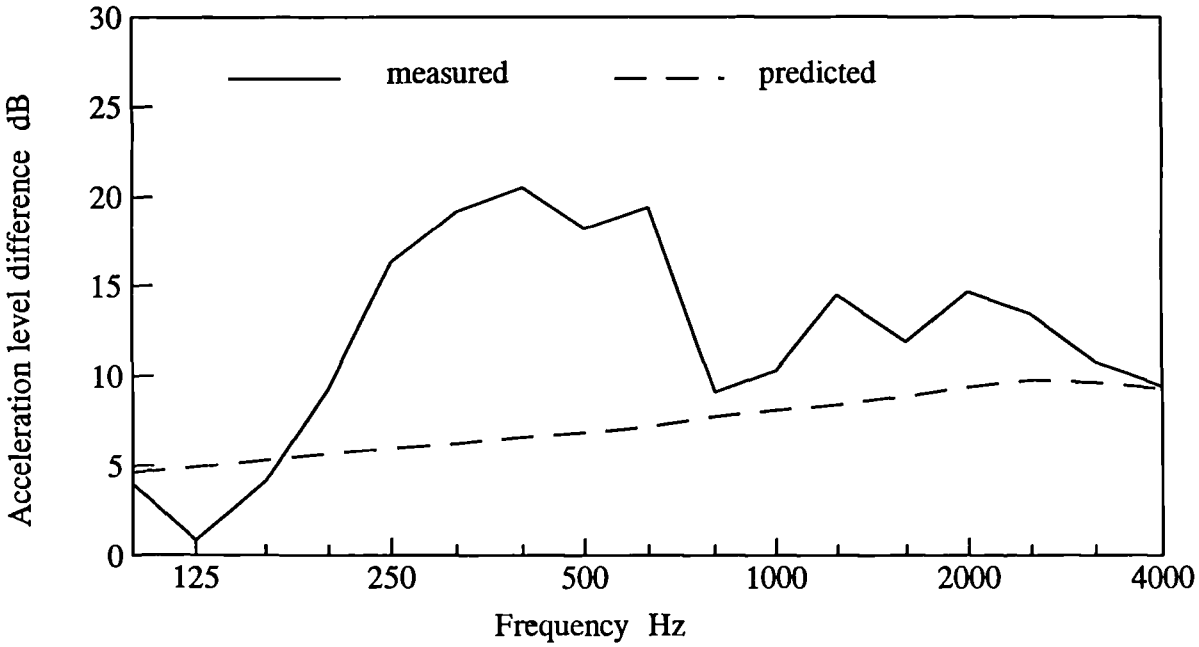

Figure 8.39 Measured and predicted acceleration level difference between two subpanels on either side of a line connected 100mm double wall due to a structural source.

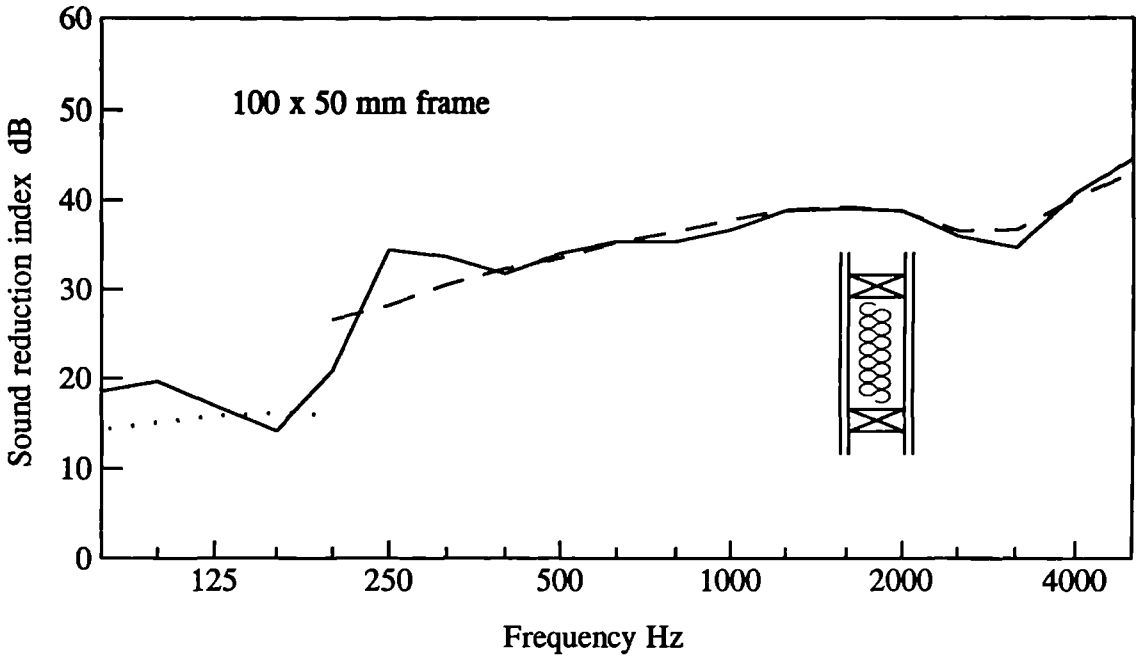

Figure 8.40 Measured and predicted sound reduction index for a 100mm line connected double wall with 50mm absorption. (____) measured, (- - -) predicted high freq. model, (....) predicted low freq. model.

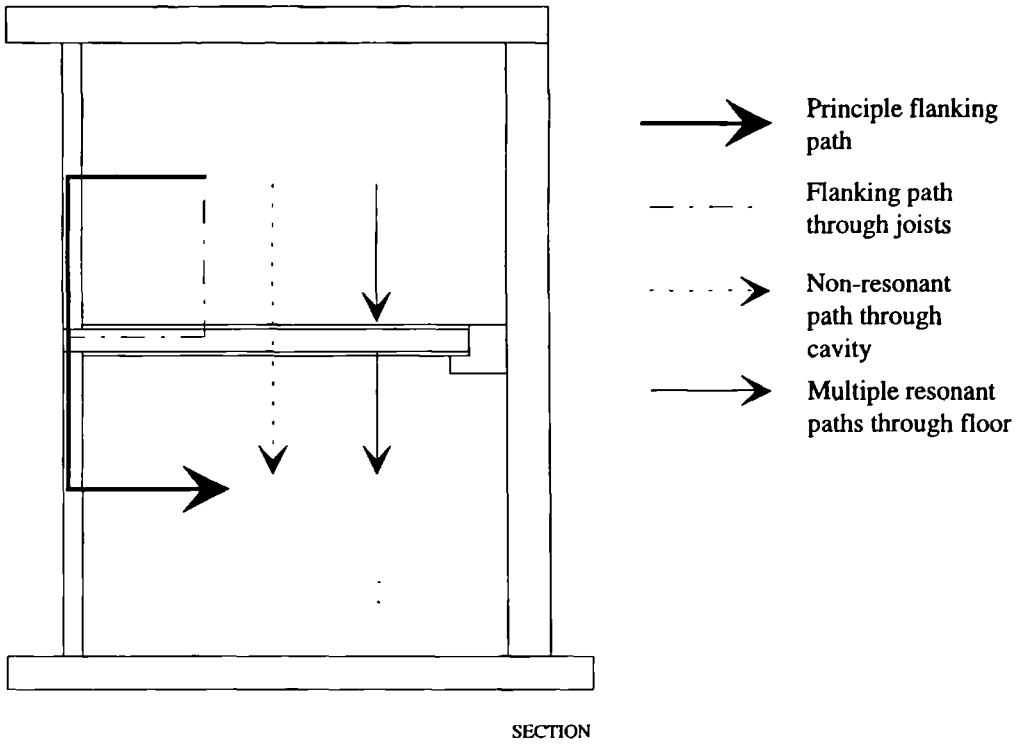

Figure 8.41 Section through built-in timber floor showing SEA transmission paths and principle flanking path through connecting wall.

Fig 8.42 shows the SEA model for the 150mm timber floor. At low frequencies coupling between the upper and lower parts of the wall, divided by the connection to the joists, was calculated using a 'tee' structure model [13]. At high frequencies the coupling from the seven joists to the wall was calculated using beam-plate theory developed by Cremer [44] and Steel [86]. The coupling from the walls to the rooms was calculated using the theory described in Chapter 2. The measured internal loss factor of the chipboard and plasterboard was 0.018 and 0.01. The total loss factor (TLF) of the various plates and walls was calculated by summing the CLF's and ILF. The TLF of the rooms and cavities was measured using the standard decay method. The chipboard floor and plasterboard ceiling were coupled to the joists by screws at 300mm centres and nails at 150mm centres respectively. No absorption was present in the cavities.

Fig 8.43 shows the acceleration level difference between the top and bottom plates of the timber floor due to an airborne source. The agreement is good over the frequency range. The lack of predicted data below 160Hz was due to the measured TLF of the cavities being less than the sum of the CLF's and ILF and hence was not included.

Fig 8.44 shows the measured and predicted acceleration level difference between the top and bottom plates of the timber floor due to a structural source. An acoustic hammer was used to excite the floor. However, not only the plate was excited directly but so was the joist as the hammer was striking at random over the floor area. Two predicted results are shown, firstly for the plate being excited and secondly for a joist being excited. It can be seen that there is much better agreement between the joist source predicted data than the plate source predicted result.

Fig 8.45 shows the measured and predicted airborne level difference from a room to a cavity in the 150mm timber floor and the agreement is good. When this result is compared with 150mm double wall cavity in Fig 7.10, which also had good agreement, this supports the findings in Chapters 7 and 8 that when the cavity is reasonably deep the theory copes well. When the cavities were of a smaller depth the agreement was poor and the error increased with decreasing frequency.

The room to room measured and predicted airborne level difference is shown in Fig

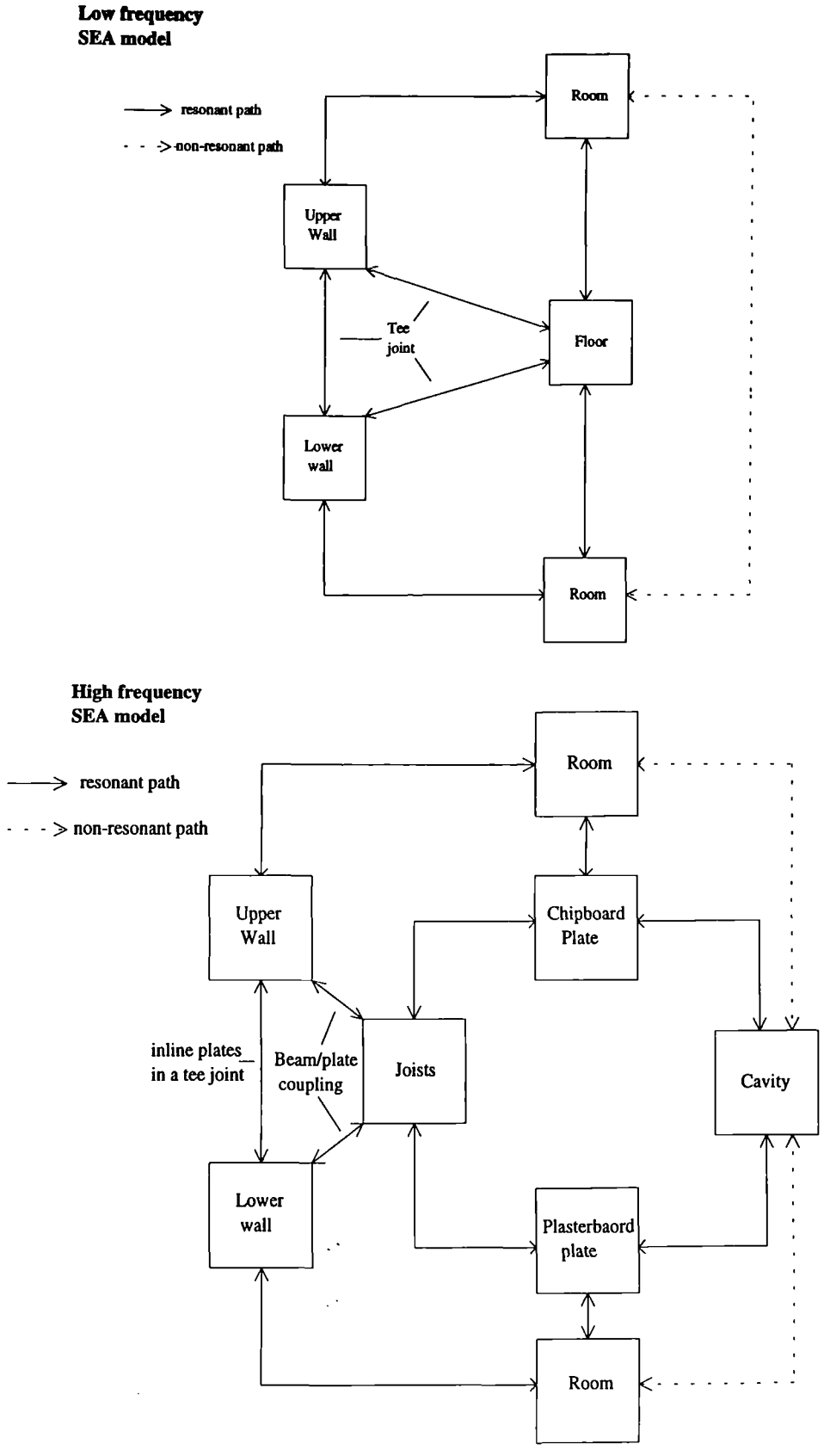

Figure 8.42 Low and high frequency SEA models for a timber floor built-in to a flanking wall.

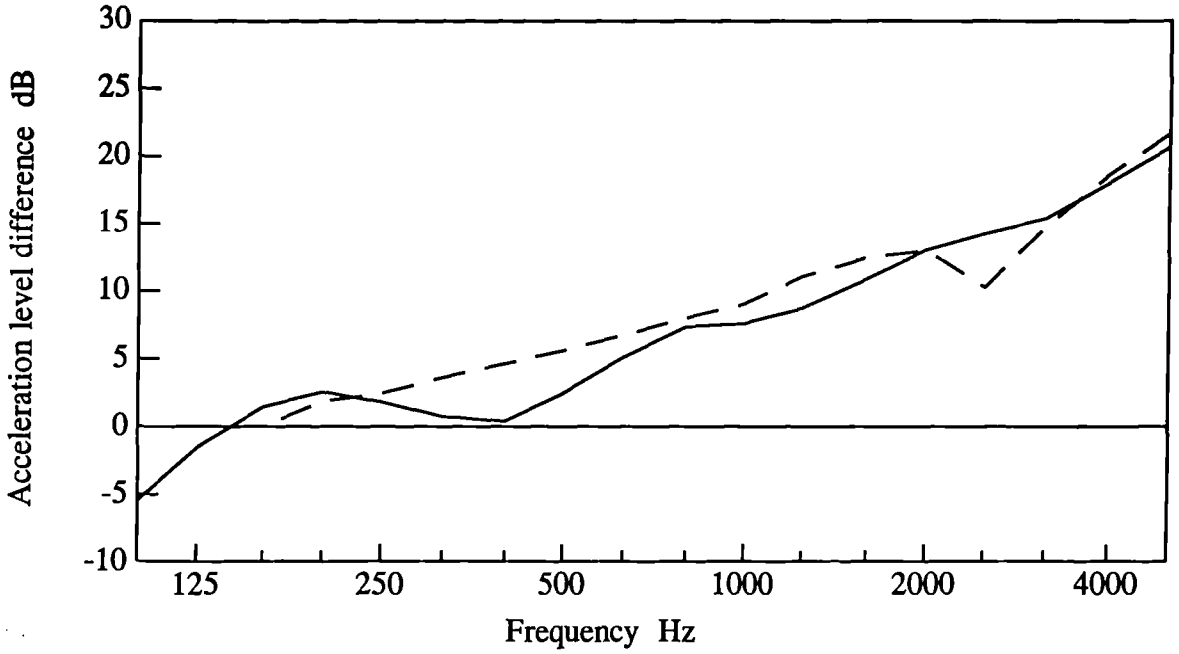

Figure 8.43 Measured and predicted acceleration level difference between the top and bottom plates of a 150mm timber floor for an airborne source. (- - -) predicted, (____) measured.

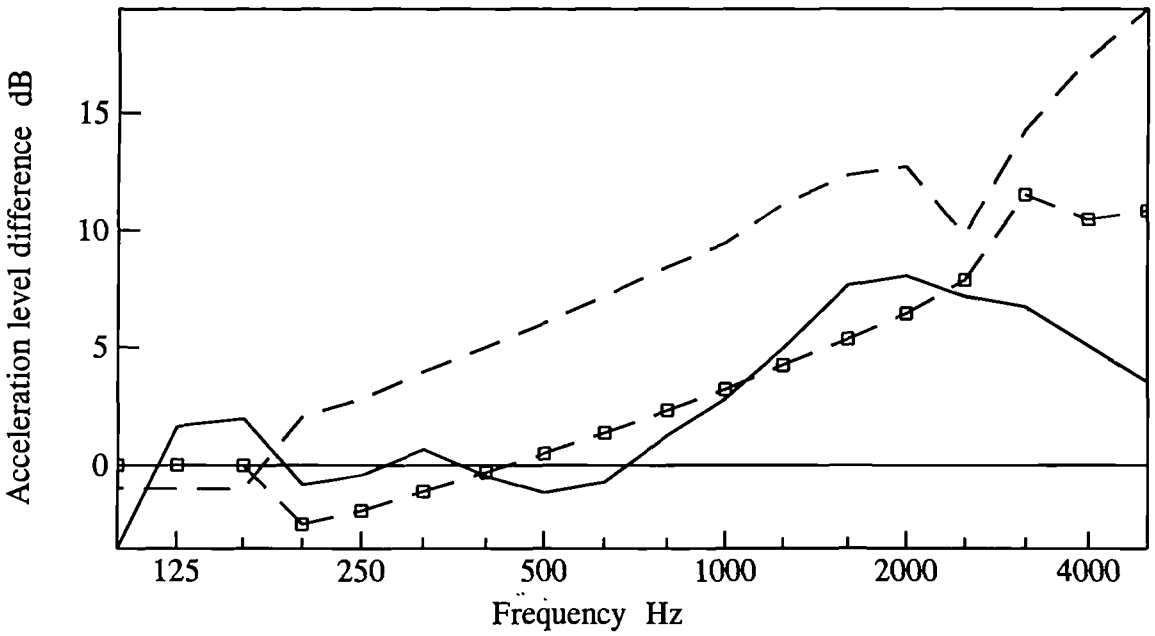

Figure 8.44 Measured and predicted acceleration level difference between the top and bottom plates of a 150mm timber floor for a structural source. (- - -) predicted-source on plates, (____) measured, (- -□- -) predicted-source on joist.

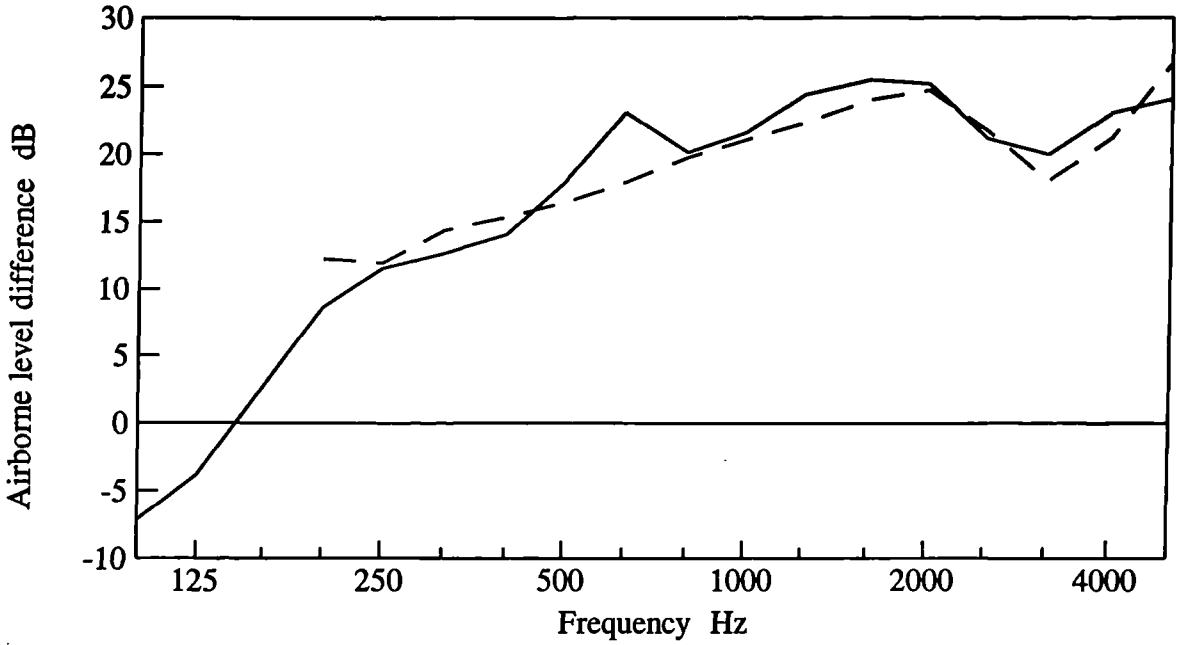

Figure 8.45 Measured and predicted airborne level difference from a room to a cavity in a 150mm timber floor.
(- - -) predicted, (____) measured.

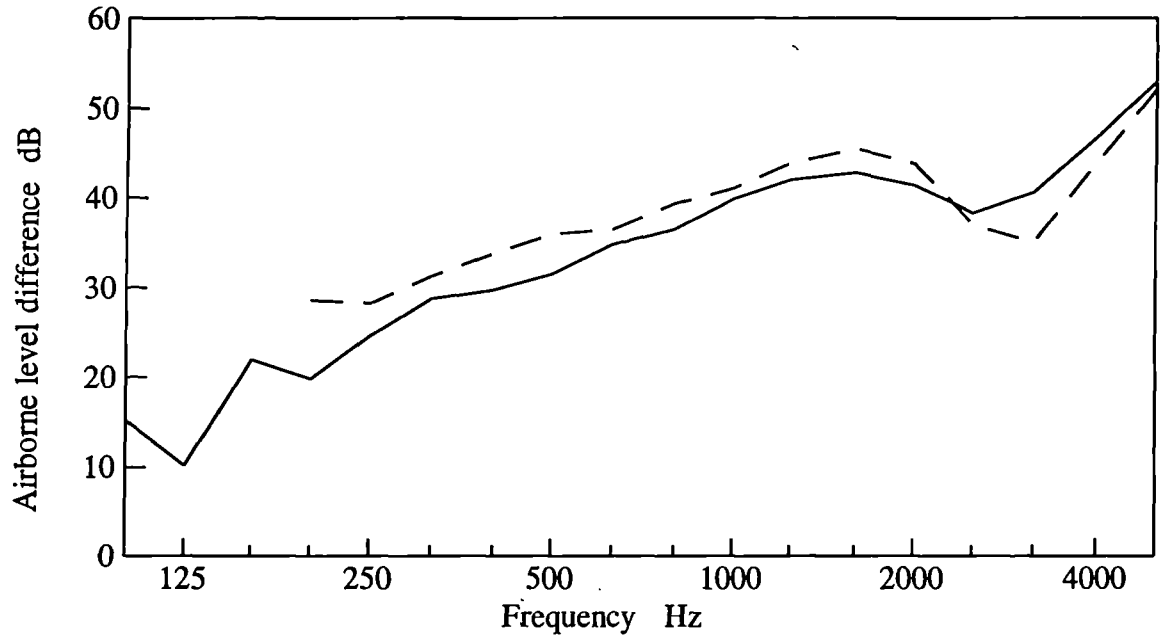

Figure 8.46 Measured and predicted airborne level difference from room to room through a 150mm timber floor.
(- - -) predicted, (____) measured.

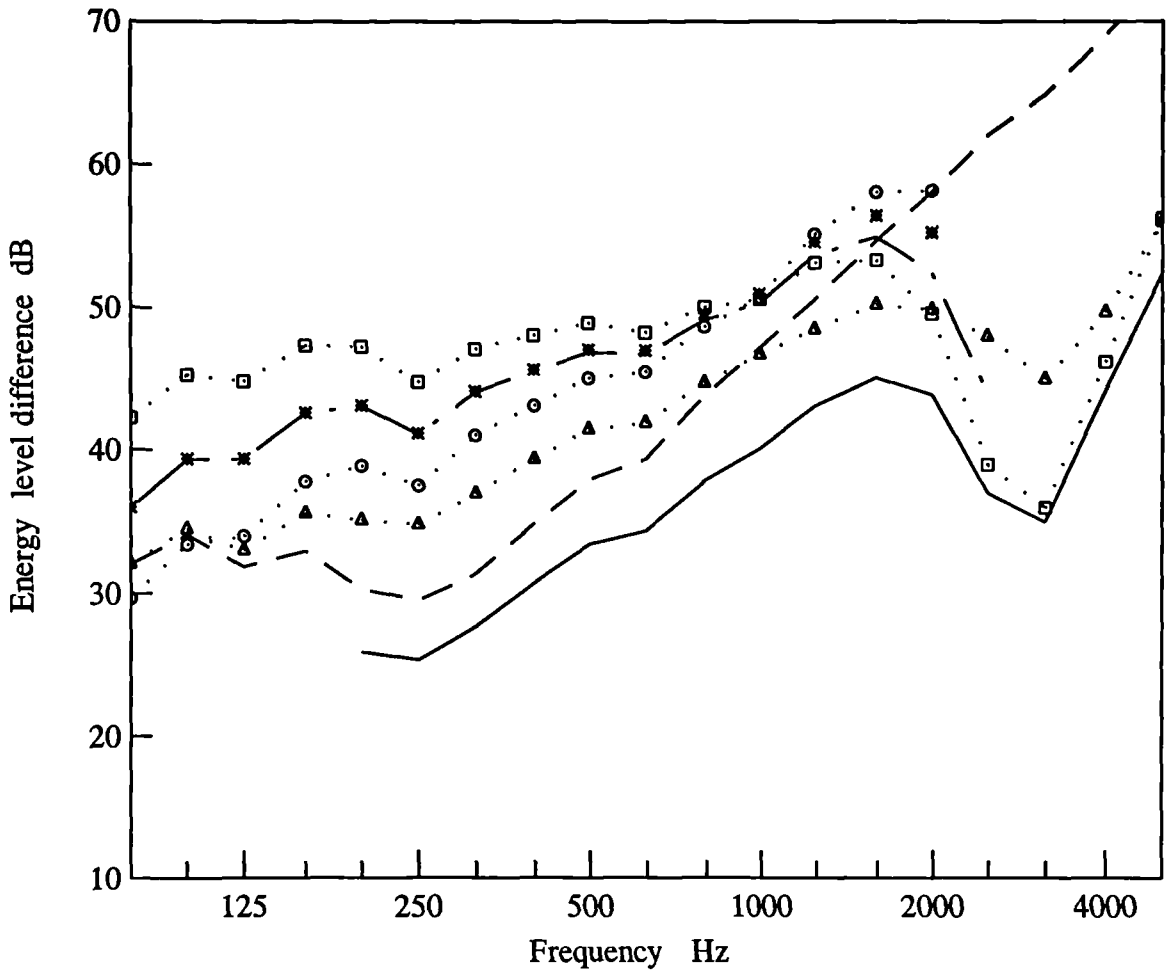

. . □ . . . . . (room-plate-cavity-plate-room)
. . o . . . . . (room-cavity-room)
. . Δ . . . . . (room-plate-joist-plate-room)
* (room-plate-cavity-room)
——— . ——— (room-cavity-plate-room)
— — — — (room-wall-room) Flanking path
——————— (sum of all predicted paths)

Figure 8.47 Predicted energy level difference from room to room through a 150mm timber floor showing the contributions of the various SEA transmission paths.

8.46. It can be seen that there is good agreement at all frequencies. It is noticeable that the agreement is better than that found for a similar depth structure shown in Fig 8.30, the 150mm double wall. Fig 8.47 shows the predicted energy level difference from room to room through the 150mm timber floor. The importance of including the flanking path in this study is shown in Fig 8.47. The dominant path at the low to mid frequencies is through the flanking wall, by as much as 4dB at 250Hz. There was attenuation of approximately 7dB between the two parts of the wall divided by the connection with the joists and it was assumed that the flanking wall could be modelled as two subsystems. At the higher frequencies the resonant path through the plates and cavity is the dominant path.

8.6 Conclusions

The results of this chapter have shown that transmission through single walls, ribbed walls, lightweight double walls, with point and line connection, and timber floors can be predicted using statistical energy analysis.

At low frequencies the double walls behave as single subsystems. Using the mass-spring-mass frequency as the transition between single and double walls works well, for both point and line connected walls. The theory copes well when predicting the behaviour of the wall as a single plate at low frequencies.

For point connected walls there is reasonable agreement between the measured and predicted data when the cavities are deep and similar in behaviour to rooms. However, there is an increasing error between the measured and predicted results as the cavity depth decreases. This error factor is double that found for transmission into double wall cavities and it is assumed that the error associated with transmission into the cavity is also occurring for transmission out of the cavity. Further work is required for predicting sound transmission into narrow cavities in double walls.

The structural coupling by point connection is well predicted as is the behaviour of the plates due to an airborne or structural source. As the number of point connections are increased so this increases the structural transmission path and increases the overall

sound transmission and the theory copes well. It appears from the results that using $\lambda_B/2$ as the criteria for the transition between point and line works well. The dominant sound transmission path has been predicted to be through the frame. But from the error associated with transmission through the cavity to the receiving room it is assumed that the cavity is the dominant transmission path for point connected walls.

When there are many nails and the spacing is smaller than $\lambda_B/2$ it is better to model the double wall plates as line connected. The agreement between the measured and predicted SRI is excellent. The predicted dominant sound transmission path for a line connected wall is through the frame.

The SEA models allowed the contributions of the various SEA sound transmission paths to be studied, including flanking paths. The timber floor results showed that the flanking path through the wall could be dominant for most of the lower frequencies. Whilst designers and architects specify floors and walls which they hope will fulfil the sound requirements of the various building regulations, section 8.5 has shown that the sound reduction may be significantly affected by a flanking transmission path. Specifying a floor or wall with high sound insulation properties does not guarantee good sound insulation if flanking paths are present.

Chapter 9
Conclusions

9.1 Introduction

The first section in this chapter draws together the important findings and conclusions from this thesis. This includes a brief discussion of the implications that these have for the performance of lightweight partition walls and timber floors. The final part of the chapter gives proposals for further research.

9.2 Conclusions

The aim of this thesis was to examine sound transmission through lightweight parallel plate structures. Theoretical models were presented using Statistical Energy Analysis (SEA) to provide predicted data to compare with measured results obtained from tests on a variety of lightweight double wall constructions and a full scale timber floor.

Chapter 2 gave a review of the previous work on double walls. It was found that the previous theories could not accurately predict the transmission through real lightweight double walls or the behaviour of the various components. The best approach was to use statistical energy analysis which could determine the individual sound transmission mechanisms involved as well as predict the overall sound transmission due to the contributions from the various transmission paths.

Chapter 3 described the experimental facilities used and test structures built for this work including methods of determining the properties of the various subsystems. Two methods were presented for measuring the total loss factor of the cavities, the standard decay method and the power injection method. Using either method it was possible to calculate

the total loss factor. When there was absorption placed in the cavity the measured reverberation time was outwith the limits of the frequency filter of the equipment.

Chapter 4 examined the coupling between parallel plates for point connection. If the nails are sufficiently spaced such that the spacing is greater than $\lambda_B/2$ then the coupling may be assumed to be point connection. Where spacing between the point connections is smaller than $\lambda_B/2$ then it may be assumed that the plates are line connected to the frame. Using mobility models theories were presented for coupling where the nails or screws are directly opposite each other or are offset from one another. The predicted acceleration level difference between the plates showed that for immediately opposite point connections the coupling was very strong. However, when compared with measured data for similar connections the results showed that the coupling was no different to that for offset point connections.

Two principle theories were presented in Chapter 5 for predicting line connection between parallel plates, where the frame may be modelled as a beam or as a finite plate. Both theories included all wave types such as bending, longitudinal, transverse and nearfield waves. From comparisons with measured data presented later in Chapter 6 it was found that the plate model had the best agreement for transmission to plates 3 & 4.

In Chapter 6 measurements were carried out on suspended line connected plate structures. To examine some of the effects of the parametric survey the depth of the frame was varied and measurements were carried out to compare with the plate and beam line prediction models. The beam model only worked well at the low frequencies up to where the first half wavelength fitted into the depth of the frame. The agreement between the plate model results and measured results was very good for transmission from plate 1 to the offset plates 3 and 4. However, predicted data for transmission from plate 1 to the inline plate 2 consistently under estimated the strength of coupling.

Chapter 7 examined the transmission into an isolated cavity and also for a double wall cavity. No new theory was presented but existing theories were examined. It was found that for transmission into an isolated cavity the existing theory and SEA models compared well with measured data. For transmission into a double wall cavity where the

cavity depth was sufficiently large that the cavity was similar in behaviour to a room the agreement was good. However, when the cavity depth decreased and the parallel plates were close together the agreement was not as good.

Chapter 8 brought together all the theories presented, from Chapter 2 to Chapter 7, into an SEA framework so that comparisons could be made between predicted and measured results for full scale double walls and a timber floor. Results were presented for single plate walls, ribbed walls, point and line connected walls and finally results from a full scale timber floor. Flanking transmission was also examined by building a timber floor which was built into a flanking wall at one end. Generally there was very good agreement between the measured and predicted acceleration level difference between the plates, whether point or line connected.

At low frequencies below the mass-spring-mass frequency, f_0, the double walls behave as single plate subsystems. An SEA model was presented for this behaviour and comparison between measured and predicted data showed good agreement. The transition between the wall behaving as a single subsystem and dividing into multiple subsystems was taken to be f_0. This predicted transition frequency agreed well with the measured data.

Analysis was undertaken of the behaviour of a ribbed wall, on the ribbed and plain sides. It was found that there was increased acceleration on the ribbed side due to the increased perimeter length provided by the ribs. In the case of the point connected double walls the overall measured and predicted sound reduction index had good agreement when the cavity was sufficiently deep. As the cavity depth decreased the error between the measured and predicted results at the lower to mid frequencies increased. The quantity of error was double that for transmission into a double wall cavity, discussed in Chapter 7. It was assumed that the error associated for transmission into the cavity was also occurring for transmission out of the cavity, and thus this could explain the larger error found for the overall sound transmission of the point connected double walls. It was found that the transmission through point connected double walls was dominated by the cavity. Measured and predicted data was also presented for a line connected double wall. It was found that the transmission through these walls was

dominated by structural transmission through the frame. There was good agreement between the measured and predicted results over the entire frequency range. Although the walls were connected by screws the spacing was smaller than $\lambda_B/2$ and was assumed to be line connect

The current Building Regulations [1,2] require the nail spacing in lightweight partitions or timber floors to be at half the spacing required for screws. This results in a significant increase in transmission at the lower frequencies due to the coupling behaving like a line connection. After the MSM frequency the double walls subdivide into the various components and the wall no longer behaves as single plate. From the standard spacings stipulated in the Building Regulations if nails are used it is within the frequency range of 100-500Hz that the reduction in sound insulation occurs. This is within the frequency range required to be tested to identify if the partition or floor has passed. Therefore from the finding of this work screws rather than nails should be used for coupling the plates to the supporting frame. Varying the material properties can change the sound insulation characteristics. If the frame has its depth or width increased this can assist in reducing the overall sound transmission. However, this may not always be possible as the designers and architects work within specified design heights and this increasing the height of a three storey building by 200mm obviously involves costs.

The SEA models presented have been able to identify the primary mechanisms of sound transmission through double walls. The agreement for most of the structures presented was very good. These models could be adopted as useful design tools in helping designers, architects and specifiers understand how the various components of the structure effect the overall sound transmission. Also the fact that the entire structure can be inserted into an SEA model allows early identification of the dominant sound transmission paths. This allows these areas to be investigated further and the design altered if required at an early stage in the design process.

9.3 Suggestions for further research

The error associated with the measured and predicted results for transmission into narrow double wall cavities is an important area of further work. It was found that when

the cavities were deep, and similar in behaviour to a room, the theory coped well. But as the cavity decreased in depth and the plates got closer the error increased.

Further work could also be undertaken on determining the total loss factor of narrow cavities with and without absorption. This is an important area as most modern walls and floors have absorption present in the cavities.

It was found that when there are point connections which are immediately opposite or offset the measured data showed no difference. However, the predicted results showed a significant increase in coupling when the point connections are immediately opposite. It may be worthwhile to investigate this area again but this time using isotropic materials to reduce the possible variables affecting the transmission.

In regard to complete buildings such as timber framed houses where all the principle structures are lightweight parallel plates, if the sound transmission can be predicted for one floor or wall, then it is possible to use SEA and the models presented in this work for a study on a complete timber framed house.

The increased transmission due to the flanking path in the timber floor test structure via the wall was significant. In domestic housing with concrete and masonry walls the floor may often be of timber construction, built-in to the walls. This study has analysed the effect of building in one end of the joists, but in reality both ends would be built-in. The SEA models used in this study predicted the transmission well but further work is required on the interaction between the joists (beams) and the walls (plates).

REFERENCES

[1] *The Building Standards (Scotland) Regulations 1990.* The Scottish Office. HMSO. 1990.

[2] *The Building Regulations (England and Wales) 1991.* IS 1991/2768.

[3] **BS 2750**:1980: Measurement of sound insulation of building elements. BSI. UK.

[4] **ISO 140** Measurement of sound insulation of building elements. BSI. UK.

[5] **BS 5821**:1984: Methods of rating sound insulation in building elements. BSI. UK.

[6] **ISO 717** Methods of rating sound insulation in building elements. BSI. UK.

[7] **A. Powell.** *Acoustical Fatigue - Foundations and future needs.* Conf. on Acoustical Fatigue, WADC TR-59-676. 1961.

[8] **R. Wilson.** *Sound Transmission through double walls.* PhD thesis, Heriot-Watt University, Edinburgh, UK. 1992.

[9] **R.J.M. Craik.** *A study of sound transmission through buildings using statistical energy analysis.* PhD thesis, Heriot-Watt University, Edinburgh, UK. 1980.

[10] **R.J.M. Craik and R. Wilson.** *Sound transmission through masonry cavity walls.* Journal of Sound and Vibration **179**, 79-96. 1995.

[11] **R.H. Lyon.** *Statistical energy analysis of dynamical systems: Theory and applications.* MIT Press, Cambridge, Massachusetts. 1975.

[12] **R.H. Lyon and R.G. DeJong.** *Theory and applications of statistical energy analysis.* (2nd edition) Butterworth Heinemann. USA. 1995.

[13] **R.J.M. Craik.** *Sound transmission through buildings using Statistical Energy Analysis.* Gower. 1996.

[14] **BS 5268**:1991: *Structural use of timber. Part 2. Code of practice for permissible stress design, materials and workmanship.* BSI. UK.

[15] **J.M. Illston.** *Construction materials - Their nature and behaviour.* (2nd edition). Spon. 1994.

[16] **BS 5234**: Parts 1 & 2. 1992. Code of Practice: Internal non-loadbearing partitions. BSI. UK.

[17] **BS 8212**: Section 6. 1995. Code of Practice: Dry lining and partitioning using gypsum plasterboard. BSI. UK.

[18] **L.L. Beranek and G.A. Work.** *Sound transmission through multiple structures containing flexible blankets.* J. Acoust. Soc. Am., Vol 21, 419-428, 1949.

[19] **Nichols, Sleeper, Wallace and Ericson.** J. Acoust. Soc. Am., Vol 19, 428, 1947.

[20] **A. London.** *Transmission of sound through double walls.* J. Acoust. Soc. Am., Vol 22, 605-615, 1950.

[21] **K.A. Mulholland, H.D. Parbrook and A. Cummings.** *The transmission loss of double panels.* J. Sound Vib., Vol 6, 324-334, 1967.

[22] **P.H. White and Powell.** *Transmission of random sound and vibration through a rectangular double wall.* J. Acoust. Soc. Am., Vol 40, 821-832, 1965.

[23] **A. Cummings and K.A. Mulholland.** *The transmission loss of finite sized double panels in a random incidence sound field.* J. Sound Vib., Vol 8, 126-133, 1968.

[24] **E.C. Sewell.** *Two dimensional solution for transmission of reverberant sound through a double partition.* J. Sound Vib., Vol 12, 33-57, 1970.

[25] **W.A. Utley and K.A. Mulholland.** *The transmission loss of double and triple walls.* App. Acoust., Vol 1, 16-20, 1968.

[26] **R.R. Hudson and K.A. Mulholland.** *The measurement of high transmission loss (The brick wall experiment).* Acustica, Vol 24, 251-261, 1971.

[27] **B.H. Sharp.** *Prediction methods for the sound transmission of building elements.* Noise Control Engineering, Vol 11, 53-63, 1978.

[28] **K.K. Schiller.** *Physical aspects of sound insulation through walls.* J. Sound Vib., Vol 6, 283-295, 1967.

[29] **M.C. Bhattacharya, K.A. Mulholland and M.J. Crocker.** *Propagation of sound energy by vibration transmission via structural junctions.* J. Sound Vib. Vol 18, 221-234, 1971.

[30] **R. Yu. Vinokur.** *The influence of linear sound bridges linking panel edges on the airborne sound insulation of double partitions.* App. Acoust., Vol 31, 19-35, 1991.

[31] **R.J. Donato.** *Sound transmission through a double-leaf wall.* J. Acoust. Soc. Am., Vol 51, 807-815, 1972.

[32] **G. Lin and J.M. Garrelick.** *Sound transmission through periodically framed parallel plates.* J. Acoust. Soc. Am., Vol 61, 1014-1018, 1977.

[33] **Q. Gu and J. Wang.** *Effect of resilient connection on sound transmission loss of metal stud double panel partitions.* Chinese Journal of Acoustics, Vol 2, 113-126, 1983.

[34] **J.L. Davy.** *Predicting the sound insulation of stud walls.* Proc. Internoise-91, Melbourne, Australia. 1991.

[35] **F.J. Fahy.** *Sound and structural vibration. Radiation, transmission and response.* Academic Press, London. 1985.

[36] **P.W. Smith.** *Statistical models of coupled dynamical systems and the transition from strong to weak coupling.* J. Acoust. Soc. Am., Vol 65, 695-98, 1979.

[37] **M.A. Heckl.*et al.*** *New methods for understanding and controlling vibratio of complex structures.* Bolt Beranek and Newman Inc., Rept. No. 875, 1961.

[38] **R.H. Lyon and G. Maidanik.** *Power flow between linearly coupled oscillators.* J. Acoust. Soc. Am., Vol 34, 623, 1962.

[39] **R.H. Lyon and E. Eichler.** *Random vibration of connected structures.* J Acoust. Soc. Am., Vol 36, 1344, 1964.

[40] **G. Maidanik.** *Response of ribbed panels to reverberant acoustic fields.* J. Acoust. Soc. Am., Vol 34, 809-826, 1962.

[41] **F.G. Leppington, E.G. Broadbent and K.H. Heron.** *The acoustic radiation efficiency of rectangular panels.* Proc. Royal Soc. Lon., A382, 245-271, 1982.

[42] **F.G. Leppington, E.G. Broadbent and K.H. Heron.** *Acoustic radiation from rectangular panels with constrained edges* Proc. Royal Soc. Lon., A393, 64-84, 1984.

[43] **F.G. Leppington, K.H. Heron, E.G. Broadbent and S.M. Mead.** *Resonant and non-resonant acoustic properties of elastic panels. II. The transmission problem.* Proc. Royal Soc. Lond., A412, 309-337, 1987.

[44] **L. Cremer, M. Heckl and E.E. Ungar.** *Structure-borne sound.* Springer-Verlag. Berlin. 1973.

[45] **T. Kihlman.** *Transmission of structure-borne sound in Buildings. A theoretical and experimental investigation.* National Institute for Building Research. Report 9, UDC 699.844, 1967.

[46] **B. Gibbs.** *The direct and indirect transmission of vibrational energy in building structures.* Ph.D. thesis, University of Birmingham, 1974.

[47] **R.S. Langley and K.H. Heron.** *Elastic wave transmission through plate/beam junctions.* J. Sound Vib. Vol 143, 241-253, 1990.

[48] **M.J. Crocker and A.J. Price.** *Sound tranmission using statistical energy analysis.* J. Sound Vib., Vol 9, 469-486, 1969.

[49] **A.J. Price and M.J. Crocker.** *Sound transmission through double walls using statistical energy analysis.* J. Acoust. Soc. Am., Vol 47, 683-693, 1970.

[50] **A. Brekke.** *Calculation methods for the transmission loss of single, double and triple partitions.* App. Acoust. Vol 14, 225-240, 1981.

[51] **M.C. Bhattacharya.** *The transmission and radiation of acoustico-vibrational energy.* Ph.D. thesis, University of Liverpool, Liverpool, UK. 1970.

[52] **A. Elmallawany.** *Criticism of statistical energy analysis for the calculation of sound insulation: Part 2 - Double partitions.* App. Acoust. Vol 13, 33-41, 1980.

[53] **M. Ohta, H. Iwashige and N. Nakasako.** *The probabilistic evaluation of discrete level type for a sound transmission through a double wall by use of a statistical energy analysis method.* Acustica, Vol 64, 1-13, 1987.

[54] **R.D. Sullivan.** *Sound insulation of brick diaphragm walls.* Ph.D. thesis, University of Liverpool, Liverpool, UK. 1994.

[55] **R.D. Sullivan and B.M. Gibbs.** *Sound insulation of wide cavity bridged heavyweight construction.* Proc. Inter-Noise 92, Toronto, Canada, 667-70, 1992.

[56] **C.E. Wallace.** *Radiation resistance of a rectangular panel.* J. Acoust. Soc. Am., Vol 51, 946-952, 1972.

[57] **K.H. Heron.** *Acoustic radiation from honeycomb sandwich plates.* Fifth European Rotorcraft and Power Lift Aircraft Forum, Amsterdam. Paper 65, 1979.

[58] **F.G. Leppington, K.H. Heron, E.G. Broadbent and S.M. Mead.** *Resonant and non-resonant acoustic properties of elastic panels. I. The radiation problem.* Proc. Royal Soc. Lond., A406, 139-171, 1986.

[59] **H. Kuttruff.** *Room acoustics.* Applied Science Publishers. London, UK. 1979.

[60] **R.J.M. Craik** *The measurement of structure-borne sound using impulsive sources.* App. Acoust. Vol 15, page 275-282, 1982.

[61] **J.R. Green ans D. Margerison.** *Statistical treatment of experimental data.* Elsevier Scientific Publishing Company, 1977.

[62] **J.E. Manning** *Formulation of SEA parameters using mobility functions*, Phil. Trans. R. Soc. Lond. A346, 477-488 (1994).

[63] **I. Bosmans and G. Vermeir.** Diffuse transmission of structure-borne sound at periodic junctions of semi-infinite plates. J. Acoust. Soc. Am., Vol 101, 3443-3456, 1997.

[64] **R.J.M. Craik, R.S. Smith and R.Wilson.** *Sound transmission through timber floors.* Proc. Inst. Acoust. Conf. Salford, Vol 2, 453-460, 1994.

[65] **BS 1202**: Part 1. 1974. Specification for nails. BSI. UK.

[66] **BS 1210**: 1963. Specification for wood screws. BSI. UK.

[67] **BS 8103**: Part 3. 1996. Code of Practice for timber floors and roofs for housing. BSI. UK.

[68] **E. Ungar.** *Transmission of flexural waves through reinforcing beams.* J. Acoust. Soc. Am Vol 33. 633-639, 1961.

[69] **L. Cremer's.** *Propagation of structure borne sound,* p137. (Sponsored Research (Germany) No. 1 (Series B))

[70] **M. Heckl.** *Wave propagation on beam plate systems.* J. Acoust. Soc. Am. Vol 33, 640-651, 1961.

[71] **H.L. Muller.** *Frequenze 11 (1957) 350.*

[72] **H.Z. Wigge.** techn. Physik (1921) 302.

[73] **V.I. Zabarov.** *Sound insulation of double walls joined at the edges.* Soviet Physics - Acoustics, Vol 11, 113-126, 1983.

[74] **D.J. Mead.** *Wave propagation and natural modes in periodic systems: Part II. Multi coupled systems, with and without damping.* J. Sound Vib., Vol 40, 19-39, 1975.

[75] **S.U. Budrin and A.S. Nikiforou.** *Wave transmission through assorted plate joints.* Soviet Physics - Acoustics, Vol 9, 1964.

[76] **T. Kihlman.** *Sound transmission through building structures of concrete.* J. Sound Vib., Vol 11, 435-445, 1970.

[77] **B.M. Gibbs and C.L.S. Gilford.** *The use of power flow methods for the assessment of sound transmission in building structures.* J. Sound Vib. Vol 49, 267-286, 1976.

[78] **P.G. Craven and B.M. Gibbs.** *Sound transmission and mode coupling at junctions of thin plates.* Part I, Representation of the problem. J. Sound Vib., Vol 77, 417-427, 1981.

[79] **R.J.M. Craik and A. Thanacanamootoo.** *The importance of inplane waves in sound transmission through buildings.* App. Acoust., Vol 37, 85-109, 1992.

[80] **J.E. Manning, R.H. Lyon and T.D. Scharton.** *Transmission of sound and vibration to a shroud - enclosed spacecraft.* Bolt Beranek and Newman, Rept. No. 143, 1966.

[81] **M.J. Crocker.** The response of structures to acoustic excitation and the transmission of sound and vibration. PhD thesis. University of Liverpool, Liverpool, 1969.

[82] **R.J.M. Craik and A.G. Osipov.** *Structural isolation of walls using elastic interlayers.* App. Acoust. Vol 46, 233-249, 1995.

[83] **R.H. Lyon and E. Eichler.** *Random vibration of connected structures.* J. Acoust. Soc. Am. Vol 36, 1344-1354, 1964.

[84] **J.E. Ashton and J.M. Whitney.** *Theory of Laminated Plates.* Stamford: Technomatic Publishing. 1970.

[85] **R.J.M. Craik and A. Thanacanamootoo.** *The importance of inplane waves in sound transmission through buildings.* App. Acoust., Vol 37, 85-109, 1992.

[86] **J.A. Steel.** *Structural vibration transmission in framed buildings using statistical energy analysis.* PhD thesis, Heriot-Watt University, Edinburgh, UK. 1990.

[87] **R.J.M. Craik.** *In-plane wave propagation in buildings.* App. Acoust. Vol 53, 273-289, 1998.

[88] **E.H. Dowell and H.M. Voss.** *The effect of a cavity on panel vibration.* AIAA Journal, Vol 1, 476, 1963.

[89] **A.J. Pretlove.** *Free vibrations of a rectangular panel backed by a closed rectangular cavity.*

[90] **R.W. Guy.** *The transmission of sound in finite surrounds.* PhD thesis, University of Liverpool, Liverpool, 1973.

[91] **A. Cummings.** *Low frequency acoustic transmission through the walls of rectangular ducts.* J. Sound Vib. Vol 61, 327-345, 1978.

[92] **F. Durka.** *Structural Mechanics.* 2nd edition, Longman Scient. Tech., 1988.

[93] **L.L. Beranek and I.L. Ver.** *Noise and vibration control engineering.-principle and applications.* J. Wiley and Sons. 1992.

[94] **K. Goesele.** *Prediction of the sound transmission loss of double partitions, (without structureborne connections).* Acustica, Vol 45, 218-227, 1980.

[95] **R.J.M. Craik, J.A. Steel and T.R.T. Nightingale.** *Sound transmission through framed buildings.*, Report IRC-IC-672, internal report of the National Research Council Canada, Institute for Research in Construction, Ottawa, Canada.

[96] **M.J. Crocker, M.C. Bhattacharya and A.J. Price.** *Sound and vibration transmission through panels and tie beams using statistical energy analysis.* Transactiosn of ASME, p775,-782, August, 1971.